UNIVERSITY OF LIVERPOOL

Dissecting the role and regulation of MRL function in Drosophila

Thesis submitted in accordance with the requirements of the University of Liverpool for the degree of Doctor in Philosophy by

Christopher James Lofthouse

June 2013

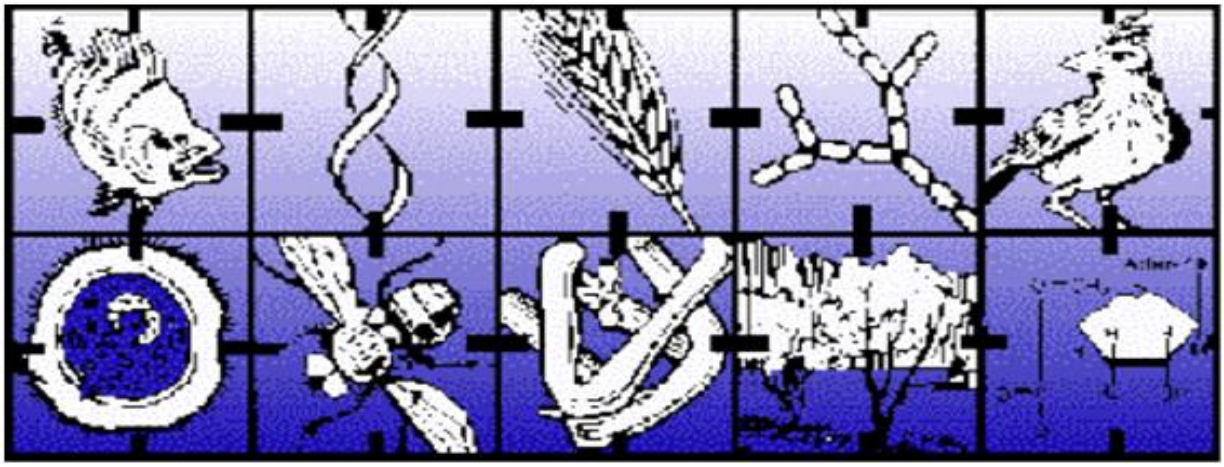

Declaration

This thesis is the result of my own work unless otherwise stated, and is based upon results from experimental and theoretical work performed as a PhD student between October 2008 and June 2013 within the Institute of Integrative Biology at the University of Liverpool.

Neither this thesis nor any part of it has been submitted in support of an application for another degree or qualification at this or any other University or Institute of Learning.

Christopher Lofthouse

June 2013

Abstract

The Mig10/RIAM/Lpd (MRL) family of adapter proteins have been recognised in transducing signals derived from growth factor receptors to alterations in cell motility and adhesion via changes in actin dynamics. Reduction in the levels of MRL proteins results in diminished cell division rates, growth retardation, an increase in monomeric (G): filamentous (F) actin ratios, loss of cell migration, and lethality. Conversely, overexpression of MRL proteins reduces the ratio of G:F actin, thereby promoting Serum Response Factor (SRF) signalling, lamellipodia formation, cellular invasion and coordinated cell growth and proliferation. Members of the MRL family all share common structural characteristics, most notably the presence of highly conserved central Ras-association (RA) and Pleckstrin homology (PH) domains in addition to an N-terminal Talin binding site and multiple C-terminal SH3 and proline rich motifs capable of interacting with Ena/VASP and Profilin.

This report extends previous work carried out on Pico, the *Drosophila* MRL homologue, by demonstrating physical interactions with Chickadee (Profilin), Rhea (Talin), Ras, and Protein Phosphatase 1 (PP1). Many of these binding partners were found to co-localise with Pico within highly dynamic membrane ruffles during *Drosophila* cell spreading, while only Enabled (Ena/VASP) co-localised at the periphery of cells once they had reached a maximal size and spreading had ceased, pointing to the existence of distinct Pico-associated complexes.

This work also details the presence of a highly conserved MAPK-binding site adjacent to the RA domain which had not been previously recorded in the literature. Site-directed mutagenesis revealed this MAPK-binding motif to be required for Pico's interactions with the Erk1/2 homologue Rolled, while conservation of MAPK binding ability was demonstrated in both human Lpd and RIAM orthologues. Further analysis showed that Rolled might phosphorylate Pico at a serine residue (Ser 819) previously identified by high-throughput phosphoproteomics, which may in turn promote Pico's interactions with PP1. Wing growth assays performed using site-directed Pico mutants indicated that PP1 plays a role in negative regulation of Pico-mediated growth, although the relevant targets of the phosphatase remain to be identified. Interestingly, reporter gene experiments confirmed that Pico induced SRF-dependent gene expression in

Drosophila cells while ectopic SRF signalling has been found to increase expression of *rolled*, suggesting the potential existence of a Rolled/PP1 mediated negative feedback loop regulating Pico functionality.

Contents

List of figures

List of tables

Abbreviations

Abl	Abelson tyrosine kinase
ADF	Actin Depolymerising Factor
ALM	Anterior lateral microtubule cells
APS	Adapter protein with PH and SH2 domains
Arp	Actin-Related Proteins
BAD	Bcl-2-associated death promoter
BLAST	Basic Local Alignment Search Tool
BPS	Between the PH and SH2
CAN	Canal-associated neurons
CDC	Cell division control protein
co-IP	Co-immunoprecipitation
CyO	Curly Oster
da	Daughterless
EGF	Epidermal growth factor
EGFR	Epidermal growth factor receptor
EMS	Ethyl methanesulfonate
en	Engrailed
Ena	Enabled
ERK	Extracellular signal-regulated kinases
EVH1	Ena/VASP homology 1
FA	Focal Adhesion
FAK	Focal adhesion kinase
FRET	Fluorescence Resonance Energy Transfer
FRT	FLP recombinase target
GAP	GTPase-Activating Protein
GFP	Green Fluorescent Protein
Grb	Growth Factor Receptor-Bound
HRP	Horseradish Peroxidase
hsp	Heat shock promoted
HSN	Hermaphrodite-specific neurons
IR	Insulin receptor
IGFR	Type I insulin-like growth factor receptor
JNK	Jun N-terminal Kinase
Lpd	Lamellipodin
MAPK	Mitogen-activated protein kinase
MEK	MAP kinase/Erk kinase
Mig-10	Abnormal cell migration protein 10
MRL	Mig-10/RIAM/Lamellipodin

mTOR	Mammalian target of rapamycin
Nedd4	Neuronal precursor cell expressed developmentally down-regulated
PDGF	Platelet-derived growth factor
PDGFR	Platelet-derived growth factor receptor
PDK-1	Pyruvate dehydrogenase kinase-1
PH	Pleckstin homology
PI	Phosphoinositide
PI3K	Phosphoinositide 3-kinase
PKA	Protein kinase A
PKC	Protein kinase C
PLC-γ	Phospholipase C-γ
PP1	Protein Phosphatase 1
PTB	Phosphotyrosine binding
RA	Ras-association
RIAM	Rap1-GTP-interacting adapter molecule
RNAi	RNA interference
S2R+	S2 receptor +
SRE	Serum response element
SRF	Serum response factor
srGAP3	SLIT-ROBO Rho GTPase activating protein
TCF	Ternary complex factor
Tft	Tufted
TSC2	Tuberous sclerosis complex 2
UAS	Upstream activating sequence
WASP	Wiskott-Aldrich syndrome protein
WAVE	WASP family Verprolin-homologous protein
WRC	WAVE regulatory complex
WT	Wild type

1. Introduction

1.1. Introducing cellular migration

Directed cell migration is a highly orchestrated, multistep process that plays a central role in many fundamental physiological mechanisms required in the development and maintenance of multicellular organisms. During early embryonic development, cell motility is essential for various morphogenic processes like gastrulation and tissue formation (Keller, 2005). Cellular migration remains crucial throughout the lifetime of higher organisms, enabling mechanisms such as wound healing and chemotactic responses of the immune system to take place (Luster et al., 2005).

Aberrant control of the migratory machinery can have serious consequences and is thought to be an underlying cause of various neurological disorders and vascular diseases. In addition, abnormal cell migration in cancerous cells often leads to the formation of secondary tumours (metastasis) and is responsible for approximately 90% of cancer related deaths (Sporn, 1996, Wang et al., 2005). Developing a comprehensive understanding of the mechanisms involved in migration is crucial for the future development of novel therapeutic treatments to combat these disorders; but it is also becoming important to emerging areas of biotechnology which focus on cellular transplantation and the manufacture of artificial tissues.

1.1.1. The mechanisms involved in migration

Migration varies significantly from one cell type to another; however, the underlying mechanisms involved are thought to be similar. To migrate, a cell must first attain a characteristic polarised morphology in response to extracellular chemical or mechanical signals, such as the presence of a Netrin gradient or increasing substrate stiffness respectively (Le Clainche and Carlier, 2008, Li et al., 2002, Lo et al., 2000). At the newly formed cell front, branched actin filaments polymerise at their barbed ends through ATP hydrolysis and depolymerise at their pointed ends at a similar rate (Theriot and Mitchison, 1991). This instigates a mechanism known as ‘treadmilling’ which allows the filaments to move forward while

maintaining the same length (Wang, 1985). The resultant force is believed to push against the membrane to drive the formation of flat membrane protrusions termed lamellipodia; enabling extension of the cell front in the direction of migration (Small et al., 2002).

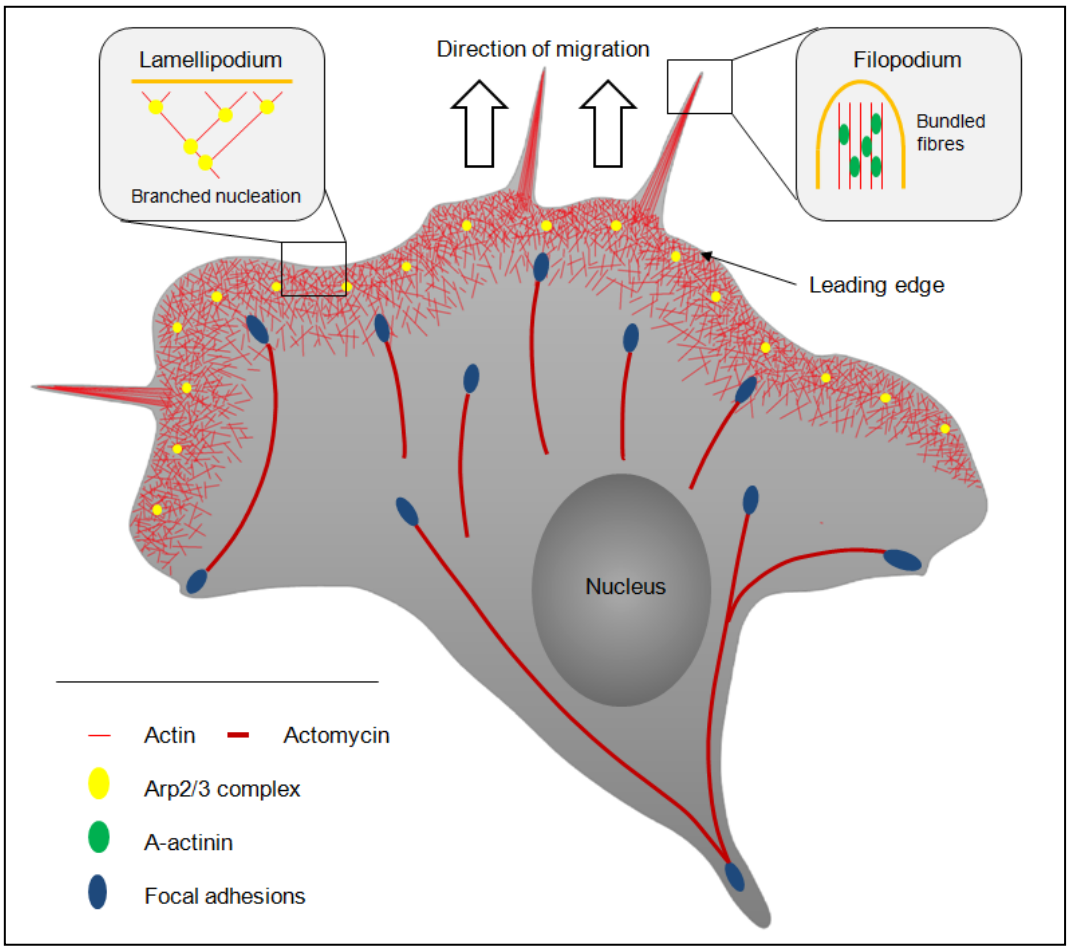

Figure 1.1.1. Schematic illustration of cellular migration. Actin assembly at the newly created cell front drives lamellipodia formation. Adhesions form at the leading edge to connect the extracellular matrix to the actin cytoskeleton enabling further extension of the protrusions. Fingerlike filopodia protrusions extend beyond the leading edge of the lamellipodia to sense the environment. Lastly, the cell combines actomyosin contractility and rear adhesion disassembly to retract its trailing edge (adapted from Le Clainche and Carlier, 2008).

At the leading edge of these advancing lamellipodia, the cell forms focal adhesions (FAs) via extracellular adhesion receptors which connect the extracellular matrix to the actin cytoskeleton (Brown et al., 2006). These attachments anchor the cell body to the substrate and enable extension of the protrusion by providing traction for the actin filaments (Le Clainche and Carlier, 2008). The migrating cells also extend fingerlike filopodia protrusions, containing 15-20 tightly bundled parallel filaments, beyond the lamellipodia leading edge to sense the environment (Lewis and Bridgman, 1992). Finally, to move forward, the cell retracts its trailing edge by combining actomyosin contractility and adhesion disassembly at the rear (Figure 1.1.1) (Le Clainche and Carlier, 2008).

1.1.2. Regulating cellular migration

Cells regulate the speed of migration by controlling the protrusive force generated by the actin filaments in the lamellipodia and filopodia. One way this is achieved is by managing the rate of actin treadmilling. As the treadmilling of pure actin is too slow to allow for the rate of movement required by many cells, control is brought about by accelerating the process.

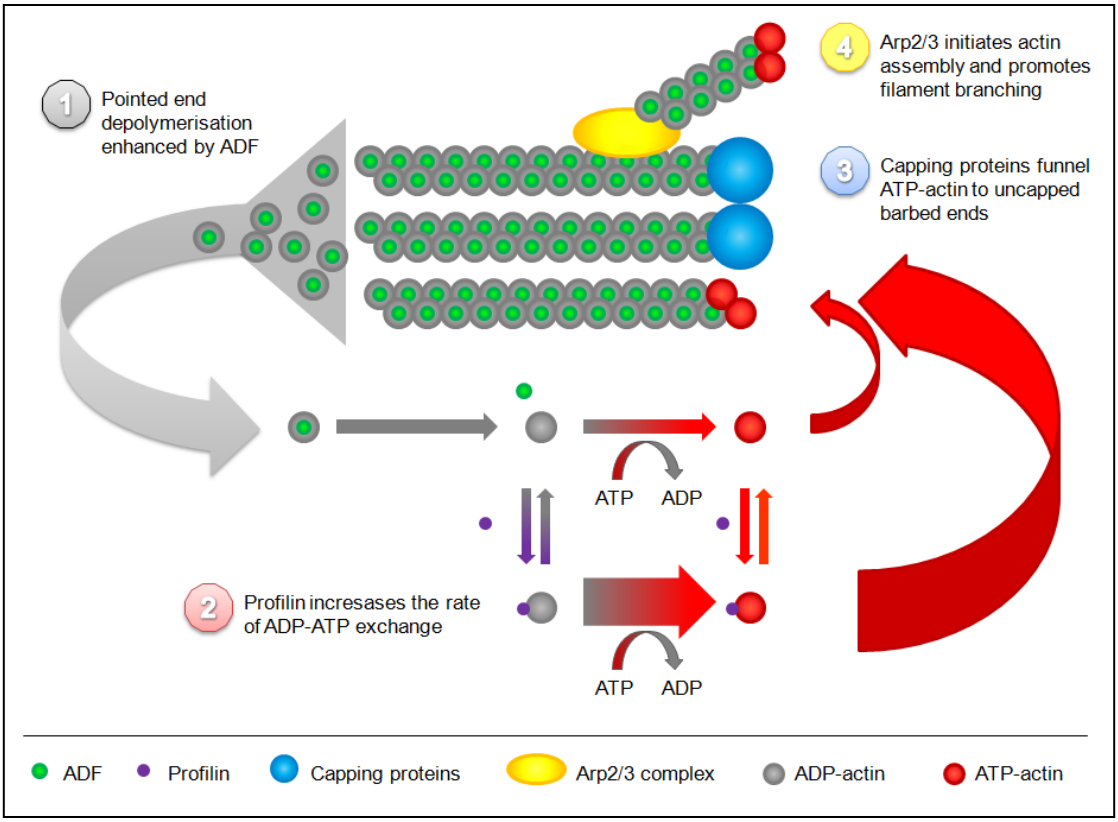

Figure 1.1.2. Regulation of actin treadmilling. (1) ADF enhances pointed end depolymerisation, increasing the concentration of monomeric actin. (2) Profilin increases the rate of exchange of ATP for ADP. (3) Capping proteins funnel ATP-actin to uncapped barbed ends. (4) Arp2/3 promotes filament branching (Le Clainche and Carlier, 2008).

ADF (Actin Depolymerising Factor) is located throughout the lamellipodium, with the exception of the leading edge, and binds to the side of ADP-actin filaments to alter their structure and induce pointed end depolymerisation (Svitkina and Borisy, 1999, Carlier et al., 1997). This increases the steady state concentration of monomeric (G) actin, which promotes faster barbed end growth to compensate for the heightened breakdown of the pointed end (Carlier et al., 1999). Profilin enhances the action of ADF by binding to G-actin and increasing the exchange rate of ADP for ATP to recycle the actin monomers near the barbed ends (Yarmola and Bubb, 2006). The combined effects of ADF and profilin alone have been shown to enhance the treadmilling rate by 125-fold (Didry et al., 1998).

The polymerisation rate is further amplified by the presence of numerous capping proteins that block the majority of actin filament barbed ends (Schafer et al., 1996). This aids in limiting filament length and funnels the flux of actin monomers to the rare, non-capped filaments, which individually grow faster (Figure 1.1.2) (Pantaloni et al., 2001, Wiesner et al., 2003). To counterbalance the effects of these capping proteins and maintain the overall treadmilling rate, migratory cells continuously generate new actin filaments.

In the lamellipodium, the nucleating factor is the Arp2/3 complex. The Arp2/3 complex localises at the leading edge of migrating cells where it mimics actin nuclei to initiate actin assembly (Svitkina and Borisy, 1999, Kelleher et al., 1995). The complex also assists in promoting filament branching by binding directly with the sides of pre-existing filaments near the barbed ends to initiate lateral branch formation (Amann and Pollard, 2001). This leads to a significant increase in the number of barbed ends (Goley and Welch, 2006). The Arp2/3 complex is normally repressed, but can be activated by members of the WASP (Wiskott-Aldrich syndrome protein) family of proteins, such as SCAR and WAVE, which are in turn activated through small G-proteins (e.g. Cdc42) that are integrated into many signalling cascades (Etienne-Manneville and Hall, 2002, Machesky et al., 1999). Through localised activation, Arp2/3 complexes are able to assist with the directionality of the protrusions in addition to their role in fuelling treadmilling with new actin filaments.

Ena/VASP proteins further aid the progression and directionality of lamellipodia through their function as anti-capping proteins (Krause et al., 2003). Ena/VASP proteins also operate within other actin associated cellular mechanisms such as morphology change, adhesion and cell-cell interactions, however their precise role is yet to be determined (Pula and Krause, 2008).

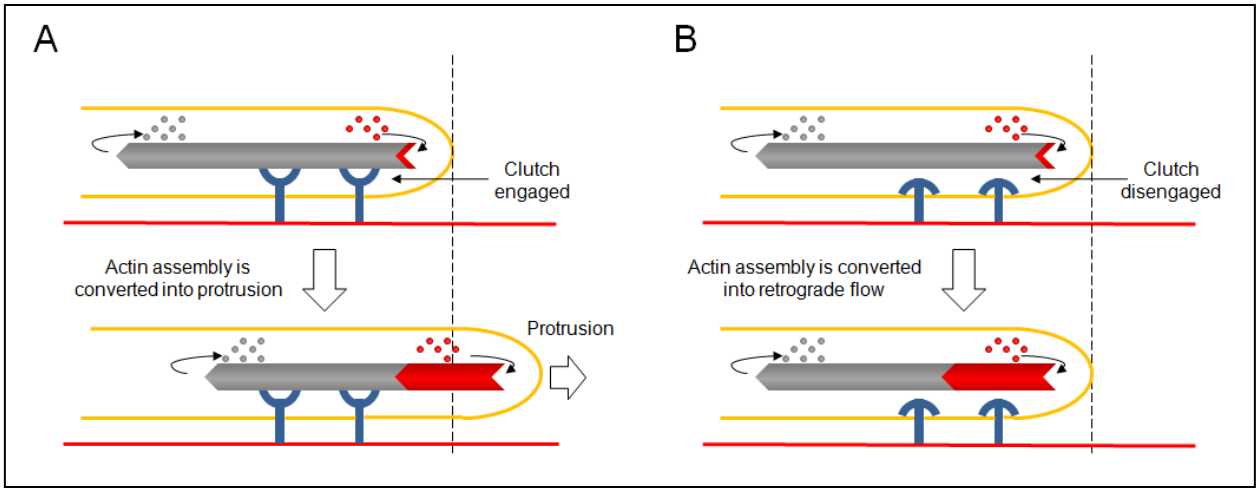

Figure 1.1.3. Regulating treadmilling force. Adhesion acts as a "molecular clutch" to convert the force generated by actin assembly into protrusion. In this figure, the actin network is represented in gray, while newly polymerized actin is represented in red. (a) The molecular clutch is engaged enabling traction between the polymerizing actin network and the substrate to result in membrane protrusion. (b) The molecular clutch is disengaged reducing traction between focal adhesions and the actin cytoskeleton preventing protrusion formation as actin treadmilling force is predominantly converted into retrograde flow (adapted from Le Clainche and Carlier, 2008).

In addition to regulating the rate of actin treadmilling, cells control migration through modulating the extent of mechanical coupling between the actin cytoskeleton and the extracellular matrix. These cell matrix adhesions act as a 'molecular clutch' which, when engaged, provide traction to the polymerising actin network. This enables the force generated through treadmilling at the leading edge of the lamellipodium to be converted into protrusion formation (Figure 1.1.3.a). Contrastingly, when the clutch is disengaged, traction is lost and slippage occurs between the polymerising actin filaments and the extracellular matrix adhesions resulting in retrograde flow and a decrease in protrusion rate (Figure 1.1.3.b) (Hu et al., 2007, Macdonald et al., 2008). The clutch also controls the transmission of the actomyosin contractile force applied on focal adhesions which facilitates traction of the cell body and retraction of tail (Webb et al., 2002).

Engagement of the molecular clutch is controlled through a variety of molecular interactions at different levels. The integrins are a large family of finely regulated heterodimeric transmembrane adhesion receptors that connect the cell to the extracellular matrix and are activated by inside-out signaling (Hynes, 2002, Humphries et al., 2006). Talin binds to the intracellular portion of the receptor, inducing a conformational change that exposes the sites of ligand binding enabling other receptors, e.g., chemokines or growth factor receptors, to control integrin activation through 'receptor cross talk' (Schwartz and Ginsberg, 2002). Talin mediated conformational change also leads to an increased affinity of the extracellular domain to components of the extracellular matrix, enhancing the overall affinity between focal adhesions and the substrate (Shattil et al., 2010).

A variety of actin binding proteins, most notably Talin, Vinculin and α-actinin, interact either directly or indirectly with the cytoplasmic tails of the integrins to 'engage the clutch' and enable traction with the extracellular matrix (Vicente-Manzanares and Horwitz, 2011). Talin is able to directly bind both integrin and actin simultaneously and plays an important role in linking integrin receptors to the actin cytoskeleton (Humphries et al., 2006). Moreover, Talin proteins are able to dimerise and may intervene in the clustering of integrin dimers to form focal adhesions (Shattil et al., 2010). Vinculin does not interact directly with the integrins, but does bind both talin and actin to play a key role in the stabilisation of the adhesive structures during the maturation of focal complexes into focal adhesions (Burridge and Mangeat, 1984, Hemmings et al., 1996). α-actinin is a homodimer that cross links actin filaments into parallel bundles to control their stiffness which is thought to potentially influence the transmission of the contractile force (Esue et al., 2009). Its direct interactions with the integrins and Vinculin are believed to play a key role in α-actinins function in linking actin filaments and focal adhesions (Otey et al., 1990, Wachsstock et al., 1987, Rajfur et al., 2002).

1.2. Cellular growth and proliferation

Cellular growth and proliferation is a tightly controlled, multifaceted process required for both the development and maintenance of all multicellular organisms. During an organism's early life, cell division is essential for morphogenesis of tissues and organs, in addition to growth of the organism itself; while throughout its existence, cellular proliferation plays a key role in mechanisms such as tissue renewal and repair, immunity, and sexual reproduction. Incorrect regulation of cell growth can lead to devastating consequences, ranging from severe developmental defects through to cancer. Indeed, analysis of the numerous factors involved in cancer progression has led to the identification of many oncogenes and tumour suppressor genes involved in controlling growth and proliferation.

1.2.1. A standard model for control

For a cell to divide, it must first respond to a series of external growth signals mediated either by environmental changes or, as is more common in multicellular organisms, the presence of growth factors such as PDGF (platelet-derived growth factor) and EGF (epidermal growth factor). In this example, PDGF and EGF are ligands for the cell surface tyrosine kinase receptors PDGFR (PDGF receptor) and EGFR (EGF receptor) respectively. In both cases ligand binding results in receptor dimerisation at the cell surface, followed by internalisation and autophosphorylation of their intracellular tyrosine kinase domains (Heldin et al., 1998, Herbst, 2004). The phosphorylated tyrosine kinase residues serve as distinct binding sites for a variety of domains such as SH2 (Src homology 2), SH3 (Src homology 3), PTB (phosphotyrosine binding), PH (pleckstin homology), and PDZ domains (Heldin et al., 1998, Herbst, 2004). This enables the recruitment and subsequent activation of numerous signal transducers and activators of intracellular substrates, such as Ras, PI3K (phosphoinositide 3-kinase) and PLC-γ (Phospholipase C-γ), which in turn stimulate further intracellular signal transduction cascades (Figure 1.2.1) (Heldin et al., 1998, Herbst, 2004).

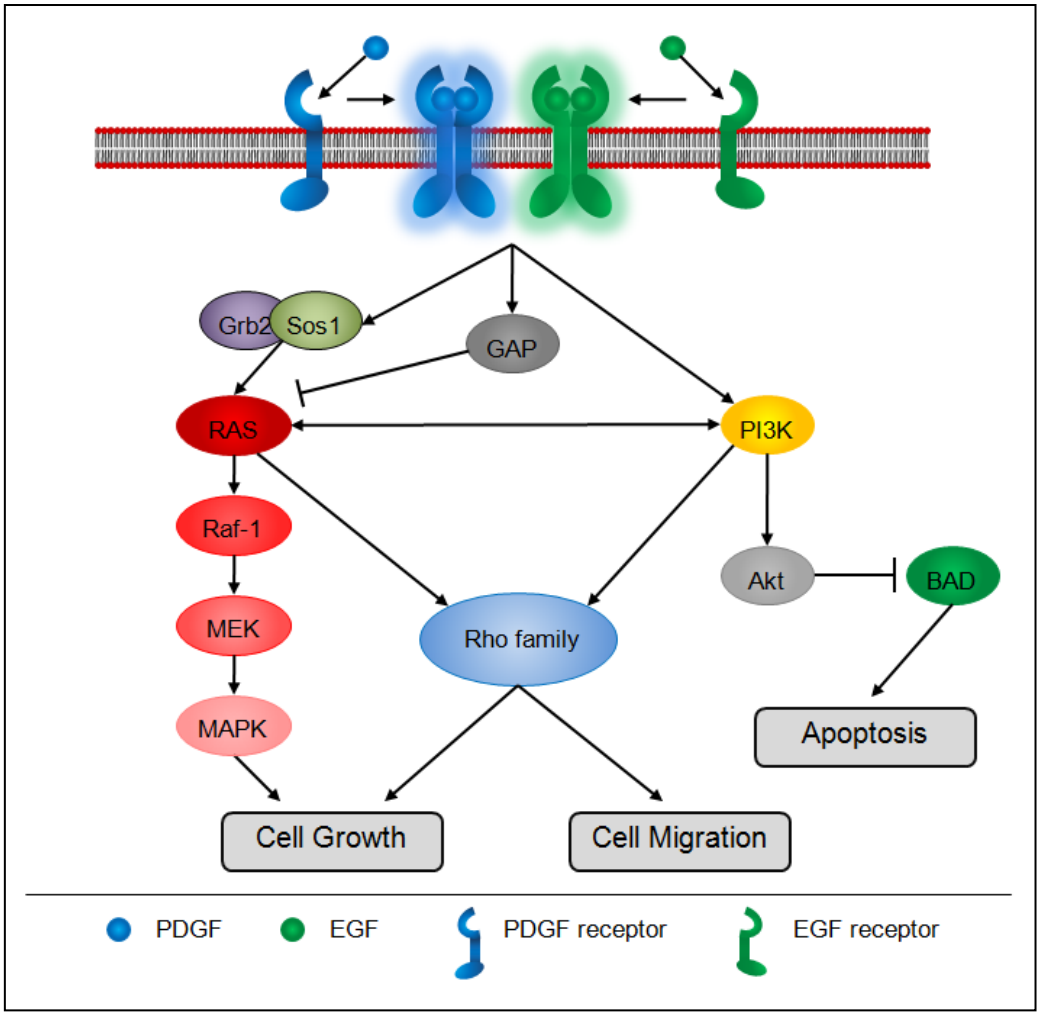

Figure 1.2.1. Schematic illustration of example signaling pathways initiated by PDGF and EGF receptor activation. Ras activity is regulated by Grb2/Sos1 mediated activation and GAP repression. Ras can initiate the RAF-MEK-MAPK signaling cascade and activate Rho GTPases, triggering cell proliferation, and cell growth and migration respectively. PI3K also regulates Rho activity and has been further implicated in Akt activation leading to suppression of apoptosis (Heldin et al., 1998, Herbst, 2004).

Ras activates several pathways, including the RAF-MEK-ERK/MAPK cascade, which transmits signals downstream and results in the transcription of genes involved in controlling several cellular mechanisms including growth, proliferation, and senescence (Santarpia et al., 2012, McCubrey et al., 2007). Net Ras activity is determined by balancing activation by Grb2/Sos1

following direct or SHP-2/Shc mediated interactions with the receptor, and deactivation by GTP hydrolysation inducing GAP (GTPase-Activating Protein) (van der Geer et al., 1997).

Ras has also been shown to bind and activate PI3K, while both proteins are able to stimulate members of the Rho GTPase family (Rodriguez-Viciana et al., 1994, Nobes et al., 1995). In its active state, Rho binds to downstream effectors and stimulates intracellular signaling pathways involved in regulating processes such as cytoskeleton organization, gene transcription, cell proliferation, migration and growth (Lazer and Katzav, 2011). In addition, PI3K is involved in activating Akt, which in turn phosphorylates the tumor suppressor TSC2 (tuberous sclerosis complex 2) and apoptosis inducing BAD (Bcl-2-associated death promoter), suppressing their growth inhibitory and apoptotic effects respectively (Huang and Manning, 2009, Datta et al., 1997). Indeed, the PI3K/Akt/mTOR (mammalian target of rapamycin) pathway has been shown to play a key role in a wide range of physiological processes, including cell cycle progression, differentiation, survival, transcription, translation, endocytosis, motility, metabolism, and autophagy (Figure 1.2.1) (Yuan and Cantley, 2008, Steelman et al., 2011).

While numerous other pathways involved in regulating cellular growth and proliferation exist, many follow a similar mechanism to the one described above, with responses to extracellular signals inducing proliferation specific signal transduction cascades, which trigger cell division. However, a surprising mechanism for actin mediated cell proliferation has been identified that links cytoskeletal dynamics to cell growth.

1.2.2. Actin mediated cellular proliferation

It originally seems remarkable that proteins implicated in the regulation of actin dynamics could be involved in nuclear gene expression of factors governing cellular growth and proliferation; however, a model whereby a depletion in the cytoplasmic levels of G-actin leads to an increase in cell division has been developed (Miralles et al., 2003).

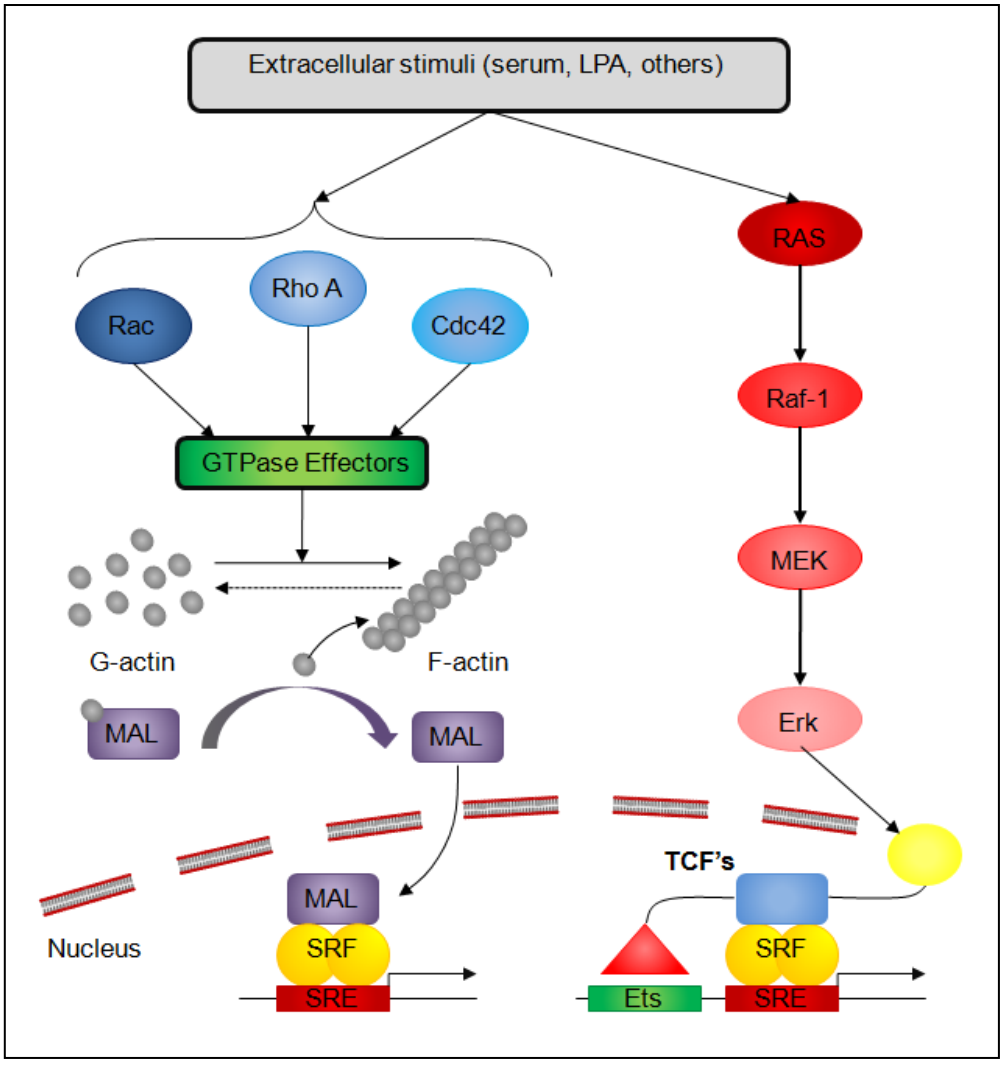

Figure 1.2.2. Pathways for SRF activation. Extracellular stimuli triggers the MAPK signaling cascade, enabling TCF-SRF complex formation and SRE binding. Conversely, activation of actin regulatory proteins leads to an increase in the F:G actin ratio. The decrease in G-actin levels reduces the binding of G-actin to MAL, allowing MAL to enter the nucleus and enhance SRF mediated gene expression (Posern and Treisman, 2006).

SRF (serum response factor) is a highly conserved mitogen responsive MADS-box transcription factor expressed in most plants and animals (Shore and Sharrocks, 1995, Arsenian et al., 1998). It binds to the SRE (serum response element) within promoter regions of 'immediate-early' genes, such as c-*fos*, when in complex with the TCF (ternary complex factor) proteins Elk-1, SAP-1 and Net; enabling regulation of apoptosis, cell growth, cell cycle control, and

differentiation (Norman et al., 1988, Treisman, 1995). This interaction with members of the TCF family enables control of transcription via MAPK (mitogen-activated protein kinase) signalling, however, a TCF independent pathway controlled by Rho-family GTPases also exists (Figure 1.2.2) (Treisman, 1994, Hill et al., 1995).

MAL, an SRF cofactor encoded by a ubiquitously expressed gene, predominantly localises to the cytoplasm where it binds directly to monomeric G-actin. These interactions with G-actin inhibit nuclear import of MAL, preventing associations with SRF and subsequent enhancement of SRE mediated gene expression (Miralles et al., 2003, Wang et al., 2002). Stimulation of actin treadmilling by Rho GTPases, such as Rac, RhoA and Cdc42, leads to an accumulation of F-actin and a commensurate depletion of G-actin, alleviating the inhibition on MALs nuclear import (Miralles et al., 2003, Settleman, 2003). Upon translocation to the nucleus, MAL complexes with SRF to enable transcription of a subset of SRE-containing genes (Figure 1.2.2) (Miralles et al., 2003, Gineitis and Treisman, 2001). Notably, not all SRF-regulated genes are sensitive to Rho-actin signaling, with the MAL-SRF complex found to selectively bind to promoter regions of Rho-sensitive genes (Gineitis and Treisman, 2001, Settleman, 2003). Indeed, NF-κB and C/EBP have been identified as transcription factors that mediate the activation of SRF by Rho, indicating that multiple downstream pathways may contribute to SRF activation and specificity (Montaner et al., 1999, Settleman, 2003).

Of course, as with the majority of signal transduction pathways, there is more complexity to the actin-MAL-SRF mechanism than can be accounted for by a simple linear cascade from the cell surface to the nucleus. For example, MAL has been found to undergo serum-induced phosphorylation that is only partially blocked by Rho inhibition, indicating that pathways independent of Rho may also influence MAL-SRF activity (Miralles et al., 2003). Indeed, Ras-RAF-MEK signalling pathways, LIM kinase, Profilin, mDia1, mDia2, VASP, WASP and N-WASP have been implicated in activating MAL and inducing nuclear translocation (Miralles et al., 2003). Also, some mutant actin monomers have been shown to remain competent for MAL binding yet promote its nuclear accumulation, which is hard to reconcile with a simple model (Posern et al., 2004, Posern and Treisman, 2006). Consequently, it has been proposed that MAL may constitutively shuttle in and out of the nucleus, and that a reduction in actin binding shifts

the balance towards import either by increasing nuclear translocation or decreasing nuclear export (Posern and Treisman, 2006). Lastly, while Rho, Rac, and Cdc42 can each promote F-actin assembly, they have been found to exhibit widely varying potency as SRF activators, further implicating downstream pathways in regulating SRF activity and specificity (Hill et al., 1995, Settleman, 2003).

1.3. The RA-PH family of adapter proteins

Adapter proteins play a fundamental role in regulating a diverse range of cellular activities through the coupling of extracellular signalling events with intracellular signal transduction pathways. While these proteins tend to lack any intrinsic enzymatic activity themselves, they often possess multiple protein and lipid binding domains which determine their function by facilitating the formation of various protein complexes. These adapter protein recruited complexes form the cornerstone of many biological processes as the close proximity of the specific binding partners enhances the control and speed of the cellular response to a signalling event.

One class of molecular adaptors are the RA (Ras-association) and PH domain containing proteins. This class of proteins are divided into two small but distinct families; the Grb (Growth Factor Receptor-Bound) 7/10/14 family and the MRL (Mig-10/RIAM/Lamellipodin) family (Figure 1.3.1) (Shen and Guan, 2004, Lafuente et al., 2004). Unlike the MRL proteins, Grb proteins are only found in higher multicellular organisms; with no orthologues identified in either *Caenorhabditis elegans* (*C. elegans*) or *Drosophila melanogaster*, indicating that the acquisition of Grb7/10/14 structure and function appears to have been relatively late in evolutionary terms (Holt and Siddle, 2005).

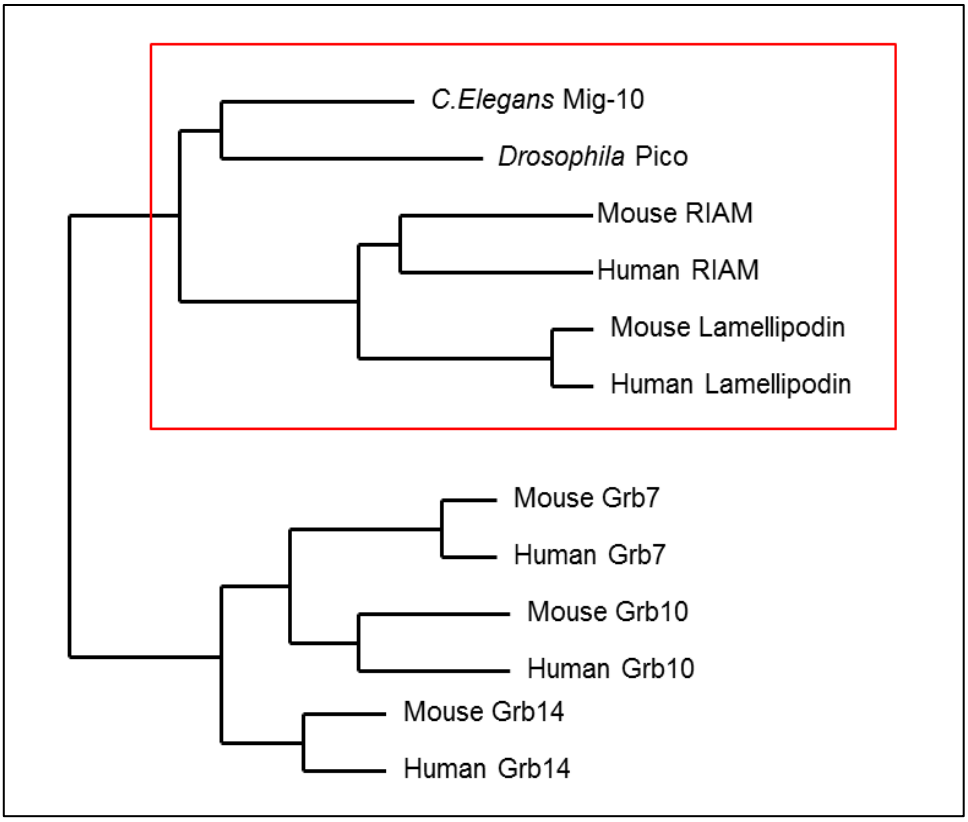

Figure 1.3.1. Dendrogram of the full-length proteins of the Grb7/10/14 and MRL families. The MRL family (boxed in red) and the Grb7/10/14 family represent two distinct sub-groups of the RA-PH superfamily. No Grb7/10/14 orthologues are found in *C. elegans* or *Drosophila melanogaster*.

1.3.1. The Grb7/10/14 family

Grb7, Grb10 and Grb14 all share a common domain structure and constitute the Grb7/10/14 family of adapter proteins. In addition to the central RA and PH domains mentioned previously, they also possess an N-terminally located proline-rich region, a C-terminal SH2 domain and a BPS (Between the PH and SH2) domain (Figure 1.3.2) (Han et al., 2001).

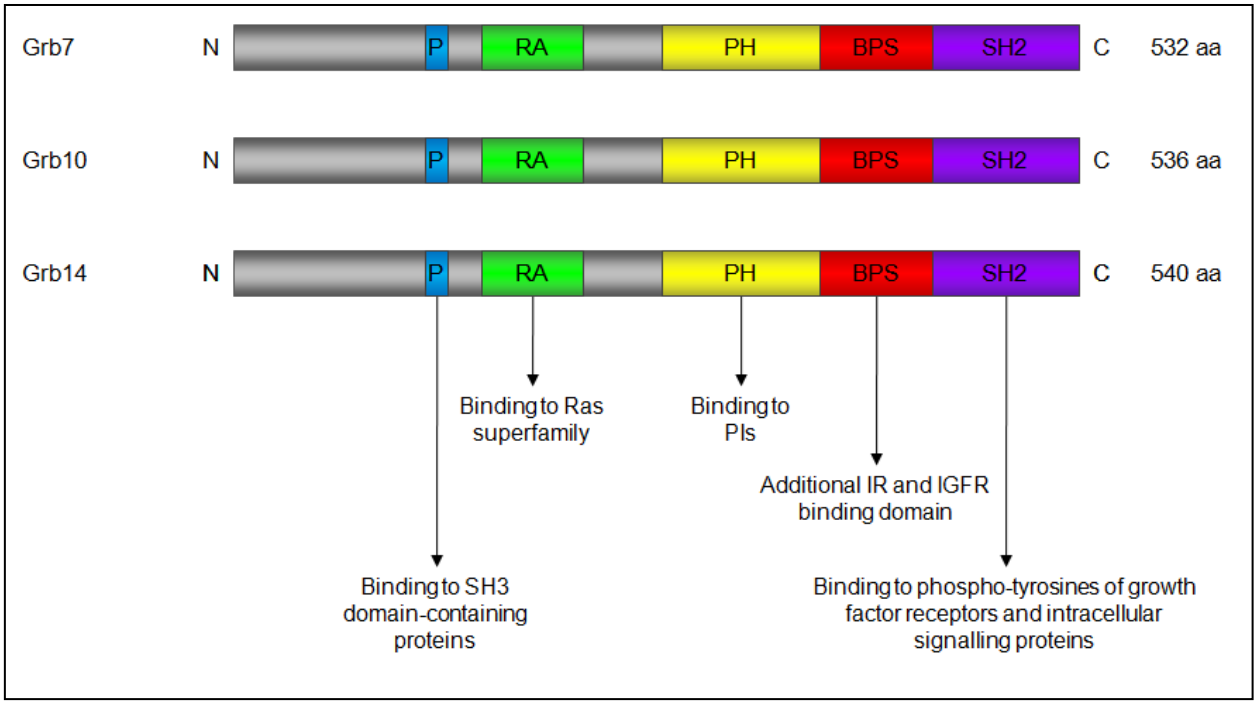

Figure 1.3.2. A schematic representation of the Grb7/10/14 family of proteins. The Grb7/10/14 all possess central RA and PH domains in addition to an N-terminal proline rich region and a C-terminal SH2 domain. The BPS domain appears to be unique to the Grb7/10/14 family.

The Ras superfamily of proteins are prolific signal-transducing GTPases that cycle between inactive GDP-bound and active GTP-bound forms. They interact with a spectrum of effector molecules enabling them to act through various signalling pathways; most notably those involved in cell proliferation, cellular adhesion, and membrane trafficking (Bourne et al., 1990, Wennerberg et al., 2005). Many Ras-like GTPases, such as R-Ras, K-Ras and Rap, activate their effectors through direct interactions with characteristic RA domains (Ponting and Benjamin, 1996). Consistently, the RA domains present in the Grb7/10/14 have been reported to facilitate interactions with members of the Ras superfamily. Grb7 has been shown to bind to N-Ras, K-Ras and H-Ras as well as activated Rap1 and Rap2, albeit with a much weaker affinity (Rodriguez-Viciana et al., 2004). Grb10 and Grb14, on the other hand, have only been found to bind to N-Ras but not Rap1 or Rap2 so far, with further experimentation required to determine if other Ras family GTPases interact (Depetris et al., 2009).

PH domains are small protein modules typically around 120 amino acids in length that are found in numerous proteins involved in cellular signalling (Haslam et al., 1993, Lemmon and Ferguson, 2000, Mayer et al., 1993). They are thought to predominantly function in targeting their host protein to the plasma membrane through direct interactions with PIs (phosphoinositides), a minor component localised on the cytosolic side of eukaryotic membranes (Lemmon, 2007, Rameh et al., 1997). In some cases PI(4,4)P_2 is the ligand, while in others, products of agonist-stimulated PI3K are the targets (Franke et al., 1995, Rameh and Cantley, 1999). While these products, PI(3,4)P_2 and PI(3,4,5)P_3, are barely detectable in resting mammalian cells, they are transiently generated in relatively significant quantities by PI3Ks following the activation of almost all known cell-surface receptors (Vanhaesebroeck and Waterfield, 1999, Lemmon and Ferguson, 2000, Cantley, 2002). In addition to their role in membrane localisation, PH domains have also been reported to interact with a small number of proteins, such as heterotrimeric G-proteins and isoforms of PKC (protein kinase C) (Tsukada et al., 1994, Robinson et al., 1993).

As expected, the PH domains of the Grb7/10/14 proteins have been shown to bind with a range of specific phosphoinositides. Grb7 has been reported to interact strongly with PI(3)P and PI(5)P, while only moderate or weak binding was observed with PI(4)P, PI(3,5)P_2, PI(3,4)P_2 and PI(3,4,5)P_3 (Shen et al., 2002). The PH domain of Grb10 was shown to have a fairly strong affinity for PI(5)P, PI(4,5)P_2, PI(3,4)P_2 and PI(3,4,5)P_3, whereas Grb14 only interacted weakly with PI(3,4,5)P_3 (Depetris et al., 2009). These differences in phosphoinositide binding specificities are generally attributed to a number of flexible loop regions attached to β-sheets that make up the domain (Fruman et al., 1999). Despite significant sequence homology (over 60%) and considerable 3D structural similarity between the Grb7/10/14 PH domains, the lengths of the aforementioned loops vary between the domains and is thought to determine phosphoinositide preference (Fruman et al., 1999, Lemmon and Ferguson, 2000). Interestingly, a loss of binding to phosphoinositide headgroups *in vitro* through a single point mutation in the PH domain of Grb14, lead to a reduction in co-immunoprecipitation with Ras; indicating that Grb14 PH domain mediated membrane association is important for the interaction of Grb14 with Ras (Depetris et al., 2009).

The SH2 domain forms the most highly conserved region amongst the Grb7/10/14 family and acts as a phosphotyrosine-binding module allowing interactions with receptor tyrosine kinases and other intracellular signaling proteins (Holt and Siddle, 2005). Despite the high degree of similarity, the binding preferences of this region generally vary between the proteins. The SH2 domains of all three Grb7/10/14 members have been shown to interact with the activated IR (insulin receptor), however, the affinity with which they associate differs significantly and may be important in influencing the outcome of IR-dependent signaling (Kasus-Jacobi et al., 2000, Hansen et al., 1996, Kasus-Jacobi et al., 1998). Grb7 associates with the receptor tyrosine kinase ErbB2 and the cytoplasmic tyrosine kinase FAK (focal adhesion kinase) via its SH2 domain, while both Grb10 and Grb14 do not (Frantz et al., 1997, Han and Guan, 1999, Janes et al., 1997). SH2 domains have also been implicated in dimerisation following structural analysis of the superficially similar APS (Adapter protein with PH and SH2 domains) SH2 region; and may be a feature of adapter proteins involved in signaling from receptors such as the IR and IGFR (type I insulin-like growth factor receptor) (Hu et al., 2003, Holt and Siddle, 2005).

The BPS domain is a short region approximately 80 amino acids long found exclusively in the Grb7/10/14 proteins and named due to its location between the PH and SH2 domains (He et al., 1998). It appears to be intrinsically unstructured yet the isolated domain retains physiological activity by interacting with activated IR and IGFR, and inhibiting IR catalytic activity (Moncoq et al., 2003, Stein et al., 2001, Bereziat et al., 2002). It is believed to function by cooperating with the SH2 domain to facilitate interactions with tyrosine-phosphorylated signalling molecules, including receptor tyrosine kinases (He et al., 1998). In addition, despite its high sequence conservation amongst the Grb7/10/14 proteins, it is thought that the BPS domain acts as an important receptor binding determinant to impart specificity amongst the family (Holt and Siddle, 2005).

Lastly, the N-terminal regions of the Grb7/10/14 proteins contain a conserved proline rich sequence in addition to other PXXP motifs, enabling interaction with SH3 domain containing proteins such as c-Abl (Abelson) by Grb10 (Frantz et al., 1997). Tandem proline rich regions in the N-terminus of Grb10 have also been found to interact with GIGYF (Grb10-interacting GYF) 1 and 2; two proteins implicated in EGFR mediated Akt activity regulation, via GYF motifs

rather than SH3 domains (Giovannone et al., 2003, Ajiro et al., 2010). In addition, the N-terminal region of Grb14 binds to an ankyrin repeat region of the poly(ADP-Ribose) polymerase tankyrase 2; however, neither the functional significance or exact site of this interaction have yet been determined (Lyons et al., 2001). No N-terminal binding partners have been identified for Grb7 thus far.

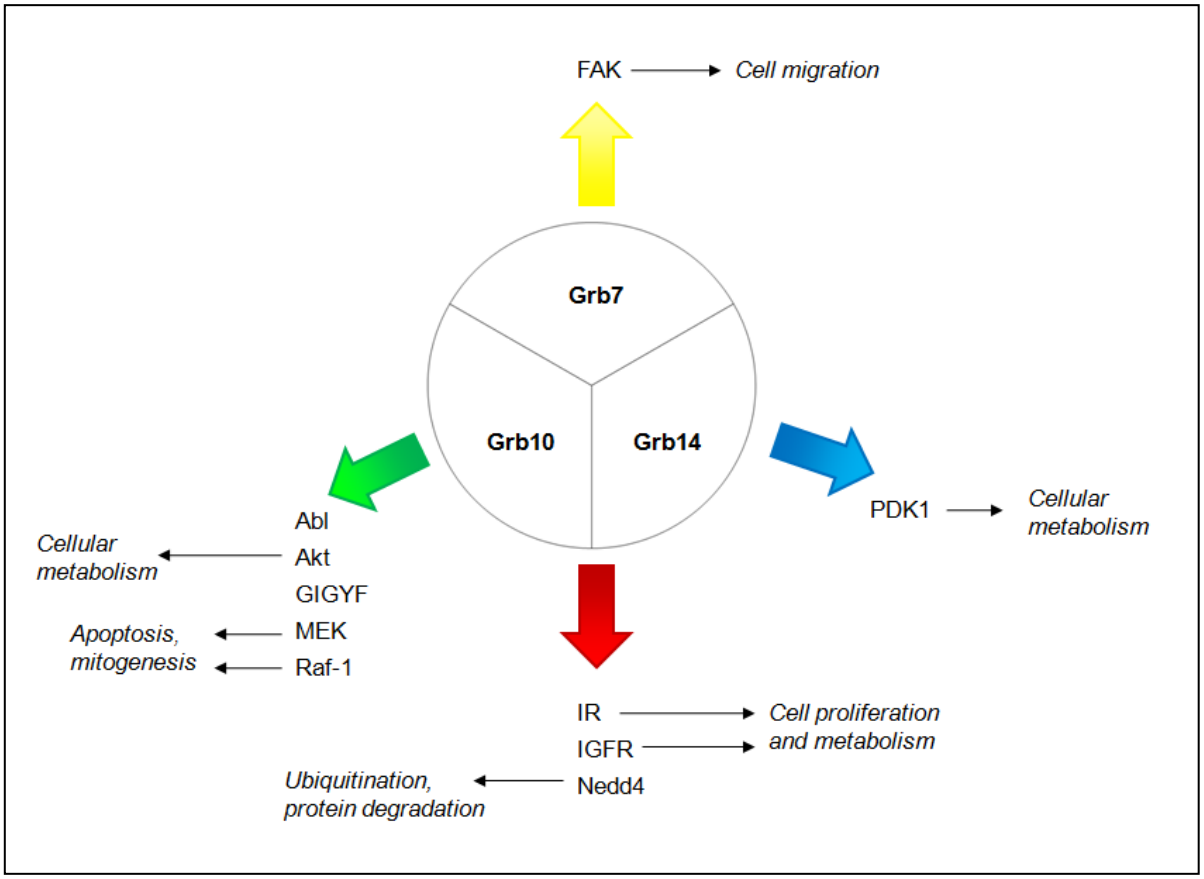

Figure 1.3.3. The differing functions of the Grb7/10/14 family. Grb7/10/14 interactions play a key role in their functionality (adapted from Holt and Siddle, 2005).

The Grb7/10/14 family proteins all share significant structural and sequence homology, however, due to their different binding partners they have been found to regulate distinct cellular functions and pathways, with only some functional overlap existing between Grb10 and Grb14 (Figure 1.3.3).

Grb7 is thought to act as a positive regulator of cell migration through its interactions with FAK and ErbB2. FAK is localised predominantly within focal adhesions and mediates several integrin signalling pathways including those involved in the promotion of cell migration, proliferation and cell spreading (Cary and Guan, 1999). ErbB2 is part of the EGFR family and has been shown to play a key role in the pathogenesis and progression of a variety of aggressive breast cancers, evolving to become an important biomarker and target for treatment of the disease (Olayioye, 2001).

Grb10 and Grb14 have been found to play a significant role in the control of cellular growth, proliferation and metabolism by directly binding and inhibiting activated IR to prevent insulin induced activation of signalling cascades involved in metabolic and mitogenic pathways (Wick et al., 2003, Kairouz et al., 2005, Kasus-Jacobi et al., 1998). Grb10 and Grb14 binding is thought to both inhibit the catalytic activity of the IR, and also block access of substrates to the activated receptor (Bereziat et al., 2002, Wick et al., 2003, Langlais et al., 2004). Contradicting this, some studies have implied that Grb10/14 might act as positive mediators of insulin signalling, with Grb10 reportedly interacting with and increasing the activity of the insulin signalling pathway molecule Akt; while Grb14 was shown to constitutively associate with PDK-1 enabling recruitment to the activated IR and promoting Akt phosphorylation and insulin signal transduction (Jahn et al., 2002, King and Newton, 2004, Holt and Siddle, 2005).

Grb10 and Grb14 have also been implicated in mediating ubiquitination and possible degradation of IGFR through interactions with Nedd4 (neuronal precursor cell expressed developmentally down-regulated), although, Grb14 has only been found to interact in yeast two-hybrid studies so far (Morrione et al., 1999, Lyons et al., 2001, Vecchione et al., 2003). Lastly, it has been suggested that Grb10 may assist in repressing apoptosis as SH2 mutated forms of Grb10 that are unable to interact with either Raf-1 or MEK (MAP kinase/Erk kinase) have induced apoptosis, while co-expression of wild type Grb10 reversed the effect (Nantel et al., 1998). It should be noted that this section should not be regarded as a comprehensive review of the Grb7/10/14 and merely exists to highlight how differential binding properties of conserved domain regions significantly affects adaptor protein functionality.

1.3.2. The MRL family

The MRL family of adapter proteins are comprised of the *C. elegans* orthologue Mig-10 (abnormal cell migration protein 10), two mammalian paralogues RIAM (Rap1-GTP-interacting adapter molecule) and Lpd (Lamellipodin), and the most recently characterised *Drosophila* orthologue Pico (Annotation symbol: CG11940) (Manser and Wood, 1990, Krause et al., 2004, Lafuente et al., 2004, Lyulcheva et al., 2008). It is thought that members of this recently identified family facilitate in transducing signals derived from membrane receptors to changes in the actin cytoskeleton enabling regulation of actin dynamics, cell adhesion, migration and growth (Krause et al., 2004, Lafuente et al., 2004, Lyulcheva et al., 2008, Colo et al., 2012b).

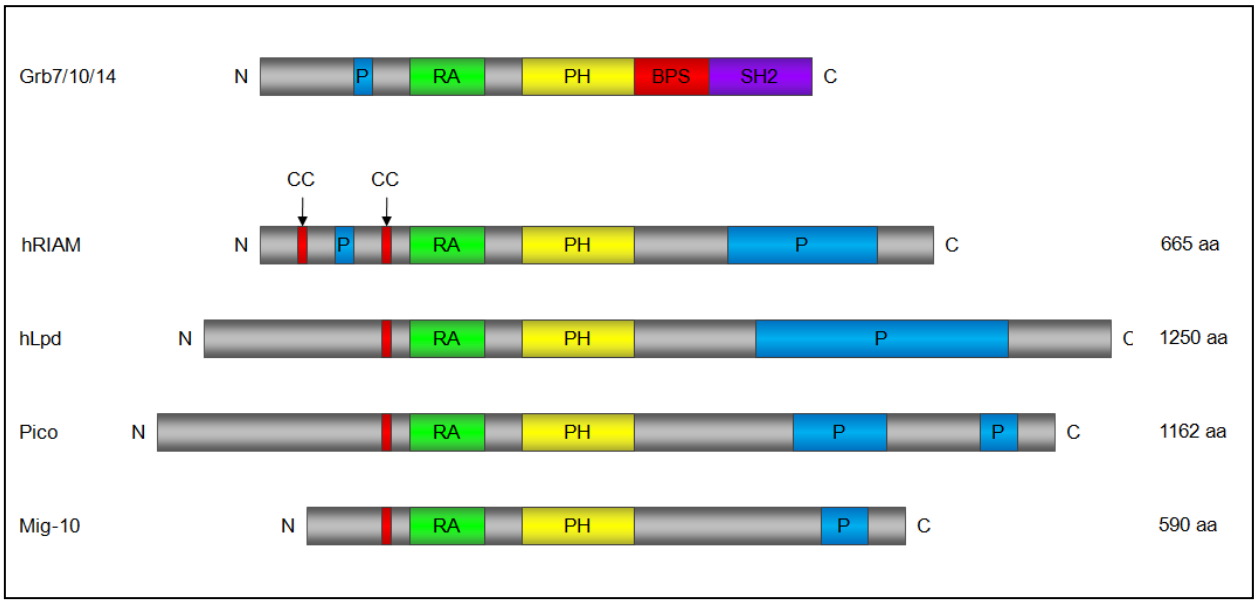

Figure 1.3.4. Schematic representation of the domain structure of Grb7/10/14 and MRL family proteins. The MRL proteins all possess central RA and PH domains in addition to an N-terminal coiled-coil motif and C-terminal proline rich regions. RIAM also contains an additional proline rich region and coiled-coil motif in its N-terminus. The MRL family do, however, lack the characteristic BPS and SH2 domains found in the Grb7/10/14 proteins (Colo et al., 2012b).

Much like the Grb7/10/14 family members, the MRL proteins all possess well defined central RA and PH domains; however, they lack the characteristic Grb7/10/14 BPS and SH2 domains while only RIAM contains an N-terminal proline rich region (Figure 1.3.4). The RA domain is approximately 90 amino acids long and directly interacts with specific Ras-like GTPases, potentially playing a crucial role in activation of the protein and/or its other associated factors (Holt and Daly, 2005). The PH domain spans roughly 100 amino acid residues and is thought to target the MRL proteins to the plasma membrane through direct interactions with phosphoinositides (Holt and Daly, 2005, Krause et al., 2004).

In addition to the RA and PH domains, the MRL proteins also possess a highly charged N-terminal region around 55 amino acids in length, while amphipathic helical structured talin binding sites have been identified within the first 100 amino acids of RIAM and Lpd (Krause et al., 2004, Lafuente et al., 2004, Lee et al., 2009). Adjacent to the N-terminus of the RA domain, MRL proteins also contain a characteristic 27 amino acid putative coiled-coil motif that may function in promoting homodimeric or heterodimeric interactions (Legg and Machesky, 2004, Lupas, 1996). Lastly, all MRL proteins possess a relatively unstructured proline rich C-terminus, with multiple FPPPP motifs allowing interactions with EVH1 (Ena/VASP homology 1) domains found in the actin regulatory proteins Enabled and VASP; as well as XPPPP motifs that bind to profilin and other SH3-binding motif containing proteins (Colo et al., 2012b, Krause et al., 2004, Lafuente et al., 2004).

The two mammalian MRL proteins, RIAM and Lpd, have well conserved RA and PH domains, however, their N-terminal and C-terminal regions show considerable divergence explaining their differing yet overlapping functionality. At its N-terminus, RIAM contains an additional proline-rich region with two putative EVH1 binding sites and an extra coiled-coil motif not found in the other MRL members (Figure 1.3.4) (Lafuente et al., 2004). The RIAM C-terminus possesses a proline-rich motif comprised of five profilin-binding sites and five EVH1 binding motifs, while the larger C-terminal proline rich region of Lpd consists of eight potential SH3 binding sites, six EVH1 domain binding regions and three profilin interacting motifs (Lafuente et al., 2004, Krause et al., 2004).

Both RIAM and Lpd interact with Ena/VASP proteins and Profilin via their EVH1 and profilin binding sites respectively; potentially facilitating their recruitment towards the leading edge to enable regulation of the actin cytoskeleton (Lafuente et al., 2004, Krause et al., 2004). Indeed, RIAM and Lpd can co-localise with Ena/VASP proteins and F-actin at lamellipodia and filopodia tips, and have been shown to regulate actin dynamics in an Ena/VASP dependent manner (Jenzora et al., 2005, Lafuente et al., 2004, Krause et al., 2004). When overexpressed, RIAM promotes cell spreading and lamellipodia formation while Lpd increases lamella protrusion velocity. The increased lamellipodial protrusion velocity resulting from Lpd overexpression can be suppressed by blocking Ena/VASP functionality (Krause et al., 2004). Contrastingly, knockdown of Lpd impaired lamella formation in addition to reducing actin branching density and F-actin levels within the lamellipodium; whilst RIAM silencing decreases F-actin quantities as well (Lafuente et al., 2004, Krause et al., 2004). RIAM and Lpd also share a capacity to bind to Talin via N-terminal amphipathic helices, enabling integrin activation and promotion of cell adhesion (Lafuente et al., 2004, Lee et al., 2009, Han et al., 2006, Watanabe et al., 2008). Furthermore, RIAM has been found to co-localise with Vinculin and actin in early focal adhesions during initial cell spreading, but is absent in more mature formations (Han et al., 2006). Fitting in with its role of controlling actin dynamics and integrin mediated adhesion, RIAM has also been shown to regulate the directionality of cell migration and play a role in FA disassembly through an integrin-RIAM dependent MEK/Erk activated feedback-loop (Hernandez-Varas et al., 2011, Colo et al., 2012a).

Despite the high level of conservation within the RA and PH domains and the presence of similar binding sites located throughout their C-terminal regions, RIAM and Lpd demonstrate differing binding preferences. RIAM interacts predominantly with active Rap-1, a well known regulator of integrin activation, although it can bind active Ras at a significantly lower affinity (Lafuente et al., 2004, Bos, 2005). This interaction requires both the RA and PH domains, and is enhanced by the RIAM N-terminus (Lafuente et al., 2004). Contrastingly, Lpd has been reported to associate with active K-Ras, N-Ras, H-Ras, R-Ras and Rac, however, no interaction with Rap-1 has yet been observed (Rodriguez-Viciana et al., 2004, Jenzora et al., 2005, Krause et al., 2004). RIAM and Lpd also display differential PH domain binding preferences, with RIAM associating with the more common PI(3)P and PI(5)P, while Lpd interacts with the relatively rarer PI(3,4)P_2

(Jenzora et al., 2005, Krause et al., 2004, Lemmon, 2008). Since PIs represent early polarizing molecules during cell activation, the differential binding capacities of the Lpd and RIAM PH domains may contribute to the characteristic temporal and spatial localisations observed in these proteins (Lemmon, 2003, Colo et al., 2012b). At the cellular level, RIAM is found both in the cytoplasm and in lamellipodia at the leading edge of the cell membrane, while Lpd is predominantly located at the plasma membrane (Lafuente et al., 2004, Jenzora et al., 2005, Krause et al., 2004).

Further protein interactions and post-translational modifications are also thought to assist in the regulation of RIAM and Lpd, enabling tight control over their divergent downstream functions. In stimulated T cells, RIAM was found to be a substrate for the tyrosine kinases Fyn, Lck and ZAP-70, enabling the C-terminal proline-rich region to interact with the SH3 domain of PLC-γ1. RIAM then assists in the translocation of PLC-γ1 to the actin cytoskeleton where, through interactions with $PI(4,5)P_2$, a signaling cascade is initiated by PLC-γ1 that increases Ras-GTP formation, MEK/Erk activation, and changes in gene expression (Patsoukis et al., 2009). Lpd, on the other hand, is able to bind the SH2 domain of c-Abl tyrosine kinase following phosphorylation of key tyrosine residues within Lpd (Michael et al., 2010). Abl family kinases are important regulators of cytoskeletal dynamics and have been implicated in axon guidance in both *Drosophila* and mammals (Lanier and Gertler, 2000). In fibroblasts, Lpd phosphorylation by c-Abl downstream of PDGF regulated dorsal ruffle formation by recruiting Ena/VASP proteins (Michael et al., 2010). Regulation of axon morphogenesis in primary hippocampal neurons is also reported to be mediated by Lpd in cooperation with c-Abl (Michael et al., 2010). Lastly, in primary fibroblasts Lpd interactions with the SH3 domain of srGAP3 (SLIT-ROBO Rho GTPase activating protein) negatively regulates lamellipodial dynamics. It is thought that srGAP3 associates with Lpd near the membrane, releasing the binding between Rac1 and Lpd, causing inhibition of membrane protrusions associated with a reduction in the local Rac1-GTP levels (Endris et al., 2011).

While RIAM and Lpd have both been implicated in cell growth and proliferation, the mechanisms through which they act are thought to be different. The reduction in integrin dependent adhesion in RIAM silenced cells was shown to correlate with decreased activation of

Erk1/2 and PI3K, two central molecules controlling cell growth and survival (Hernandez-Varas et al., 2011). These cells exhibited inhibition of anchorage-independent growth, as well as impaired tumor growth and delayed metastasis; suggesting that RIAM mediated activation of Erk1/2 and PI3K may contribute to cellular proliferation (Hernandez-Varas et al., 2011, Colo et al., 2012b). Lpd, on the other hand, has been implicated in mammalian cell proliferation through regulation of SRF. Lpd is thought to trigger an increase in F-actin levels, releasing the cofactor MAL from its association with G-actin, and allowing its transport to the nucleus where it acts as a cofactor for SRF mediated growth related gene expression (Pinheiro et al., 2011, Colo et al., 2012b, Lyulcheva et al., 2008). Indeed, the ability of Lpd to regulate SRF activity has already been implicated in directing pyramidal neurons to select a radial migration pathway along glia rather than a tangential migration mode (Pinheiro et al., 2011).

Mig-10, the only *C. elegans* MRL homologue, possesses the characteristic central RA and PH domains, C-terminal proline rich regions and N-terminal coiled-coil motif common in all MRL proteins (Manser and Wood, 1990, Colo et al., 2012b). It shares significant homology with Lpd and is required for successful long-range antero-posterior migration of embryonic CANs (canal-associated neurons), ALMs (anterior lateral microtubule cells) and HSNs (hermaphrodite-specific neurons), as well as efficient development of excretory canals used in osmoregulation; processes requiring well controlled directional migration (Colo et al., 2012b, Manser et al., 1997, Manser and Wood, 1990, Chang et al., 2006). However, unlike the other members of the MRL family, Mig-10 has not yet been found to play a role in cellular growth and proliferation (Colo et al., 2012b).

MIG-10, much like Lpd, contains consensus EVH1 binding sites thought to mediate interactions with members of the Ena/VASP family to assist in their recruitment to the leading edge, enabling cytoskeletal changes and enhancement of migration (Holt and Daly, 2005, Drees and Gertler, 2008). Indeed, disrupted embryonic cell migration responses instigated by *mig-10* mutants resemble those of mutants for *unc-34*, the *C. elegans* Ena/VASP ortholog (Forrester and Garriga, 1997). Moreover, during neuronal development, MIG-10 and UNC-34 cooperate to guide axons toward UNC-6 (Netrin) and away from SLT-1 (Slit), with UNC-34 required for the formation of filopodia and MIG-10 enhancing their numbers (Chang et al., 2006, Quinn et al., 2006).

However, double mutants of *unc-34* and *mig-10* cause much more severe defects than either mutant separately, while in *unc-34* mutants alone, developing axons that lack filopodia are still guided to UNC-6 through MIG-10 mediated lamellipodial growth; suggesting that the two proteins may act in overlapping functional pathways (Chang et al., 2006). In particular, it is thought that MIG-10 is likely to associate with actin polymerization machinery via additional partner molecules, although interactions with UNC-34 through a common pathway are still probable (McShea et al., 2013, Chang et al., 2006).

MIG-10 has also been found to localise asymmetrically in response to external directional signals such as UNC-6 or SLT-1, enabling control over the directionality of cellular migration (Quinn et al., 2006). Experiments showed that overexpression of MIG-10 in the absence of these guidance cues led to the development of a multipolar phenotype with undirected outgrowths, while the addition of UNC-6 or SLT-1 resulted in the monopolar formation of a single overgrowth with enhanced guidance (Quinn et al., 2006). It has been proposed that in the absence of UNC-6, its receptor UNC-40 (DCC) is distributed uniformly, however, when a UNC-6 gradient is present, UNC-40 becomes polarized to the side of the growth cone closest to the source of UNC-6, leading to localised $PI(3,4)P_2$ production by AGE-1 (PI3K) and activation of Rac (Adler et al., 2006, Quinn et al., 2008). As with Lpd, localisation of MIG-10 is thought to be mediated by upstream Ras superfamily controlled interactions with $PI(3,4)P_2$ via the PH domain (Krause et al., 2004, Quinn et al., 2008). Indeed, a fragment of MIG-10 containing only the RA and PH domains bound specifically to the activated Rho GTPase CED-10 (Rac1); however, mutation of *ced-10*, or either *age-1* or *daf-18* (PTEN) which have also been implicated in regulating $PI(3,4)P_2$ turnover, disrupted correct MIG-10 localisation in response to UNC-6 (Quinn and Wadsworth, 2008, Quinn et al., 2008, Adler et al., 2006). Consequently, it is thought MIG-10 binds to the UNC-40 co-localised $PI(3,4)P_2$ and activated Rac, enabling asymmetric actin-based protrusive activity and control over the directionality of migration (Adler et al., 2006, Quinn et al., 2008). Recently, MIG-10 has been shown to localise to presynaptic regions in response to this pathway, mediating synaptic vesicle clustering and F-actin organisation (Stavoe and Colon-Ramos, 2012). This involvement in vesicle trafficking may be related to MIG-10's function in excretory cell outgrowth, as formation of the lumen of these tubule shaped single

cells, fundamental to the development and function of many tissues and organs in metazoan organisms, requires localisation and fusion of vesicles (Buechner, 2002).

As described previously, the Arp2/3 complex is responsible for nucleating branched actin filaments, and plays a crucial role in regulating lamellipodial dynamics (Goley and Welch, 2006). WAVE (WASP family Verprolin-homologous protein) is a WASP family protein involved in activating the Arp2/3 complex downstream of Rac and is constitutively associated with the WRC (WAVE regulatory complex) proteins ABI-1 (Abi-1), GEX-2 (Sra-1), GEX-3 (Nap-1), and HSPC300 (Miki et al., 1998, Eden et al., 2002, Stovold et al., 2005). The WRC inhibits WAVE activity in the absence of migratory signalling events and is critical for controlling WAVE localisation and stability (Chen et al., 2010, Ismail et al., 2009, Kunda et al., 2003). Recently, it was demonstrated that MIG-10 directly interacts with the SH3 domain of ABI-1 and that *abi-1* mutant or *abi-1 RNAi* treated animals show similar defects in ALM migration and excretory cell canal outgrowth as those with mutant *mig-10*; indicating that MIG-10 and ABI-1 are involved in a common pathway (McShea et al., 2013). Additionally, in *C. elegans* ABI-1 and ABL-1 (Abl) have been shown to interact *in vitro* and have opposing functions in the regulation of cell engulfment of apoptotic cells (Hurwitz et al., 2009). In mammals, Abi-1 is a downstream target and modulator of Abl activity, with their interaction shown to promote phosphorylation of the Ena/VASP family member Mena, although it remains unclear how this influences Enabled activity (Shi et al., 1995, Michael et al., 2010, Tani et al., 2003). Lpd is also a target of Abl, however a role for Abi-1 in this interaction has not been described (Michael et al., 2010). It is therefore not beyond reason to suggest that MIG-10 may interact with ABL-1 to mediate ABI-1 regulation of downstream ARP2/3 actin filament branching.

The *Drosophila* ortholog Pico (CG11940) is the most recently characterised MRL family member and, akin to Mig-10, comprises the only MRL member in *Drosophila* and shares considerable homology with Lpd. Two transcripts generated from alternative transcription start sites were identified, pico and pico-L; with Pico-L encoding an 1159 amino acid protein identical to the shorter form, except for the presence of additional 128 N-terminal amino acids (Lyulcheva et al., 2008). Unsurprisingly, Pico contains the distinctive RA and PH domains, as well as the N-

terminal coiled-coil motif and C-terminal proline-rich Ena/VASP binding sites characteristic of all MRL members (Lyulcheva et al., 2008).

Studies in *pico* mutant larvae revealed a dramatic reduction in size and early death, suggesting that Pico is required for tissue and organismal growth, as well as viability. In addition, RNAi mediated silencing of *pico* in *Drosophila* wing discs led to a significant reduction in wing area, due primarily to a reduction in cell proliferation and size rather than induced apoptosis (Lyulcheva et al., 2008). Further investigations demonstrated that homozygous *pico* mutant clones generated in *Drosophila* imaginal discs, exhibited severe growth and proliferation defects and were gradually extruded from the otherwise wild type tissue (Lyulcheva et al., 2008). Conversely, overexpression of Pico was shown to induce hyperplastic growth at both the tissue and whole organism level, owing to a co-ordinated increase in both cell number and cell size (Lyulcheva et al., 2008).

It has been reported that Pico's ability to regulate cell growth and proliferation is dependent on EGFR activity. Indeed, ectopic expression of a dominant negative form of *EGFR* ($EGFR^{DN}$), thought to interfere with signaling by forming inactive heterodimers with the wild type receptors, resulted in dramatically reduced, narrow wings (Kashles et al., 1991, Guichard et al., 1999). Wings coexpressing Pico and $EGFR^{DN}$ resembled those of $EGFR^{DN}$ alone, while RNAi mediated silencing of *pico* suppressed the overgrowth effects of EGFR overexpression (Lyulcheva et al., 2008). Consequently, it is thought that EGFR may activate Ras-like GTPases, which in turn binds to and activates the MRL proteins (Rodriguez-Viciana et al., 2004).

The Pico RA-PH region was reported to be capable of binding constitutively active forms of Ras and Rap1 in yeast two hybrid studies, suggesting that Pico may constitute a Ras or Rap1 GTPase effector downstream of EGFR. Furthermore, Pico interacts with the EVH1 domain of the *Drosophila* Ena/VASP homologue Ena (Enabled), and influences actin dynamics in an Ena dependent manner (Lyulcheva et al., 2008). Overexpression of Pico alone promoted F-actin formation in imaginal wing discs, while *pico RNAi* reduced F-actin levels; although total actin content was consistent throughout indicating that Pico regulates the ratio of G:F actin (Lyulcheva et al., 2008). Homozygous *ena* mutants dominantly suppressed Pico-mediated F-actin

accumulation and wing growth, suggesting that Ena is limiting for Pico function. Wings expressing Ena with *pico RNAi* resembled those with *pico RNAi* alone while co-overexpression of Ena and Pico phenotypically resembled the effect of overexpressing either gene alone, indicating that both function in the same pathway (Lyulcheva et al., 2008).

As with Lpd, Pico has been implicated in mediating cellular growth and proliferation through regulation of MAL/SRF dynamics (Lyulcheva et al., 2008). Genetic analysis has revealed that MAL/SRF levels are important for pico-mediated regulation of tissue growth. Co-overexpression of MAL and Pico in wings phenotypically resembled the effect of overexpressing MAL alone, while MAL-mediated overgrowth could not be suppressed by *pico RNAi*; implying MAL acts downstream of Pico. Furthermore, Pico-mediated wing overgrowth was dominantly suppressed by a hypomorphic mutation in *bs* (blistered), the *Drosophila* SRF homologue (Lyulcheva et al., 2008). It is thought that by increasing F actin levels, Pico promotes the release of the SRF cofactor MAL from its interaction with G-actin. MAL then translocates to the nucleus where it associates with, and activates SRF, leading to increased transcription of growth related genes (Pinheiro et al., 2011, Colo et al., 2012b, Lyulcheva et al., 2008). Conversely, a recent report has challenged this finding by demonstrating that *pico RNAi* leads to a crumpled wing phenotype rather than a clean tissue undergrowth phenotype, suggesting that Pico is required for correct wing morphogenesis (Thompson, 2010). However, this report neglected to highlight the predicted off-target effects of commercially available *Pico RNAi* strains potentially used to generate this contradictory data, despite the Lyulcheva *et al.* 2008 paper employing a customised strain with no anticipated erroneous targeting outcomes.

1.4. Using *Drosophila melanogaster* as a model for growth and migration

While studies using cultured cell lines have significantly improved our understanding of cellular migration and growth, it is not possible to effectively replicate the full complexity of these processes within this system alone. One of the principal limitations is the lack of a natural cell microenvironment, although cultured cells also often exhibit changes to their normal morphology, function and gene expression. Indeed, various studies have served to highlight the importance of interactions between cells and their surrounding tissues on coordinated cell growth and migration; a process that cannot be reproduced *in vitro* (Bissell and Radisky, 2001). Consequently, *in vivo* models have been utilised to complement and verify the research conducted with cultured cells.

Experiments in mice have contributed extensively to our understanding of cellular migration and proliferation within the context of the whole organism. Indeed, genetically engineered mice with gain-of-function mutations in oncogenes, and loss-of-function mutations in tumour-suppressor genes, have enabled the functionality of a range of proteins involved in growth and migration to be extensively characterised (Singh and Johnson, 2006, Van Dyke and Jacks, 2002). However, the genetic alterations required to investigate how these multiple proteins operate remain exceptionally difficult and time-consuming to generate (Brumby and Richardson, 2005). Analysis within the model system *C. elegans* has also provided a wealth of insight into pathways related to growth and migration. This is in part due to the successful work mapping the developmental fate of every single somatic cell, although their optical transparency and ease of gene overexpression and RNAi mediated silencing have also contributed (Johnson, 2003). Nonetheless, *C. elegans* is evolutionarily far from humans, with many physiologically important systems absent in the nematode and approximately 35% of genes possessing human homologues (Johnson, 2003).

Drosophila melanogaster, represents a simple model system in which cellular growth and migration can be analysed *in vivo*. *Drosophila* has been extensively used as a model organism for over a century, due in part to the ease with which stocks can be reared in the laboratory, its short generation time and the abundance of powerful genetic techniques that have been developed

within the system (Matthews et al., 2005, St Johnston, 2002). Furthermore, despite assumptions indicating that humans and flies diverged from one another over 700 million years ago, a significant number of biological and developmental processes have been shown to be conserved between the two organisms; with about 75% of known human disease genes having a recognizable match in the genetic code of fruit flies, and over 50% of fly protein sequences possessing mammalian analogues (Reiter et al., 2001). Moreover, many of the genes known to influence cellular growth and migration in mammals possess homologous genes in *Drosophila* which have been shown to produce similar phenotypes and act in similar signalling pathways as their human counterparts. It is for these reasons that *Drosophila melanogaster* has become an important model system for investigating cellular growth and migration.

1.4.1. Genetic techniques available in Drosophila

As mentioned previously, an assortment of powerful genetic tools have been developed in the *Drosophila* system, allowing a wide variety of *in vivo* experiments to be performed. Large scale forward genetic screens can be carried out to identify genes involved in the regulation of specific biological processes, such as development, growth, or migration. Multiple independent gene mutations can be generated within the *Drosophila* genome through either chemical mutagenesis following exposure to mutagens such as EMS (ethyl methanesulfonate), or transposable element insertion using *P*-elements (St Johnston, 2002, Adams and Sekelsky, 2002). This allows a large number of genes to be screened for a specific phenotype of interest, however, genes with redundant functions often fail to produce a visible phenotype when mutated (St Johnston, 2002, Brumby and Richardson, 2005).

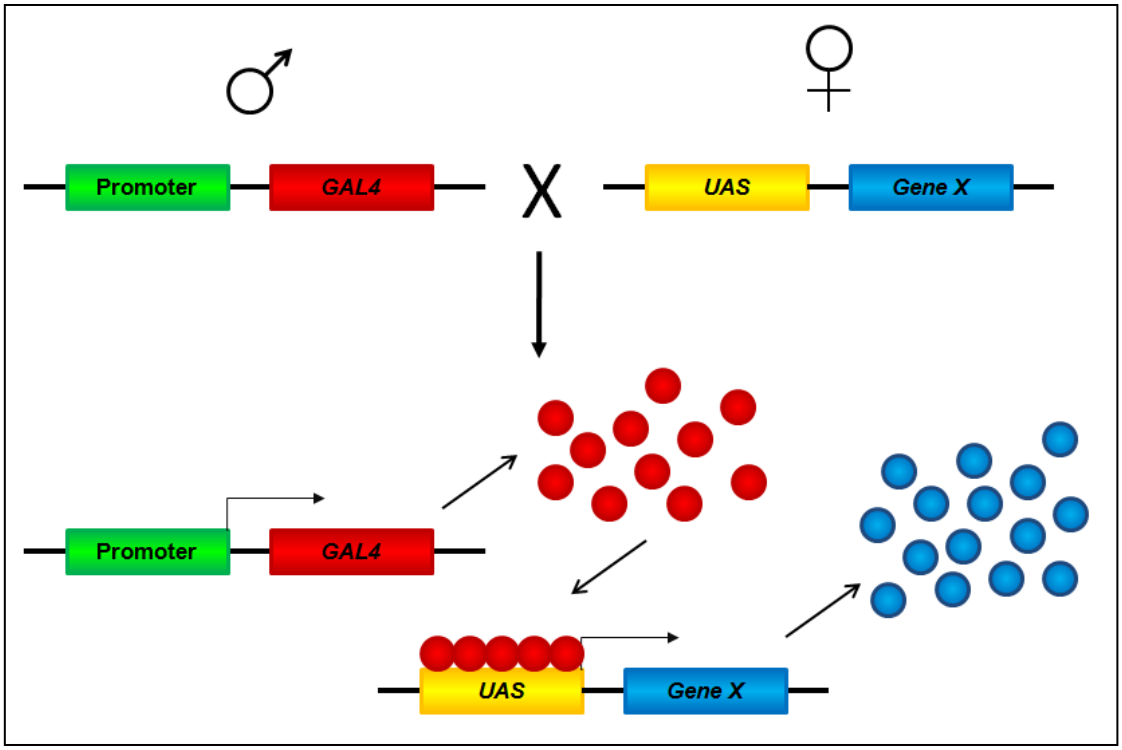

Figure 1.4.1. The *Gal4-UAS* bipartite expression system. *GAL4* gene expression is controlled by nearby genetic enhancers. A range of *GAL4* enhancer lines are available which express the transcription activator in tissue- and temporal-specific patterns. The GAL4 protein binds to any *UAS* sites present in the *Drosophila* genome and any gene that lies immediately downstream of the activating sequence will be expressed in the same spatial and temporal pattern as the *GAL4* gene (Duffy, 2002, Adams and Sekelsky, 2002, St Johnston, 2002).

This issue can be circumvented by performing mis-expression screens that exploit the yeast *GAL4-UAS* bipartite expression system to induce tissue specific ectopic gene expression (St Johnston, 2002, Adams and Sekelsky, 2002). In brief, *P*-elements carrying the yeast upstream activating sequence (*UAS*) element and a gene of interest are initially inserted into the *Drosophila* germline. Progeny that have the *UAS* construct incorporated into their genome are subsequently crossed to flies which, under the control of an endogenous promoter, express the yeast transcriptional activator *GAL4* in a defined spatial and temporal pattern. Once expressed, GAL4 binds to the *UAS* site and enables expression of any gene that lies immediately downstream of the activating sequence in the same tissue/temporal specific pattern (Figure 1.4.1)

(Duffy, 2002, Adams and Sekelsky, 2002, St Johnston, 2002). It is also possible to knockdown expression of genes by using the *GAL4-UAS* system to express double-stranded hairpin RNA resulting in sequence-specific post-translational silencing of the targeted gene through RNAi (Duffy, 2002). This allows a number of genes of interest to be overexpressed or silenced in relevant specific tissues, permitting easy screening for phenotypic changes. Any genes producing a phenotype of interest can then be used to identify further genes acting in the same pathway. This is achieved by analysing the ability of other genes to enhance or suppress the original phenotype (St Johnston, 2002, Adams and Sekelsky, 2002).

Once genes regulating a biological process of interest have been identified, further analysis using similar techniques can be performed to characterise the proteins they encode. For example, overexpression or knockdown studies can be carried out using the *GAL4-UAS* system to examine the effects of ectopic protein expression within a range of different tissues (Brand and Perrimon, 1993, Duffy, 2002). Similarly, known homologues of the genes of interest can be ectopically expressed to determine if they can produce similar phenotypes. Lastly, modified proteins produced by *in vitro* genetic alterations can be expressed, enabling examination of the various binding domains and post translational modification sites' responsibility in correct protein function.

In addition to whole tissue or organism expression analysis, techniques have been developed that allow small areas of cells containing genetic alterations to be produced in a wild type background. This mosaic patterning is created using the FLP recombinase – *FLP recombinase target* (FLP/*FRT*) system, and can be exploited to allow both mis-expression and homozygous mutant clones (Golic, 1991). Briefly, tissue or developmental specific expression of the yeast FLP recombinase drives mitotic recombination between two *FRT* sites present on homologous chromosome arms. If one chromosome arm contains a mutant allele of the gene of interest, clones of homozygous mutant cells can be produced (Figure 1.4.2.a) (Theodosiou and Xu, 1998). On the other hand, mis-expression clones are generated by coupling the FLP/*FRT* recombination system with the *UAS-GAL4* system. In this instance, induction of FLP recombinase induces recombination between two *FRT* sites flanking a reporter/silencer cassette. The excision of this cassette brings the *GAL4* gene *in trans* with a constitutive promoter enabling expression of

GAL4, which in turn drives the expression of any *UAS*-linked genes (Figure 1.4.2.b) (Theodosiou and Xu, 1998).

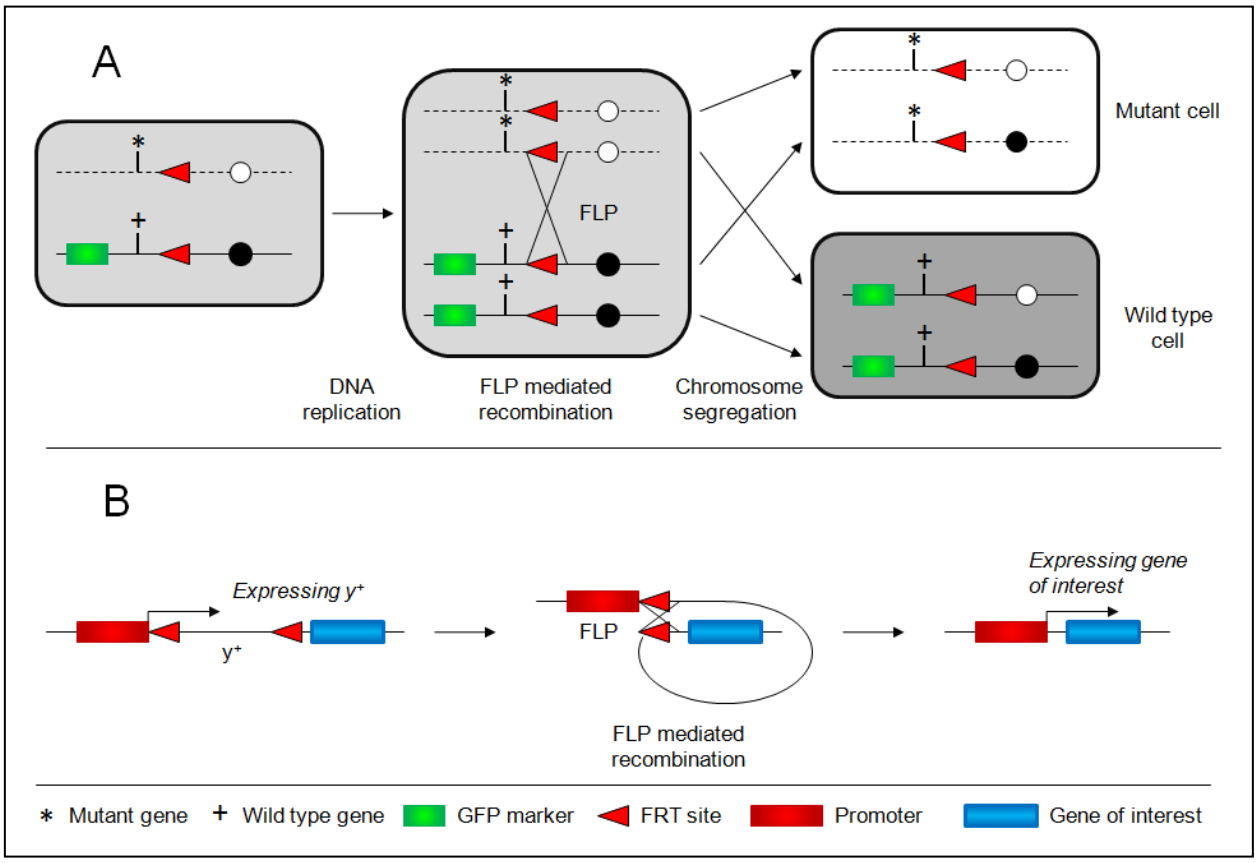

Figure 1.4.2. Generating mosaic clones using FLP/*FRT*-mediated mitotic recombination. (a) Expression of the FLP enzyme can induce recombination between *FRT* sites on homologous chromosomes, enabling daughter cells homozygous for a mutant allele to be generated. (b) Conversely, activation of FLP can initiate recombination between two *FRT* sites flanking a reporter/silencer cassette leading to its excision. This brings the *GAL4* gene *in trans* with a constitutive promoter enabling expression of *GAL4*, and in turn *UAS*-linked genes (Theodosiou and Xu, 1998).

1.5. Research Aims

The overarching aim of the research presented in this report was to elucidate the molecular mechanisms by which the *Drosophila* MRL homologue Pico functions to promote tissue overgrowth and identify the pathways involved in the regulation of its function. Due to the notable homology between the MRL proteins in flies and higher eukaryotes, it was anticipated that any insights obtained would be of use in guiding future studies within more complex systems, such as mammals. As a first step towards understanding Pico's role as an adapter protein and the potential mechanisms involved in its regulation, bioinformatic software was utilised to identify novel binding motifs and characterise the key functional domains present within MRL proteins. The findings from this work was then used in the development of site-directed *pico* mutants affecting motifs deemed fundamental to Pico's role in the hope of disrupting or altering their function. The ability of wild type or mutant Pico variants to interact with a selection of actin modifying and regulatory proteins then was assessed through co-immunoprecipitation assays. Due to the ectopic nature of these experiments, additional investigations were also carried out to confirm whether endogenous Pico was expressed within the same tissues as the associated proteins, and therefore have the potential to naturally come into contact *in vivo*. Lastly, as a means of identifying novel interaction partners not previously described in the literature, mass spectrometry was also employed on Pico pulldowns.

The next objective was to ascertain the subcellular localisation of Pico and determine if any of Pico's interactions contributed to its positioning. This was achieved by analysing the location of fluorescently tagged Pico wild type and mutant constructs within *Drosophila* cells spreading across a substrate. Co-localisation studies were also performed via immunostaining to visualise the endogenous proteins.

The final aim of this project was to determine the ability of *pico* mutants to induce overgrowth of the developing *Drosophila* wing. These data were collated with findings from interaction and localisation studies to identify putative roles for the domains of Pico investigated in this thesis. This subsequently enabled a preliminary model for the regulation of Pico by a phosphorylation cascade involving MAPK and PP1 to be proposed.

2. Materials and methods

2.1. Commonly used media and solutions

LB (Lysogeny broth) Media:

LB medium required for growth of bacterial strains was composed of 1.0% Tryptone, 0.5% Bacto-yeast Extract, and 1.0% NaCl dissolved in RO water with a pH of 7.0. The resultant solution was autoclaved before use.

LB Agar:

LB agar required for growth of bacterial strains on solid plates was comprised of 1.0% Tryptone, 0.5% Bacto-yeast Extract, 1.0% NaCl, and 1.6% agar dissolved in RO water with a pH of 7.0. The mixture was autoclaved and left to cool to 55°C before an appropriate antibiotic was added and the mixture poured into plates to set.

SOC (Super Optimal Broth) media:

SOC media is a nutrient-rich bacterial broth enabling heightened transformation efficiencies of plasmids. It was comprised of 2.0% Tryptone, 0.5% Bacto-yeast Extract, 0.05% NaCl, and 2.5 mM KCl dissolved in RO water and possessing a pH of 7.0. The solution was autoclaved before the addition of 1 mM $MgCl_2$ and 20mM glucose.

Complete S2 Media:

The complete medium required for S2 cells is Schneider's *Drosophila* Medium (Sigma) modified with 10% (v/v) heat-inactivated Foetal Calf Serum (FCS) (Sigma) and Penicillin-Streptomycin (Invitrogen) to a final concentration of 50 units Penicillin G and 50 µg Streptomycin sulphate per millilitre of medium.

Kinase Buffer:

Kinase buffer was used to assay protein kinase activity and contains 50 mM Tris-HCl, 100 µM ATP, 10 mM $MgCl_2$, 1 mM EGTA (Ethylene Glycol Tetraacetic Acid), 2 mM DTT (Dithiothreitol), and 0.01% Brij 35.

TE Buffer:

TE buffer was used to solubilise DNA or RNA, while protecting it from degradation and contains 10 mM Tris-Cl pH 7.5 and 1 mM EDTA (Ethylenediaminetetraacetic acid).

RIPA (Radio-Immunoprecipitation Assay) Buffer:

RIPA buffer enabled efficient cell lysis and protein solubilisation while avoiding protein degradation and interference with the proteins immunoreactivity and biological activity. It was composed of 50 mM Tris (pH 7 - 8), 150 mM NaCl, 0.1% SDS (Sodium Dodecyl Sulfate), 0.5% sodium deoxycholate, and 1% Triton X 100.

ChromoTek lysis buffer:

ChromoTek lysis buffer has been optimised by the manufacturer for GFP-Trap co-immunoprecipitation and enables efficient cell lysis and protein solubilisation while avoiding protein degradation and interference with the proteins immunoreactivity and biological activity. It contains 10 mM Tris/Cl pH 7.5, 150 mM NaCl, 0.5 mM EDTA, and 0.5% NP-40.

2x SDS-Sample Buffer:

2x SDS-Sample buffer was used for preparation and loading of protein samples into an SDS-polyacrylamide gel for SDS-PAGE and Western blotting. It was composed of 50 mM Tris-Cl pH6.8, 100 mM dithiothreitol, 2% SDS, 0.1% bromophenol blue, and 10% glycerol.

1x SDS-PAGE Running Buffer:

1x SDS-PAGE running buffer enables protein separation by SDS-polyacrylamide gel electrophoresis to occur and was comprised of 25 mM Tris, 250 mM glycine pH 8.3, and 0.1% SDS.

Coomassie Staining Solution:

Coomassie stain is used to visualise proteins within polyacrylamide gels and is made up of 0.1% Coomassie G-250, 10% acetic acid, and 40% methanol.

Coomassie Destaining Solution:

Coomassie destain was used to enhance visualisation and clarity of coomassie stained proteins within polyacrylamide gels and was composed of 20% methanol and 10% acetic acid.

Tris-glycine Transfer Buffer:

Tris-glycine transfer buffer allows protein transfer from SDS-polyacrylamide gels to a solid phase support, such as nitrocellulose or PVDF membranes. The solution was comprised of 25 mM Tris, 193 mM glycine, and 20% methanol.

PBS (Phosphate Buffered Saline)/PBST:

PBS is a buffer solution designed to replicate the osmolarity and ion concentrations of normal cells and was composed of 137 mM NaCl, 2.7 mM KCl, 8 mM Na_2HPO_4, and 1.46 mM KH_2PO_4. PBST is made up of 1 x PBS with 0.1% Tween-20.

2.2. Commonly used strains

2.2.1. Bacterial lines utilised

One Shot® Top 10 chemically competent E. coli (Invitrogen)

F- *mcr*A Δ(*mrr-hsd*RMS-*mcr*BC) φ80*lacZ*ΔM15 Δ*lac*X74 *rec*A1 *ara*D139 Δ(*ara-leu*) 7697 *gal*U *gal*K *rps*L (StrR) *end*A1 *nup*G

One Shot® ccdB Survival™ 2 T1R competent cells (Invitrogen)

F- *mcr*A Δ(*mrr-hsd*RMS-*mcr*BC) Φ80*lacZ*ΔM15 Δ*lac*X74 *rec*A1 *ara*Δ139 Δ(*ara-leu*) 7697 *gal*U *gal*K *rps*L (Str^R) *end*A1 *nup*G *fhu*A::*IS2*

Growth and storage of bacterial cells were as described in Sambrook (2001) unless stated otherwise. Frozen stocks were generated by adding 50% filter-sterilised glycerol to cell cultures to give a final concentration of 15% and stored at -80ºC. Ampicillin and kanamycin were prepared as 100 mg/ml and 50 mg/ml filter-sterilised stock solutions respectively and stored at -20ºC. Ampicillin was used at a concentration of 100 µg/ml and kanamycin used at 50 µg/ml.

2.2.2. Cell lines used

Drosophila Schneider (S2) Cells

Drosophila Schneider (S2) cells are a cell line derived from a primary culture of late stage (20-24 hours old) *Drosophila melanogaster* embryos and formed a loose, semi-adherent monolayer in tissue culture flasks (Schneider, 1972).

Drosophila Schneider Receptor + (S2R+) Cells

Drosophila Schneider Receptor + (S2R+) cells are a line, again derived from the Schneider lab, which possess the wingless receptors Dfrizzled-1 and Dfrizzled-2 and formed a highly adherent monolayer in tissue culture flasks (Yanagawa et al., 1998).

The cells were initiated, maintained and stored using the following procedures:

Initiating cultures from frozen stocks:

To initiate cultures from a frozen stock, cells were quickly thawed at 30ºC and transferred to a 25cm^2 flask containing 5 ml of room temperature Complete S2 Medium. The cells were then incubated at 28ºC for 30 minutes before being resuspended and centrifuged at 1000 x g for 5 minutes. The medium was decanted to remove DMSO, and the cells plated in 5 ml fresh Complete S2 Medium in a new 25cm^2 flask. The cells were incubated at 28ºC for 3-4 days until they reached a density of 6-20 x 10^6 cells/ml.

Passaging S2 cells:

When cells reached an optimum density of 6–20 x 10^6 cells/ml, the conditioned medium was pipetted up and down several times to break up clumps of cells and wash the surface of the flask to remove adherent cells. The cells were split at a 1:2 to 1:5 dilution into new culture vessels and fresh Complete S2 Medium added to create a final density of 2-4 x 10^6 cells/ml. The cells were then incubated at 28ºC until an optimum density was reached.

Freezing S2 cells:

To create a frozen stock, cells were grown to a density of 1-2 x 10^7 cells/ml and pelleted by centrifuging at 1000 x g for 5 minutes. The cells were then washed in 10 ml PBS and pelleted again before being resuspended at a density of 1.1 x 10^7 cells/ml in Freezing Medium (45% conditioned Complete S2 Medium, 45% fresh Complete S2 Medium, and 10% DMSO). 1 ml of the cell suspension was aliquoted per vial and the cells were frozen in a control rate freezer to -80ºC for 24 hours before being transferred to liquid nitrogen for long term storage.

2.2.3. Drosophila stocks employed

act5C-GAL4

w; 13B/CyO; *act5C-GAL4*/MKRS

Expresses GAL4 ubiquitously in the pattern of the *Act5C* gene.

da-GAL4

w; 13B/CyO; *da-GAL4*/MKRS

Ubiquitous expression of GAL4 under the control of *daughterless*.

enGAL4

w; *enGAL4*/CyO

Expresses GAL4 in the posterior compartment of embryonic segments in the pattern of the *engrailed* gene.

hsGAL4

w; *hsp70-GAL4*/ *hsp70-GAL4*

Heat shock inducible ubiquitous expression of GAL4.

MS1096-GAL4

MS1096-Gal4 on X

Expresses GAL4 across the wing pouch in early third instar larval wing discs and predominantly in the in dorsal half of the wing disc in mid-late third instar larvae.

Fly stocks were kept at 18ºC or 25ºC on standard yeast/dextrose medium (1% (w/v) agar, 7.3% (w/v) dextrose, 5% (w/v) yeast, 6.7% (w/v) organic wholemeal flour, 0.25% (v/v) nipagin, 0.3% (v/v) propionic acid) in 30/50ml vials or 250ml bottles as appropriate. Flies were anaesthetised with CO_2 and examined using Nikon SMZ-645 or Nikon SMZ-800 microscopes and Photonics 200 lightsources using standard fly-pushing techniques (Roberts, 1998, Greenspan, 2004). All fly stocks described were obtained from the Bloomington *Drosophila* Stock Centre (http://flystocks.bio.indiana.edu) unless stated otherwise.

2.3. Bioinformatic analysis

2.3.1. Identification and alignment of MRL family proteins

BLAST (Basic Local Alignment Search Tool) analysis was performed on human Lpd, human RIAM, *C. elegans* MIG-10, and *Drosophila* Pico protein sequences using the NCBI (http://blast.ncbi.nlm.nih.gov/), Uniprot (http://www.uniprot.org/), and Ensemble (http://www.ensembl.org/) databases to identify corresponding homologues within a range of apposite species. T-Coffee accurate, an enhanced version of the multiple sequence alignment T-Coffee package incorporating additional 3D structural and homology extension algorithms, was employed to align the MRL sequences discovered during the BLAST searches (Notredame et al., 2000, Armougom et al., 2006, Di Tommaso et al., 2011). As a means of manually assessing the accuracy of the alignments, BOXshade 3.21 (http://www.ch.embnet.org/software/BOX_form.html) and Ali2D 2.17 (http://toolkit.tuebingen.mpg.de/ali2d) were used to assess respective sequence and secondary structure homology between the aligned sequences, allowing adjustments to be made when necessary.

2.3.2. Phylogenetic analysis

MRL alignments from T-Coffee accurate were assessed for pairwise distances using Tree-Puzzle 5.2 (Schmidt et al., 2002) and the outcomes analysed further with the distance based phylogeny reconstruction algorithm FastME 2.07 (Desper and Gascuel, 2002). The highly accurate PHYML 3.0 algorithm (Guindon et al., 2010), commonly used to estimate large phylogenies by maximum likelihood, was then utilised to enhance precision before the resulting tree was visualised by FigTree 1.4 (http://tree.bio.ed.ac.uk/software/figtree/).

2.3.3. Domain conservation/sequence analysis

Individual T-Coffee accurate alignments were generated for the single orthologue, Lpd, and RIAM groupings alone, in addition to the complete MRL alignments from Chapter 2.3.1. These alignments were analysed by Plotcon (EMBOSS) to ascertain the extent of conservation between

the sequences using the EBLOSUM62 scoring matrix and a window size of 16. Those areas displaying a high degree of sequence similarity were then assessed using the ELM (Eukaryotic Linear Motif) resource which, in addition to utilising the more standard SMART/Pfam, GlobPlot, and IUPred searches, identifies short linear motifs within unstructured protein regions (Dinkel et al., 2012, Davey et al., 2012).

2.4. Phosphorylation site analysis

2.4.1. Peptide array design and production

A peptide array was designed consisting of diminutive 15mer peptides representing every serine, threonine and tyrosine residue contained within Pico. The residue to be assessed was positioned in the centre of each short peptide to increase the opportunity for prospective target sequences flanking either side to be recognised, while substituting the amino acid with a suitable alanine or phenylalanine acted as a negative control. As some peptide regions contained more than one potentially phosphorylatable residue, control peptides were also included whereby serine, threonine or tyrosine residues not under investigation were replaced with an appropriate alanine or phenylalanine. A further set of peptides containing specific consensus target sequences for a variety of MAPKs was included to act as a positive control. The complete list of 598 peptide sequences proposed for use in this study can be found in Appendix 2. The peptide array was synthesised using the SPOT-synthesis technique (Frank, 2002) by the Peptide Synthesis Core Technology Facility (CRUK London Research Institute).

2.4.2. Kinase phosphorylation analysis

The peptide array was thoroughly moistened in ethanol before being incubated overnight at room temperature in Kinase buffer (New England Biolabs) supplemented with 0.2 mg/ml BSA (Bovine Serum Albumin) (Sigma) and 100 mM NaCl, but lacking ATP. The membrane was then incubated in 15 ml blocking solution consisting of 1x Kinase Buffer with 1 mg/ml BSA (New England Biolabs) and 100 mM NaCl at 30˚C for 45 minutes after which the array was exposed to 13 ml Kinase buffer (New England Biolabs) supplemented with 0.2 mg/mL BSA, 120 units of an

appropriate kinase, and 24μCi γ-32P-ATP for 2 hours at 30˚C. Ten 15 minute washes in 1 M NaCl, three 5 minute washes in H_3PO_4, three 5 minute washes in distilled water, and two 2 minute washes in 100% ethanol were performed. The membrane was allowed to air dry before being wrapped in Saran wrap, placed on a phosphor cassette overnight, and subjected to autoradiography analysis using a Storm 860 Phosphorimager (GE Healthcare).

2.4.3. Phosphatase analysis

The peptide array was thoroughly moistened in ethanol before being incubated overnight at room temperature in NEBuffer for PMP (Protein MetalloPhosphatases) (New England Biolabs). The membrane was then incubated in 15 ml PMP buffer (New England Biolabs) supplemented with 1 mM $MnCl_2$ and either 10 units of activated PP1 (New England Biolabs) or 2000 units of active λ Phosphatase (New England Biolabs) for 2 hours at 30˚C. Ten 15 minute washes in 1 M NaCl, three 5 minute washes in H_3PO_4, three 5 minute washes in distilled water, and two 2 minute washes in 100% ethanol were performed. The membrane was allowed to air dry before being wrapped in Saran wrap, placed on a phosphor cassette overnight, and subjected to autoradiography analysis using a Storm 860 Phosphorimager (GE Healthcare).

2.5. Polymerase Chain Reaction (PCR)

Synthetic oligonucleotides complementary to the ends of the nucleotide sequence were designed in the region to be amplified, while annealing temperatures were ascertained using the formula $T_A = (2 \times TA) + (4 \times GC)$. Repeated cycles of heating, primer hybridisation and DNA synthesis allow the nucleotide sequence flanked by the two oligonucleotides to be selectively amplified exponentially. All PCR reactions were performed using a Technie TC-512. The reaction mixes and typical cycling programs are given below:

Reaction mixes

Taq Polymerase (Qiagen) 20 μl reaction mix

10x reaction buffer - 2.0 μl; 100 mM dNTPs - 0.6 μl; Forward Primer - 1.0 μl; Reverse Primer - 1.0 μl; Template DNA – 10 pg – 200 ng; Taq Polymerase (5 units/μl) - 0.3 μl; ddH_2O to 20 μl.

Platinum® Pfx DNA Polymerase (invitrogen) 20 µl reaction mix

10x reaction buffer - 2.0 µl; 50 mM $MgSO_4$ – 0.4 µl; 100 mM dNTPs - 0.6 µl; Forward Primer - 1.0 µl; Reverse Primer - 1.0 µl; Template DNA – 10 pg – 200 ng; Pfx Polymerase (2.5 units/µl) - 0.3 µl; ddH_2O to 20 µl.

Typical Cycling Programs

Two-step Cycling:

94ºC for 2 min 30sec,
92ºC for 20 sec, ← x 35
68ºC for 1 min per kb*,
68ºC for 5 min
4 ºC forever

Three-step Cycling:

94ºC for 2 min 30sec,
92ºC for 20 sec, ← x 35
T_m-5ºC for 45 sec,
68ºC for 1 min per kb*,
68ºC for 5 min
4ºC forever

*Extension times were 1min/kb for Platinum® Pfx polymerase (Invitrogen) at 68°C and 15-30 sec/kb for Taq polymerase (Qiagen) at 72°C.

2.6. List of oligonucleotides

All oligonucleotides were designed according to general primer design guidelines (PremierBiosoft International) and synthesized by MWG Biotech. The lyophilised primers were diluted in TE buffer pH 8.0, to make 100 µM stocks and stored at -20 ºC. Dilutions of 10 µM and 3.2 µM were used for PCR and sequencing reactions respectively.

Primers for pico mutagenesis:

-A270K-fwd: 5’ - CCGCCTGCTGAAGGACAAGAACCACGTGCAGATGCAGAG - 3’

-A270K-rev: 5’ - GGTTCTTGTCCTTCAGCAGGCGGGTCACGTGTCCGC - 3’
-K272A-fwd: 5’ - GCTGGCCGACGCGAACCACGTGCAGATGCAG - 3’
-K272A-rev: 5’ - GCACGTGGTTCGCGTCGGCCAGCAGGCG - 3’

Primers for testing pico insertion:
-M13-fwd: 5’ - TTGTAAAACGACGGCCAGTC - 3’
-M13-rev: 5’ - TGCCAGGAAACAGCTATGAC - 3’
-Pico-fwd: 5’ - GTAGCTCCAGCGGCATCAGC - 3’
-Pico-rev: 5’ - CGGCGTAGTTCATGGCCAGC - 3’

Sequencing primers for pico constructs:
-Pico_Seq1: 5’ - GGCATGATGGTCCAACCGC - 3’
-Pico_Seq2: 5’ - GGGCTGCGGACACGTGACC - 3’
-Pico_Seq3: 5’ - CTGTTCCACGGCCACAACGTG - 3’
-Pico_Seq4: 5’ - ACGCCTTCGATAGCGAGTTC - 3’
-Pico_Seq5: 5’ - GCTGTCGCTGGCCTCCCTG - 3’
-Pico_Seq6: 5’ - TGAGCAGCCTGTCCAACGGC - 3’
-Pico_mut: 5’ - AACAGCTCCCACTACTACCG - 3’

2.7. Agarose gel electrophoresis

DNA molecules were separated by size using agarose gel electrophoresis. Agarose gels were prepared and run as described in Sambrook (2001). Ethidium bromide (Sigma) was added to the gel at a final concentration of 0.2-0.5 μg/ml. Samples were diluted with 1 x loading buffer (10 x agarose loading buffer, 30% (v/v) glycerol, 0.35% (v/v) bromophenol blue) before being loaded on the gel. The samples were electrophoresed in 1 x TAE at 100 volts for 30-45 minutes, using a GIBCO BRL electrophoresis power supply and Fisher Brand gel tank. SmartLadder I (Eurogentec), a molecular weight marker, was used to determine DNA concentration as well as fragment size. The DNA fragments were visualised using an ultraviolet light source (Syngene) and documented with a PULNiX TM-300 video camera system and Syngene UP-895MD video graphic printer.

2.8. Gel extraction

Desired DNA fragments were cut from the gel by scalpel blade and purified using the QIAquick Gel Extraction Kit (Qiagen) as per manufacturer's instructions. Briefly, agarose is dissolved to release the DNA, which is then bound to an anion-exchange membrane before the purified DNA fragment is eluted in an appropriate volume of TE buffer. Due to the nature of the protocol, DNA could only be semi-quantified by gel electrophoresis.

2.9. Restriction digestion

Restriction digests were performed using enzymes and compatible buffers (New England Biolabs) according to the manufacturer's guidelines. Typically, 20 µl reactions were carried out using 3 units of each enzyme and 0.1-2 µg of DNA. For double digests i.e. those containing two restriction endonucleases, buffers compatible with both enzymes were used. Reactions were typically incubated at 37ºC for 2 hours or overnight.

2.10. DNA ligation

Digested products were run on an appropriate percentage agarose gel and fragments extracted using the Gel extraction protocol (Chapter 2.8.). Complementary linear DNA fragments formed from digestion and extraction were ligated into circular plasmids using a T4 DNA ligase Kit (Roche). For ligation, two fragments totalling an approximate 3:1 molar ratio of insert:vector were used as per manufacturer's instructions. The following equation was used to calculate appropriate amounts of DNA to use for a 3:1 molecular ratio:

$$\frac{\text{ng of vector} \times \text{kb size of insert}}{\text{kb size of vector}} \times \text{insert : vector molar ratio} = \text{ng of insert}$$

Molecular ratios could be altered as needed depending on experimental success. One unit of T4 DNA ligase was incubated with a total of 100 ng of DNA in T4 reaction buffer (Roche). Reaction volumes were kept at 20 µl as per manufacturers guidelines. Reaction mixtures were

incubated at 16°C for 20 hours before 2-4µl of the ligation reaction was transformed into One Shot® Top 10 chemically competent *E. coli* (Invitrogen). Ligations were screened by PCR and restriction digestion before sequencing was carried out.

2.11. Gateway® LR Recombination Reaction

Gateway® LR reactions were performed to shuttle the RNAi resistant Pico wild type and mutant construct ORFs (open reading frames) from the pDONR™221 entry vector into the desired destination vectors pTVW (*UASt* promoter, N-terminal Venus tag), pAVW (act5c promoter, N-terminal Venus tag) (*Drosophila* Genomics Resource Center), and pMt-PtA (metallothionein promoter, N-terminal Protein A tag) (Paolo D'Avino-University of Cambridge). 50-150 ng of the entry clone containing the gene of interest was mixed with 150 ng of the destination vector and TE buffer pH 8.0, to give a final volume of 8 µl. The LR clonase II enzyme mix (Invitrogen) was thawed on ice for 2 minutes, vortexed briefly, then 2 µl of the enzyme mix was added to the reaction mix. Reactions were incubated at 25ºC for a minimum of 1 hour, although overnight incubation is recommended for large plasmids (over 10 kb). Following incubation, 1 µl of Proteinase K (Invitrogen) solution was added to the reaction mix and incubated at 37ºC for 10 minutes to stop the reaction. 5 µl of the reaction mix was then transformed into One Shot® Top10 Chemically Competent Cells (Invitrogen). The transformed cells were plated onto ampicillin-LB agar plates and incubated at 37ºC overnight. Plasmids were extracted from colonies and screened by restriction digestion.

2.12. Transformation of chemically competant cells

For each transformation one vial of One Shot® Top10 Chemically Competent Cells (Invitrogen) or One Shot® ccdB Survival™ 2 T1R competent cells (Invitrogen) was thawed on ice and 1-5 µl of the DNA (10 pg to 100 ng) added and mixed gently. The cells were incubated on ice for 30 minutes before being heat shocked at 42ºC for exactly 30 seconds. Following heat shock, the cells were placed on ice for two minutes and 250 µl of pre-warmed S.O.C Medium (Invitrogen) added to each vial. The vial(s) were then shaken horizontally at 225 rpm for 1 hour at 37ºC in a shaking incubator before each transformation reaction was spread on pre-warmed selective

plates. The plates were inverted and incubated overnight at 37ºC. The following day colonies were picked and isolated plasmids analysed by restriction digestion, PCR or sequencing.

2.13. DNA extraction

Small-scale plasmid purification (≤20 µg) was carried out using QIAprep Spin Miniprep Kits (Qiagen), while medium (≤100 µg) and large-scale (≤2.5 mg) plasmid purification was carried out using QIAfilter Plasmid Midi kits or Mega kits (Qiagen) respectively according to the manufacturer's instructions. Briefly, cells grown overnight in selective LB media were lysed under alkaline conditions and clear cell lysates were applied to columns containing a silica gel membrane capable of binding DNA, yet allowing contaminants to be washed away. DNA was eluted from the columns with an appropriate volume of Qiagen Elution Buffer (Qiagen). The concentration of DNA obtained was then measured using a NanoDrop.

2.14. DNA quantification

DNA concentrations were quantified by the Thermo Scientific NanoDrop™ 1000 Spectrophotometer. The NanoDrop uses a 1-2 µl sample held in place by surface tension of the liquid and measures absorbance of the sample over a 220nm-750nm spectrum, reporting DNA concentration and relative purity of the sample with 230/260 and 260/280 ratio measurements. The NanoDrop was able to measure samples up to 3700 µg/µl and so removed the need for serial dilution of DNA samples to ensure accurate measurement. DNA could also be semi-quantified by analysing the intensity of DNA run on an agarose gel compared to reference ladder of known concentration.

2.15. DNA sequencing

DNA sequencing was carried out by GATC, Germany (gmbH) (http://www. gatc-biotech.com/en). Enough DNA was provided for a total of 6 reactions at a concentration of 30-100 ng/µl in 20 µl of ultra pure ddH_2O. Sequencing primers were designed with a theoretical melting temperature of 60°C and a Guanine/Cytosine composition as close as possible to 50%.

Sequencing analysis was performed with MegAlign software (DNA Star) which aligned results to predicted sequences allowing comparative assessments to be made.

2.16. Insertion of constructs into flies

Transgenic flies expressing the previously described Venus tagged Pico constructs under the control of the upstream activator sequence (*UAS*) were generated through *P*-element mediated germline transformation by Genetic Services, Inc (Cambridge, MA, USA) (Rubin and Spradling, 1982, Sentry and Kaiser, 1992). The Pico constructs were injected into W^{1118} embryos along with the helper plasmid pUC*hs*Delta2-3, which provided a source of *P*-element transposase.

The progeny were screened for non-white eyes indicating that the constructs, which carried a *white*$^{+}$ minigene, had successfully been transformed into the germline cells. The chromosome harbouring each independent insert was determined by crossing individual transgene-carrying males to *w; Tft/CyO* and then crossing the progeny to *w; Tft/CyO; MKRS/TM6B.* Each insert was then balanced with an appropriate, dominantly marked, balancer chromosome (Greenspan, 2004). Verification and analysis of ectopic protein expression was carried out by visualisation of fluorescent Venus in larvae carrying the *engrailed-GAL4* driver and one copy of the transgene of interest.

2.17. Transfection of S2 and S2R+ cells

2.17.1. Transient transfection with Effectine

For transient transfection S2R+ cells were plated at 3.5 x 10^5 in 4 ml growth media (approximately 60% confluency) in 6 well dishes. The cells were then transfected with Effectene as per manufacturer's instructions (Qiagen). Briefly, 0.4 µg total plasmid DNA was condensed by interactions with 3.2 µl of Enhancer in EC Buffer to a final volume of 100 µl and incubated for 5 minutes. 10 µl Effectene Reagent was then added to the condensed DNA to produce condensed Effectene–DNA complexes. The Effectene–DNA complexes were mixed with 1.4 ml

medium to aid faster diffusion and directly added to the cells. Cells were incubated for 48 hours following transfection to enable suitable gene expression.

2.17.2. Generating stable lines using Cellfectin

3 x 10^6 S2 cells were plated into each well of a 6 well dish in a final volume of 2 ml Complete S2 Medium without antibiotics. The cells were then allowed to adhere to the bottom of the plate for a minimum of 2 hours at 25ºC. A solution containing 5 µg of the pAVW Pico constructs and 0.5 µg of the pCoBlast (Blasticidin reistance) plasmid (Invitrogen) in 0.1 ml Complete S2 Medium without antibiotics was combined and mixed gently with a solution containing 15 µl Cellfectin (Invitrogen) in 0.1 ml Complete S2 Medium without antibiotics.

The resultant mixture was incubated at room temperature for 30 minutes before 0.8 ml Complete S2 Medium without antibiotics was added. The 2 ml of original medium was then removed from the S2 cells and replaced with the new solution containing the DNA/Cellfectin mix. The cells were incubated overnight at 25ºC before the media containing the transfection mix was removed and replaced with 3 ml of fresh Complete S2 Medium (containing antibiotics). Following incubation at 25ºC for 48 hours, the old medium was removed and fresh Complete S2 Medium containing 20 µg/ml Blasticidin (Sigma) added.

If the cells were in suspension, they were centrifuged at 1000 g for 5 minutes before the fresh medium was added. After 1-2 days the contents of each well were transferred into single 25cm^2 flasks in a final volume of 6 ml Complete S2 Medium containing 20 µg/ml Blasticidin. When the cells became over confluent they were transferred into single 75cm^2 flasks in a final volume of 15 ml Complete S2 Medium containing 20 µg/ml Blasticidin. The cells were maintained using normal procedures and Complete S2 Medium containing 20 µg/ml Blasticidin.

2.18. Immunoprecipitation

2.18.1. Pulldown of Myc/FLAG-tagged proteins

Appropriate flies expressing Myc or FLAG tagged proteins were selected, snap frozen in liquid nitrogen, and then crushed before 0.5 ml of ice cold RIPA buffer was added. The flies were crushed further in the RIPA buffer until completely lysed and immediately place on ice. The resulting lysate was centrifuged for 10 minutes at 10,000 rpm at 4°C to pellet the fly debris before the supernatant was carefully removed using a pipette, transferred to a clean labelled eppendorf tube and set on ice. A small sample was taken as a positive control and 5 µl of anti-Myc (A14) (Santa Cruz) or anti-FLAG (M2) (Sigma) was added to the eppendorf. The contents were then briefly mixed using a vortex mixer and subjected to over-end mixing for 1 hour at 4°C. Before the hour long incubation was complete, 50 µl of EZview Red Protein G Affinity beads (Sigma) were added to a clean labelled eppendorf tube. 750 µl of ice-cold RIPA buffer was added to the beads and the solution briefly mixed using a vortex mixer. The tube was then centrifuged at 10,000 rpm for 30 seconds at 4°C and the supernatant removed and discarded. This washing process was performed two more times before the bead pellet was placed on ice.

Once the hour long incubation of lysate with antibody was finished, the tube was briefly centrifuged for 2-3 seconds to collect the contents in the bottom of the tube. The entire sample was then removed, transferred to the tube containing the EZview beads, and the resulting solution mixed using a vortex mixer. The contents were then subjected to over-end mixing for 1 hour in the cold room before being spun down at 10,000 rpm for 30 seconds at 4°C and placed on ice. The supernatant was removed and the beads washed three times in 750 µl of ice-cold RIPA buffer, after which 25 µl of ice-cold RIPA buffer and 25 µl of 2x SDS-sample buffer were added to the beads and the samples boiled for 10 minutes. The tube was again centrifuged at 10,000 rpm for 30 seconds to pellet the beads and the supernatant directly loaded into a polyacrylamide gel for SDS-PAGE (Chapter 2.19.).

2.16.2. GFP-Trap mediated pulldown of Venus-Pico

Flies expressing Venus-Pico were selected by detection of the Venus-tag under a fluorescent sterodissecting microscope, snap frozen in liquid nitrogen and then crushed. 200 µl of ChromoTek lysis buffer (ChromoTek) was added and the sample placed on ice before being repeatedly crushed every 5 minutes for 30 minutes. The lysate was then centrifuged at 10,000 rpm for 10 minutes at 4°C to pellet the fly debris before the supernatant was carefully removed using a pipette, transferred to a clean labelled eppendorf tube and set on ice. The volume was adjusted to 500 µl with ice cold ChromoTek dilution buffer (ChromoTek) and 50 µl of sample removed to act as a positive control. Next, 20 µl of GFP-Trap beads were equilibrated by washing three times in 500 µl ice cold ChromoTek dilution buffer. Between each wash step the beads were pulled down using a DiaMag1.5 magnetic separator (Diagenode) and the supernatant removed. Once equilibrated, the *Drosophila* lysate was added to the beads and subjected to over-end mixing for 2 hours at 4°C.

Following the 2 hour incubation, the GFP-Trap beads were pellated using the magnetic separator and the supernatant removed. The beads were then washed five times 500 µl ice cold ChromoTek dilution buffer before being boiled for 20 minutes in 100 µl 2x SDS-Sample buffer. The beads were once again pulled down using the magnetic separator and the remaining supernatant loaded into a polyacrylamide gel for SDS-PAGE.

2.16.2. Pulldown of SUBO-tagged peptides

Hela and S2R+ cells were harvested and pelleted by centrifugation at 1000 x g for 5 minutes. The cell medium was removed and the pellet transferred to an eppendorf to which 0.5 ml of ice cold RIPA buffer was added. The cells were lysed for 20 minutes on ice and centrifuged at 10,000 rpm for 10 minutes at 4°C to remove the cell debris. The supernatant was carefully removed using a pipette, transferred to a clean labelled eppendorf tube. Meanwhile, thirty W^{1118} flies were collected, snap frozen in liquid nitrogen, and then crushed before 0.5 ml of ice cold RIPA buffer was also added. The flies were crushed further in the RIPA buffer until completely lysed and immediately place on ice. The resulting lysate was centrifuged for 10 minutes at

10,000 rpm at 4°C to pellet the fly debris before the supernatant was carefully removed using a pipette and transferred to a clean labelled eppendorf tube.

200 µg of a SUBO-tagged RIAM fragment corresponding to residues 147-174 (Thomas Zacharchenko-University of Liverpool) was added to each of the lysates and the solutions subjected to over-end mixing at 4˚C for 2 hours. For each sample, 10 µl of SUMO-Qapture resin (Enzo Life Sciences) was equilibrated in separate eppendorfs by adding 500 µl ice cold RIPA buffer and mixing the solution briefly using a vortex mixer. The tubes were then centrifuged at 10,000 rpm for 30 seconds at 4°C and the supernatant removed and discarded. This washing process was performed two more times before the resin pellet was placed on ice.

Once the 2 hour incubation of lysates with SUBO-RIAM was finished, the tubes were briefly centrifuged for 2-3 seconds to collect the contents in the bottom of the tube. The entire samples were then removed, transferred to tubes containing the SUMO-Qapture resin, and incubated for 1 hour at 4˚C with over-end mixing. Next the samples were spun down at 10,000 rpm for 30 seconds at 4°C and placed on ice. The supernatant was then removed from each sample and the resin washed three times in 750 µl of ice-cold RIPA buffer, after which 25 µl of ice-cold RIPA buffer and 25 µl of 2x SDS-sample buffer was added to the resin and the samples boiled for 10 minutes. The tubes were again centrifuged at 10,000 rpm for 30 seconds to pellet the beads and the supernatant directly loaded into a polyacrylamide gel for SDS-PAGE (Chapter 2.19.).

2.19. SDS-PAGE

Proteins were separated on the basis of molecular weight on SDS-polyacrylamide gels as described in Sambrook (2001). In brief, whole flies or third instar larvae were frozen in liquid nitrogen and then ground up in 2x SDS-Sample buffer. The resulting mixture was then boiled for 10 minutes and centrifuged at 10,000 rpm for 3 minutes to remove debris. The supernatant was run on Tris-buffered SDS-polyacrylamide gels in 1 x SDS-PAGE Running Buffer, with the acrylamide concentration of the separating gel varying depending on the size of the proteins being separated. A pre-stained protein ladder (New England Biolabs) was employed to allow the

size of separated proteins to be estimated and Mini-Protean II Vertical Electrophoresis apparatus (Bio-Rad) was used according to the manufacturer's instructions.

2.19.1. Coomassie staining

Following protein separation by SDS-PAGE gel electrophoresis, Coomassie staining was performed as a means of visualising proteins present at 0.5 μg or above within loaded samples. The polyacrylamide gel was initially removed from the glass plates and placed into a suitably sized container and rinsed once in ddH_2O (Sambrook, 2001). The gel was then incubated with Coomassie stain solution for 1 hour on a rocking table before being rinsed again in ddH_2O two more times. Next, the gel was incubated with Coomassie de-stain solution to remove excess dye from the background gel matrix. The de-stain solution was replaced every 30-60 minutes until a sufficient level of de-staining had been reached.

2.19.2. Western blotting

Following sufficient separation of proteins by SDS-PAGE, proteins were transferred overnight, at 4ºC, to a pre-wetted Immobilon-P PVDF membrane (Millipore) in Tris-glycine transfer buffer, using Bio-Rad electrophoretic transfer apparatus as per the manufacturer's instructions. After blotting, membranes were stained briefly with Ponceau S solution (Sigma Aldrich) to determine adequate electrophoretic transfer. The lanes were appropriately marked with a pencil and the membranes rinsed with water and PBST to remove the stain.

Membranes were incubated in blocking buffer (PBST + 5% w/v Marvel skimmed milk powder) for 90 minutes, at room temperature, to reduce non-specific binding of the antibody before being incubated a suitable primary antibody, diluted in blocking buffer, under optimised conditions detailed in Table 2.19.1. The membranes were then washed three times in PBST for 10 minutes and incubated with an appropriate horseradish peroxidase (HRP)-conjugated secondary antibody (Table 2.19.2.), diluted in blocking buffer, for 90 minutes at room temperature. Next, the membranes were washed three times in PBST for 10 minutes and once in PBS for 10 minutes.

1˚ Antibody	Supplier	Species	Concentration	Conditions	Predicted Size
Myc (A14)	Santa Cruz	Rabbit	1:100	2 hrs at RT	-
FLAG (M2)	Sigma	Rabbit	1:300	2 hrs at RT	-
GFP (ABfinity)	Invitrogen	Rabbit	1:2000	O/N at 4˚C	-
GFP (12A6)	DSHB	Mouse	1:500	2 hrs at RT	-
Chickadee (chi 1J)	DSHB	Mouse	1:2000	O/N at 4˚C	18 kDa
Talin (A22A)	DSHB	Mouse	1:2000	O/N at 4˚C	200-250 kDa
Ras (05-516)	Millipore	Mouse	1:2000	2 hrs at RT	22 kDa
Rap-1 (121)	Santa Cruz	Rabbit	1:500	O/N at 4˚C	24 kDa
PP1 (3529)	In-house	Rabbit	1:2000	O/N at 4˚C	37 kDa
Erk1/2 (137F5)	Cell Signalling	Rabbit	1:2000	2 hrs at RT	42-44 kDa
pErk1 (ab24157)	Abcam	Rabbit	1:1000	O/N at 4˚C	42-44 kDa
pPico (0140)	In-house	Rabbit	1:1000	O/N at 4˚C	124 kDa

Table 2.19.1. Primary antibodies used in Western blots.

N.B. Anti-GFP (12A6) used to detect Venus in Figure 5.5.1.a has only been available since April 2013 and therefore could not be used for examination of Venus-Pico expression levels in flies or co-IP controls.

2˚ Antibody	Supplier	Species	Concentration	Conditions
Anti-mouse HRP	Cell Signalling	Goat	1:2000	2 hrs at RT
Anti-rabbit HRP	Cell Signalling	Goat	1:2000	2 hrs at RT

Table 2.19.2. Secondary antibodies used in Western blots.

SuperSignal® West Pico chemiluminescent substrate (Pierce) was used according to the manufacturer's instructions to detect the HRP-conjugated secondary antibodies. Light emitted from the chemiluminescent reagent was detected by exposure to Amersham Hyperfilm ELC (GE Healthcare Ltd) for 30 seconds to 2 hours depending on the signal intensity before the X-ray film was subsequently developed and fixed with Kodak developer/fix according to the manufacturer's instructions.

2.20. Mass Spectrometry

GFP-Trap mediated pulldowns of *hs-GAL4* Venus-Pico^{WT} and W^{1118} were carried out and the beads from each sample split in separate eppendorf tubes. One half of the beads were boiled in 50 µl 2x SDS-Sample buffer and directly loaded into a polyacrylamide gel for SDS-PAGE, while the other half were stored in 40 µl of 25 mM ammonium bicarbonate. Once SDS-PAGE was complete, the polyacrylamide gel was stained using the Coomassie staining protocol (Chapter 2.19.1.) and used for SDS-PAGE mediated mass spectrometry.

2.20.1. SDS-PAGE mediated mass spectrometry

SDS-PAGE mediated mass spectrometry was carried out by Lynn McLean, (Protein Function Group, Institute of Integrative Biology). Briefly, excised bands (plugs) were de-stained with 50% acetonitrile/50% 100 mM ammonium bicarbonate. Gel plugs were reduced with 10 mM dithiothreitol for 30 minutes at 37°C, then alkylated for 60 minutes at 37°C in 55 mM iodoacetamide. The plugs were then dehydrated using acetonitrile at 37°C for 15 minutes. The acetonitrile was removed and the gel plugs allowed to dry. Finally, trypsin (0.02 µg/µl final concentration) was added and the digestion proceeded for 16 hours at 37°C. At the end of the digestion, the reaction was stopped and the surfactant inactivated and precipitated by addition of formic acid to a final concentration of 0.5%. Peptides were analysed using a Bruker Amazon ion trap mass spectrometer coupled to a Waters nanoACQUITY UltraPerformance liquid chromatography® (UPLC®) system. The samples were injected onto a reverse phase column (Acquity BEH C18, 75µm x 150mm 1.7µm) and eluted over a 1 hour gradient. The mass spectrometer was set up in positive ion mode and calibrated with Bruker calibration mix. Spectra were acquired between 300-1800m/z with an ICC target of 200,000. Up to five precursor ions above a threshold of 10,000 were selected for MSMS fragmentation per MS scan. Each precursor was fragmented twice and then the mass was excluded for 1 minute. Singly charged ions were excluded. Data was analysed using both Peaks and Mascot software.

2.20.2. Mass spectrometry of total pulldowns

Mass spectrometry of total pulldowns was performed by Lynn McLean using the GFP-Trap magnetic beads stored in 40 µl of 25 mM ammonium bicarbonate. Briefly, 2.5 µl of 1% RapiGest^{TM} (Waters MS Technologies) was initially added to the samples and the solutions incubation at 80°C for 10 minutes. Samples were reduced with 2.5 µl of 60 mM dithiothreitol for 10 minutes at 60°C and then alkylated for 30 minutes at room temperature in the dark, with 2.5 µl of 180 mM iodoacetamide. Finally, trypsin (0.01 µg/µl final concentration) was added and the digestion proceeded for 16 hours at 37°C. At the end of the digestion, the reaction was stopped and the surfactant inactivated and precipitated by addition of trifluoroacetic acid to a final concentration of 0.5%. After incubating for 45 minutes at 37°C, samples were clarified by centrifugation at 15,000 x *g* for 15 minutes. Digests were analysed as tryptic peptides, resolved by high resolution liquid chromatography (Waters nanoAcquity) prior to tandem mass spectrometry on a Thermo LTQ-Orbitrap Velos system. For each digested sample analysed by LC MS, 1 µl was injected onto a 75µm x 150 mm BEH C18 column and the peptides resolved over a 90 minute linear organic gradient of 3-40% buffer B (0.1% FA in acetonitrile). Data acquisition was data dependent, with the top 20 most intense peptides in each MS scan selected for fragmentation. Data was analysed using Peaks and Mascot searches.

2.21. S2R+ spreading on ConA coated substrates

500 µl of 15 µg/ml Concanavalin A (Sigma) was plated onto glass bottomed 6-well dishes (IWAKI) and allowed to dry overnight at room temperature. 2 ml of S2R+ cells at $2x10^5$ cells/ml were plated into each well and allowed to adhere for either 20 or 30 minutes before being fixed in 10% paraformaldehyde in PBST for 10 minutes.

2.21.1. Staining S2R+ cells

The fixed cells were subjected to three 10 minutes washes with PBS and then blocked with PBST + 5% FCS for a minimum of two hours at 4ºC. Cells were then incubated with primary antibodies diluted in PBST + 5% FCS (Table 2.21.1.) overnight at 4ºC before being washed a

further three times for 20 minutes in PBST. Secondary antibodies were diluted in PBST + 5% FCS (Table 2.22.2.), added to the wells and incubated at room temperature in the dark for two hours. The cells were then subjected to a further three 15 minute PBST washes and one 15 minute wash in PBS. Lastly, 0.5 ml of mounting medium (85% glycerol, 2.5% n-propylgallate) was added to each well and the dishes stored in the dark for no longer than a week at 4ºC.

1˚ Antibody	Supplier	Species	Concentration
Chickadee (chi 1J)	DSHB	Mouse	1:1000
Enabled (5G2)	DSHB	Mouse	1:2000
Talin (A22A)	DSHB	Mouse	1:1000
Ras (05-516)	Millipore	Mouse	1:200
Erk1/2 (137F5)	Cell Signalling	Rabbit	1:200
PP1 (0140)	In-house	Rabbit	1:500

Table 2.21.1. Primary antibodies used in S2R+ staining.

1˚ Antibody	Supplier	Species	Concentration
Anti-mouse AF555	Invitrogen	Goat	1:500

Table 2.21.2. Secondary antibodies used in S2R+ staining.

2.22. Wing disc dissection and staining

Wing imaginal discs were dissected from wandering third instar larvae in cold PBS, transferred to a watchglass, and fixed with 4% paraformaldehyde in PBST for 20 minutes at room temperature. The tissues were subjected to three 10 minutes washes with PBS and then blocked with PBST + 5% FCS for a minimum of two hours at 4ºC. The wing discs were then incubated with primary antibodies diluted in PBST + 5% FCS (Table 2.22.1.) overnight at 4ºC before being washed a further three times for 20 minutes in PBST. Secondary antibodies were diluted in PBST + 5% FCS (Table 2.22.2.), added to the tissues and incubated at room temperature in the dark for two hours. The tissues were then subjected to a further three 15 minute PBST washes

and one 15 minute wash in PBS. Lastly, the wing discs were mounted on microscope slides in 17.5 µl of Vectashield mounting medium (Vector Laboratories) and covered with a raised coverslip. The sides were sealed with clear nail polish and slides stored in the dark for no longer than a week at 4ºC.

1˚ Antibody	Supplier	Species	Concentration
Pico (3531)	In-house	Rabbit	1:1000
Chickadee (chi 1J)	DSHB	Mouse	1:2000
Enabled (5G2)	DSHB	Mouse	1:2000
Talin (A22A)	DSHB	Mouse	1:1000
Ras (05-516)	Millipore	Mouse	1:500
Erk1/2 (137F5)	Cell Signalling	Rabbit	1:500
PP1 (0140)	In-house	Rabbit	1:2000

Table 2.22.1. Primary antibodies used in wing disc staining.

1˚ Antibody	Supplier	Species	Concentration
Anti-rabbit AF488	Invitrogen	Goat	1:500
Anti-mouse AF555	Invitrogen	Goat	1:500

Table 2.22.2. Secondary antibodies used in wing disc staining.

2.23. Confocal microscopy

Tissues prepared using the above immunostaining protocols were examined using an LSM 710 confocal microscope (Zeiss) and Zen 2011 confocal software (Zeiss). GFP and Venus fusion proteins were excited at 488nm using an argon laser and Cy3 conjugates excited with a He/Ne laser operating at 561nm. Fluorescence was measured by the 32-channel internal detector and images visualised using Zen 2011 Lite (Zeiss). S2R+ cells were imaged using 2 µm slices while wing discs were assessed by multiple 2.5 µm sliced z-stacks.

Quantification of the relative fluorescence intensity was carried out using the linear plot profile tool within ImageJ (National Institute of Health) and data analysed within Microsoft Excel 2010. Maximal Venus-Pico intensity within S2R+ cells was calculated by averaging the six highest intensity values reported in the linear plot profile results.

2.24. SRF luciferase assay

SRF-luciferase assays were carried out using the Qiagen Cignal SRE Reporter Kit and Dual-Glo® Luciferase Assay System (Promega) as per manufacturer's instructions. Briefly $2x10^4$ S2R+ cells were plated into individual wells in a 96-well plate and transfected with 100 ng *pA*-renilla and 100 ng *SRE*-firefly either alone as a control, or alongside 200 ng of a vector of interest using Effectine (Qiagen). Triplicate transfections were carried out on the same batch of cells to minimise variability among treatment groups after which the cells were incubated for 48 hours enable suitable gene expression. Cells were then lysed in 20 µl Passive Lysis Buffer (Promega) for 15 minutes at room temperature on an orbital shaker before the lysate was transferred to a new 96-well plate. 100 µl of Luciferase Assay Reagent II (Promega) was added to each well and analysis carried out using an automated luminometer to record the firefly luciferase activity. Next, 100 µl of Stop & Glo® Reagent (Promega) was added to the wells and analysis of the Renilla luciferase activity performed using the automated luminometer. Firefly luciferase activity was divided by Renilla luciferase activity to determine the degree of SRF activity. Single factor Anova tests were then performed on the data to determine if there were statistically significant differences between groups (p-values less than 0.05 were deemed statistically significant.

2.25. Wing size analysis

For wing preparations, appropriate adult flies were stored in 75% ethanol for at least 24 hours to dehydrate and preserve the wings. Wings were removed from flies using dissection tweezers (Dumont Medical) and placed on a microscope slide to dry. Twenty-five wings, from individual flies, were dissected per genotype. Once dry, the wings were transferred to a small drop of mounting medium (1:1 methylsalicylate/ Canada balsam) where air bubbles could be removed.

The wings were then transferred to a fresh 15µl drop of mounting medium on a new slide and covered with a coverslip. The slides were examined using a Leica MZ10F microscope. A Leica DFC420 digital camera and Leica application suite software (Version 2.8.1) were used to take images of the tissues. Wing areas were measured using the polygon tool within ImageJ to mark the area of the wing to be measured, and the area calculated using the measurement function. The wing blade but not the wing hinge was included in this measurement as shown in Figure 2.25.1. T-tests were carried out to validate apparent mean differences and p-values of less than 0.05 considered to be statistically significant.

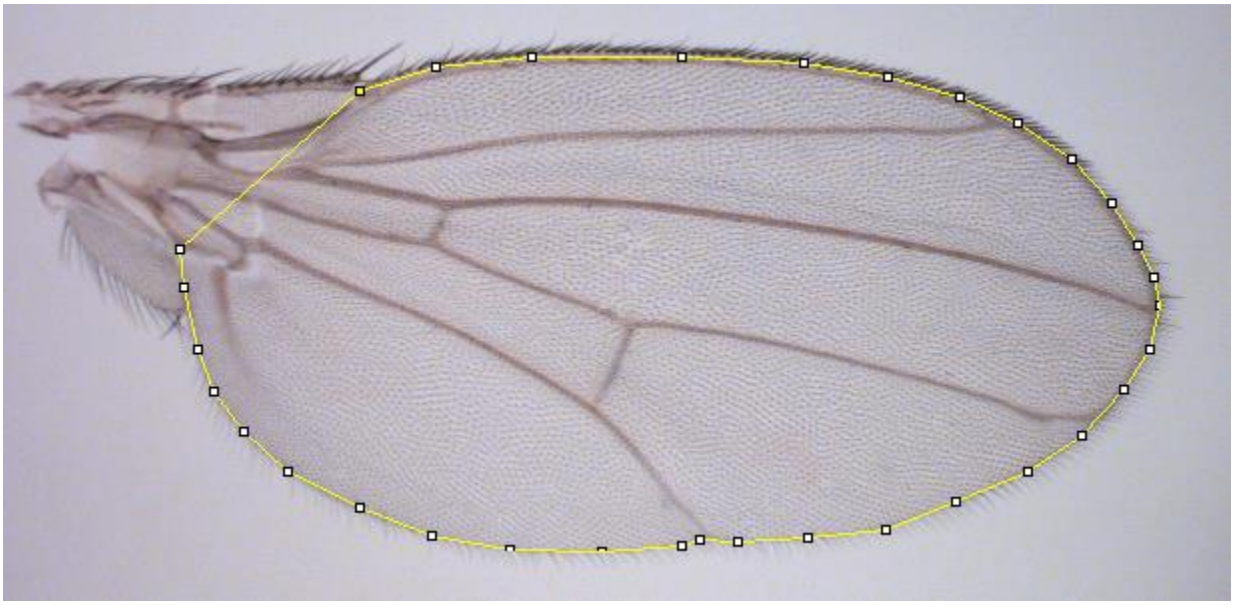

Figure 2.25.1. Example of wing size analysis in ImageJ. The wing blade but not the wing hinge was used to calculate the tissue size of adult *Drosophila* wings.

3. Bioinformatic analysis of the MRL family

3.1. Introduction

The MRL family constitutes a group of molecular adaptor proteins which facilitate the transduction of signals derived from membrane receptors to changes in cytoskeletal dynamics, enabling regulation of cell shape, adhesion, migration and growth (Krause et al., 2004, Lafuente et al., 2004, Lyulcheva et al., 2008). As adapter proteins, the MRLs possess numerous protein and lipid binding domains, but have no intrinsic enzymatic activity, instead functioning by bringing specific binding partners into close proximity to enhance and control the cellular response to signalling events.

Previous research has already identified and characterised many of these binding domains, with the most notable being the highly conserved and well defined central RA and PH domains (Figure 3.1.1.) (Colo et al., 2012b). Briefly, the RA domain has been shown to directly interact with specific Ras-like GTPases and is thought to play a crucial role in activation of the MRL protein or its other associated factors, while the PH domain binds to PIs and is believed to enable recruitment of MRL protein complexes to the plasma membrane (Holt and Daly, 2005, Krause et al., 2004). Adjacent to the N-terminus of the RA domain, MRL proteins contain a characteristic putative coiled-coil motif which is thought to promote homo- or hetero-dimeric interactions, although the biological function of this interaction has yet to be ascertained (Chang et al., 2013, Legg and Machesky, 2004, Lupas, 1996).

In addition, the MRL proteins possess a relatively unstructured proline rich C-terminus with multiple FPPPP and XPPPP motifs allowing interactions with the actin regulatory proteins Ena/VASP and Profilin respectively (Krause et al., 2004, Lafuente et al., 2004). Amphipathic helical structured talin binding sites have also been identified within the first 100 amino acids of RIAM and Lpd, and are thought to assists in linking associated proteins to FAs (Lee et al., 2009, Han et al., 2006). Lastly, a PP1 binding motif has been found within a C-terminal proline rich region of Pico and most likely functions in regulating the activity of either Pico or its interaction partners (Lyulcheva, 2006).

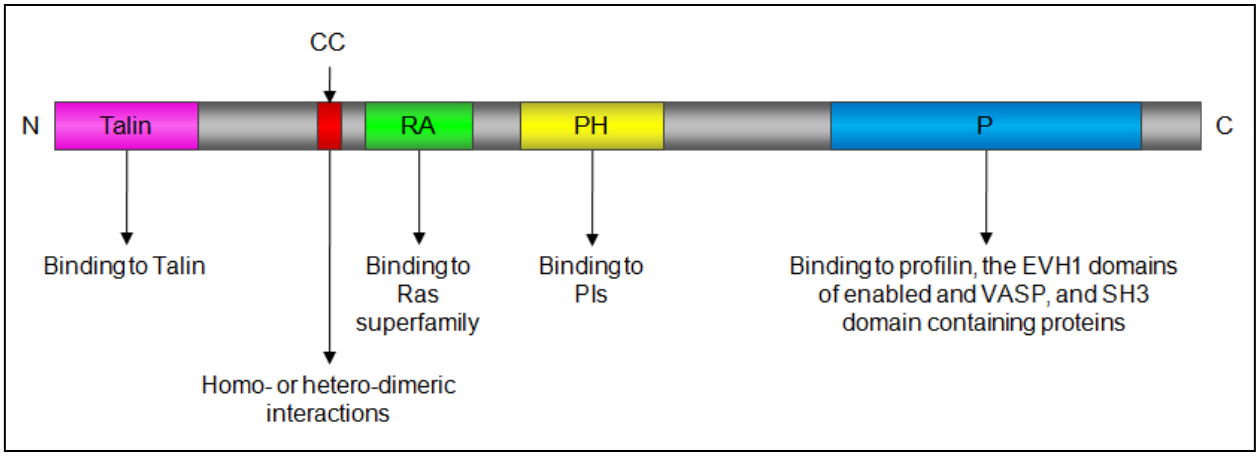

Figure 3.1.1. A schematic representation of the MRL family functional domains. The MRL proteins all possess central RA and PH domains in addition to an unstructured proline rich C-terminus (P) and a putative coiled-coil motif (CC) adjacent to the RA domain. Talin binding sites have also been identified within the first 100 amino acids of RIAM and Lpd.

Taken together, it is clear to see how binding partner interactions may play a key role in MRLs functionality, with Ras and PP1 potentially assisting in the regulation of associated cytoskeletal modification proteins such as Enabled, Profilin and Talin. Consequently, to better understand the mechanisms through which the MRL proteins act, further comprehension of their domain structure must first be established so that fundamental interactions can be ascertained.

3.1.1. Aims

The aim of the research presented in this chapter was to characterise, through examination of conserved regions, key MRL binding domains with a view to identifying novel functional motifs present within the protein sequence. To perform this analysis effectively, MRL protein alignments were generated using BLAST identified sequences from a wide variety of multicellular eukaryotes. Phylogenetic analysis was performed on the alignments to confirm correct MRL sequence identification before investigating potential domain occurrence within those regions possessing a high level of sequence conservation. Further sequence analysis was carried out as a means of isolating potentially important binding motifs that displayed a conserved presence, but lacked consistent structural localisation.

3.2. Phylogenetic analysis of the MRL family

Basic Local Alignment Search Tool algorithms were initially used to identify MRL homologues in a wide variety of species. Sequence alignments were then performed on all rational hits using the T-Coffee Accurate alignment tool before being manually assessed for accuracy with BoxShade and Ali2D. Lastly, a phylogenetic tree of the MRL proteins was generated using Tree-Puzzle, FastME and PHYML. This was used to verify correct MRL sequence identification as well as accurately separate and categorise the Lpd and RIAM paralogues.

Initial BLAST screening revealed no orthologues to be present in Protista, Plantae or Fungi kingdoms, indicating that the MRL proteins emerged exclusively during animal evolution. MRL homologues were identified in both *Amphimedon queenslandica* (sponge) and *Trichoplax adherens* (placazoa), suggesting MRLs emerged at an early stage in animal evolution. *Tetraodon nigroviridis* (pufferfish) and *Danio rerio* (zebrafish) represent the earliest organisms to possess the two paralogues Lpd and RIAM, while only a single orthologue was found in *Ciona intestinalis* (sea squirt), part of the phylum Chordata. This implies that the duplication event leading to two copies of the MRL gene occurred at some point during primitive vertebrate evolution. Interestingly, the recently sequenced early vertebrate *Petromyzon marinus* (lamprey) appears to have copies of both Lpd and RIAM, however, the protein sequence for both is currently incomplete (Smith et al., 2013) and was therefore not included in later analysis.

Figure 3.2.1. shows a radial dendrogram of the phylogenetic tree generated (a rectangular arrangement can be found in Appendix 1). Three distinct groups can be clearly seen representing the single MRL orthologues (green), Lpd (red) and RIAM (blue), enabling accurate classification of the Lpd and RIAM paralogues. In addition, no significant outliers were observed, validating the MRL sequences identified through the BLAST screen. The data from this figure also shows that considerable divergence of the protein sequence has occurred amongst those species possessing only one MRL homologue. This is demonstrated by the long lines emerging from each branch point in this grouping, and isn't surprising given the substantial evolutionary distances between these organisms. The single orthologue sequences also appear to show a greater similarity to Lpd than RIAM.


Amphimedon queenslandica Ortho
Trichoplax adhaerens Ortho
Nematostella vectensis Ortho
Ciona intestinalis Ortho
Strongylocentrotus purpuratus Ortho
Caenorhabditis elegans Mig10
Apis mellifera Ortho
Drosophila melanogaster Pico
Anopheles gambiae Ortho
Aedes aegypti Ortho
Tetraodon nigroviridis RIAM
Danio rerio RIAM
Xenopus tropicalis RIAM
Anolis carolinensis RIAM
Zebra finch RIAM
Gallus gallus RIAM
Monodelphis domestica RIAM
Mus musculus RIAM
Rattus norvegicus RIAM
Oryctolagus cuniculus RIAM
Macaca mulatta RIAM
Homo sapiens RIAM
Pan troglodytes RIAM
Equus caballus RIAM
Canis familiaris RIAM
Sus scrofa RIAM
Tetraodon nigroviridis Lpd
Danio rerio Lpd
Xenopus tropicalis Lpd
Pan troglodytes Lpd
Homo sapiens Lpd
Macaca mulatta Lpd
Oryctolagus cuniculus Lpd
Sus scrofa Lpd
Equus caballus Lpd
Canis familiaris Lpd
Rattus norvegicus Lpd
Mus musculus Lpd
Monodelphis domestica Lpd
Gallus gallus Lpd
Zebra finch Lpd
Anolis carolinensis Lpd

Figure 3.2.1. Radial dendrogram of MRL phlogenetic tree. MRL sequence alignments were used to generate a phylogenetic tree to confirm appropriate MRL sequence identification and classification of Lpd and RIAM paralogues. Three distinct groupings representing the single MRL orthologues (green), Lpd (red) and RIAM (blue) can be seen enabling characterisation of Lpd and RIAM, while a lack of outliers substantiates the accuracy of sequences identified through BLAST searches.

Interestingly, Lpd displays a significant degree of sequence conservation, with only *Tetraodon nigroviridis* and *Danio rerio* exhibiting relatively slight variance. RIAM, on the other hand, exhibits notably greater divergence, albeit nowhere near the levels found within the single orthologues. This result implies that the more constrained Lpd probably functions within core processes, while RIAMs divergence may have assisted in the more complex structural development found in vertebrates.

3.3. Domain Analysis

3.3.1. Domain conservation analysis

Once the accuracy of the MRL sequence characterisation had been confirmed, new individual T-Coffee Accurate alignments were generated for the single orthologue, Lpd and RIAM groupings alone. These new alignments, in addition to the complete MRL alignment used for the phylogenetic tree, were analysed by plotcon to ascertain the extent of conservation between the sequences. Those areas displaying a high degree of sequence similarity were then assessed using the Eukaryotic Linear Motif (ELM) resource which, in addition to utilising the more standard SMART/Pfam, GlobPlot, and IUPred searches, identifies short linear motifs within unstructured protein regions not previously assessed within the MRLs (Dinkel et al., 2012, Davey et al., 2012). Domain conservation analysis was performed on the basis that regions containing key functional domains will be highly conserved and show little divergence compared to those lacking fundamental functionality. Similarity plots annotated with the predicted functional domains from each alignment are shown in Figure 3.3.1.

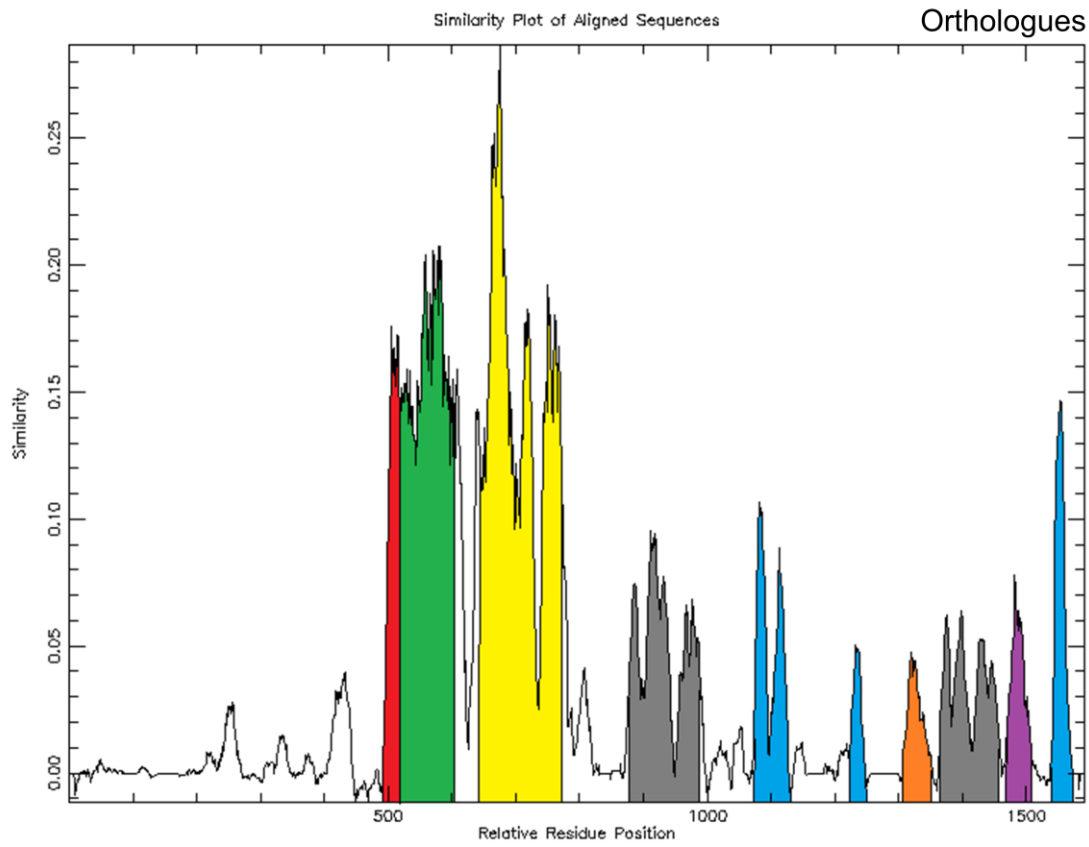
Similarity Plot of Aligned Sequences
Orthologues
Similarity
0.00
0.05
0.10
0.15
0.20
0.25
500
1000
1500
Relative Residue Position

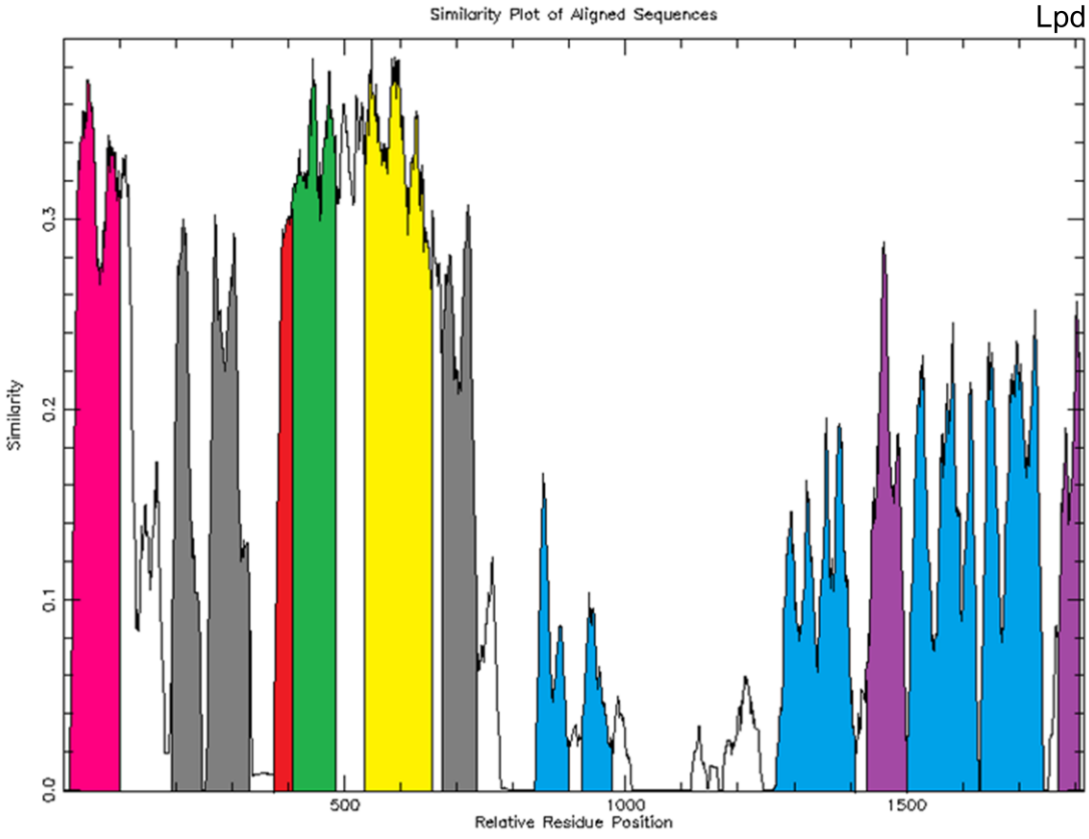
Similarity Plot of Aligned Sequences
Lpd
Similarity
0.0
0.1
0.2
0.3
500
1000
1500
Relative Residue Position

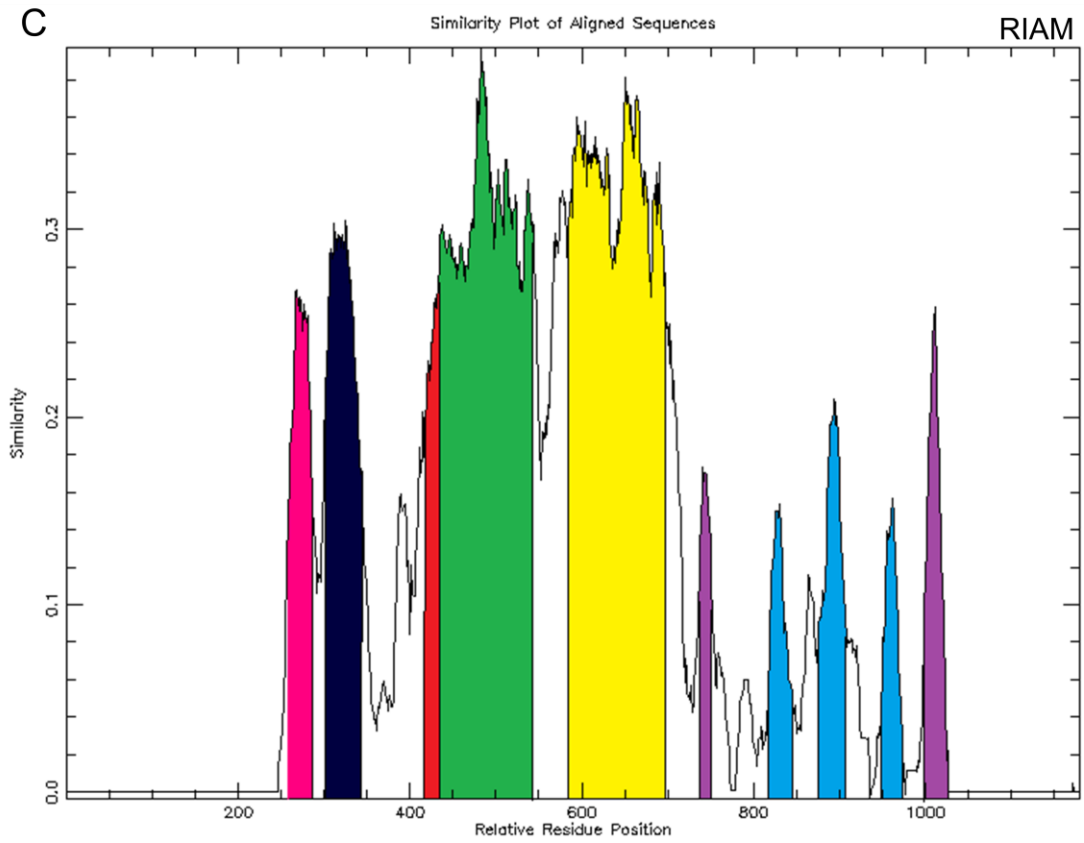
C
Similarity Plot of Aligned Sequences
RIAM
Similarity
0.0
0.1
0.2
0.3
200
400
600
800
1000
Relative Residue Position

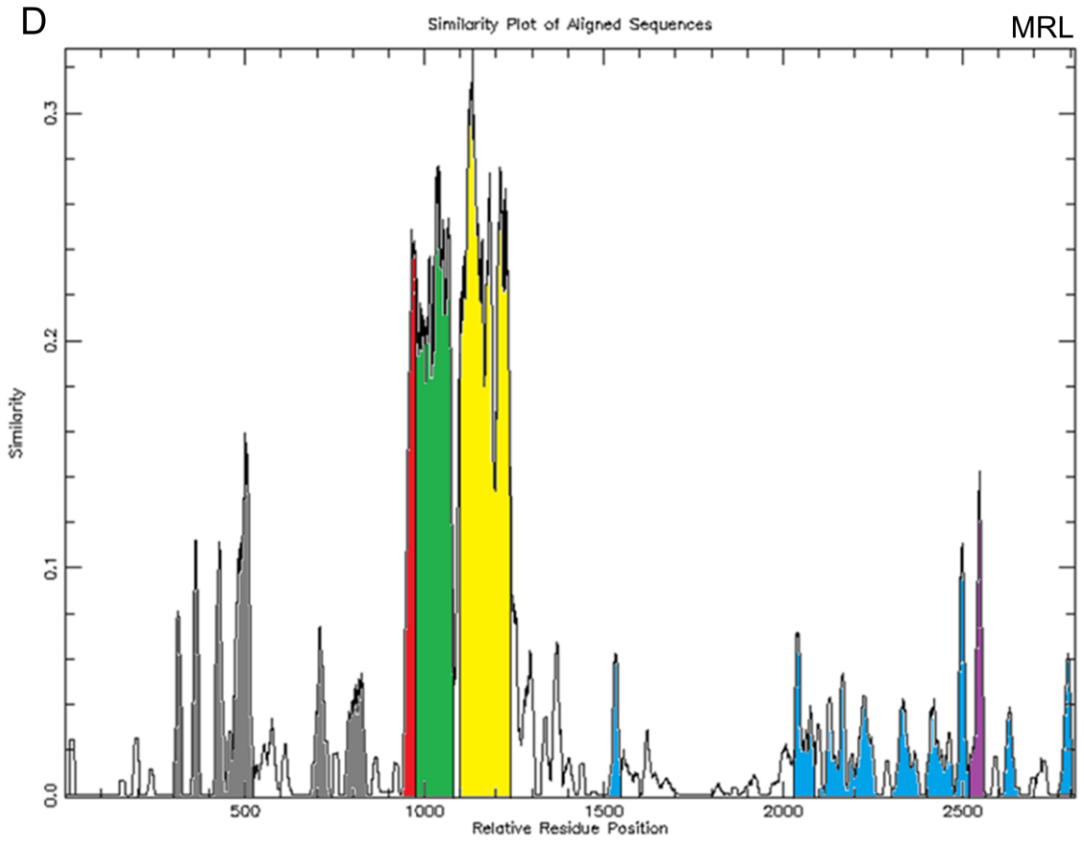
D
Similarity Plot of Aligned Sequences
MRL
Similarity
0.0
0.1
0.2
0.3
500
1000
1500
2000
2500
Relative Residue Position

Figure 3.3.1. Predicted MRL conserved functional sites. Sequence alignments for all (a) single orthologue, (b) Lpd, (c) RIAM, and (d) MRL proteins were analysed to identify highly conserved areas before predicted functional sites present within these regions were characterised. Functional domains are represented using the following colour scheme: RA domain (green); PH domain (yellow); MAPK binding site (red); Proline rich region (blue); SH3 binding site (Purple); Talin binding region (Pink); coiled-coil motif (dark blue); ambiguous/potential modification site (grey); PP1 binding site (orange).

Data from all the alignments studied in Figure 3.3.1. highlighted considerable conservation within the characteristic RA and PH domains. Even the relatively divergent single orthologue species displayed significant sequence homology within these two regions, emphasising their importance to MRL functionality. The data also revealed a previously uncharacterised, yet highly conserved, MAPK binding site adjacent to the RA domain. This binding motif was present in all MRL proteins analysed and displayed a comparable level of similarity to that found within the RA and PH domains, underlining its potentially significant role in the fundamental functionality of MRLs.

As expected, multiple proline rich regions and SH3 binding sites were identified within the unstructured C-terminus of all MRL sequences analysed, while a highly conserved talin binding motif is present at the N-terminus of both Lpd and RIAM. Contrastingly, the single orthologues do not appear to possess a conserved talin binding site, raising questions as to whether this interaction is limited to vertebrate species. Interestingly, a highly conserved coiled-coil region was only observed in RIAM, with neither Lpd or the single orthologues found to possess one using this method. Further analysis revealed this site to be the second coiled-coil region previously described in RIAM, while the characteristic coiled-coil domain recognised as a common feature amongst all MRL proteins is lacking. This highlighted the limitations of ELM in identifying short secondary structures.

Numerous conserved regions with no putative binding properties were also observed, particularly in the single orthologues and Lpd. This may be an artefact of the alignment software actively seeking homology, however, these areas of sequence were characterised as potential sites of

post-translational modification. While this hypothesis may indeed be true, it is worth noting that these regions do not appear to be spatially conserved amongst the MRL proteins; with RIAM containing none, the single orthologues possessing them exclusively within the N-terminus, and Lpd's being found in both the N-terminus and adjacent to the C-terminus of the PH domain.

Finally, a reasonably well conserved PP1 binding motif was observed in the single orthologues, however, similar sites were not found within either Lpd or RIAM. Upon closer inspection, it was established that this conserved site was exclusive to the four insecta species sequences studied, although all MRL proteins appeared to possess a common PP1 binding site at the C-terminus of the RA domain (data not shown).

3.3.2. Domain sequence analysis

While domain conservation analysis proved a useful tool in identifying key domains common to all MRLs, the issues emanating from the partially conserved PP1 binding site drew attention to the limitations of this method in recognising potentially important domains that may display a conserved presence, but lack a consistent position within the protein structure. Consequently, analysis was performed whereby the entire protein sequence was examined to identify all functional domains present. Employing ELM analysis on all the MRL sequences from the BLAST screen was deemed impractical, therefore only the previously well characterised peptides from *H. sapiens* and the model organisms *C. elegans* and *D. melanogaster* were examined. Accordingly, hRIAM, hLpd, Mig10 and Pico full peptide sequences were analysed using ELM and the predicted functional domains rationalised to remove apparent false positives. Figure 3.3.2. shows an alignment of the protein sequences annotated with predicted functional sites displaying either significant homology or a role in regulation, migration, and growth. A rough similarity scoring system has been included to aid with the assessment of domain conservation.

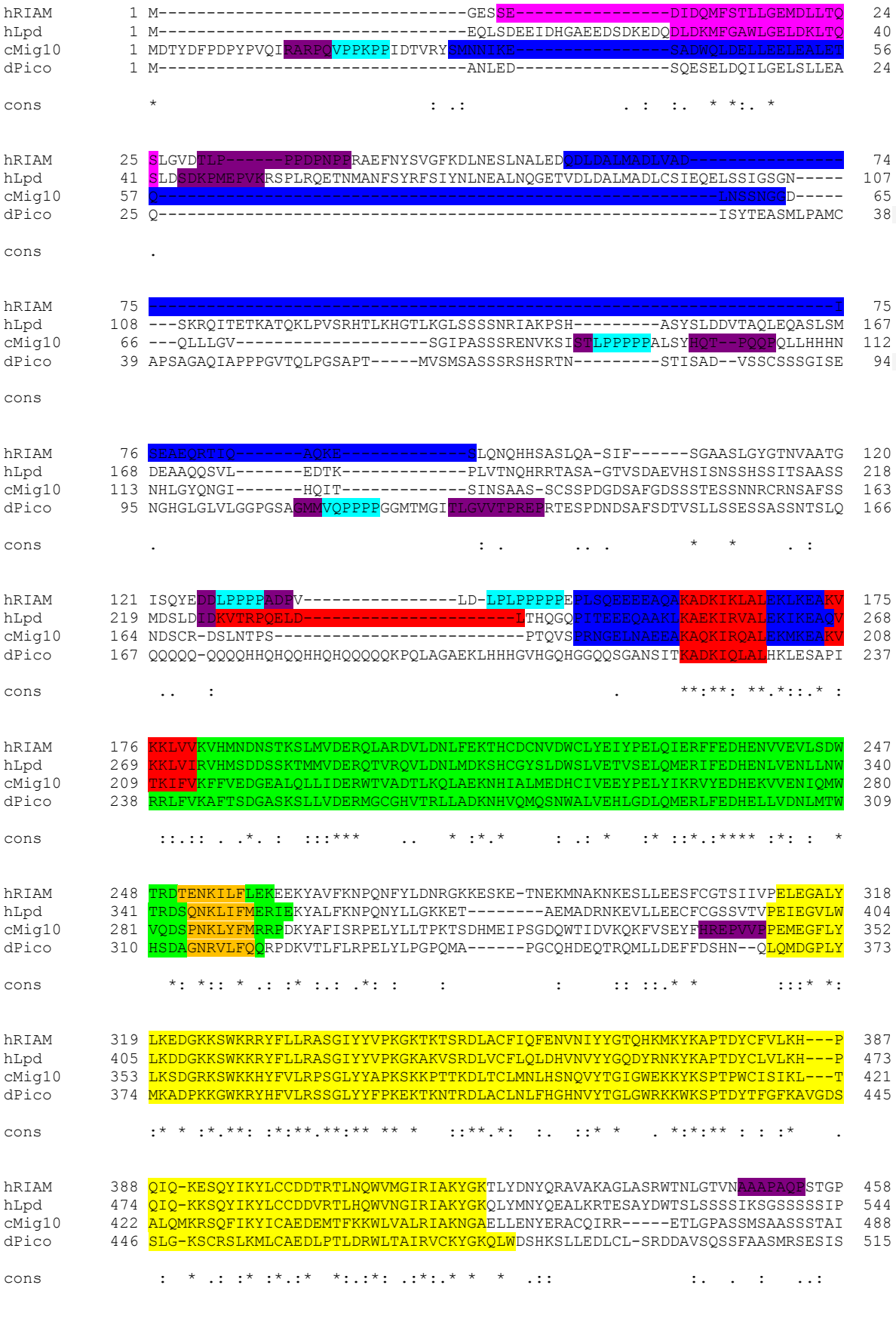

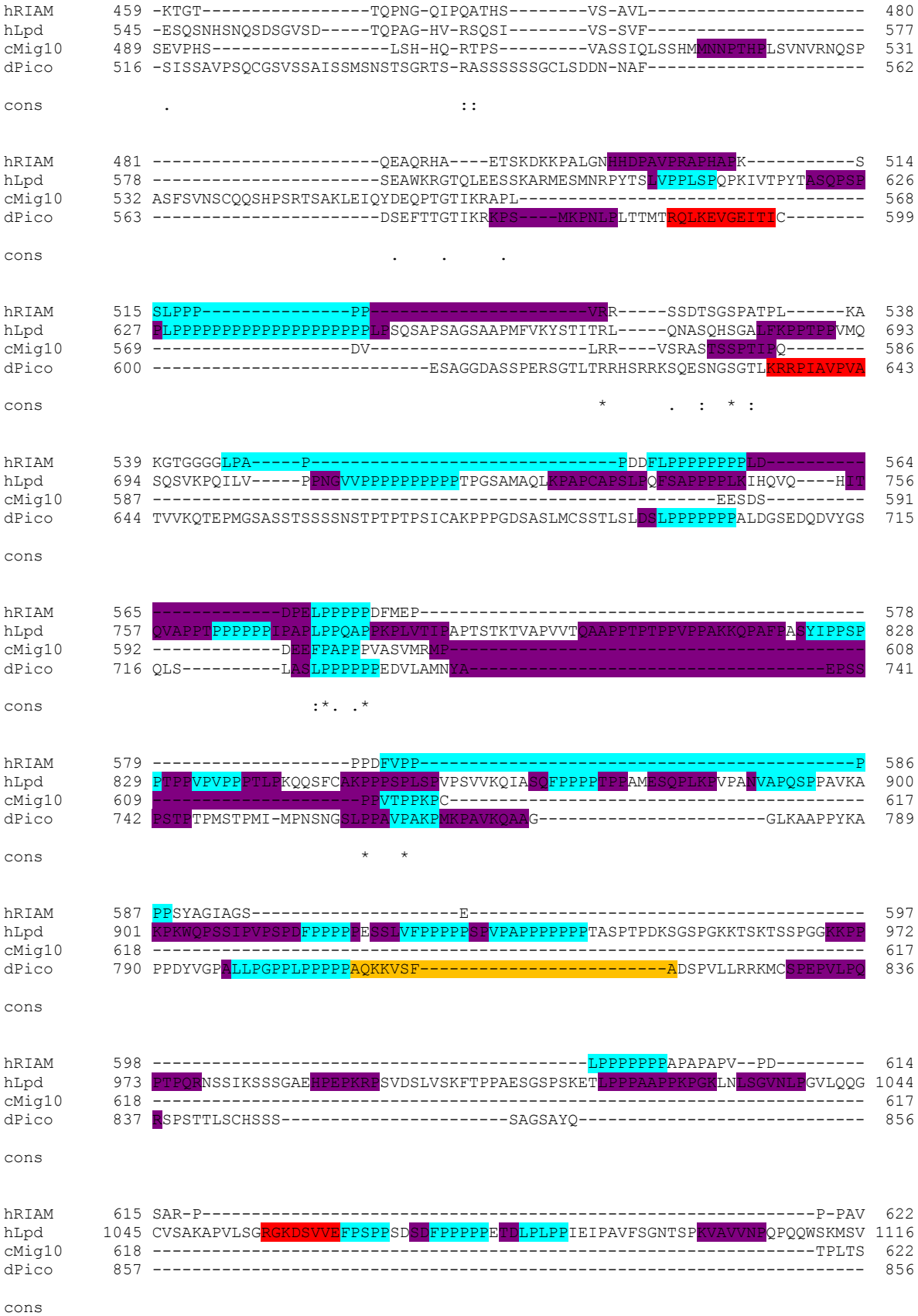
hRIAM 459 -KTGT----------TQPNG-QIPQATHS--------VS-AVL---------- 480
hLpd 545 -ESQSNHSNQSDSGVSD-----TQPAG-HV-RSQSI--------VS-SVF---------- 577
cMig10 489 SEVPHS----------LSH-HQ-RTPS---------VASSIQLSSHMMNNPTHPLSVNVRNQSP 531
dPico 516 -SISSAVPSQCGSVSSAISSMSNSTSGRTS-RASSSSSSGCLSDDN-NAF---------- 562
cons
hRIAM 481 ----------QEAQRHA----ETSKDKKPALGNHHDPAVPRAPHAPK----------S 514
hLpd 578 ----------SEAWKRGTQLEESSKARMESMNRPYTSLVPPLSPQPKIVTPYTASQPSP 626
cMig10 532 ASFSVNSCQQSHPSRTSAKLEIQYDEQPTGTIKRAPL---------- 568
dPico 563 ----------DSEFTTGTIKRKPS----MKPNLPLTTMTRQLKEVGEITIC-------- 599
cons
hRIAM 515 SLPPP----------PP----------VRR-----SSDTSGSPATPL------KA 538
hLpd 627 PLPPPPPPPPPPPPPPPPPPLPSQSAPSAGSAAPMFVKYSTITRL-----QNASQHSGALFKPPTPFVMQ 693
cMig10 569 ----------DV----------LRR----VSRASTSSPTIPQ-------- 586
dPico 600 ----------ESAGGDASSPERSGTLTRRHSRRKSQESNGSGTLKRRPIAVPVA 643
cons
hRIAM 539 KGTGGGGLPA-----P----------PDDFLPPPPPPPLD---------- 564
hLpd 694 SQSVKPQILV-----PPNGVVPPPPPPPPPTPGSAMAQLKPAPCAPSLPQFSAPPPPLKIHQVQ----HIT 756
cMig10 587 ----------EESDS---------- 591
dPico 644 TVVKQTEPMGSASSTSSSSNSTPTPTPSICAKPPPGDSASLMCSSTLSLDSLPPPPPPPALDGSEDQDVYGS 715
cons
hRIAM 565 ----------DPELPPPPPDFMEP---------- 578
hLpd 757 QVAPPTPPPPPPTPAPLPPQAPPKPLVTIPAPTSTKTVAPVVTQAAPPTPTPPVPPAKKQPAFPASYIPPSP 828
cMig10 592 ----------DEEFPAPPPVASVMRMP---------- 608
dPico 716 QLS----------LASLPPPPPPEDVLAMNYA----------EPSS 741
cons
:*. .*
hRIAM 579 ----------PPDFVPP----------P 586
hLpd 829 PTPPVPVPPPTLPKQQSFCAKPPPSPLSPVPSVVKQIASQFPPPPTPPAMESQPLKPVPANVAPQSPPAVKA 900
cMig10 609 ----------PPVTPPKPC---------- 617
dPico 742 PSTPTPMSTPMI-MPNSNGSLPPAVPAKPMKPAVKQAAG----------GLKAAPPYKA 789
cons
*
hRIAM 587 PPSYAGIAGS----------E---------- 597
hLpd 901 KPKWQPSSIPVPSPDFPPPPPESSLVFPPPPPSPVPAPPPPPPPTASPTPDKSGSPGKKTSKTSSPGGKKPP 972
cMig10 618 ---------- 617
dPico 790 PPDYVGPALLPGPPLPPPPPAQKKVSF----------ADSPVLLRRKMCSPEPVLPQ 836
cons
hRIAM 598 ----------LPPPPPPPAPAPAPV--PD---------- 614
hLpd 973 PTPQRNSSIKSSSGAEHPEPKRPSVDSLVSKFTPPAESGSPSKETLPPPAAPPKPGKLNLSGVNLPGVLQQG 1044
cMig10 618 ---------- 617
dPico 837 RSPSTTLSCHSSS----------SAGSAYQ---------- 856
cons
hRIAM 615 SAR-P----------P-PAV 622
hLpd 1045 CVSAKAPVLSGRGKDSVVEFPSPPSDSDFPPPPPETDLPLPPIEIPAVFSGNTSPKVAVVNPQPQQWSKMSV 1116
cMig10 618 ----------TPLTS 622
dPico 857 ---------- 856
cons

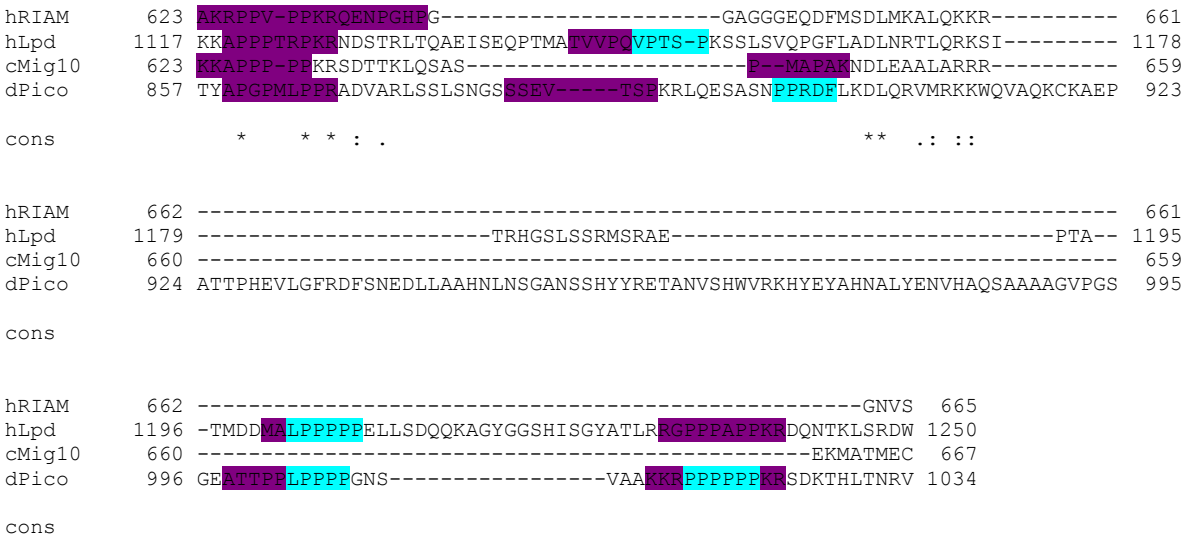

Figure 3.3.2. MRL sequence alignment with predicted functional domains. Complete human RIAM, human Lpd, *C. elegans* Mig-10, and *Drosophila* Pico sequences were assessed individually for potential functional sites. This figure shows an annotated protein alignment were the predicted functional regions are represented by the following colour scheme: RA domain (green); PH domain (yellow); MAPK binding site (red); Proline rich region (blue); SH3 binding site (Purple); Talin binding region (Pink); coiled-coil motif (dark blue); PP1 binding site (orange).

The data presented in Figure 3.3.2. further supports the findings from the domain conservation analysis described earlier. All of the MRL proteins were found to possess clear central RA and PH domains, as well as multiple proline rich and SH3 binding regions distributed amongst an unstructured C-terminus. The novel MAPK binding site bordering the RA domain ($MAPK^{site1}$) was also observed and showed significant sequence conservation, while a talin binding region was identified in both RIAM and Lpd, but not Mig-10 or Pico.

Interestingly, while the second coiled-coil motif commonly attributed to RIAM was identified, a potentially novel coiled-coil region was observed near the N-terminus of Mig-10. It must be noted that the characteristic coiled-coil motif neighbouring the RA domain, highlighted in Lpd, RIAM, and Mig-10, but not Pico, was established through a literature search and not by ELM analysis. Consequently, assuming this coiled-coil region is common to all MRL proteins as

stated in the literature, this result implies that Mig-10, much like RIAM, may contain a second coiled-coil structure within its N-terminus (Colo et al., 2012b). Also worthy of note is the existence of numerous proline rich regions within the N-terminal region of RIAM, Mig-10 and Pico, while SH3 binding sites were identified in the N-terminus of all the proteins studied. Whether these motifs play a significant role in MRL functionality remains to be seen, however previous investigations had only focused on their presence in RIAM.

An additional MAPK binding domain ($MAPK^{site2}$) was also observed in both Lpd, RIAM, and Mig-10 close to the highly conserved novel $MAPK^{site1}$ motif described previously in section 3.3.1. This site lies adjacent to the C-terminal side of the common coiled-coil region, but is not present in Pico. Pico and Lpd do, however, possess further MAPK binding regions within their C-terminus, though they do not appear to be conserved and display low ELM probability scores. A conserved PP1 binding motif located at the C-terminus of the RA domain was found in all the proteins analysed, while an extra PP1 binding site was also revealed within the unstructured C-terminal region of Pico only. These sites had already been discovered during the domain conservation analysis, however, no further potential PP1 binding motifs were identified.

3.4. Establishing the MAPK consensus sequence

Both domain conservation and domain sequence analysis have highlighted the existence of a highly conserved MAPK binding motif present in all MRL proteins. Given the potential importance of this site in MRL functionality, accurate characterisation was required not only to ascertain the reliability of these findings, but to also assist in the development of site specific mutants beneficial for future investigations. Accordingly, an alignment of all the MRL sequences identified from the BLAST screen was generated and the region containing the proposed MAPK motifs isolated and analysed using ELM (Figure 3.4.1.).

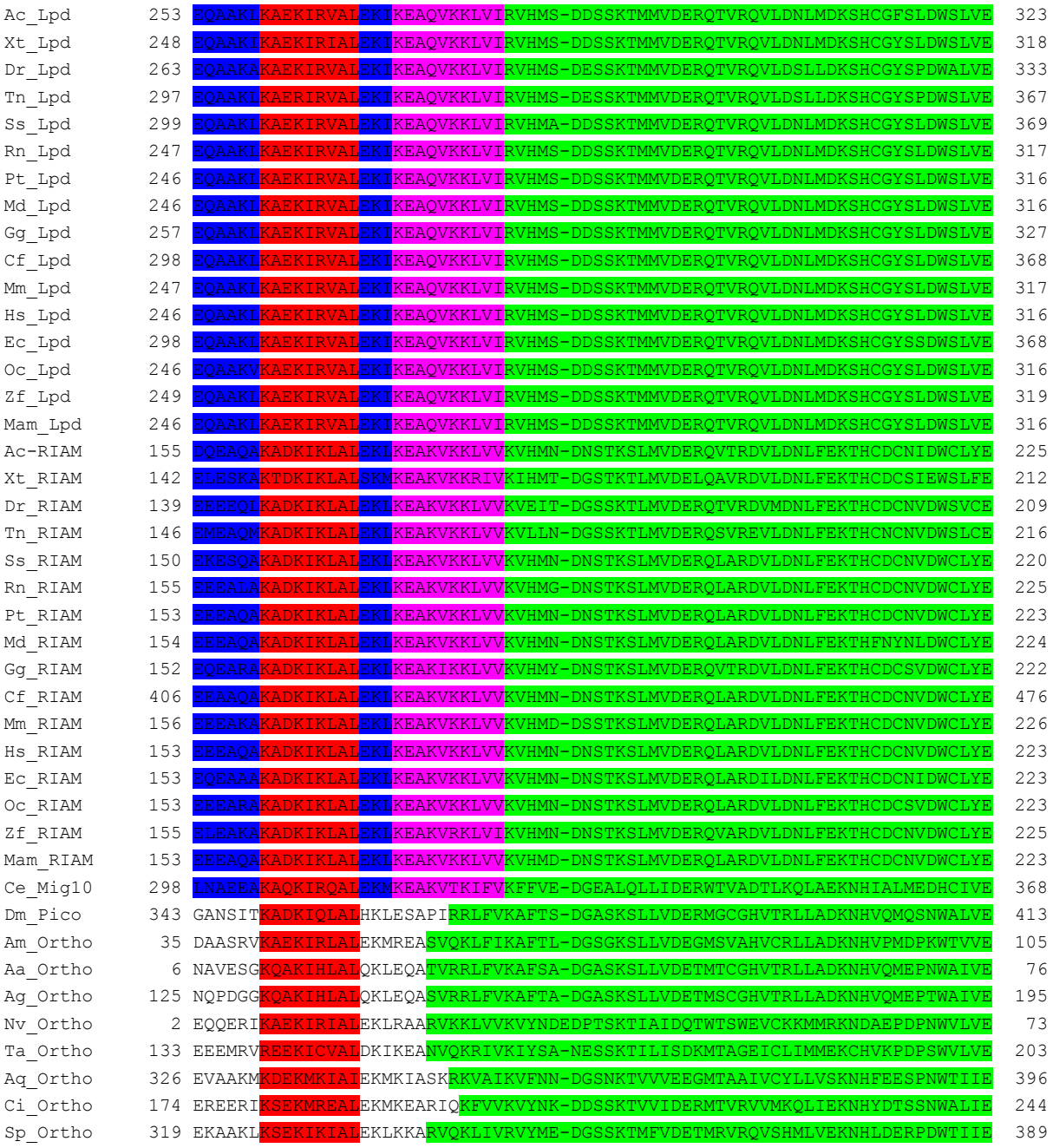

Figure 3.4.1. Annotated alignment of the conserved MAPK region present in MRL proteins. MRL sequence alignments were generated and the area possessing the proposed MAPK motif isolated and examined. A highly conserved MAPK binding site ($MAPK^{site1}$) (red) is present throughout all the MRL proteins, while a second adjacent motif ($MAPK^{site2}$) (pink) is found only in Lpd, RIAM and Mig-10. This additional site lies between the boundaries of the coiled-coil region (dark blue) and the RA doamin (green).

The data presented in Figure 3.4.1. confirmed the presence of a highly conserved MAPK binding (red) site neighbouring the RA domain in all MRL proteins. In RIAM, Lpd, and Mig-10, this site is situated within the coiled-coil motif previously characterised within the literature (Colo et al., 2012b). However, Lpd, RIAM and Mig-10 also possess a second conserved MAPK binding motif (pink) not found in the other single orthologues. This domain is positioned between the characteristic coiled-coil motif and RA domains, overlapping the boundary of each slightly. Analysis of both domains reveals the presence of conserved consensus sequences distinctive to each site. $MAPK^{site1}$ found in all the MRL proteins has a consensus sequence of KXXKIZXAL, were X denotes any amino acid and Z represents a basic residue; while $MAPK^{site2}$ has KEAK/QVKKLVV/I as its consensus. The presence of a clear consensus sequence for both proposed binding sites offers significant support for the concept of MAPK binding. Further evidence is provided by the exceptionally high level of sequence similarity that occurs in this region; with the MAPK binding sites exhibiting 73%[1] and 80%[2] sequence identity compared with the 44% and 52 % found within the characteristically conserved RA and PH domains respectively.

3.5. Discussion

The methods employed in this chapter were able to identify the highly conserved central RA and PH domains, as well as the proline rich and SH3 binding regions present in the unstructured C-terminus, features previously reported as common to all MRL proteins (Krause et al., 2004, Lafuente et al., 2004, Lyulcheva et al., 2008, Colo et al., 2012b). They also detected the talin binding sites located at the N-terminus of Lpd and RIAM, but failed to recognise coiled-coil motifs present in all MRLs, exposing potential limitations in the prediction of short secondary structures (Lee et al., 2009, Colo et al., 2012b, Chang et al., 2013). Due to the generally strong correlation with previous findings described in the literature, these results provided sufficient confidence in the analytical processes carried out; and as such, novel findings were deemed satisfactory enough to warrant further investigative effort. Consequently, the results from the investigations carried out in this chapter were used as the basis for much of the research presented in this work.

3.5.1. Potential MAPK binding

The presence of highly conserved MAPK binding sites close to the RA domain is extremely interesting. Given the well established roles MAPK plays in regulation and signal transduction, this finding offers potentially key insights into the pathways involved in control of the MRL proteins and their associated factors. Indeed, a recent study has already identified a link between RIAM and the MAPK Erk1/2 in promoting FA disassembly (Colo et al., 2012a). MAPKs have been shown to tightly cooperate with Ras-like GTPases in numerous signalling cascades (Krishna and Narang, 2008, Wittinghofer and Nassar, 1996). Consequently, the closeness of the MAPK binding sites to the well defined RA domain may be linked to this collaboration and should be investigated further.

The conserved MAPK motif present in all MRL proteins is located within the coiled-coil region recently shown to contribute to homodimeric binding in Lpd (Chang et al., 2013). How this might affect potential MAPK or homodimeric interactions is still unclear, although it could be hypothesised that binding to one may influence the ability of the peptide to associate with the other. The presence of a second conserved MAPK binding site situated outside the coiled-coil motif in Lpd, RIAM, and Mig-10 could represent a newly formed binding motif that is not influenced by homo- or hetero-dimeric interactions. As such, further questions surrounding the role of these coiled-coil mediated interactions need to be answered before a more complete mechanistic insight can be developed; however, a much more pressing issue is whether MAPKs actually bind directly, and if so, where?

3.5.2. Other potential findings of note

In addition to the discovery of a potential MAPK binding site, the results presented in this chapter also alluded to other possible findings of note, with the first being the identification of a second coiled-coil motif at the N-terminus of Mig-10. A second coiled-coil region present in RIAM is already commonly acknowledged, however, the motif recognised in Mig-10 was not aligned with that found in RIAM (Lafuente et al., 2004). Instead, this site appears to align with the talin binding domains present at the N-terminus of Lpd and RIAM (Lee et al., 2009).

No distinguishable talin binding sites were identified and no direct interaction has yet been reported in either Mig-10 or Pico. Given the key role Talin plays in linking FAs to the cytoskeletal matrix, and the clear associations already identified in Lpd and RIAM, it would be surprising if this was not a common feature in all MRLs (Goult et al., 2013, Lee et al., 2009). Interestingly, the talin binding sites present in RIAM and Lpd were found to possess an amphipathic helical structure (Lee et al., 2009). Taken together, the coiled-coil motif identified in Mig-10 may act as a site for Talin binding, however, the lack of any such motif in Pico does raise questions as to whether this interaction occurs in simpler organisms. As such, determining whether Pico can also interact with Talin will be of some importance, even if a precise binding site cannot be determined at this stage.

A well conserved PP1 binding site was also identified at the C-terminus of the RA domain in all the MRL proteins analysed, while a second C-terminal PP1 motif was found only amongst the insecta. Previous work performed in the Bennett lab has confirmed that *Drosophila* Pico is able to interact directly with PP1, however, mutational analysis revealed this association to only take place at the insect specific C-terminal site (Lyulcheva, 2006, Bennett et al., 2006). While this finding does not preclude the possibility of PP1 binding in the non insecta MRLs, doubts obviously exist, even though an interaction with such a fundamental phosphatase would usually be mechanistically conserved. It may indeed be the case that PP1 can bind to the site present in the RA domain, although it is also possible that another phosphatase may bind or PP1 might interact via one of the other MRL associated proteins eg Profilin (Shao and Diamond, 2012). Either way, it is essential to discern the role PP1 plays in Pico's overall functionality so that the responsibility phosphatases could have in MRL regulation can be ascertained, even if the phosphatases in question are not PP1.

Little is currently known about the effects of posttranslational modifications or phosphorylation on the MRL proteins. The presence of numerous sites with the potential to be modified in some way certainly offers a likely explanation for how MRL protein interactions and/or localisation may be regulated. This is especially true considering the presence of conserved MAPK binding motifs and the proposed interaction with PP1. Consequently, developing an understanding of

how these modifications, particularly phosphorylation, affect MRL interactions and functionality will be crucial.

4. Tool Generation

4.1. Introduction

To identify proteins that interact with the MRL proteins and determine the precise sites of binding, researchers have utilised a variety of techniques; most notably yeast-two-hybrid and immunoprecipitation assays to confirm direct interactions of both full and incomplete peptides with their associated proteins, and co-localisation studies as further corroboration of their findings. Identification of specific binding regions has been achieved by domain mapping experiments and the use of arrays consisting of diminutive 15-20mer peptides spotted onto membranes (Krause et al., 2004, Lafuente et al., 2004, Jenzora et al., 2005, Lee et al., 2009). While these methods have provided clear evidence supporting the existence of various interactions, due to the nature of the investigations performed, only limited information can be inferred about how these associations affect MRLs binding affinities and overall functionality.

Although deletion analysis where single or multiple binding domains are completely removed from the peptide sequence may appear to offer a suitable investigative route, the elimination of large binding regions, such as the RA or PH domains, is liable to impair correct tertiary protein formation and introduce erroneous findings. Given the complex nature of many protein configurations, even the deletion of small motifs may have significant effects. Consequently, studies have begun to focus on mutating a small number of key residues required for a specific interaction to minimise off-target effects on other regions within the protein structure.

While identifying functionally important amino acids to substitute is straightforward for the majority of short, simple motifs such as the PP1 or MAPK binding sites, the more substantial and complex RA and PH domains present a significantly tougher challenge. Works published by Fridman *et al.* 2000 and Shirouzu *et al.* 1999 have gone some way to addressing these issues within the RA domain, as modifications to key consensus residues were found to enhance or reduce Ras binding respectively in other RA domain containing proteins. Hence, by comparing the RA domains used in these studies to those found within the MRL proteins, it may be possible to identify the crucial residue changes required to recreate these alterations in Ras affinity.

In addition to studying the effects of individual binding site mutations on MRL functionality, it is also important to assess the role modifications, such as phosphorylation, play in regulating their interactions and overall activity. This is especially true following the identification of MAPK and PP1 binding sites, as well as the presence of numerous potential post-translational modification sites outlined in the previous chapter. Serine, threonine and tyrosine represent the three most commonly phosphorylated amino acids in eukaryotes, however, analysing the effects of phosphorylation unequivocally is often impractical. Instead, phosphorylation of these residues can be imitated by replacing the amino acid of interest with one displaying structural similarity to the phosphorylated form. An illustration of serine phospho-mimicry is shown in Figure 4.1.1.

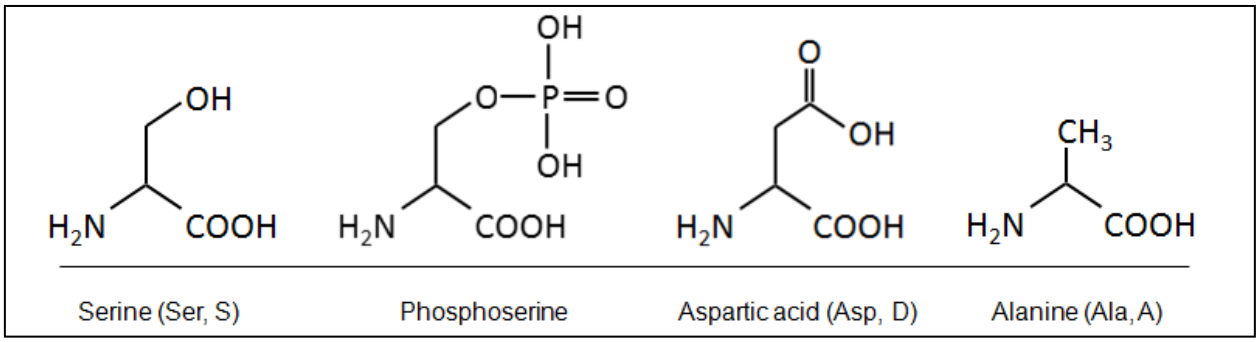

Figure 4.1.1. A structural representation of phospho- and dephospho-mimicry of serine. Aspartic acid, with its negatively charged carboxylate (COO^-) ion, is able to partially mimic the structure and charge of phosphoserine. Conversely, alanine lacks the -OH group required for phosphorylation and can therefore act as a permanently dephosphorylated form of serine.

Serine possesses a characteristic CH_2OH group attached to the standard amino acid backbone. When phosphorylated, a distinctive highly charged PO_4^{3-} phosphate group replaces the hydroxyl (OH^-) ion which typically lacks any resonance structures when attached to R-CH_2, and therefore carries no formal charge. Aspartic acid, one of only two acidic amino acids occurring naturally, displays a very similar backbone to serine, differing only in the presence of a carboxylic acid (COOH) group in place of the hydroxyl ion. This acidic group readily loses its hydrogen leading to the formation of a negatively charged carboxylate (COO^-) ion. While this carboxylate ion exhibits a lesser charge than a phosphate group, it is often strong enough to mimic the effects of

phosphoserine on local tertiary peptide structure, especially when considering the lack of any significant charge normally present within serine alone.

The slightly larger glutamic acid forms the second acidic residue present in nature and is commonly used as a phosphomimetic for both threonine and tyrosine. Glutamic acid shares a reasonable degree of structural homology with threonine and emulates phosphothreonine in a similar way to aspartic acid with serine. Tyrosine, on the other hand, possesses a distinctive aromatic ring not present in glutamic acid, however, no other suitably structured amino acid exists naturally that can replicate a phosphomimetic form of this residue. As such, glutamic acid is often used due to its larger size, but must be extensively validated before any decisive conclusions are made as this change often displays an effect reminiscent of tyrosine to alanine mutations.

As well as mimicking phosphorylation, it is also possible to generate non-phosphorylatable mutants where the addition of a phosphate group is impossible. For serine and threonine, alanine is utilised as a replacement residue as the lack of an -OH group prevents phosphorylation from taking place (Figure 4.1.1.). It must be noted that alanine is smaller than both serine and threonine and does not display the nucleophilic properties found in the aforementioned amino acids. In the case of tyrosine, phenylalanine can act as a dephosphomimetic residue as it possesses the characteristic aromatic ring, but lacks the critical -OH group.

4.1.1. Aims

The purpose of the research untaken in this chapter was to design, and subsequently generate, the tools required to achieve the overarching objectives set out for this project. Initially, the potential sites of phosphorylation in Pico were assessed by analysing the ability of activated kinases to phosphorylate short 15mer peptides representative of every serine, threonine and tyrosine residue present in the protein. The ability of PP1 to dephosphorylate these sites was then investigated to pinpoint sequences capable of displaying reversible phosphorylation and to better understand the role PP1 may play in Pico regulation. The results from these investigations were employed in conjunction with previous findings mapping protein phosphorylation sites from a large scale

screen of Kc167 cells (Bodenmiller et al., 2007), to assist in the design of phospho- and dephospho-mimetic forms of Pico. Protein binding mutants possessing alterations to key residues within specific motifs were also devised using the data presented in Chapter 3. The aforementioned mutants were then generated and shuttled into appropriate vectors enabling their expression in both *Drosophila melanogaster* and S2 cells. Following incorporation of the apposite constructs into fruit flies, the resulting lines were characterised to ascertain the inserts chromosome location and relative expression levels. Attempts were also made to generate both stable and transiently transfected S2 lines expressing each of the mutant constructs.

4.2. Phosphorylation site analysis

A previous screen carried out by Bodenmiller *et al.* 2007 mapping phosphorylation sites in a variety of proteins identified three distinct phosphorylated serine residues in Pico at position 624, 627, and 819. In order to confirm these findings and discover potential phosphorylation sites not identified by this screen, a peptide array consisting of diminutive 15mer peptides representing every serine, threonine and tyrosine residue contained within Pico was produced. The residue being assessed was positioned in the centre of each short peptide to increase the opportunity for prospective target sequences flanking either side to be recognised, while substituting the amino acid with a suitable alanine or phenylalanine acted as a negative control. As some peptide regions contained more than one potentially phosphorylatable residue, control peptides were also incorporated whereby serine, threonine or tyrosine residues not under investigation were replaced with an appropriate alanine or phenylalanine. A further set of peptides containing specific consensus target sequences for a variety of MAPKs was included to act as a positive control. The complete list of the 598 peptide sequences used in this study can be found in Appendix 2.

The array was exposed to radiolabelled (γ-^{32}P) ATP combined with a selection of individual kinases considered likely regulators of MRL activity to ascertain potential phosphorylation target sites for each enzyme. An activated form of the tyrosine kinase Abl was initially investigated due to its previously identified interaction with Lpd (Michael et al., 2010). The resultant findings from autoradiography analysis are shown in Figure 4.2.1.

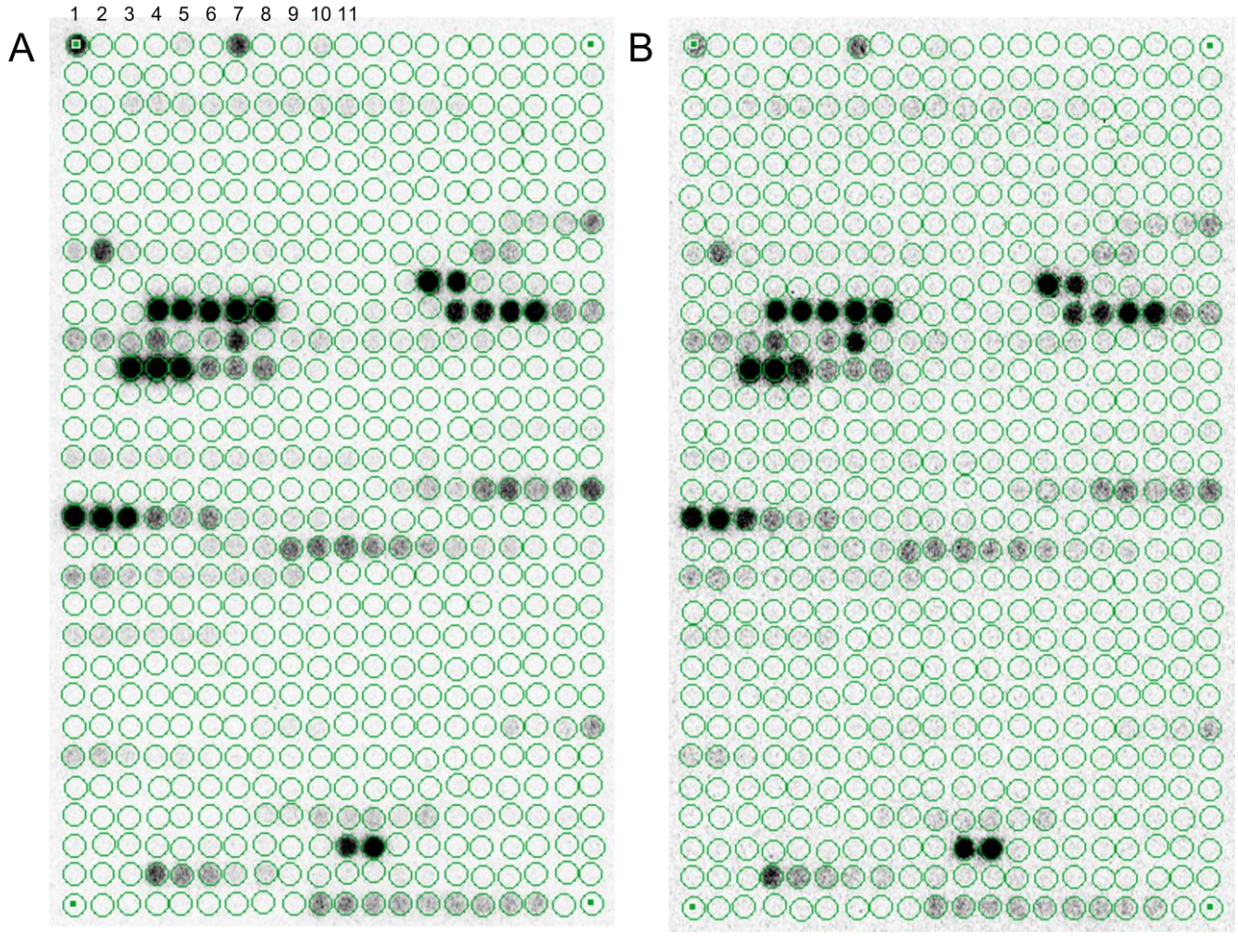

Figure 4.2.1. Results of peptide array following exposure to γ-^{32}P ATP and the tyrosine kinase Abl. (a) The peptide array was exposed to γ-^{32}P ATP and activated Abl kinase before autoradiography fluorescence was assessed to determine the sites of phosphorylation. This analysis identified Y395 and Y396 as potential residues phosphorylated by Abl. Peptides corresponding to target consensus sequences for 1) PKC, 2) c-Abl, 3) EGFR, 4) INSR, 5) JNK1, 6) PKA, 7) CDC2, 8) Erk1/2, 9) APK, 10) GSK3, and 11) p38, were included as positive controls. (b) The array was then incubated with the phosphatase PP1 to identify sites capable of displaying PP1 mediated reversible phosphorylation. The results from subsequent autoradiography analysis demonstrated very little dephosphorylation occurring at any of the scoring peptides.

Initial assessments of the results obtained in Figure 4.2.1.a indicated that the positive controls for Protein Kinase C (PKC) (peptide 1) and Cell Division Controlling Protein 2 (CDC2) (peptide 7) were phosphorylated, however, the Abl target sequence (peptide 2) was not. They also showed that many of the peptides were capable of being phosphorylated by Abl kinase, however, closer inspection of scoring sequences revealed that many of the negative controls had been phosphorylated as well. By only considering those phosphorylated peptides where the negative control did not register as a hit, the results indicated that Y395 and Y396 (peptides 184-188), may represent sites of Abl phosphorylation.

Next, due to its previously described interaction with Pico, the array was incubated with an activated form of the phosphatase PP1. The subsequent results generated following examination of autoradiography fluorescence (Figure 4.2.1.b) revealed very little decrease in the levels of phosphorylation across all of the peptides. Any reduction in signal observed was in line with the expected decay of γ-^{32}P, indicating that no PP1 mediated dephosphorylation occurred at these sites. While this result may have been expected given PP1s preference towards serine and threonine compared to Abl's predilection for tyrosine, many of the scoring peptides only contained serine or threonine. Taken together with the appearance of phosphorylated negative controls and apparent serine/threonine phosphorylation by a predominantly tyrosine specific kinase, this finding raised some significant questions over the validity of this investigation.

Lastly, as a means of cleaning the peptide array for further investigations with other kinases, the membrane was exposed to λ protein phosphatase (λPP). λPP displays activity towards phosphorylated serine, threonine and tyrosine residues, however, much like PP1, very little change in phosphorylation state was observed across all of the peptides following autoradiography analysis (data not shown). Consequently, before any further investigations could be performed, the peptide array was left for a sufficient amount of time to allow the γ-^{32}P to decay through numerous half lives.

The next kinase assessed was the serine/threonine specific Erk1/2, selected due to its role in many growth and migration related signalling cascades although, the recent link with RIAM mediated FA disassembly has lent further support for this choice (Colo et al., 2012a). Before

commencing the investigation, autoradiography analysis was performed to confirm sufficient γ-^{32}P decay (data not shown), and following a satisfactory outcome, the peptide array was incubated with γ-^{32}P ATP and activated Erk1. Erk1 was chosen over Erk2 as it showed slightly greater homology with the *Drosophila* homolog Rolled, although both peptides display significant sequence identity (over 85%) with each other (Boulton and Cobb, 1991). The results generated following autoradiography examination are shown in Figure 4.2.2.

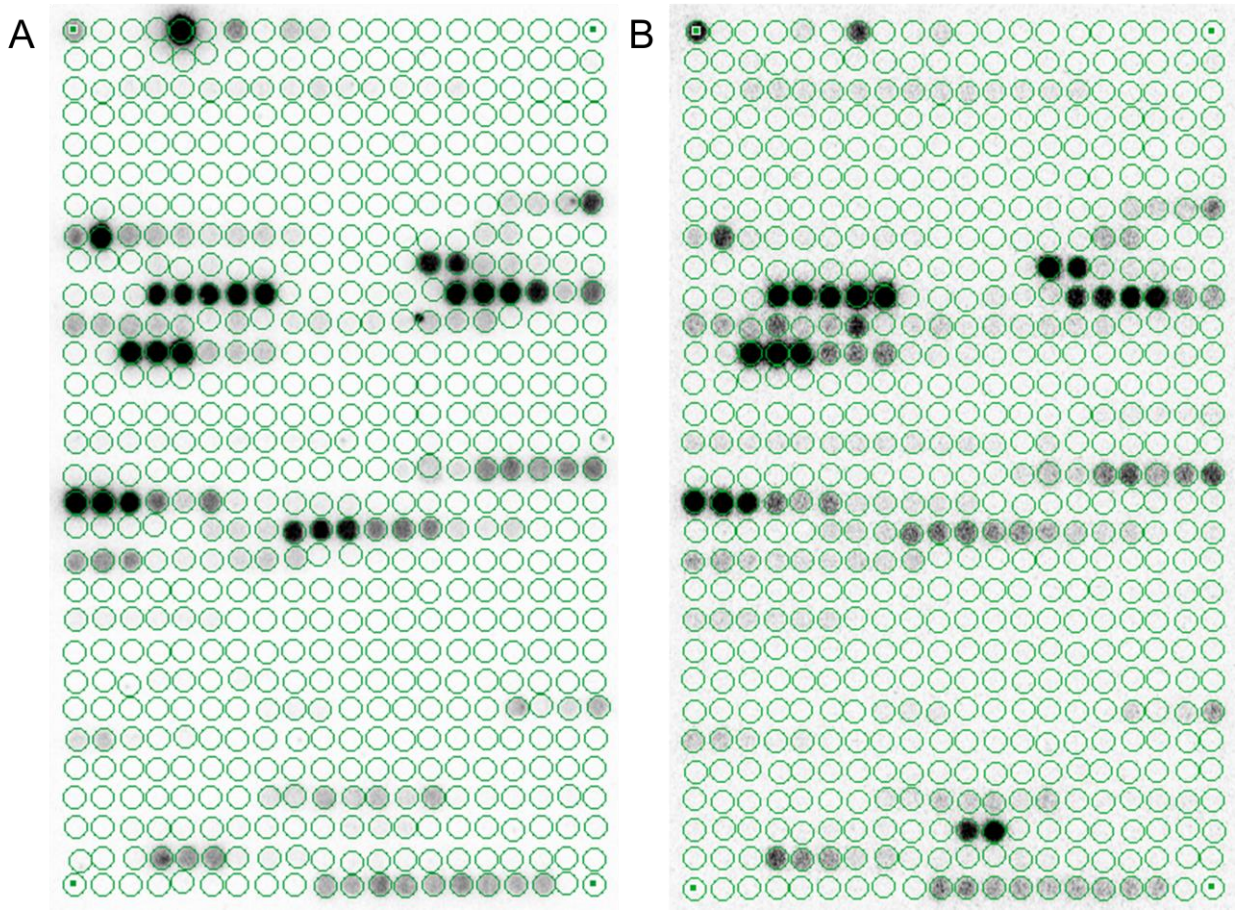

Figure 4.2.2. Results of peptide array following exposure to γ-^{32}P ATP and the serine/threonine kinase Erk1. (a) The peptide array was incubated with γ-^{32}P ATP and activated Erk1 kinase before being assessed by autoradiography to determine the sites of phosphorylation. Analysis revealed the results obtained were almost identical to (b) those observed following exposure to Abl kinase, casting significant doubts over all findings made from this investigation.

Analysis of the results shown in Figure 4.2.2. revealed that the sites of phosphorylation identified following exposure to Erk1 were almost identical to those observed in Abl kinase. Significant differences were only detected in the positive controls, where the Jnk target sequence (peptide 5) displayed notable levels of phosphorylation by Erk1, and at S949 (peptides 551-552), which exhibited phosphorylation of the WT peptide and negative control by Abl but not Erk1. Similar results were also obtained following incubation with both PP1 and λPP as neither phosphatase yielded any discernable reduction in phosphorylation levels across all peptides (data not shown).

While these findings cast significant doubts over the viability of the peptide array in ascertaining potential sites of phosphorylation within Pico, one final experiment was carried out using the serine/threonine p38 kinase. As with Erk1, before any experimentation was carried out the array was left for a period of time to allow the γ-^{32}P to decay thoroughly. The results obtained from autoradiography analysis following incubation of the membrane with γ-^{32}P ATP and p38 were exactly the same as those acquired after exposure to Erk1. Indeed, a similar lack of detectable dephosphorylation was observed when the array was incubated with PP1 and λPP. Consequently, given the seemingly erroneous results obtained from this analysis, the design of phospho- and dephospho-mimetic mutants was performed using data from the Bodenmiller *et al.* 2007 screen alone.

4.3. Designing Pico mutant constructs

Previous work performed in the Bennett lab has demonstrated that overexpression of the Pico short transcript, but not the long, leads to an increase in tissue growth and cell migration. Conversely, knockdown of Pico through RNAi caused reduced growth and retarded migration (Lyulcheva et al., 2008, Lyulcheva, 2006, Taylor, 2010). As a means of confirming that these knockdown phenotypes did not result from erroneous off target effects of the dsRNA, an RNAi resistant WT Pico short construct was designed by exploiting codon redundancy to enable confirmatory rescue experiments to be performed. The resulting transcript was intended to be resistant to both commercially available and in house RNAi constructs, while the codon usage was also tailored for efficient translation within the *Drosophila* system. All subsequent mutants were designed using this WT construct as their foundation, making them RNAi resistant as well.

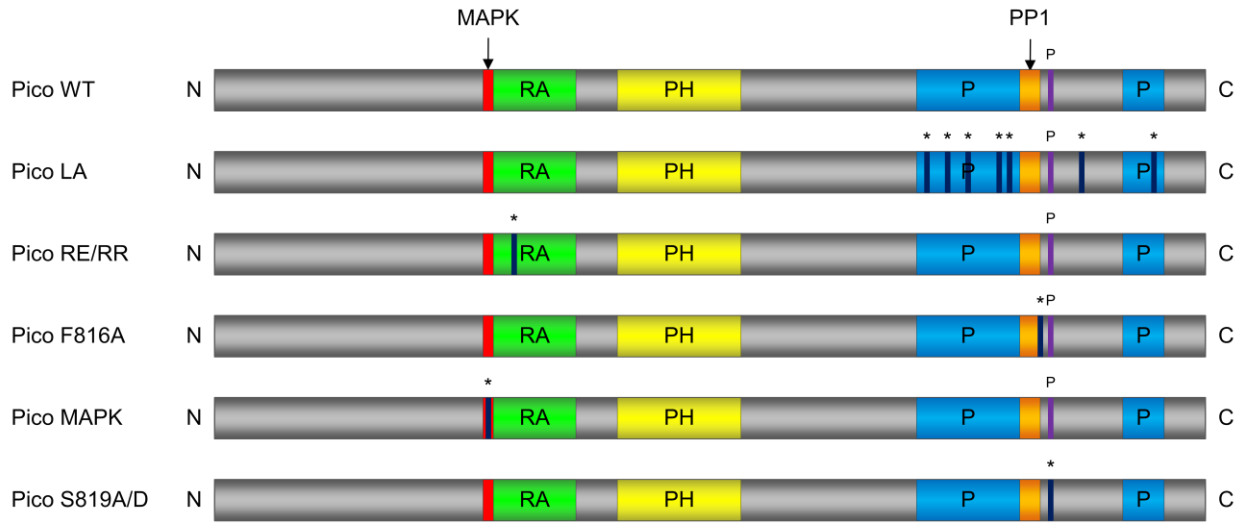

Figure 4.3.1. Schematic representation of the Pico mutant constructs designed. A variety of RNAi resistant mutant constructs have been generated with potential alterations to binding of Enabled (LA), Ras (RE/RR), PP1 (F816A), and MAPKs (MAPK). Two further mutants displaying phosphomimetic (S819D) and permanently dephosphorylated (S819A) properties for the serine at position 819 were also generated. 'P' denotes the site of phosphorylatyion while '*' designates modified regions within each of the constructs.

Based on domain analysis and previous work presented in the literature, the following binding site and de/phosphomimetic mutants were designed (Figure 4.3.1.):

LA Seven leucine to alanine point mutations introduced to characteristic *Drosophila* EVH1 binding sites (LPPPP) identified within the C-terminus of Pico are predicted to interfere with direct Enabled interactions. As Enabled has previously been shown to interact with Profilin, it is possible this alteration may also affect associations with chickadee (Krause et al. 2002).

RE (A270K) Previous work performed by Fridman *et al.* assisted in the identification of an alanine at position 270 that may enhance Pico's ability to interact with Ras or Rap when exchanged for lysine (Fridman et al., 2000).

RR (K272A) Findings presented by Shirouzu *et al.* formed the basis for changing a lysine at residue 272 to alanine in the hope of diminishing Pico's capacity to bind with Ras or Rap (Shirouzu et al., 1999).

F816A Previous work performed in the Bennett lab identified a phenylalanine at position 816 which prevents direct interactions with PP1 when replaced with an alanine (Lyulcheva, 2006, Bennett et al., 2006).

MAPK Using the MAPK consensus sequence developed in Chapter 3, it was hoped that exchanging two lysines and a leucine found within the conserved $MAPK^{site1}$ binding region to alanine (K221A; K224A; L229A) will inhibit Pico's potential ability to interact with MAPKs.

S819A The phosphorylation mapping screen performed by Bodenmiller *et al.* identified the serine at residue 819 as a potential site of phosphorylation. Substituting the serine for an alanine would yield a peptide incapable of being phosphorylated at this position (Bodenmiller et al., 2007).

S819D Replacing the serine at position 819 with a phosphomimetic aspartic acid was hoped to sufficiently replicate the effects of phosphorylation previously observed by Bodenmiller *et al.* at this site (Bodenmiller et al., 2007).

The precise sites of each mutation, along with the WT construct DNA sequence, is shown in Appendix 3. It should be noted that despite Bodenmiller *et al.* 2007 identifying three potentially phosphorylated residues in Pico, phospho- and dephospho-mimetic mutants were only generated for the serine found at position 819. This was due to low confidence in phosporylation at positions 624 and 627 as they were each detected only once in the screen, while pS819 was observed 18 times (Bodenmiller et al., 2007).

4.4. Generatinging Pico constructs

Once designed, the RNAi resistant Pico^{WT} construct was synthesised by BioPioneer Inc and inserted into a Gateway® pDONR221 entry vector to enable simple shuttling of the gene into appropriate destination vectors via LR recombination. As the Pico^{LA}, Pico^{F816A}, Pico^{S819A} and Pico^{S819D} mutants had also been devised by that point, BioPioneer developed these constructs as well using the pDONR221 Pico^{WT} vector as a backbone.

To create the Pico^{RE}, Pico^{RR} and Pico^{MAPK} mutant constructs, site-directed mutagenesis of the pDONR221 Pico^{WT} vector was attempted using PCR. Briefly, overlapping primers complementary to the proposed mutational sites, but possessing specific changes required for each construct, were synthesised. They were used in conjunction with a high fidelity Taq based DNA polymerase to amplify the complete pDONR221 Pico^{WT} vector via PCR, before the resultant products were exposed to the endonuclease *Dpn*I. *Dpn*I specifically cleaves methylated DNA created by DNA methyltransferases (DNMTs) present within the host cell of the parental Pico^{WT} strand, but not the PCR reaction mix. Consequently, only the pDONR221 Pico^{WT} vector DNA was digested, leaving the new mutants untouched and able to be transformed into chemically competent cells following end joining by DNA ligase. However, despite repeated rounds of gradient PCR and various alterations to the reaction mix's composition, neither agarose gel electrophoresis nor direct transformation into competent cells yielded any positive results (data not shown).

Instead, as the Pico^{RE}, Pico^{RR} and Pico^{MAPK} mutational sites were in close proximity, it was deemed practical to employ BioPioneer to generate short inserts corresponding to a region of Pico situated between single *Sac*I and *Sal*I sites containing the desired modifications (Figure 4.4.1.). These sequences were then inserted into an appropriate vector to enable replication within transformed cells. Both the mutant and pDONR221 Pico^{WT} vectors were digested with *Sac*I and *Sal*I and run on an agarose gel to separate the products (data not shown). The resultant 444bp and 4790bp bands were cut from the mutant and pDONR221 Pico^{WT} lanes respectively, before being purified with a gel extraction kit. T4 DNA ligase was utilised to join the cohesive end termini together and the products transformed into competent cells. These cells were

subsequently plated onto selective media and single colonies picked. A variety of techniques, such as PCR, restriction digestion, and sequencing, were then employed to validate the newly formed constructs (data not shown).

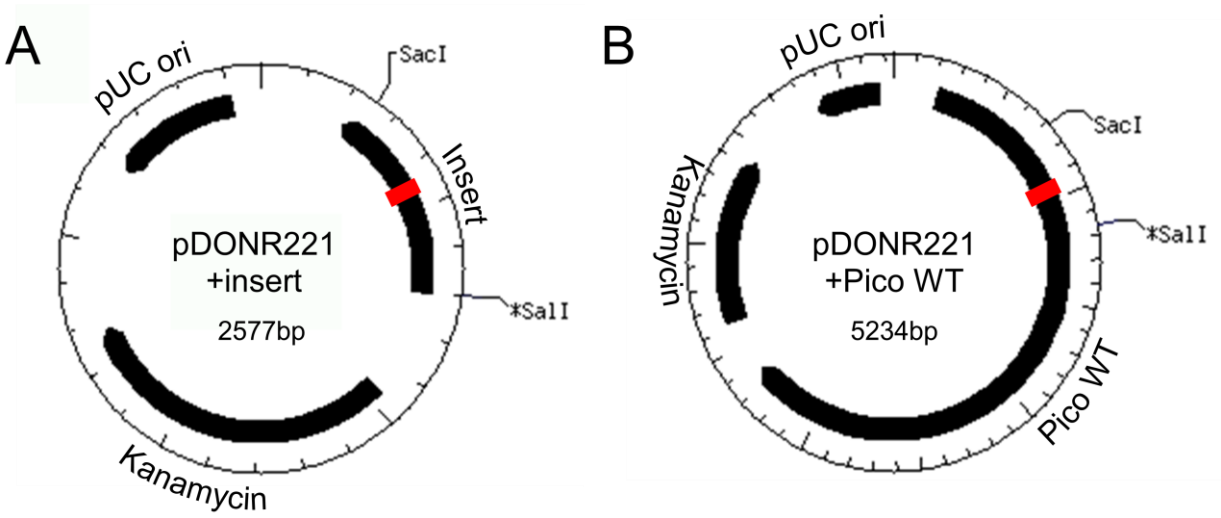

Figure 4.4.1. Schematic diagram showing *Sac*I-*Sal*I restriction sites within the Pico$^{RE/RR/MAPK}$ mutant and pDONR221 Pico^{WT} vectors. a) Pico^{RE}, Pico^{RR} and Pico^{MAPK} mutant vector SacI-SalI restriction map. b) pDONR221 Pico^{WT} vector SacI-SalI restriction map. The regions mutated in the Pico^{RE}, Pico^{RR} and Pico^{MAPK} constructs are highlighted in red.

4.5. Insertion of constructs into flies

Following successful generation of the RNAi resistant Pico constructs within the pDONR221 entry vector, an appropriate destination vector needed to be selected to enable their expression within flies using the *Drosophila GAL4-UAS* system. As the constructs had been designed with a stop codon, an appropriate tag could only be translated at the N-terminus. Accordingly, the pTVW (1091) vector from the Drosophila Genomics Resource Centre (DGRC) was identified as a suitable candidate. pTVW (1091) possesses a *UASt* promoter to enable expression under the direction of GAL4, and an N-terminal Venus tag. Venus is an enhanced Yellow Fluorescent Protein (YFP) flurophore derived from Green Fluorescent Protein (GFP) following the addition of several mutations (Rekas et al., 2002). Venus was chosen due to its superior and robust

fluorescent properties, in addition to its successful use in pulldown and Fluorescence Resonance Energy Transfer (FRET) experiments (Nagai et al., 2002).

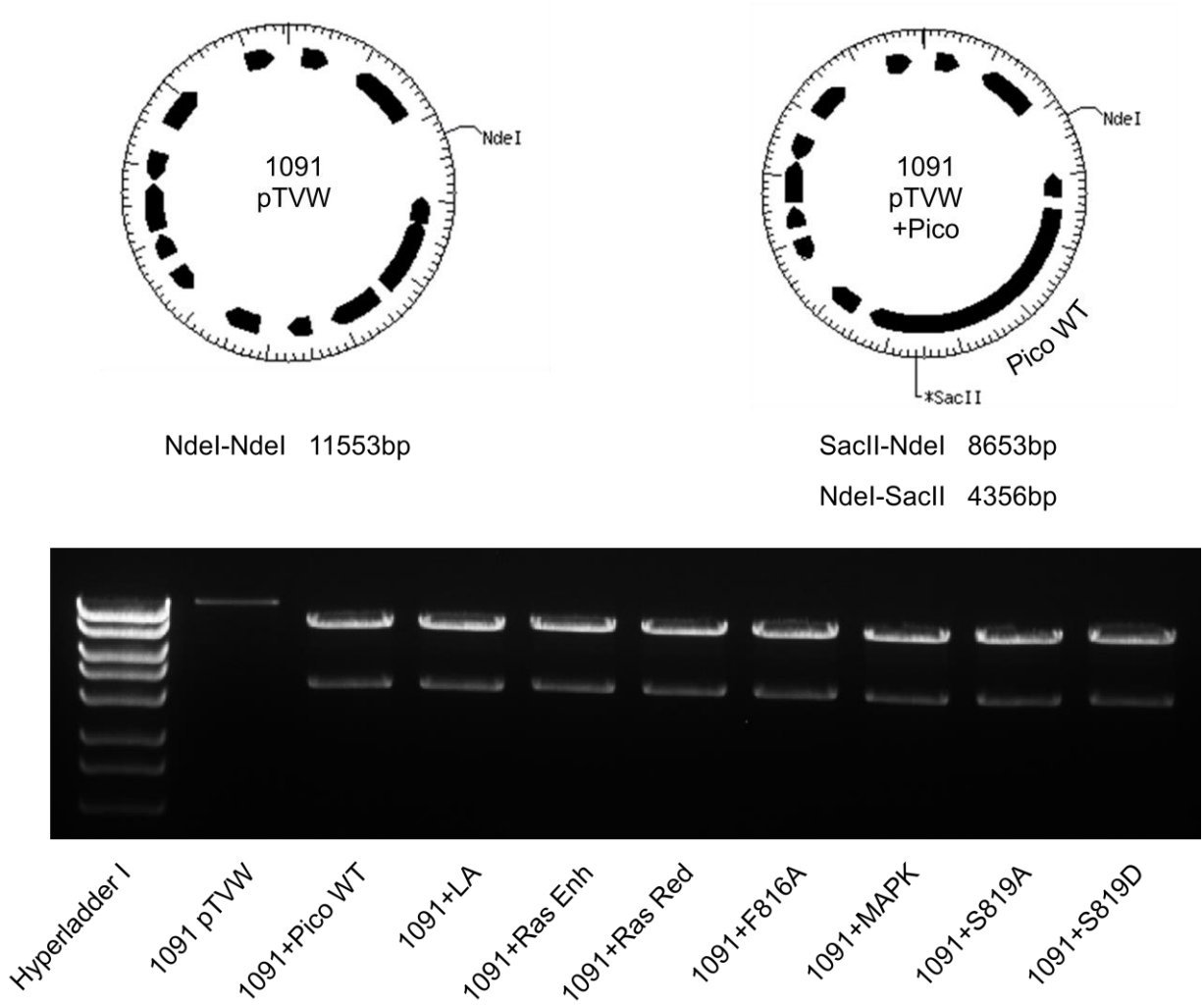

Figure 4.5.1. Agarose gel electrophoresis to validate *pTVW* Pico vectors following LR recombination. *Nde*I-*Sac*II restriction digests were performed on *pTVW* Pico vectors following LR recombination. The resulting products were run on an agarose gel and confirmed correct orientation of the inserted constructs.

LR recombination was performed to shuttle the constructs from the pDONR entry clones into *pTVW* destination vectors. The products of this reaction were transformed into competent cells selected for the presence of amp^r and the absence of a toxic *ccdB* gene in unrecombined

destination vectors. *Nde*I and *Sac*II restriction digestion was used to verify accurate insertion and orientation of the Pico constructs within the *pTVW* vectors. The results confirming correct incorporation by gel electrophoresis of the restriction products is shown in Figure 4.5.1.

Following validation of the destination vectors, transgenic flies possessing copies of the *UAS*-controlled Venus tagged Pico constructs were generated through *P*-element mediated germline transformation by Genetic Services. Briefly, the Pico constructs, positioned between *P*-element ends and alongside a *white*$^{+}$ minigene marker within the *pTVW* vectors, were injected into W^{1118} embryos along with the helper vector pUC*hs*Delta2-3 to provide a source of *P*-element transposase. The *P*-element, with *UASt*-Venus Pico as its cargo, was then randomly transposed to an indiscriminate chromosomal site (Spradling and Rubin, 1982, Sentry and Kaiser, 1992). The resulting flies were then returned for further analysis.

4.6. Characterisation of Venus Pico fly lines

A total of 10 lines were created for each Venus-Pico mutant construct by Genetic Services, however, not all progeny were viable as the random nature of *P*-element insertion can lead to the formation of sickly stocks. Those that did survive were characterised to determine the insert's chromosome location and relative expression level.

4.6.1. Analysis of insert chromosome location

The progeny were initially screened for non-white eyes indicating that the constructs, now permanently associated with a *white*$^{+}$ minigene, had successfully been transformed into the germline cells. The chromosome harbouring each independent insert was determined by crossing individual transgene-carrying males to *w; Tft/CyO* and then crossing the male progeny to *w; Tft/CyO; MKRS/TM6B.* Table 4.6.1. details which chromosome the constructs were inserted into for each line. Following characterisation, each insert was then balanced with an appropriate, dominantly marked, balancer chromosome to prevent recombination and enable stock maintenance (Greenspan, 2004).

Fly Line	Chromosome Loc.	Fly Line	Chromosome Loc.
Pico WT Line 1	**3**	F816A Line 8	**1**
Pico WT Line 2	**3**	F816A Line 9	**3**
Pico WT Line 3	**3**	F816A Line 10	**3**
Pico WT Line 4	**2**	MAPK Line 1	**3**
Pico WT Line 5	**3**	MAPK Line 2	**1**
Pico WT Line 6	**3**	MAPK Line 3	**3**
Pico WT Line 7	**3**	MAPK Line 4	**3**
Pico WT Line 8	**3**	MAPK Line 5	**3**
Pico WT Line 9	**1**	MAPK Line 8	**2**
Pico WT Line 10	**1**	MAPK Line 9	**3**
LA Line 2	**3**	MAPK Line 10	**3**
LA Line 3	**2**	S819A Line 1	**3**
LA Line 5	**3**	S819A Line 2	**2**
LA Line 6	**3**	S819A Line 3	**1**
LA Line 7	**2**	S819A Line 5	**3**
LA Line 8	**3**	S819A Line 6	**2**
LA Line 9	**3**	S819A Line 7	**2**
LA Line 10	**3**	S819A Line 8	**2**
Ras Enh Line 1	**2**	S819A Line 9	**2**
Ras Enh Line 2	**3**	S819A Line 10	**2**
Ras Red Line 2	**2**	S819D Line 2	**3**
Ras Red Line 3	**2**	S819D Line 3	**2**
Ras Red Line 4	**3**	S819D Line 4	**1**
Ras Red Line 8	**3**	S819D Line 5	**3**
Ras Red Line 10	**2**	S819D Line 6	**3**
F816A Line 2	**3**	S819D Line 7	**3**
F816A Line 3	**2**	S819D Line 8	**2**
F816A Line 5	**2**	S819D Line 9	**3**
F816A Line 6	**2**	S819D Line 10	**3**
F816A Line 7	**2**		

Table 4.6.1. Chromosomal location of Venus tagged Pico inserts. Chromosomal location of UAS-Venus tagged Pico inserts in each transgenic fly line.

4.6.2. Analysis of Venus Pico expression levels

Due to the random nature of *P*-element insertion, constructs may be located in regions of generally high (euchromatin) or low (heterochromatin) gene expression, dictating in turn the expression levels of the construct itself. As such, the relative Venus-Pico expression level was assessed for each line. Initial attempts to express the transgenes using the ubiquitous *da-GAL4* and *act5C-GAL4* drivers failed to produce any viable larvae or adult flies expressing the Pico constructs, indicating high Pico levels may significantly disrupt correct larval development and cause lethality.

To combat this lethal effect, the characteristically segmented *enGAL4* driver was used and found to yield viable larvae. Consequently, verification and analysis of ectopic protein expression was first carried out by visualisation of fluorescent Venus in larvae carrying the *enGal4* driver and one copy of the transgene of interest (Figure 4.6.1.). Subsequent attempts to confirm expression levels through Western blot analysis using anti-Pico (3531) and anti-GFP (ABfinity) proved unsuccessful, however, the images generated from the initial visualisation experiments were deemed sufficiently accurate to enable appropriate lines for each construct to be selected for future use (Figure 4.6.1.).

Pico WT

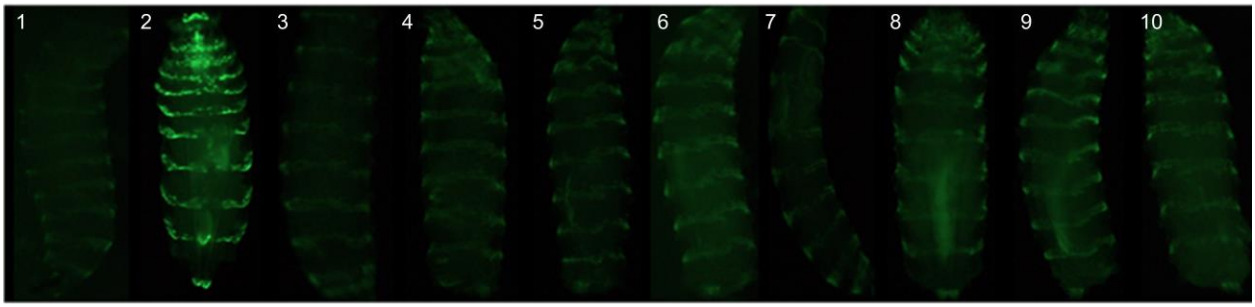

LA

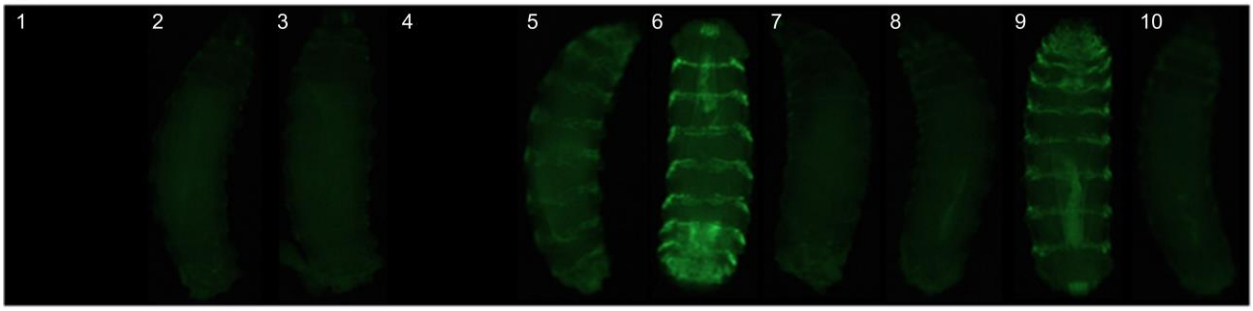

Ras Enhanced

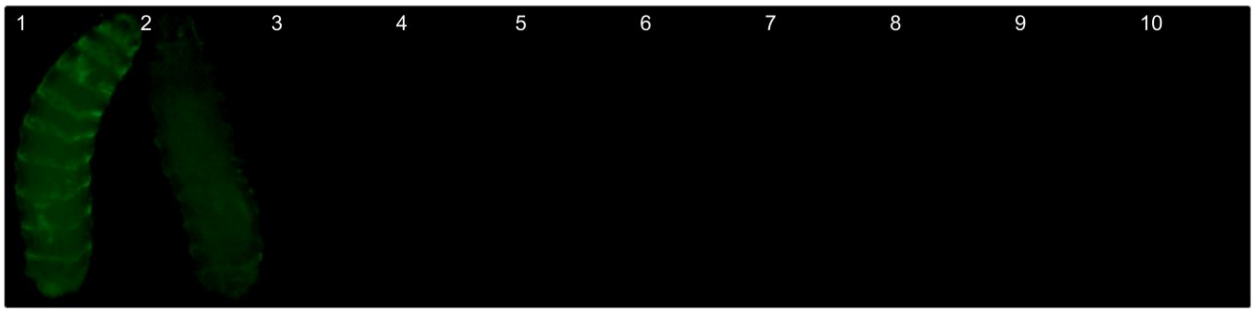

Ras Reduced

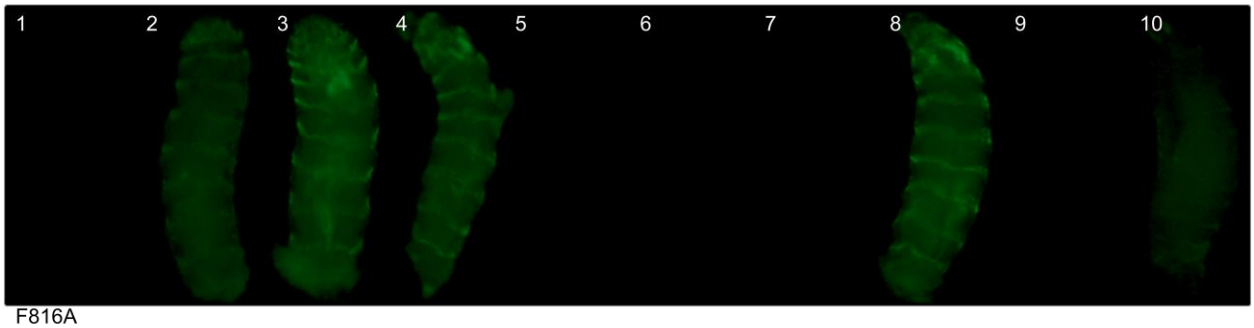

F816A

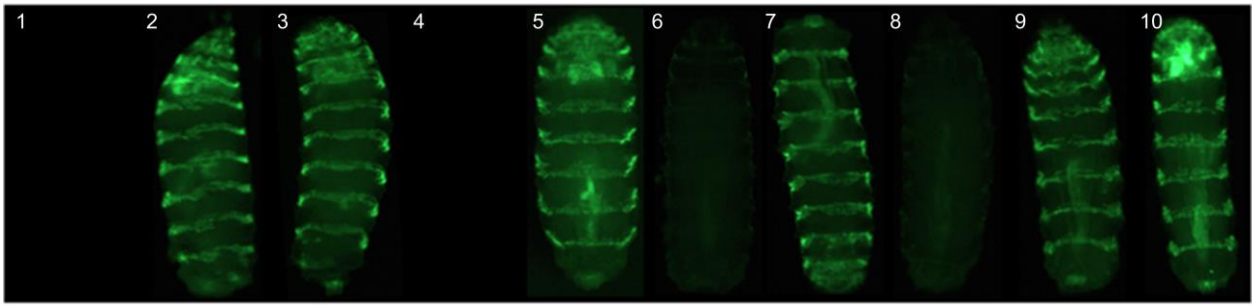

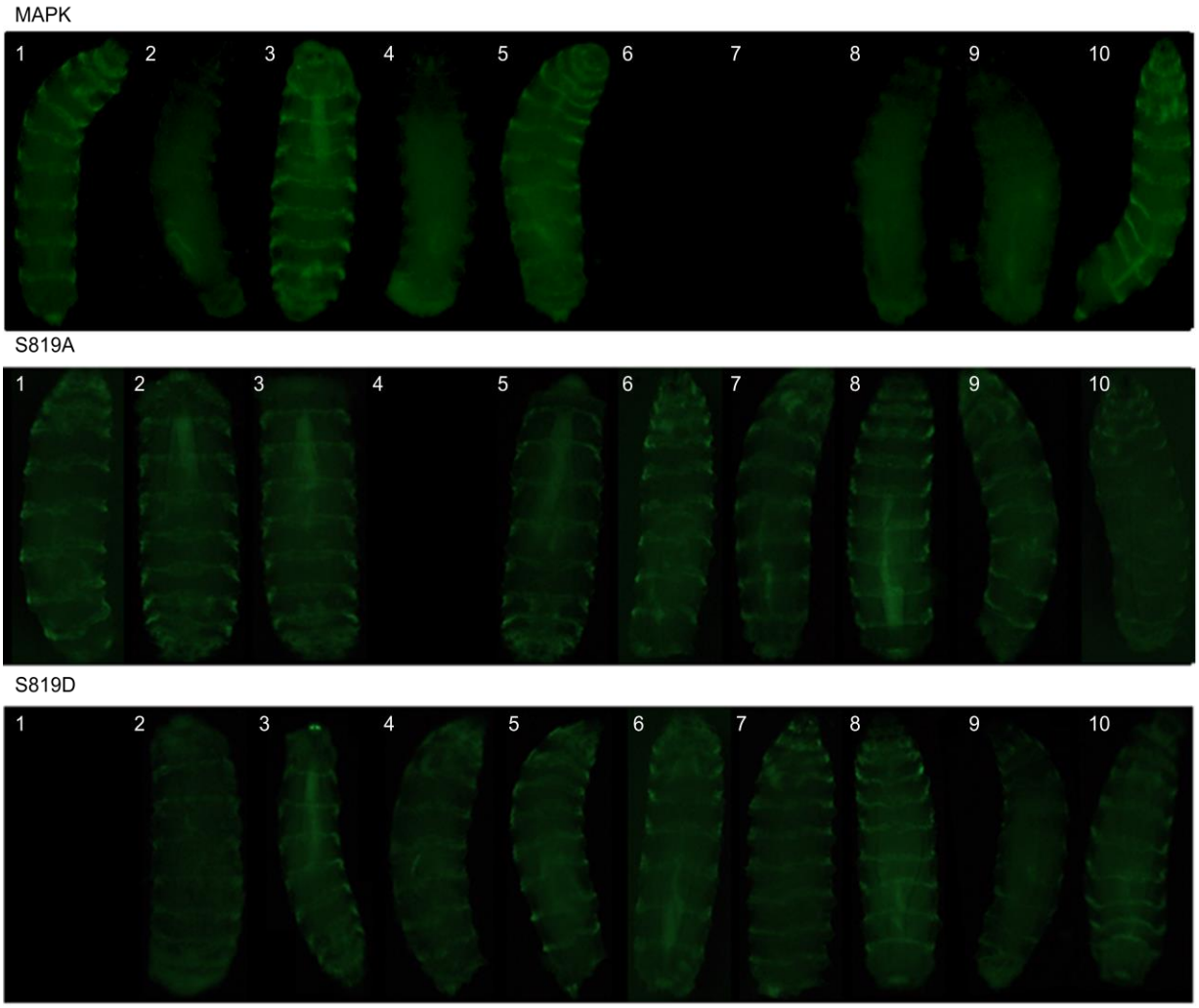

Figure 4.6.1. Visualisation of Venus-Pico expression under the control of *enGAL*. Visualisation experiments were carried out to assess the relative expression levels of Venus-Pico under the control of *enGAL4* for each mutant construct line.

4.6.3. Selection of Venus-Pico lines

Once characterisation was completed, appropriate lines were selected from each construct for use in future experiments. Only lines with constructs located on either the second or third chromosome were considered as some prospective investigations would not be possible with transcripts located on the first. From those lines remaining, suitable choices were made based on their relative expression levels, characterised as either high (e.g. $Pico^{WT}$ 2), moderate (e.g.

Pico^{WT} 4), or low (e.g. Pico^{LA} 2). As some constructs, such as Pico^{F816A} and Pico^{S189A}, possessed lines displaying only high or moderate expression levels, selected lines were placed into one of two apposite groupings (high expression or moderate expression) in accordance with their observed level of transcription. Pico^{WT} line 2 and Pico^{WT} lines 4 and 6 were chosen as comparative controls for the high and moderate groups respectively, enabling accurate conclusions to be made about the mutational effects without confounding expressional effects when analysing phenotypic outcomes of the mutant constructs. Figure 4.6.2. displays the line selected for each construct and indicates which of the two expression groupings they have been placed into.

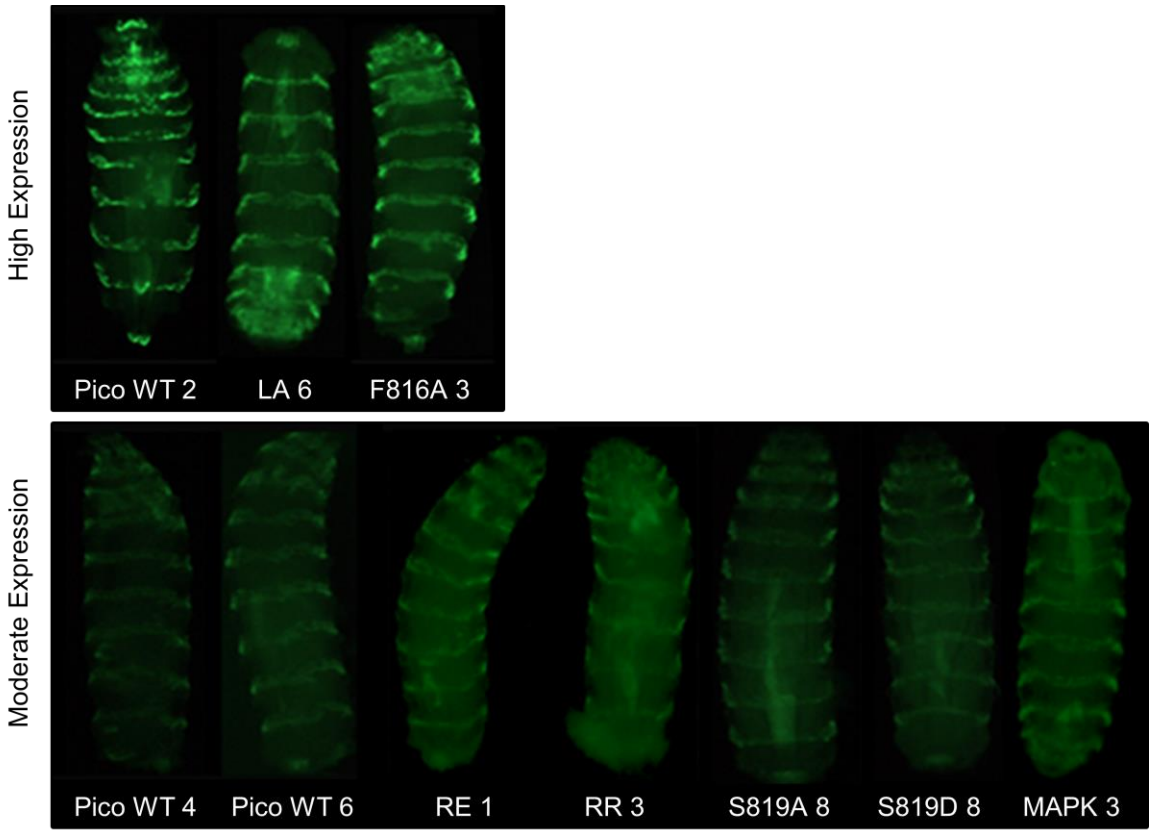

Figure 4.6.2. Visualisation of selected Venus-Pico lines. Venus-Pico lines were selected based on their chromosome location and relative expression levels. Selected lines were subsequently placed into high or moderate expression groupings to enable suitable comparisons to be made during analysis of their phenotypic effects.

4.7. Expressing constructs in S2 cells

As with expression of the transcripts in flies, appropriate destination vectors needed to be selected to enable expression of the Pico constructs within *Drosophila* embryo derived S2 cells (Schneider, 1972). Two suitable vectors were subsequently identified, the first of which was a metallothionein promoted N-terminal Protein A tag (*pMt-PtA*) vector kindly supplied by Paolo D'Avino (University of Cambridge). The use of a copper sulphate induced metallothionein promoter allowed tight control over the expression of each construct, limiting any potential toxicity and enabling a range of time course assays to be carried out. *pAVW* (1087) from the DGRC was the second vector deemed appropriate and consists of a constitutively active *act5c* promoter and an N-terminal Venus-tag to facilitate in a variety of imaging experiments.

Again, LR recombination was performed to shuttle the constructs from pDONR entry clones into the selected destination vectors. The resulting products were transformed into competent cells and selected for on ampicillin plates. As no sequence data was available for *pMt-PtA*, accurate confirmation of correct insertion for this vector was not possible. However, *Sac*I-*Sal*I restriction digestion was at least able to verify insertion had taken place (data not shown). *Nde*I and *Sac*II restriction digestion was used to verify correct insertion and orientation of the Pico constructs within the *pAVW* vectors, with the confirmatory results from gel electrophoresis shown in Figure 4.7.1.

Stably transfected lines were generated by co-transfecting S2 cells with each construct and the Blasticidin resistance gene pCoBlast using Cellfectin. The cell lines were maintained with Complete Schneider's medium containing toxic Blasticidin to continually select for successfully transfected cells. Despite repeated attempts using a wide range of $CuSO_4$ concentrations, it was not possible to express PtA tagged Pico. In addition, constitutive expression of the Venus-Pico constructs appeared to be toxic, with the stably transfected cell lines all demonstrating significantly diminished growth rates and sickly appearance. Consequently, investigations were performed to assess the potential use of transiently transfected cells for imaging and pulldown experiments.

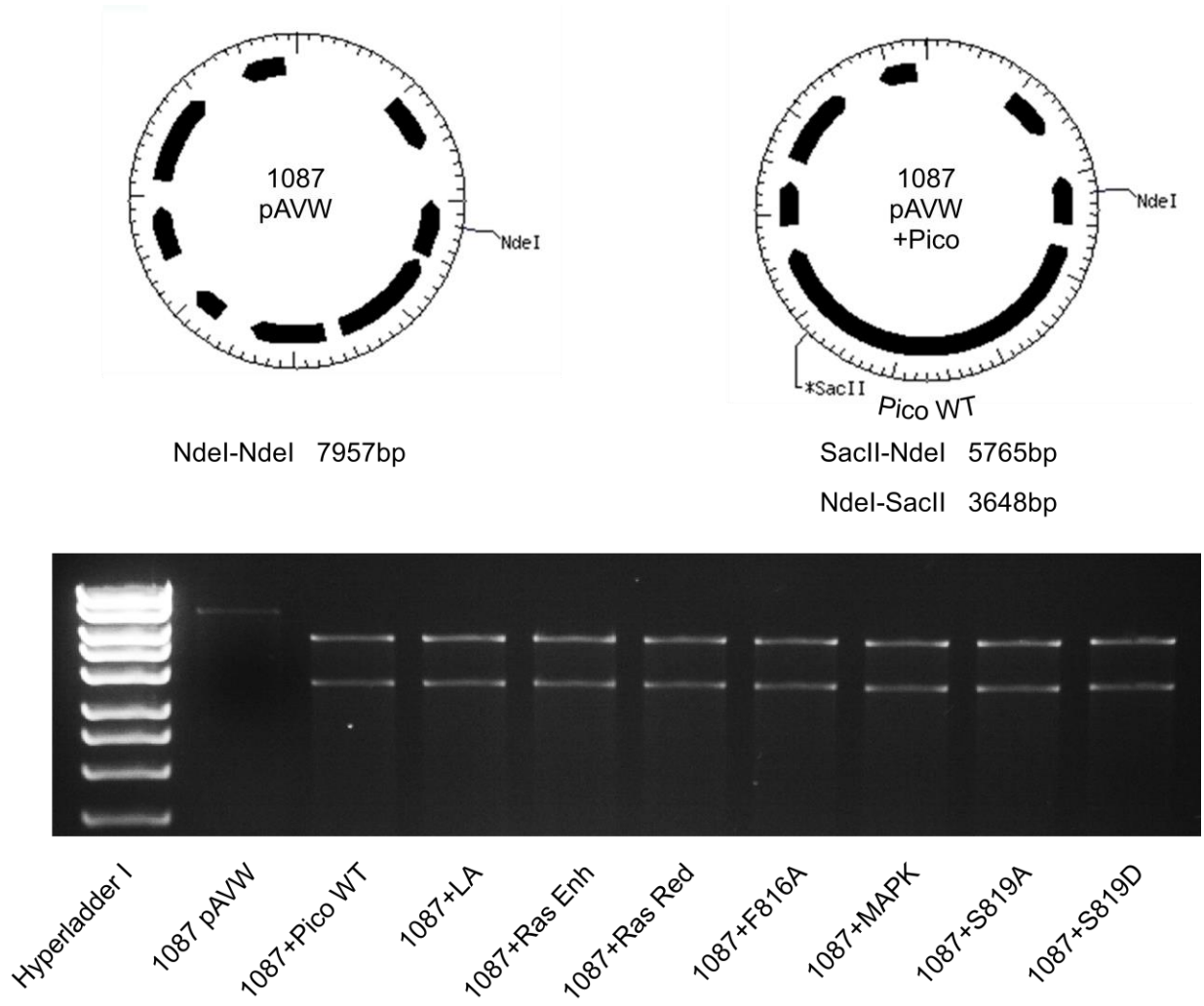

Figure 4.7.1. Agarose gel electrophoresis to validate *pAVW* Pico vectors following LR recombination. *Nde*I-*Sac*II restriction digests were performed on *pAVW* Pico vectors following LR recombination. The resulting products were run on an agarose gel and confirmed correct orientation of the inserted constructs.

Initial investigations using Cellfectin as a reagent for transient transfection of *pAVW* Pico yielded promising results, with an estimated efficiency of approximately 70-80% being observed in a number of experiments (data not shown). However, at an early stage in this study, Cellfectin was discontinued by the manufacturer and replaced with Cellfectin II, which despite its namesake, had a different composition to its predecessor (Invitrogen, personal communication). Despite repeated attempts to optimise, Cellfectin II failed to exhibit a transfection efficiency above 1%.

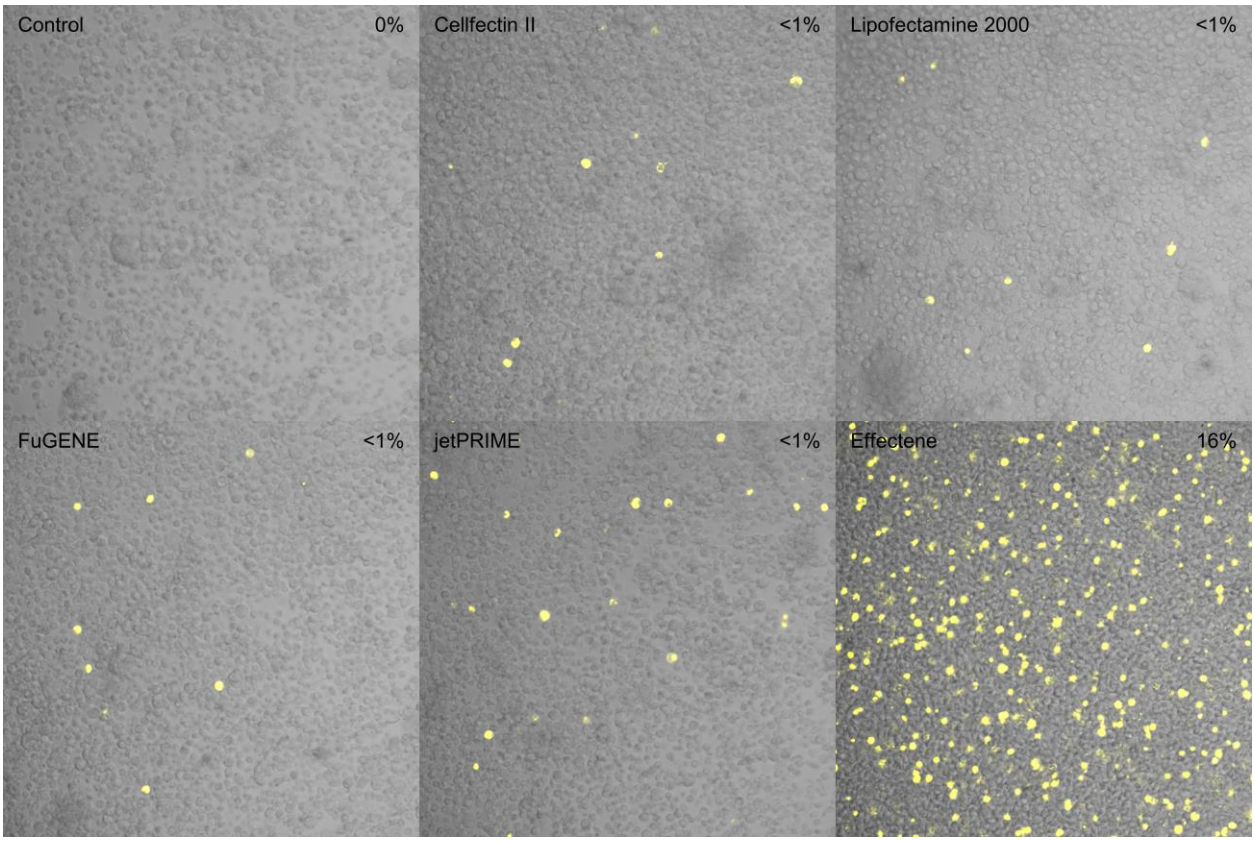

Figure 4.7.2. Confocal analysis of suitable reagent for transient transfection of S2 cells. A range of commercial reagents were examined by confocal microscopy to identify the most suitable for transient transfection of S2 cells with *pAVW* Pico. Effectene was established as the most appropriate with a transfection efficiency of around 15-20%.

Consequently investigations were carried out to identify a suitable transfection reagent for use in S2 cells. Figure 4.7.2. shows results from the most successful compounds tested. The majority of reagents examined failed to achieve a transfection efficiency above 1%. However, Effectene consistently displayed an efficiency between 15-20%. Indeed, co-transformation of more than one construct regularly exhibited an efficiency of around 10% when the Effectine dose was increased in proportion to the number of constructs used. As such, all subsequent analysis of the Pico constructs in S2 cells utilised Effectine mediated transient transfection.

4.8. Discussion

The work described in this chapter has led to the design and generation of an RNAi resistant $Pico^{WT}$ construct capable of being used in a range of rescue experiments. It has also facilitated in the development of Pico mutant constructs predicted to have a reduced affinity for Enabled, Chickadee, Ras, PP1, and MAPK, enabling the role that these interactions play in MRL functionality to be ascertained. In addition, phospho and dephospho mimetic constructs have been created to examine the effects of phosphorylation on Pico's associations and overall activity. Lastly, the constructs were inserted into flies subsequently characterised to allow selection of lines suitable for future work, while a mechanism for transient expression in S2 cells has been developed to enable localisation experiments to be performed.

4.8.1. Prospective investigations

Previous work performed in the Bennett lab had already examined Pico's capacity to directly bind with several factors through yeast two-hybrid assays. However, these investigations were limited to confirming interactions *in vitro* and did not assess the role of these associations on Pico functionality (Taylor, 2010). By examining the protein binding capabilities of the WT and mutant constructs through co-immunoprecipitation, it is hoped that a more complete understanding of the responsibility certain interactions have on Pico's functionality will be developed. Initially, it was intended that pulldown experiments would be performed using S2 cells as they generally offer cleaner extracts than flies, however, as it was only possible to transiently express the constructs at a relatively low efficiency in this system, other means of precipitating ectopic Pico complexes were ultimately utilised.

Past analysis of Lpd and RIAM have found that both predominantly localise to lamellipodial tips, providing significant support for their role in cellular migration. (Krause et al., 2004, Lafuente et al., 2004). Prior to this report, only preliminary research had been carried out to assess Pico's localisation, however, this was performed within whole tissues with very little work done in single cells (Lyulcheva, 2006). Work performed by Rogers *et al.* 2002 has demonstrated a method for inducing lamella formation in S2 cells through the use of Concanavalin A (ConA)

coated coverslips. Subsequent experimentation completed in the Valle lab using the aforementioned technique confirmed the presence of numerous actin regulatory proteins within the lamellae of S2 cells and validated the ConA mediated approach for studying localisation (Rogers et al., 2003). Evaluating Pico's localisation within S2 cells will be crucial for accurately understanding its function, while assessing the positioning of the mutant constructs may enable a greater comprehension of how interactions affect Pico's ability to localise and operate correctly. Analysis of Pico's co-localisation with various binding partners could further assist with understanding how its associated proteins aid in overall functionality while lending further support to findings from the co-immunoprecipitation experiments.

Given the plethora of powerful tools available within the *Drosophila* system, a wide range of prospective investigations can be carried out to assess the effects of the mutant constructs on growth and migration. Previous investigations have already confirmed Pico's role in growth and proliferation, with overexpression in wing discs leading to an increase in wing size, while RNAi mediated knockdown caused smaller wings to develop (Lyulcheva et al., 2008). Similar experiments performed in border cells has demonstrated a role for Pico in cellular migration. Ectopic overexpression of Pico was found to promote migration of the border cell cluster towards the oocyte, while depletion of pico by RNAi resulted in retarded migration of the cluster relative to wild type (Figure 4.8.1.a) (Taylor, 2010). Pico's ability to promote Ras mediated overgrowth has also been demonstrated through analysis of larval brains and a *Drosophila* metastasis model (Taylor, 2010, Pagliarini and Xu, 2003). Expression of constitutively active Ras^{V12} alone was found to cause some tissue overgrowth, however, when overexpressed in conjunction with ectopic Pico, a dramatic increase in tissue overgrowth was observed, with some cases of secondary metastases being reported (Figure 4.8.1.b) (Taylor, 2010, Lyulcheva, 2006). Using these methods to analyse the mutant constructs will enable a thorough understanding of how protein interactions and phosphorylation function in determining Pico's role in growth and migration.

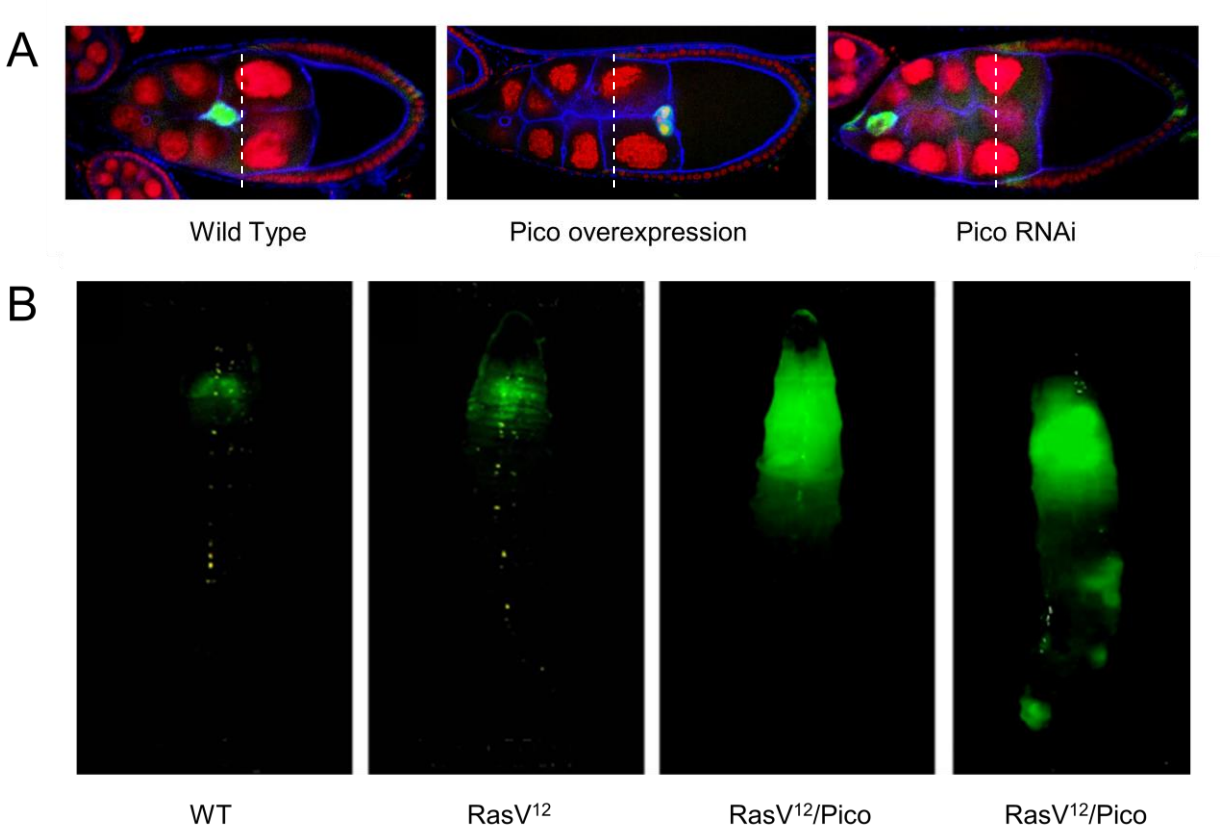

Figure 4.8.1. Examples of phenotypic analysis to assess Pico's functional effects. (a) In wild type egg chambers, the position of the migrating border cells labelled with GFP (green) is typically in line with, or slightly behind, the end of the columnar follicle cells (signified by the dotted lines). Ectopic overexpression of Pico promoted migration of the cluster towards the oocyte while depletion through RNAi slowed migration of the border cell cluster relative to wild type (Taylor, 2010). (b) As a means of assessing overgrowth, *UAS*-GFP was expressed in the eye-antennal discs of *Drosophila* larvae. When constitutively active Ras^{V12} was expressed alone, a small amount of overgrowth was observed compared to wild type, however, when overexpressed in conjunction with ectopic Pico, a dramatic increase in GFP-marked tissue was seen with some larvae exhibiting metastases at ectopic sites (Lyulcheva, 2006).

5. Pico's interactions

5.1. Introduction

Given the substantial role associated proteins play in determining overall MRL functionality, a significant amount of work has focused on identifying potential partners and their respective binding sites. Previous research has confirmed that RIAM and Lpd interact with the actin regulatory proteins Ena/VASP and profilin through the proline rich and SH3 binding motifs distributed amongst their unstructured C-terminal regions (Lafuente et al., 2004, Krause et al., 2004). In addition, RIAM and Lpd share a capacity to bind to the cytoskeletal protein Talin via N-terminal amphipathic helices, enabling Integrin activation and promotion of cell adhesion (Lee et al., 2009).

Despite retaining significant sequence homology and possessing the ability to interact with many similar proteins, Lpd and RIAM display subtle differences in their binding preferences. RIAM has been shown to interact predominantly with active Rap-1 in a process requiring both the RA and PH domains, although it can bind active Ras with a lower affinity (Lafuente et al., 2004, Bos, 2005). In contrast, Lpd associates with active K-Ras, N-Ras, H-Ras, R-Ras and Rac, however no interaction with Rap-1 has yet been observed (Rodriguez-Viciana et al., 2004, Jenzora et al., 2005, Krause et al., 2004). RIAM and Lpd also differ in their PI binding preferences, with RIAM associating with PI(3)P and PI(5)P, while Lpd interacts with PI(3,4)P_2 (Jenzora et al., 2005, Krause et al., 2004, Lemmon, 2007). Since PIs represent early polarizing molecules during cell activation, the differential binding capacities may contribute to the distinct localisations characteristic of these proteins (Lemmon, 2003, Colo et al., 2012b). More recently, associations specific to each paralogue have been described, with Lpd shown to bind both srGAP3 and the tyrosine kinase c-Abl, while an interaction between RIAM and PLC-γ1 has also been reported (Endris et al., 2011, Michael et al., 2010, Patsoukis et al., 2009). The binding differences between these two similar paralogues highlights the need to properly assess the precise associations found within the other, more divergent orthologues if they are to be used in furthering our understanding of MRL function.

Surprisingly, though a plethora of phenotypic data has been reported, very little is currently known about Mig10s binding partners. To date, only interactions with an activated form of the Rac1 homolog CED-10, and the WRC protein ABI-1, have been described (Quinn et al., 2008, McShea et al., 2013). All other potential associations have only been theorised upon using co-localisation studies, mutational analysis, and direct interactions of other MRL homologues presented in the literature (Quinn and Wadsworth, 2008). A little more has been reported concerning the binding partners of Pico, with yeast-two-hybrid assays confirming direct interactions with activated Ras and Rap, Enabled, Chickadee, and PP1 (Taylor, 2010). However, further validation of these interactions using an *in vivo* system has yet to be performed and identification of the sites of binding had not been carried out.

5.1.1. Aims

The intention of the investigations performed in this chapter was to first confirm the findings of the yeast-two-hybrid assays *in vivo* through co-immunoprecipitation studies, while the ability of Pico to interact with homologues of the other MRL binding partners described in the literature was also assessed. Following identification of a potential MAPK binding site in Chapter 3, a selection of apposite MAPKs were examined for associations with Pico, as well as RIAM and Lpd. Subsequent hits were assessed further using the MAPK mutant construct to ascertain if the proposed site was necessary for binding, before mass spectrometry was performed to identify novel binding proteins of Pico to be later verified by co-IP studies.

The mutant constructs generated in Chapter 4 were then assessed by co-immunoprecipitation to determine their effect on Pico's interactions before further analysis was performed to elucidate the involvement of Pico-bound MAPKs in the phosphorylation of Pico-Ser 819 through the use of a phospho-specific antibody. Finally the functional role of this phosphorylation site in Pico was investigated to determine how it affected Pico’s associations with other proteins by using the phospho- and dephospho-mimetic constructs.

5.2. Pico's interactions

As a means of confirming and broadening the findings from the yeast-two-hybrid assays performed previously within the Bennett lab showing interactions with Ras, Rap, Enabled, Chickadee, and PP1, co-IPs were carried out using ectopically expressed Venus-Pico^{WT}. Due to the low transient transfection efficiency and general toxicity observed in stable lines, S2 cells could not be used as an expression vehicle for Venus-Pico. Consequently, expression of Venus-Pico^{WT} was carried out in flies However, as with S2 cells, ectopic Venus-Pico was found to be toxic and caused lethality during early larval development when used in combination with a ubiquitous driver such as *act5C-GAL4* and *da-GAL4*. The alternative *enGAL4* driver, employed during the analysis of Pico expression levels, only appeared to initiate transcription during the larval stage as no discernable expression was observed in adult flies (Harrison et al., 1995). Attempts to precipitate Venus-Pico from *enGAL* driven larvae failed due to insufficient quantities of the transcript and difficulties in sufficiently lysing the tissues (data not shown). Instead, the heat shock inducible *hsGAL4* driver was used to express the Venus-Pico constructs from which Venus-positive flies were selected for before co-immunoprecipitation, SDS-PAGE, and western blotting was carried out to identify complexed proteins (Halfon et al., 1997).

For each experiment, total extracts made from lysed samples before the addition of GFP-Trap magnetic particles were used to confirm the presence of the protein under investigation, while co-IPs from W^{1118} flies lacking Venus-tagged Pico were employed as a negative control. To avoid overexposure of the positive control lanes, the quantities of total lysates and co-IP samples were normalised to yield broadly similar band intensities. This typically meant positive control lanes represented roughly 1/4 of a fly, while the IPs corresponded to approximately 7 flies. For all experiments where a negative result was observed, the corresponding co-IP sample was examined for the presence of Talin to confirm successful precipitation had occurred.

5.2.1. Pico co-immunoprecipitates with expected binding partners

To verify previous findings from the yeast-two-hybrid assays (Taylor, 2010), immunoblotting was performed on Venus-tagged Pico^{WT} co-IP samples to test for the presence of PP1, Enabled,

and Chickadee. The results presented in Figure 5.2.1. show the existence of both PP1 and Chickadee within the Pico^{WT} immunoprecipitates, indicating that Pico interacts with both proteins. It was not possible, however, to prove Enabled association as optimisation of the 5G2-Enabled specific antibody for use in western blots was unsuccessful (data not shown). Lastly, due to the previously documented interaction of Talin with both Lpd and RIAM (Lee et al., 2009), the presence of Rhea, the *Drosophila* Talin homologue, was also examined in Pico^{WT} precipitates. The data shown in Figure 5.2.1. confirmed the presence of Rhea in the co-IP sample and demonstrates Pico's ability to complex with the Talin homolog *in vivo*.

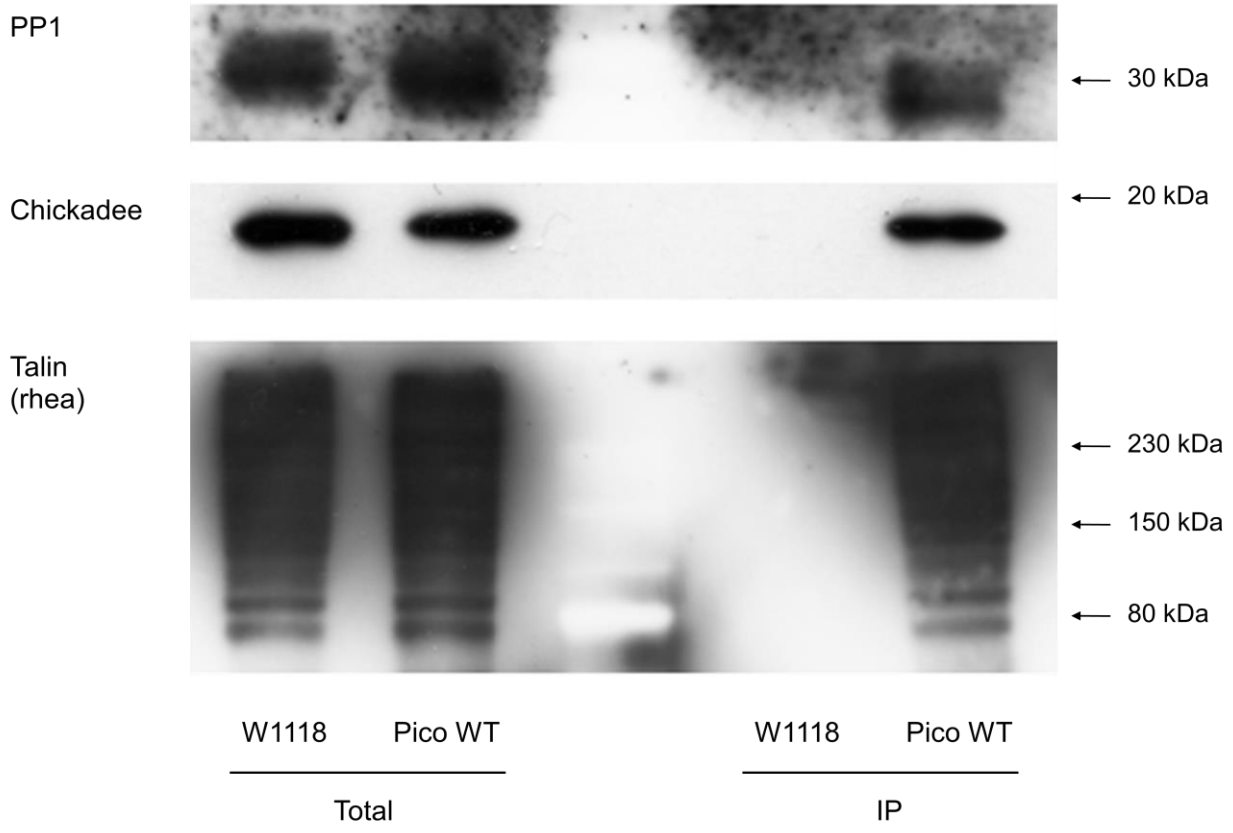

Figure 5.2.1. Immunoblots of PP1, Chickadee, and Talin from Venus-Pico^{WT} pulldown expreriments. Co-immunoprecipitation was performed on flies expressing Venus-Pico^{WT} using GFP-Trap magnetic beads. The resulting samples were examined via immunoblot analysis to ascertain the presence of PP1, Chickadee, Enabled, and Rhea in the pulldown. The findings indicate that Pico associates with PP1, Chickadee and Rhea *in vivo*, however, analysis of Enabled was inconclusive.

5.2.2. Pico interacts with Ras but not Rap

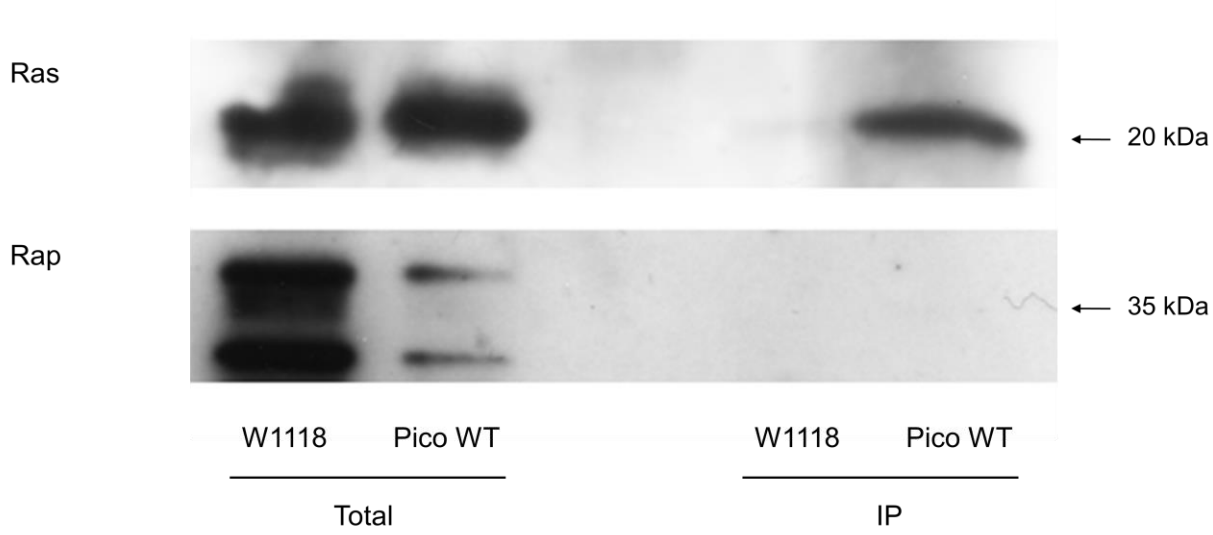

Figure 5.2.2. Immunoblots of Ras and Rap from Venus-Pico^{WT} pulldown experiments. Pulldowns were carried out on flies expressing Venus-Pico^{WT} under the control of *hs-GAL4* using GFP-Trap. The samples were then examined by western blotting to determine if Ras or Rap interact with Pico. The results showed Pico complexes with Ras but not Rap, although it is possible interactions with Rap occur at low levels.

Previous work performed within the Bennett lab had already demonstrated by yeast-two-hybrid analysis that Pico directly binds the active forms of both Ras and Rap, but not their wild type or dominantly negative forms. Furthermore, these associations were observed using both a full-length Pico construct and a partial fragment containing only the RA and PH domains (Taylor, 2010). Consequently, co-IP and immunoblotting was performed to ascertain if these interactions also occurred *in vivo*.

The results shown in Figure 5.2.2. suggest that Pico binds Ras but not Rap *in vivo*, although, care should be noted in this result as a failure to detect Rap interaction does not necessarily confirm an inability to bind Rap. Indeed, it may be that Pico, much like RIAM, is capable of associating with both GTPases, but displays a preference for Ras or binds Rap only under certain circumstances (Lafuente et al., 2004, Bos, 2005).

5.2.3. Pico interacts with activated Rolled but not Jnk

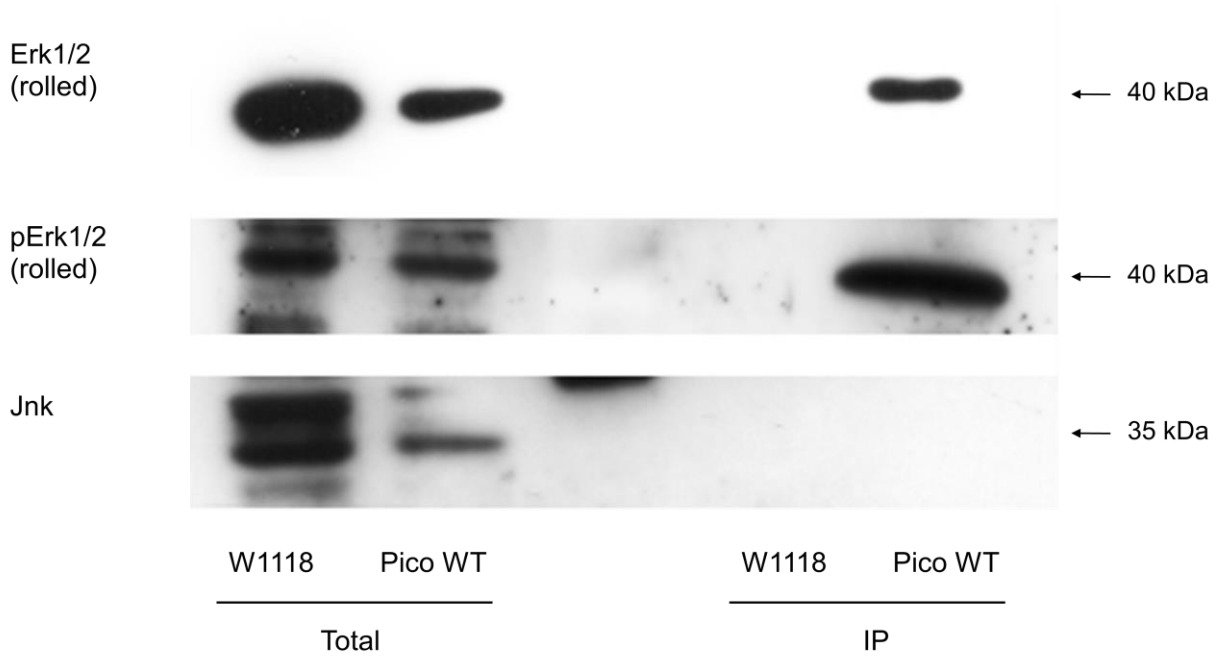

Figure 5.2.3. Western blots of Erk1/2, activated Erk1/2 and Jnk using Venus-Pico^{WT} co-IP samples. Pulldowns were performed on flies expressing Venus-Pico^{WT} using GFP-Trap magnetic beads before being examined by immunoblot analysis to establish the presence of Rolled, activated Rolled, and Jnk within the co-IPs. The findings showed Pico was able to interact with both Rolled and activated Rolled, but not Jnk.

Identification of the highly conserved MAPK binding site described in Chapter 3 strongly suggested MRL may have a conserved ability to bind MAPK. As such, Pico's capacity to associate with members from each of the three principal MAPK families, Erk, Jnk, and p38, was assessed (Muda et al., 1996). Initially, interactions with the Erk1/2 homologue, encoded by *rolled*, was examined by co-IP and immunoblotting due to the well documented role Erk family kinases play in both cell growth and migration (Cargnello and Roux, 2011). The data presented in Figure 5.2.3. suggests Pico can associate with Rolled *in vivo*. Next, the ability of Pico to interact with activated Rolled was investigated through the use of an antibody specific to the di-phosphorylated form of Erk1/2. Results shown in Figure 5.2.3. confirm Pico's capacity to interact

with activated Rolled, however, the data was unable to determine if Pico associates exclusively with the active form or not.

Lastly, analysis was performed to determine if Pico associates with Jnk family members. The evidence from Figure 5.2.3. suggests Pico does not interact with Jnk family kinases, although, as with Rap, this cannot be considered categorical due to the nature of co-IPs. Unfortunately it was not possible to assess p38 associations as an antibody capable of detecting the *Drosophila* isoform could not be procured.

5.2.4. Pico binds directly to Rolled at the conserved MAPK binding site

Figure 5.2.4. Immunoblot of Erk1/2 from Venus-Pico^{WT} and Venus-Pico^{MAPK}. Co-immunoprecipitation was carried out on *hs-GAL4* flies expressing Venus-Pico^{WT} and Venus-Pico^{MAPK} using GFP-Trap beads. The subsequent pulldowns were examined by western blotting to determine if Rolled was present. The findings indicated that while Pico^{WT} can associate with Rolled, the MAPK-binding mutant was unable to, suggesting that Pico might bind directly to Rolled via the conserved MAPK binding site.

Following confirmation of Pico-Rolled associations, the capability of the MAPK-binding mutant Pico^{MAPK} to also interact with Rolled was assessed to determine if the conserved MAPK binding site was critical for binding. The results presented in Figure 5.2.4. indicates Pico^{WT} associates with Rolled, however, Pico^{MAPK} failed to interact. Taken together with the known properties of the MAPK motif, this finding implies Pico binds Rolled directly through the conserved MAPK binding site described in Chapter 3.

5.2.5. Lpd and RIAM also exhibit Erk1/2 interactions at the conserved MAPK binding site

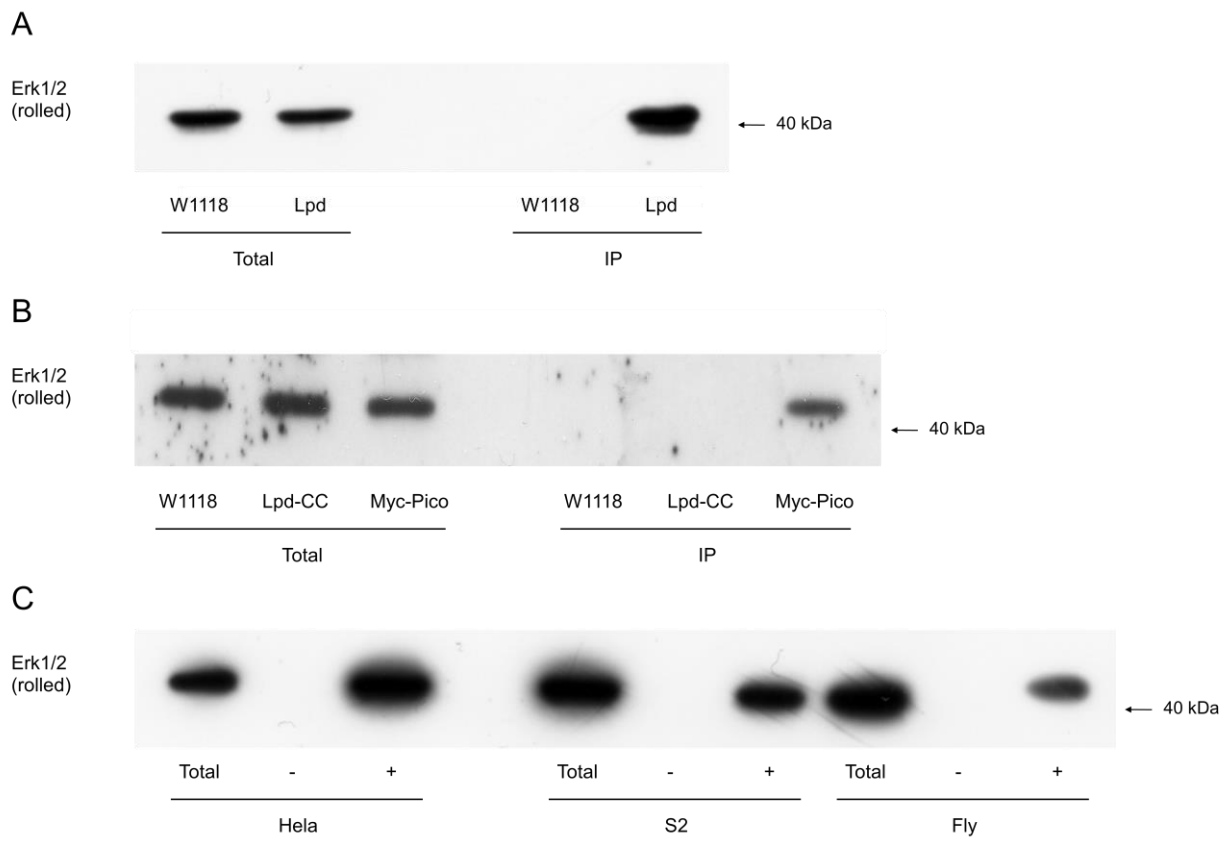

Figure 5.2.5. Western blots of Erk1/2 from Lpd-S, Lpd-CC, and RIAM pulldowns. Co-immunoprecipitation was carried out on *arm-GAL4* flies expressing (a) FLAG-Lpd-S, and (b) Myc-Lpd-CC before western blotting was performed to ascertain the presence of Rolled. The results showed wild type Lpd-S was able to interact with Rolled, while the Lpd coiled-coil mutant (Lpd-CC) could not. (c) A SUMO tagged RIAM fragment (residues 147-174) was incubated with total lysates from Hela cells, S2 cells and whole adult flies. The protein was then pulled down using SUMO-Qapture resin and immunoblot analysis carried out to establish whether associations with either Erk1/2 or Rolled had occurred. '-' indicates samples incubated with SUMO-Qapture resin alone, while '+' denotes lysates where SUMO-RIAM peptide had been added before co-immunoprecipitation took place. The findings revealed that the shortened RIAM peptide was sufficient to enable interactions with Erk1/2 and Rolled within Hela, S2 and *Drosophila* systems.

Having shown direct binding of Pico to Rolled through the conserved MAPK motif, experiments were carried out to determine whether Lpd and RIAM displayed a similar ability. A FLAG-tagged wild type Lpd construct expressed in adult flies using the *arm-GAL4* driver was immunoprecipitated using anti-FLAG bound to Protein G Sepharose before Western blot analysis was performed to ascertain if Rolled was present in the precipitates. As with the Venus-Pico^{WT} experiments, W^{1118} flies lacking any tagged ectopic protein were utilised as a negative control, while total lysates confirmed the presence of the protein under investigation. The results shown in Figure 5.2.5.a confirm that Lpd is able to associate with the *Drosophila* Erk1/2 homologue Rolled, despite being from a highly diverged species.

Next, the ability of Myc tagged Lpd-CC, a construct possessing a mutated coiled-coil motif, to interact with Rolled was assessed to establish if direct binding also occurred at the conserved MAPK site in Lpd. Again, using the *arm-GAL4* driver, Myc-Lpd-CC and a Myc-tagged Pico WT construct were expressed in adult flies and pulled down through co-immunoprecipitation. The resulting samples were then assessed by western blotting to determine if Rolled was present. Figure 5.2.5.b reveals that Myc-Pico, but not Myc-Lpd-CC, was able to bind Rolled, suggesting that Lpd, much like Pico, binds Erk1/2 or Rolled directly via one of its conserved MAPK sites. While it may seem this data points to interactions occurring at the site positioned within the coiled-coil motif, it is possible that disruption to this region also interferes with the second site situated at the N-terminus of the RA domain.

As a means of determining whether RIAM is able to interact with Erk1/2 or Rolled, and also to ascertain whether the MAPK binding motif within the coiled-coil region plays a role in this association, a short SUBO-tagged peptide consisting of RIAM residues 147-174 was kindly provided by Thomas Zacharchenko (University of Liverpool). This region contains the coiled-coil motif enclosing the conserved MAPK^{site1} site, but lacks the MAPK^{site2} binding motif positioned at the N-terminus of the RA domain. Structural studies were performed by the Barsukov lab (University of Liverpool) to confirm protein folding had occurred and verify purity of the peptide prior to any analysis being carried out.

Extracts were made from Hela cells, S2 cells, and whole adult flies using RIPA buffer before the SUMO-RIAM peptide was incubated with each sample. The RIAM peptide was then pulled down by SUMO-Qapture resin and the resulting samples boiled in SDS-PAGE buffer and analysed by western blotting for the presence of Erk1/2 and Rolled. Samples of total extracts were used to confirm presence of the protein under investigation, while lysates incubated with SUMO-Qapture resin alone acted as negative controls. The findings presented in Figure 5.2.5.c demonstrate that the short RIAM peptide was able to bind Erk1/2 and Rolled within Hela, S2 and *Drosophila* systems. Further control experiments demonstrated that the RIAM peptide was unable to associate with either Ras or Talin (data not shown), validating the procedures carried out. Taken together, these results suggest that Erk1/2 binds directly to both Lpd and RIAM via the conserved $MAPK^{site1}$ binding motif situated within the coiled-coil region, however, the binding ability and functionality of $MAPK^{site2}$ remains unclear.

5.3. Novel interactions identified by Mass Spectrometry

Pico had so far been shown to associate with Chickadee, Rhea, Ras, Rolled and PP1 *in vivo*, while potential Enabled interactions were also deemed highly likely based on previous work performed within the lab and findings presented in the literature (Taylor, 2010, Colo et al., 2012b). As a means of identifying novel interaction partners and generating further evidence to support the current findings, mass spectrometry was carried out on Venus-$Pico^{WT}$ pulldowns. Co-IPs performed on W^{1118} flies using GFP-Trap were also analysed by mass spectrometry to provide a comparable control.

5.3.1. SDS PAGE mass spectrometry identifies Fasciclin 1 as a potential complex partner

Initially, mass spectrometry on coomassie-stained bands cut out SDS-PAGE gels was carried out to identify proteins in complex with Pico. Co-IP samples were run out on a gel alongside controls (Figure 5.3.1.) and eight individual bands subjected to mass spectrometry by the Beynon lab using a Bruker AmaZon before analysis of the raw data was completed using PEAKS 6. Initial findings appeared perplexing and were eventually considered inaccurate as manual examination of the unprocessed data highlighted more appropriate solutions that corresponded

better with the expected outcomes. Consequently Mascot was employed instead to assess the raw data, with the findings displayed in Figure 5.3.1.

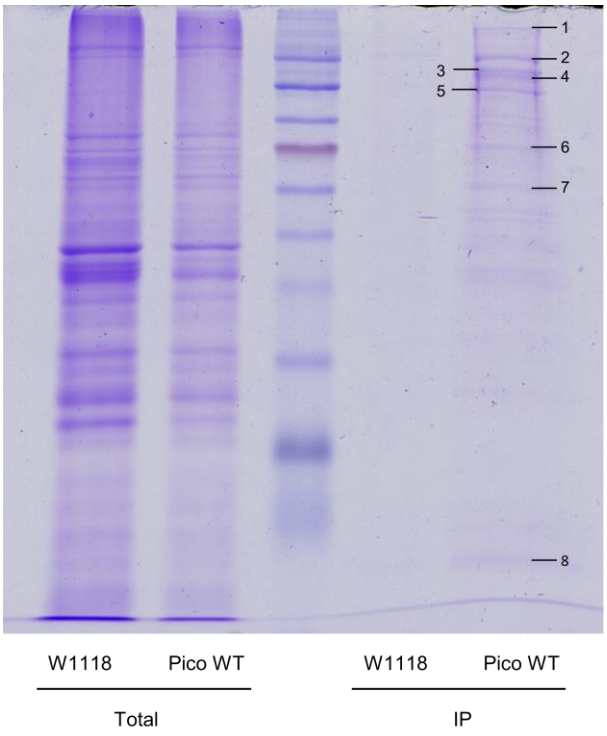

1)	KDVVVAGG	Fasciclin I
2)	VISQQSLER	Myosin heavy chain
3)	SPTDYTFGFK	Pico
4)	SSGLYYFPK	Pico
5)	TVDGVTNIELEEK	Fragile X mental retardation syndrome protein I
6)	SPTDYTFGFK	Pico
7)	SGVGNFIK	Polyadenylate binding protein
8)	VMPAVVIR	60S ribosomal protein

Figure 5.3.1. Results from SDS-PAGE mass spectrometry. Co-immunoprecipitation was performed on W^{1118} and *hs-GAL4* Venus-$Pico^{WT}$ flies using GFP-Trap magnetic beads. The resulting samples were separated by one dimensional SDS-PAGE and stained using coomassie blue. The eight bands highlighted in the figure were cut out and analysed by mass spectrometry to determine their spectral pattern before their identity was confirmed by Mascot. Pico, Fasciclin, FXR1, PABP, and 60S ribosomal protein were classified from the $Pico^{WT}$ pulldown.

Pico was recognised in multiple bands (bands 3, 4, and 6), most likely representing degradation products of the full-length protein, confirming its successful precipitation by GFP-trap. Myosin heavy chain was also discovered (band 2), however a faint band of approximately the same weight can be seen in the W^{1118} co-IP, indicating that this may be an artefact of pulldowns using GFP-Trap. It is unclear why this banding is much stronger in the Venus-$Pico^{WT}$ pulldown,

although it may be caused by actual interactions with Pico or an increase in myosin levels following Pico overexpression.

Strangely, the RNA binding Fragile X mental retardation syndrome protein 1 (FXR1) (band 5), Polyadenylate binding protein (PABP) (band 7), and 60S ribosomal protein (band 8) were identified, with no comparative bands being seen in the W^{1118} co-IP. It is thought these factors may have been pulled down with partially synthesised Pico still undergoing translation, as the targeted Venus tag is situated at the N-terminus and will have been generated first. Interestingly, the homophilic cell adhesion molecule Fasciclin 1 was also discovered from a very distinctive high molecular weight band (band 1). No corresponding band of equal size was observed in the W^{1118} co-IP and given its established role in cell adhesion, represents a respectable novel candidate for further study (Elkins et al., 1990). However, it should be noted that Fasciclin 1 has a predicted weight of 73 kDa, while the band analysed appears to have a molecular weight well in excess of 150 kDa, which is far in excess of what might be expected even if the protein were extensively glycosylated (Wang et al., 1993).

5.3.2. Mass spectrometry of total pulldowns isolates cdc42 as another potential Pico interactor

Despite yielding some potentially useful findings, various flaws were identified in the SDS-PAGE mediated mass spectrometry. Notably, numerous bands were observed in the Venus-$Pico^{WT}$ lane of the coomassie stained SDS gel, however, only a few were extracted and analysed due to them being deemed either too close together or insufficiently stained to enable accurate selection. Also, of those bands examined, none corresponded to the already well characterised associated proteins identified from the yeast-two-hybrid and co-IP investigations, highlighting the limitations of this process. Consequently, mass spectrometry was performed on total GFP-trap pulldowns from Venus-$Pico^{WT}$ and W^{1118} flies using an LTQ Velos. The overall spectral readouts from each pulldown is shown in Figure 5.3.2.

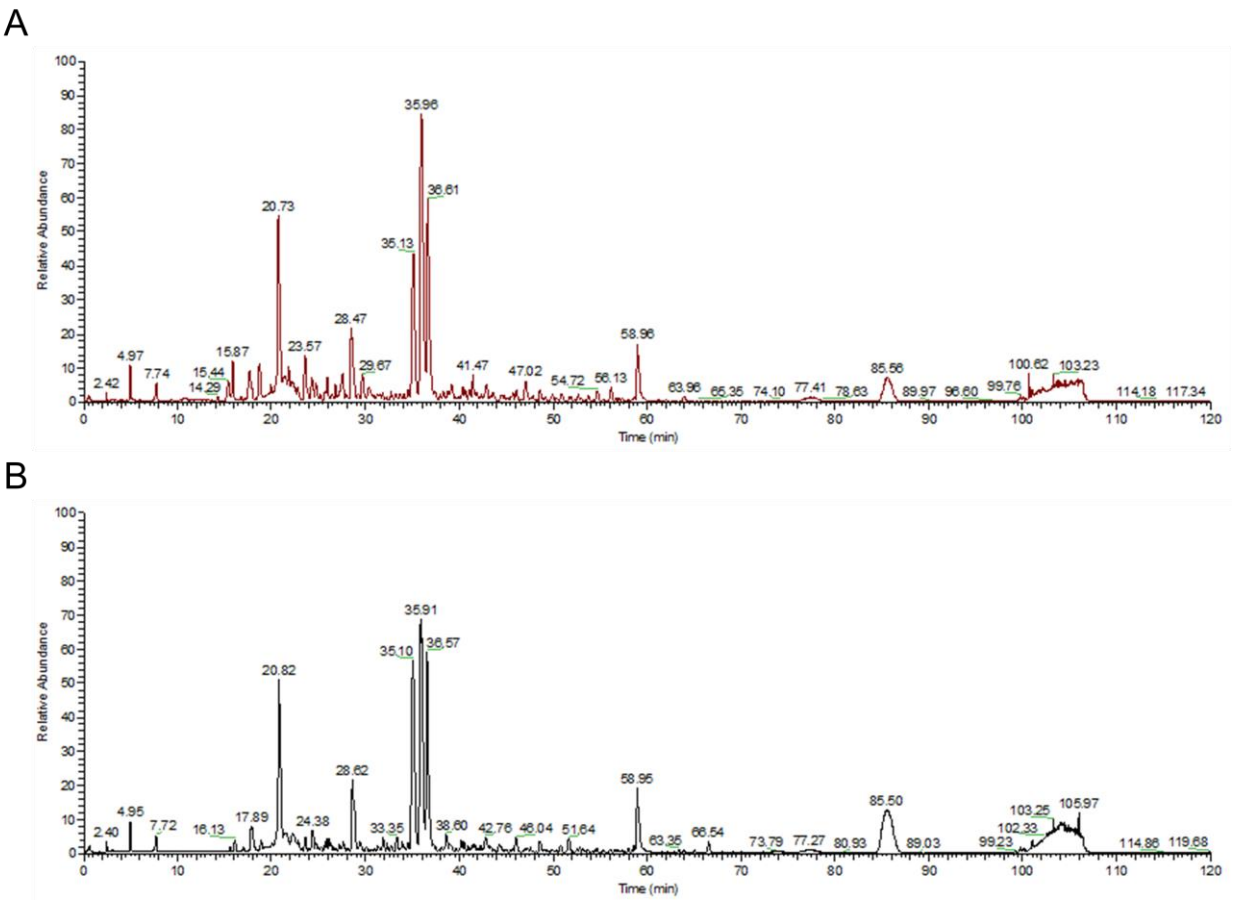

Figure 5.3.2. Complete spectra from total W^{1118} and Venus-$Pico^{WT}$ pulldowns. Complete spectra of GFP-trap pulldowns from (a) W^{1118} and (b) Venus-$Pico^{WT}$ expressing flies. The spectra show significant similarities and indicate that many of the proteins identified may be artefacts bound to the GFP-Trap beads.

The complete spectral readouts from Venus-$Pico^{WT}$ and W^{1118} pulldowns shown in Figure 5.3.2. revealed numerous individual proteins in both samples. In addition, the similarities of the peak distributions suggested many of the proteins were present in both samples, implying that the majority of recognised peptides were probably artefacts bound to the GFP-trap beads and not specifically complexed with Pico. Indeed, closer inspection revealed over 350 different proteins had been identified by PEAKS 6 and Mascot in each sample, of which only 35 were unique to the Venus-$Pico^{WT}$ co-IP. A complete list of proteins found exclusively in each pulldown can be found in Appendix 4.

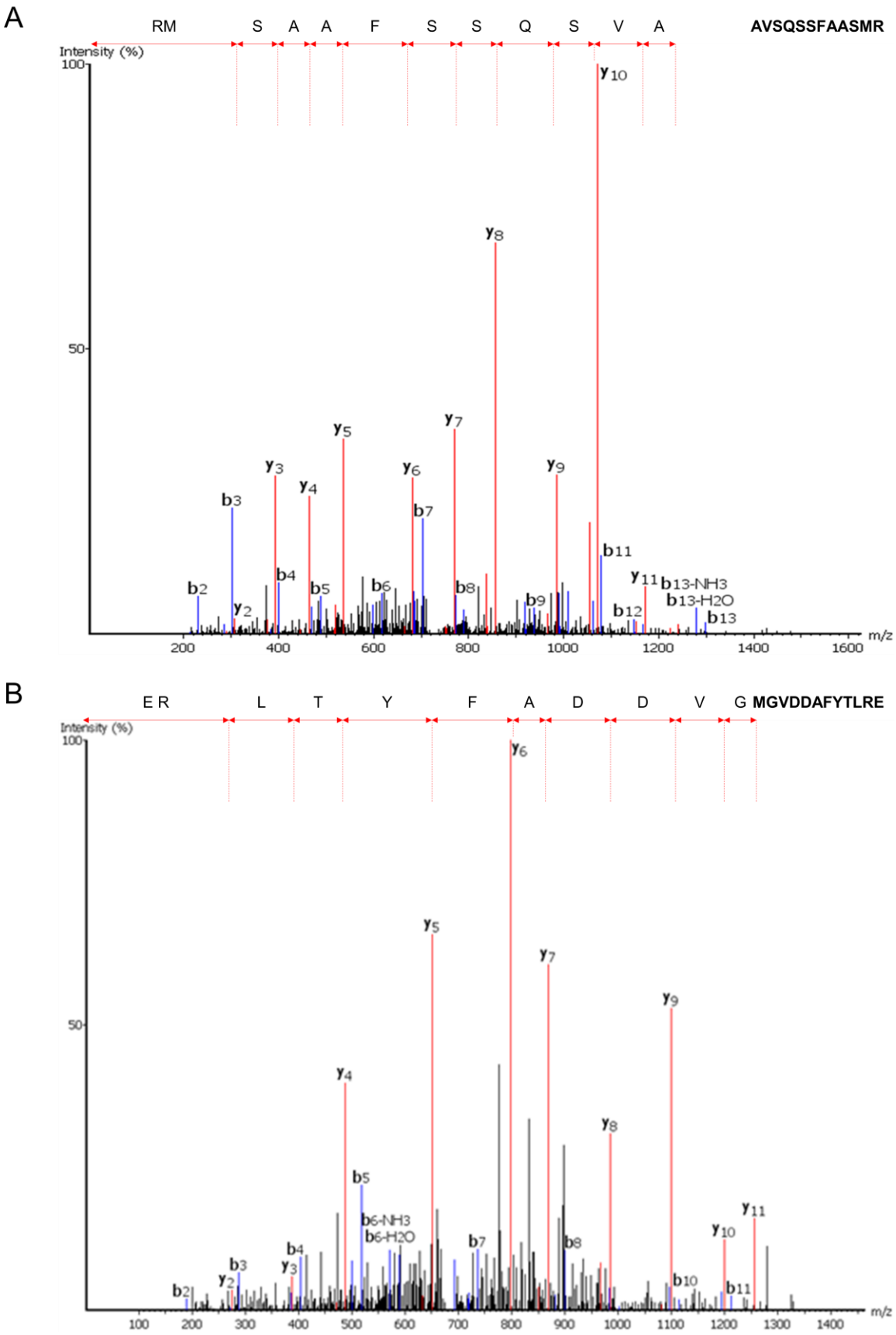
A
RM S A A F S S Q S V A
AVSQSSFAASMR
Intensity (%)
100
50
y10
y8
y7
y5
y3
y6
y4
y9
b3
b7
b11
b4
b2
b5
b6
b8
b9
y11
b13-NH3
b13-H2O
y2
b12
b13
m/z
200
400
600
800
1000
1200
1400
1600
B
E R L T Y F A D D V G
MGVDDAFYTLRE
Intensity (%)
100
50
y6
y5
y7
y9
y4
y8
b5
b6-NH3
b6-H2O
y11
y10
b4
b7
b8
b3
y3
y2
b2
b10
b11
m/z
100
200
300
400
500
600
700
800
900
1000
1100
1200
1300
1400

C

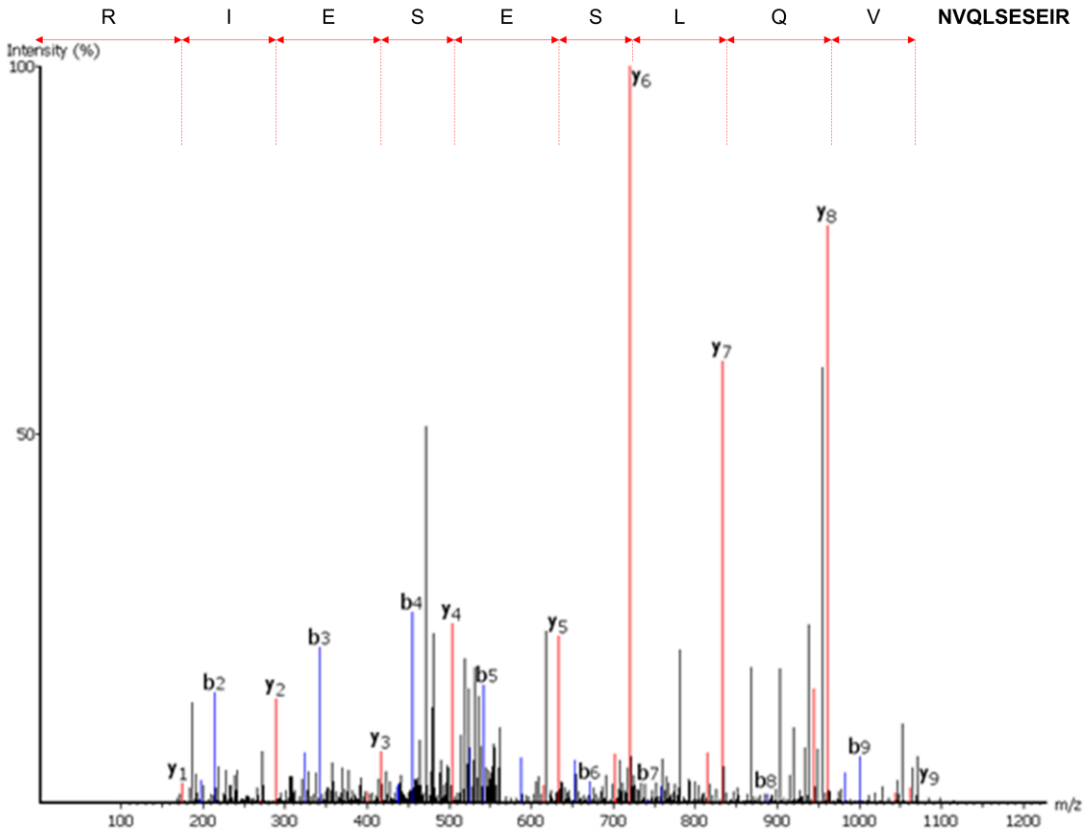
R I E S E S L Q V
NVQLSESEIR
Intensity (%)
100
50
y6
y8
y7
b4
y4
y5
b3
b2
y2
b5
y3
y1
b6
b7
b8
b9
y9
m/z
100 200 300 400 500 600 700 800 900 1000 1100 1200

D

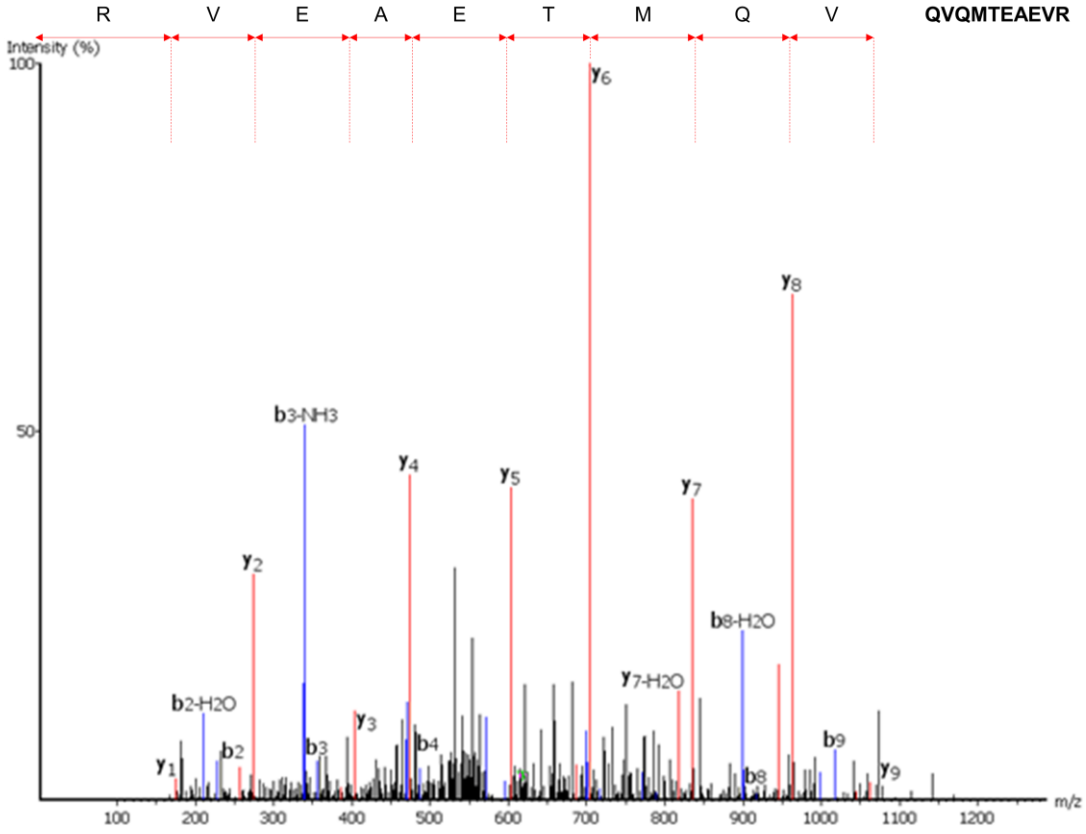
R V E A E T M Q V
QVQMTEAEVR
Intensity (%)
100
50
y6
y8
b3-NH3
y4
y5
y7
y2
b8-H2O
y7-H2O
b2-H2O
y3
b2
b3
b4
y1
b9
y9
b8
m/z
100 200 300 400 500 600 700 800 900 1000 1100 1200

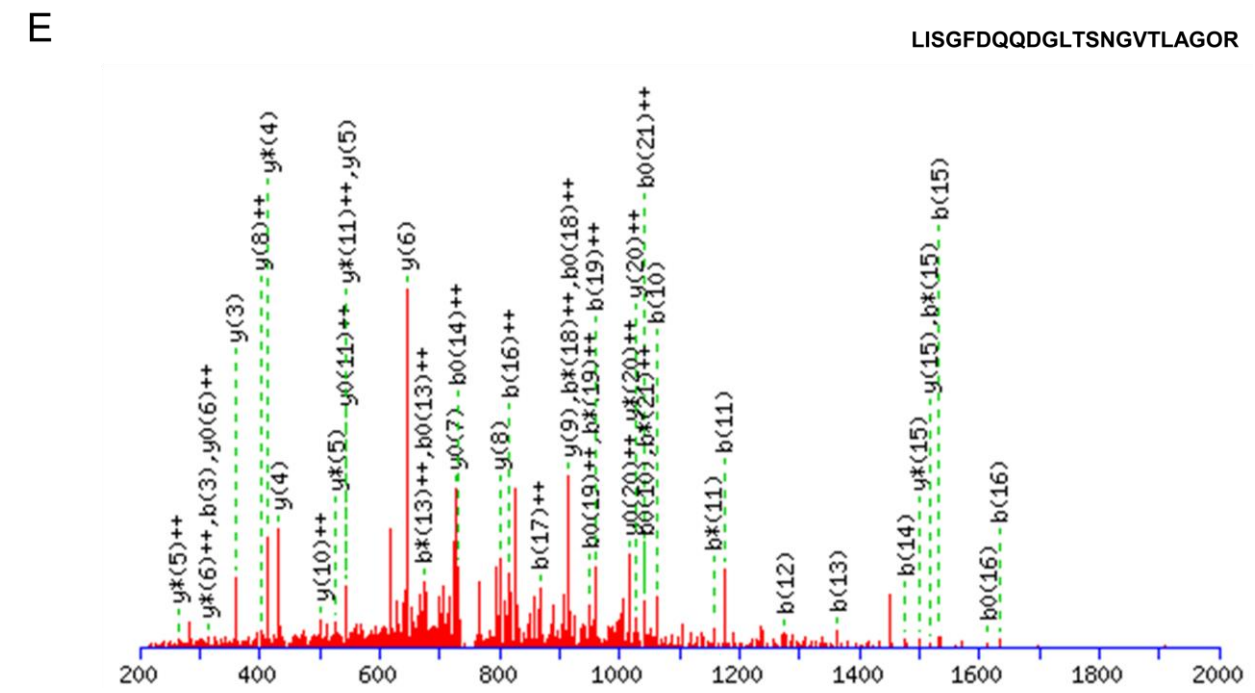

Figure 5.3.3. Manually annotated example spectra for Pico and its previously identified associated partners. Total GFP-Trap mediated pulldowns from Venus-Pico^{WT} and W^{1118} were analysed by mass spectrometry. The resulting data was examined by PEAKS 6 and Mascot before proteins unique to the Venus-Pico^{WT} co-IP were rationalised to select for those involved in regulation, growth, and migration only. (a) Pico, along with its previously identified interacting proteins (b) Ras, (c) PP1 α87B, and (d) PP1 β9C were identified by both programs, while (e) Chickadee was only detected using the more sophisticated Mascot software. To confirm these findings, manual analysis of the mass spectra was performed and compared to the software's calculated sequence shown in the top right corner of each graph.

A rationalisation process was carried out to eliminate proteins unrelated to regulation, growth, or migration. Those remaining were manually assessed to confirm correct identification before further conclusions were made. As expected, Pico was identified numerous times, with 39 unique peptides recognised covering 40% of the total sequence (Figure 5.3.3.a). Interestingly, the previously characterised Pico binding partners Ras and PP1 were detected by both software packages, whereas Chickadee was only pinpointed via the more advanced Mascot software. Distinctive Ras peptides were detected twice and corresponded to 11% of the total sequence

(Figure 5.3.3.b), while peptides for PP1 α87B (Figure 5.3.3.c) and PP1 β9C (Figure 5.3.3.d) were each observed only once and covered just 3% of their respective sequences. PEAKS 6 was unable to identify Chickadee as the complex nature pertaining to the large 22mer peptide, containing various modifications and di/tri-meric residue states, could only be resolved using the more sophisticated Mascot software (Figure 5.3.3.e). Although just one peptide corresponding to Chickadee was discovered, it did cover 17% of the total sequence and had a low degree of calculation error.

In addition to identifying the previously characterised Pico binding partners, PEAKS 6 and Mascot both revealed the presence of cdc42 exclusively within the Venus-Pico^{WT} co-IP sample. A total of two unique peptides were observed and found to correspond with 11% of the total protein sequence, while the manual analysis shown in Figure 5.3.4. confirmed correct software identification. Given cdc42's acknowledged role in stimulating signalling cascades controlling cytoskeletal remodelling, cell polarity establishment, migration, proliferation, and transcription, it represents another suitable candidate for further study (Chi et al., 2013).

Interestingly, neither Enabled, Rolled, or Fasciclin 1 were identified by either PEAKS 6 or Mascot in either the Venus-Pico^{WT} and W^{1118} total pulldowns. Regardless of this, repeated attempts were made to determine whether fasciclin1 and cdc42 were associated with Pico via immunoblot analysis of Venus-Pico^{WT} co-IPs. Unfortunately, it was not possible to optimise the available antibodies for use in western blotting, preventing any auxiliary investigations from being carried out (data not shown).

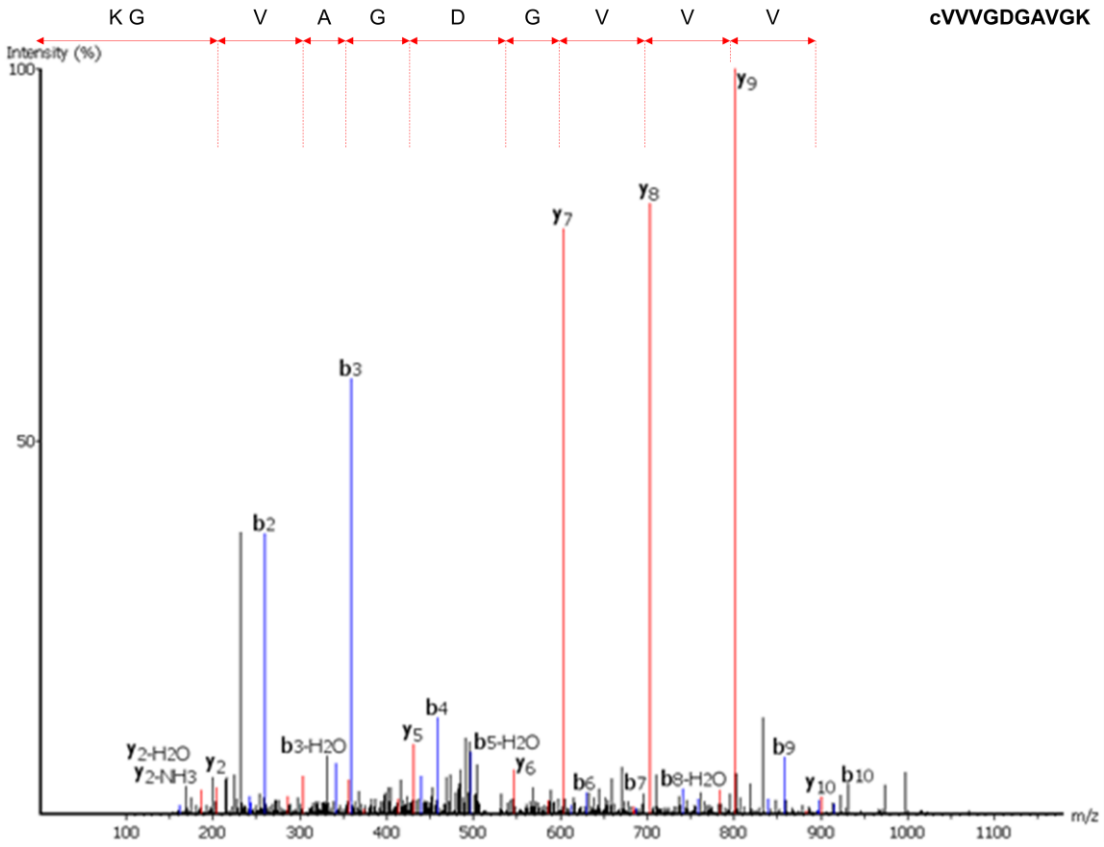
K G V A G D G V V V
cVVVGDGAVGK
Intensity (%)
100
50
y9
y8
y7
b3
b2
b4
y5
b5-H2O
y6
b3-H2O
y2-H2O
y2-NH3
y2
b6
b7
b8-H2O
b9
y10
b10
m/z
100 200 300 400 500 600 700 800 900 1000 1100

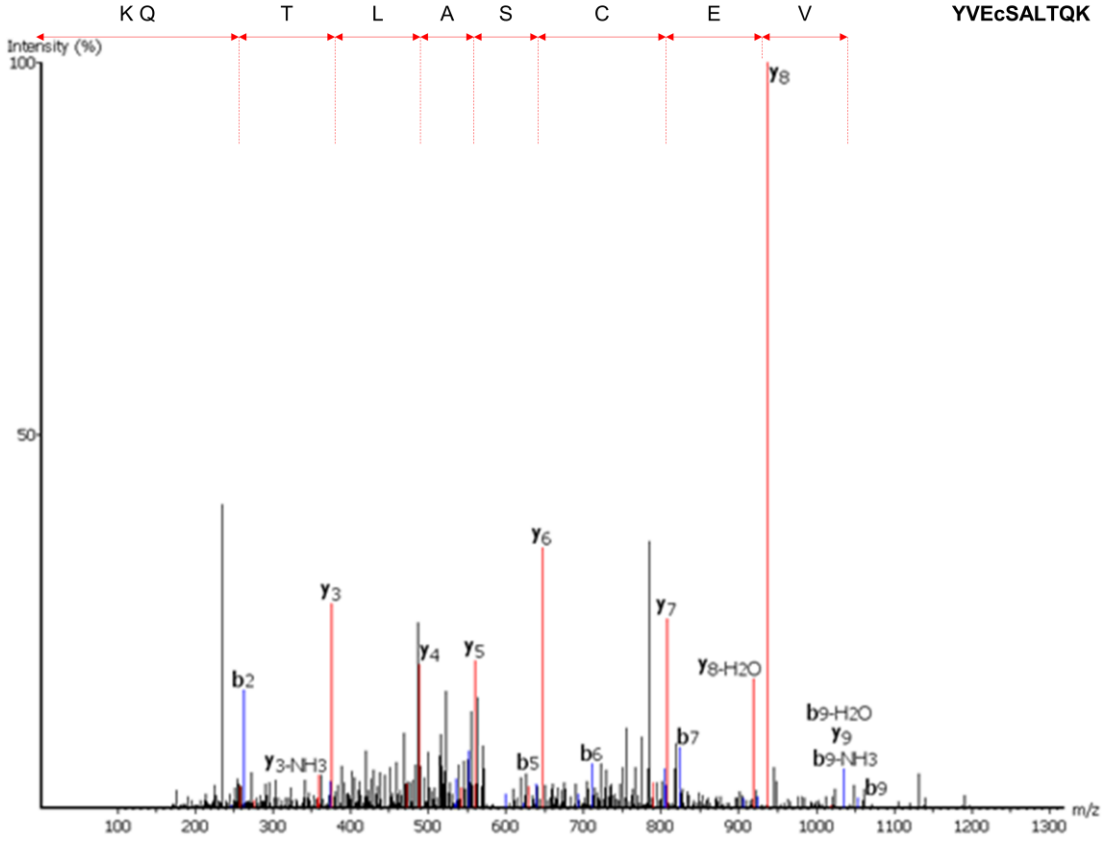
K Q T L A S C E V
YVEcSALTQK
Intensity (%)
100
50
y8
y6
y3
y7
y4
y5
y8-H2O
b2
b9-H2O
y9
b9-NH3
b7
y3-NH3
b5
b6
b9
m/z
100 200 300 400 500 600 700 800 900 1000 1100 1200 1300

Figure 5.3.4. Manually annotated mass spectrums corresponding to the two cdc42 peptides detected. Mass spectrometry was performed on total co-IPs from W^{1118} and Venus-$Pico^{WT}$ and analysed by PEAKS 6 and Mascot. Proteins unique to the Venus-$Pico^{WT}$ pulldown were rationalised to select for those involved in regulation, growth, and migration. In addition to identifying the well characterised Pico associated proteins Ras, PP1 and Chickadee, this investigation also discovered cdc42 as a potentially novel interacting protein, a finding confirmed by manual analysis of the spectra. The software's predicted sequence is shown in the top right corner of each graph (lower case letters indicate some uncertainty in residue identity).

5.4. Analysis of Pico mutant constructs

Having established the binding properties of wild type Pico, experiments assessing the binding abilities of the site-directed Pico mutants were performed. As with the Venus-$Pico^{WT}$ investigations, *hs*-GAL4 was used to express the Venus-tagged mutant constructs, while pulldowns were carried out with GFP-Trap. Also, total extracts made from lysed samples before the addition of GFP-Trap magnetic particles were utilised to confirm the presence of the protein under investigation, whereas co-IPs from W^{1118} were employed as a negative control.

5.4.1. The putative EVH1-binding motifs are not crucial for interactions with Chickadee

Co-IPs of the Venus-$Pico^{LA}$ mutant were assessed to determine whether the seven leucine to alanine mutations introduced to the characteristic *Drosophila* EVH1 binding sites (LPPPP) interfered with Pico's potential associations. Enabled is predicted to bind to Pico via one or more of Pico's EVH1-binding motifs, however, since both Pico and Chickadee have been reported to bind to Enabled (Lyulcheva et al., 2008, Krause et al., 2002), association of Chickadee with Pico may be indirect. The results shown in Figure 5.4.1. indicate that $Pico^{LA}$ can successfully complex with Chickadee as well as Rolled, PP1, Ras, and Rhea. This indicates that the leucine containing proline rich regions are not crucial for Chickadee interactions and although it was not possible to confirm whether $Pico^{LA}$ disrupted binding to Enabled, an equivalent set of mutations in Lpd does abrogate Enabled binding (Matthias Krause, personal communication), therefore suggesting that binding of Chickadee to Pico is not via Enabled.

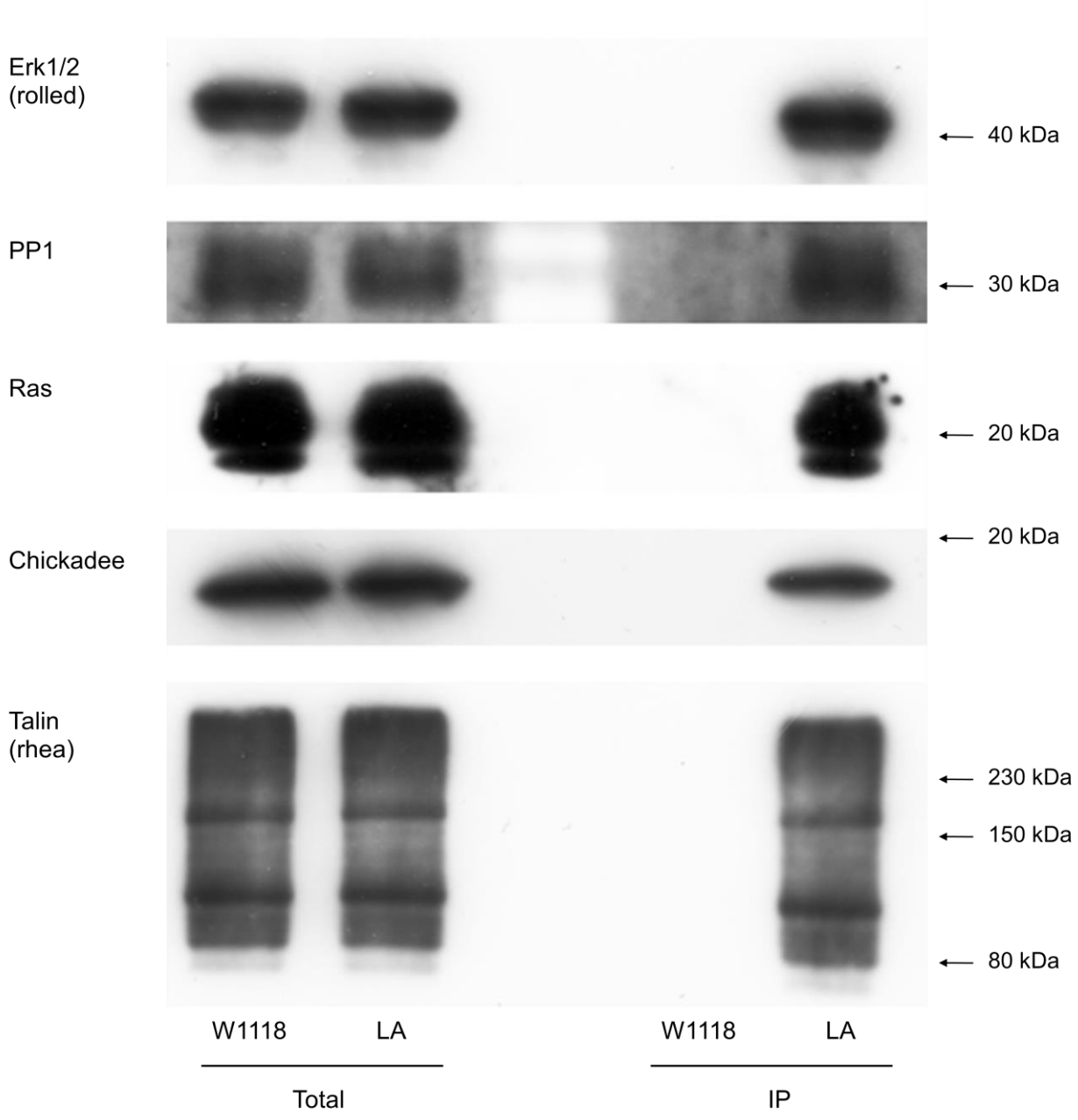

Figure 5.4.1. Immunoblots of Erk1/2, PP1, Ras, Chickadee, and Talin from Venus-Pico^{LA} mutant pulldowns. Co-immunoprecipitation was performed on flies expressing the Venus-Pico^{LA} mutant using GFP-Trap magnetic beads. The resulting samples were examined via immunoblot analysis to confirm the presence of Rolled, PP1, Ras, Chickadee, and Rhea in the pulldown. The findings showed that the Pico^{LA} mutant can associate with Rolled, PP1, Ras, Chickadee, and Rhea *iv vivo*, indicating that the leucine containing proline rich regions are not crucial for Chickadee interactions, although they may still be involved in binding with Enabled.

5.4.2. RA mutations have no discernable effect on Ras or Rap binding

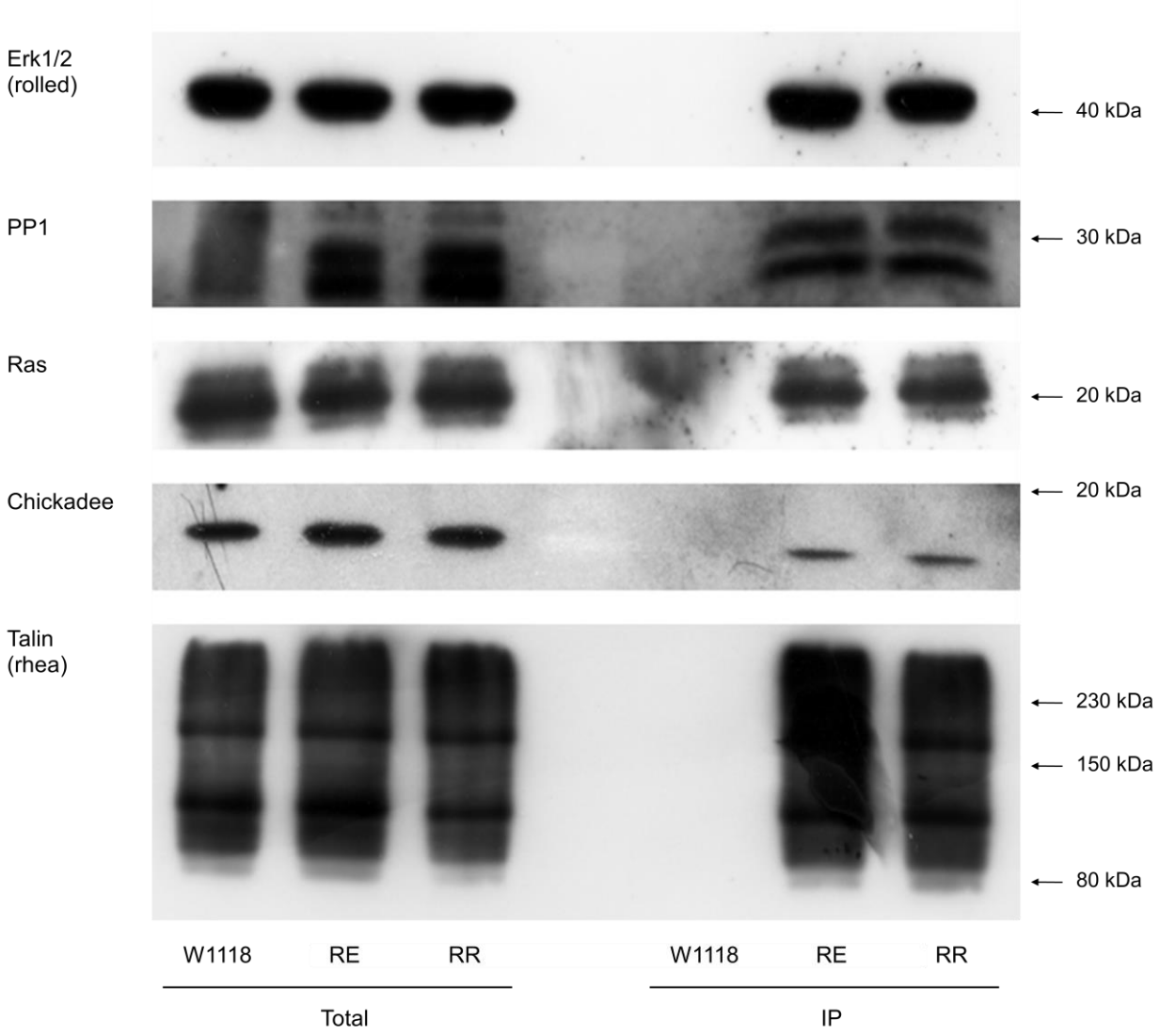

Figure 5.4.2. Western blots of Erk1/2, PP1, Ras, Chickadee, and Talin from Venus-Pico^{RE} and Pico^{RR} mutant pulldowns. Pulldowns were carried out on *hs-GAL4* flies expressing the Venus-tagged Pico^{RE} and Pico^{RR} mutant constructs using GFP-Trap. The resulting samples were then examined by western blotting to determine if Rolled, PP1, Ras, Chickadee, and Rhea were present. The results showed that both the Pico^{RE} and Pico^{RR} mutants were able to interact with Rolled, PP1, Ras, Chickadee, and Rhea *iv vivo*, implying that the desired alterations to Pico's affinity for Ras had not been achieved.

Pulldowns from the Venus-tagged Pico^{RE} and Pico^{RR} mutant constructs, designed to exhibit increased and reduced affinities for Ras respectively, were examined. The findings displayed in Figure 5.4.2. indicate no discernable alterations in Ras binding had been achieved in either mutant, and that they were both still capable of interacting with Rolled, PP1, Chickadee, and Rhea. A further investigation assessing Rap interactions was also carried out to determine if the modifications present in either construct enabled Rap binding, however, as with wild type Pico, no association was observed (data not shown).

5.4.3. Protein Phosphatase 1 (PP1) is not required for Pico's interactions

At first the Venus-tagged Pico^{F816A} mutants ability to interact with Protein Phosphatase 1 was assessed to determine whether replacement of the phenylalanine at position 816 with an alanine was sufficient to prevent direct binding as had been previously described (Lyulcheva, 2006). The results presented in Figure 5.4.3. show that PP1 is unable to bind Pico^{F816A}, therefore providing further evidence that direct binding between the two proteins occurs via the N-terminally located site and not at the conserved motif positioned within the RA domain (Chapter 3.3.).

Accordingly, the effects of PP1 binding on Pico's interactions with its other associated factors was examined. The outcomes illustrated in Figure 5.4.3. showed that the PP1 binding mutant was able to complex with Rolled, Ras, Chickadee, and Rhea, suggesting that binding of Pico to PP1 is not required for Pico to interact with these associated factors.

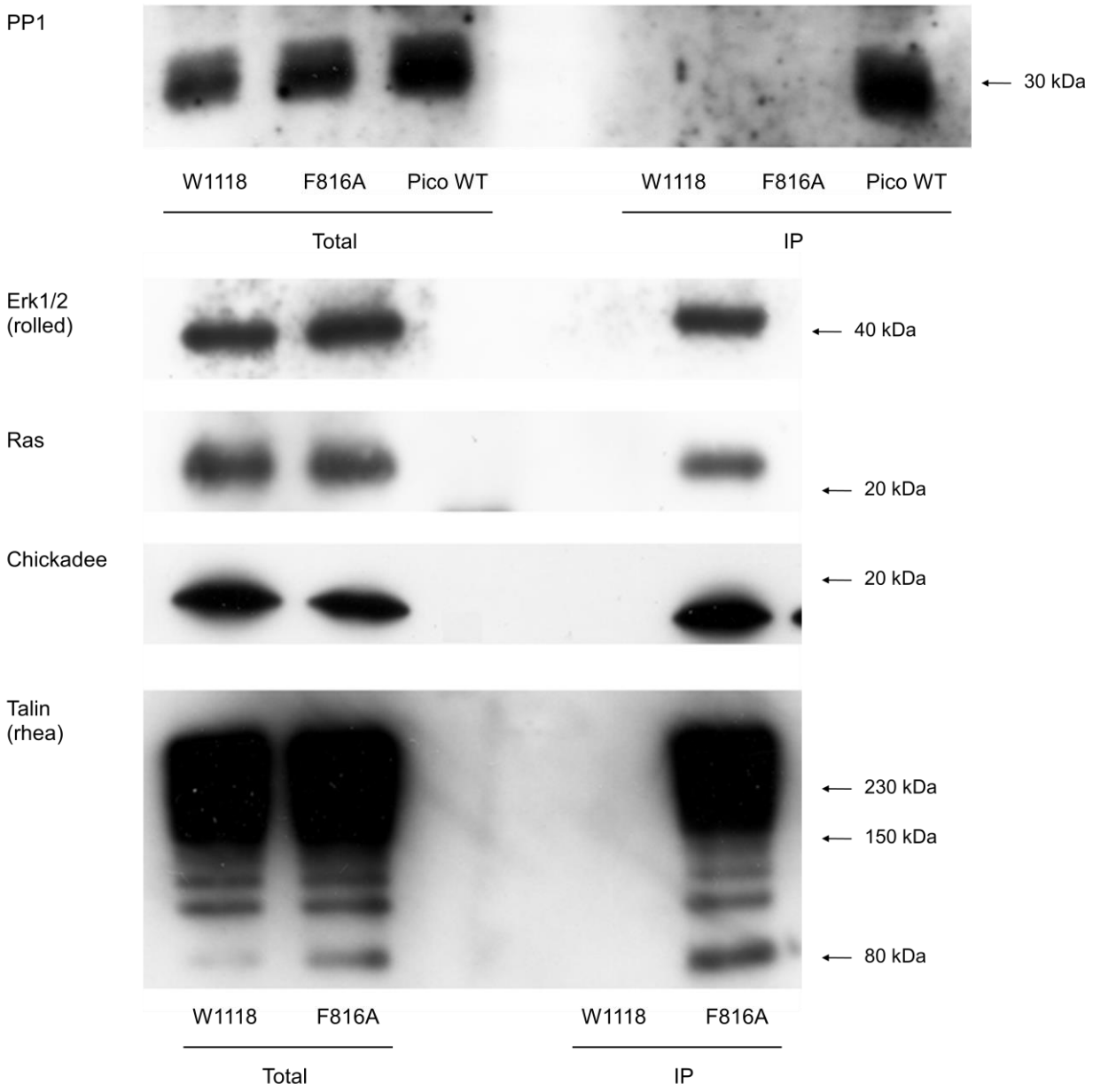

Figure 5.4.3. Immunoblots of PP1, Erk1/2, Ras, Chickadee, and Talin from Venus-Pico^{F816A} mutant pulldowns. Co-immunoprecipitation using GFP-Trap was performed on flies expressing the Venus-Pico^{F816A} mutant construct. The resulting pulldowns were studied by western blot analysis to detect for the presence of PP1, Rolled, Ras, Chickadee, and Rhea. The results indicated that Pico^{F816A} was incapable of interacting with Protein Phosphatase 1, but could still complex with Rolled, Ras, Chickadee, and Rhea; indicating that PP1 binds directly to Pico via this site and that association with PP1 is not required for the other interactions to occur.

5.4.4. MAPK binding is required for interactions with PP1

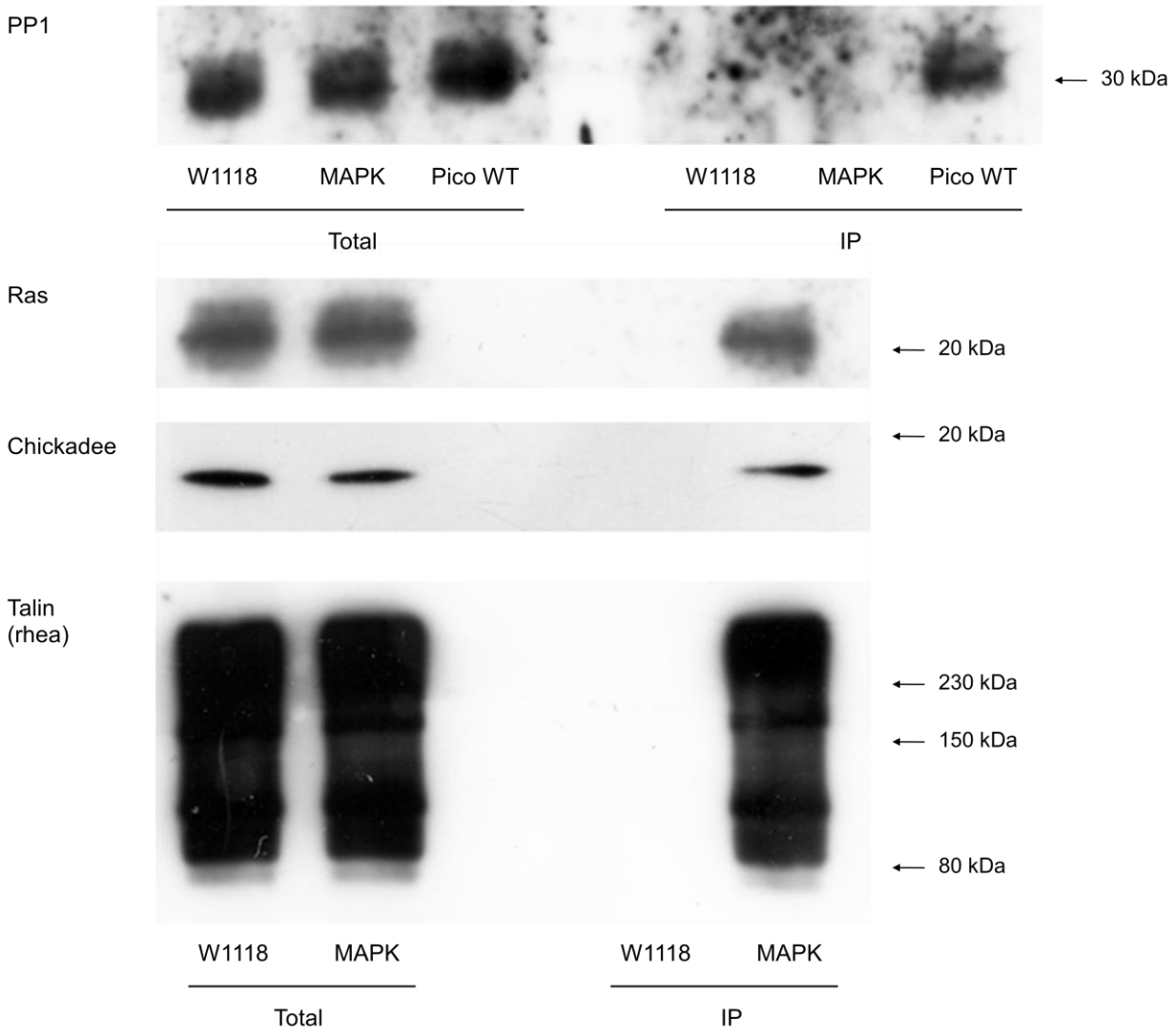

Figure 5.4.4. Western blots of PP1, Ras, Chickadee, and Talin from Venus-Pico^{MAPK} mutant pulldowns. Pulldowns using GFP-Trap were carried out on *hs-GAL4* flies expressing the Venus-tagged Pico^{MAPK} construct already shown to lack binding with Rolled. The resulting samples were then examined by immunoblotting to determine if PP1, Ras, Chickadee, and Rhea were present in the pulldowns. The findings showed that not only was the Pico^{MAPK} mutant unable to bind Rolled, but it was also incapable of interacting with PP1, indicating that Rolled plays a role in PP1 binding. The results also revealed that the MAPK-binding mutant could associate with Ras, Chickadee, and Rhea, demonstrating that Rolled was not required for the

other interactions to occur and that the residue changes within this construct had not caused extensive disruption to the tertiary structure.

Earlier work (Figure 5.2.4.) had already demonstrated that Pico^{MAPK} was incapable of binding Rolled. Consequently, pulldowns from Venus-tagged Pico^{MAPK} were examined to determine whether Rolled binding had any effect on PP1, Ras, Chickadee and Rhea interactions. The results shown in Figure 5.4.4. indicate that Pico^{MAPK} mutant is unable to bind to PP1, but can still complex with Ras, Chickadee and Rhea. This suggests that Rolled is involved in PP1 binding but is not required for the other interactions to occur. Furthermore, these findings show that the residue changes within this construct does not cause extensive disruption to the tertiary protein structure.

5.5. Effects of Phosphorylation

In addition to studying the effects of individual binding site mutations on MRL functionality, it was also important to assess the role phosphorylation played in regulating Pico's interactions, especially following confirmation that Pico binds MAPK and PP1, and the effect Rolled interactions had on PP1s association.

5.5.1. Rolled is involved in phosphorylation of serine 819

Previous work presented in the literature had identified the Ser 819 as a site of phosphorylation within Pico (Bodenmiller et al., 2007), while earlier findings discussed in this chapter showed direct interactions between the MAPK Rolled and Pico. Taken together with the discovery that Rolled may be involved in PP1 binding at a motif adjacent to the proposed phosphorylation site, it was hypothesised that Rolled might phosphorylate the serine at this position. Subsequent target-sequence analysis using Phospho.ELM revealed Pico-Ser 819 to be a potential target of Erk1/2 (Dinkel et al., 2012), while more direct approaches utilising a phospho-specific antibody designed to specifically recognise Pico phosphorylated at this site was also carried out.

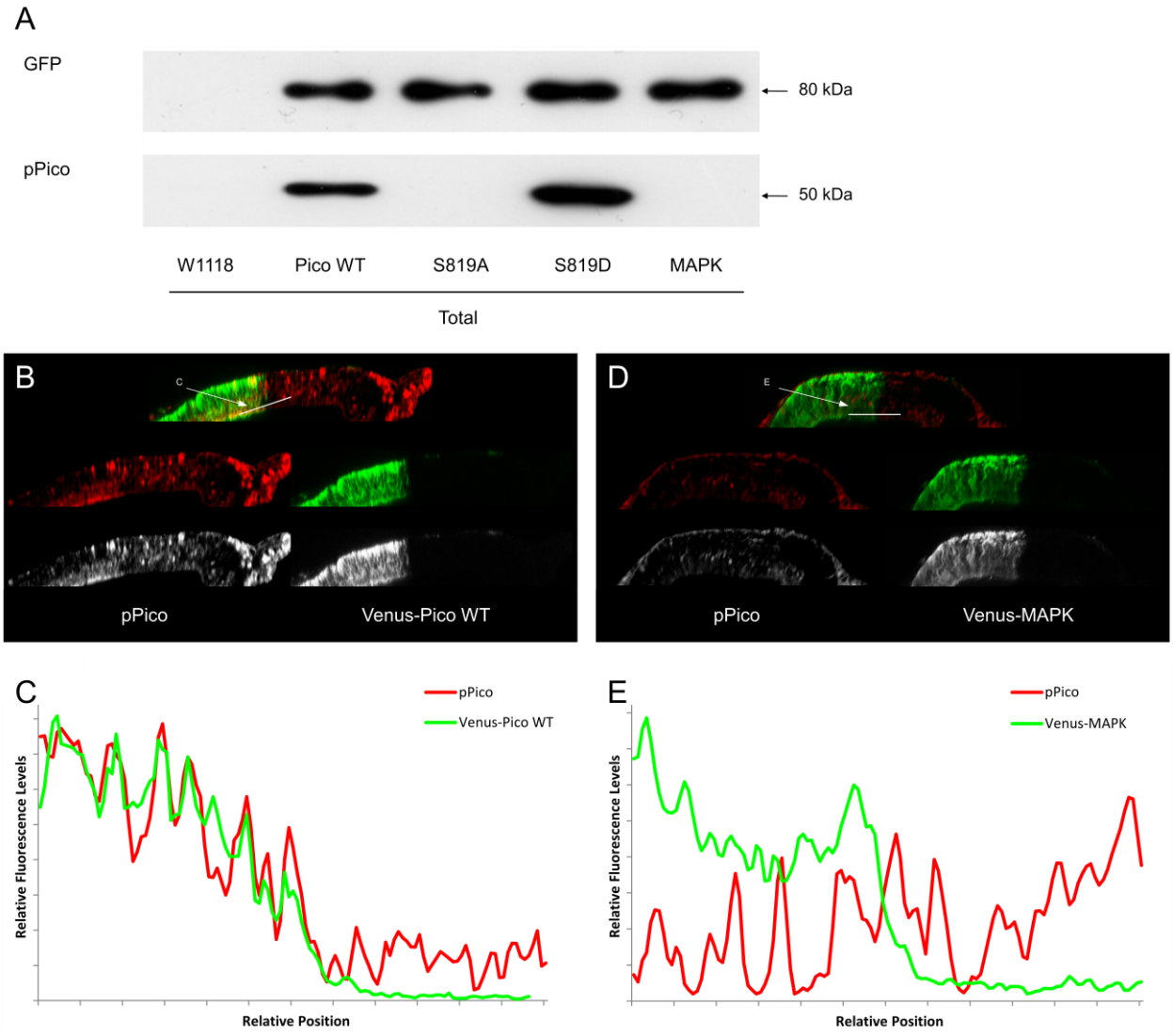

Figure 5.5.1. Confirmation of Rolled's involvement in phosphorylation of serine at position 819. (a) Total extracts from W^{1118}, *hs-GAL4* $Pico^{WT}$, and *hs-GAL4* $Pico^{MAPK}$ flies were analysed by western blotting to ascertain the levels of serine 819 phosphorylation using a phospho specific antibody. The results showed that the MAPK-binding mutant displayed very little apparent phosphorylation at this site compared to Venus-$Pico^{WT}$, even though GFP staining indicated slightly higher levels of the ectopic protein within the $Pico^{MAPK}$ sample. $Pico^{S819A}$ and $Pico^{S819D}$ total extracts were also included to enable validation of the phospho-Pico antibody (b) Wing discs expressing Venus-tagged $Pico^{WT}$ (green) under the control of *en-GAL4* were stained with the phospho specific antibody (red) and visualised by confocal microscopy. (c) The findings following linear plot profiling indicate that the levels of phosphorylated Pico are notably higher

in cells expressing the ectopic protein compared with those that are not. (d) *en-GAL4* Pico^{MAPK} (green) was also expressed in wing discs subsequently stained with the phospho specific antibody (red) and visualised under a confocal microscope. (e) The linear plot profiling results show that the levels of phosphorylated Pico remain the same between cells expressing ectopic Pico^{MAPK} and those that do not, implying that Pico^{MAPK} cannot be phosphorylated at Ser 819. When combined, these data suggest that Pico-bound Rolled is involved in phosphorylation of the Serine at position 819 within Pico.

Extracts from W^{1118} and *hs-GAL4* flies expressing Venus-Pico^{WT} and Venus-Pico^{MAPK} were examined by immunoblotting with an antibody raised against a Pico peptide mimicking phosphorylation at Ser 819. Further control blots were carried out using anti-GFP to determine the amount of ectopic protein present in the samples. The results displayed in Figure 5.5.1.a indicate that the MAPK-binding mutant exhibits very little phosphorylation compared to Venus-Pico^{WT}, even though the GFP staining indicates comparable levels of ectopically expressed Pico protein. The ability of the phospho-specific antibody to recognise Pico^{S819D} but not Pico^{S819A} in total extracts indicates that the antibody fails to recognise Pico that is not phosphorylated at this site. Overall, these findings provide support for the specificity of the phospho-Pico antibody and suggest that Rolled is involved in the phosphorylation of Pico at position 819.

As a means of providing further evidence to support this conclusion, wing discs dissected from *en-GAL4* larvae characteristically expressing Venus-Pico^{WT} in the posterior compartment were stained with the phospho-specific antibody and visualised by confocal microscopy (Figure 5.5.1.b). The graphical representation of relative fluorescence levels presented in Figure 5.5.1.c shows that the levels of phosphorylated Pico were considerably higher in cells expressing Venus-Pico^{WT} compared with those that did not. Contrastingly, wing discs from *en-GAL4* Venus-Pico^{MAPK} larvae stained with the phospho specific antibody shown in Figure 5.5.1.d indicated that the levels of phosphorylated Pico were the same in cells expressing the ectopic MAPK-binding mutant and those that did not (Figure 5.5.1.e). This confirmed that Pico^{MAPK}, unable to interact with Rolled, could not be phosphorylated at serine 819. When combined with the findings from *en-GAL4* Venus-Pico^{WT}, this result further supports the hypothesis that Rolled is involved in phosphorylation of Pico at position 819.

5.5.2. Phosphorylation of Serine 819 is important for PP1 binding

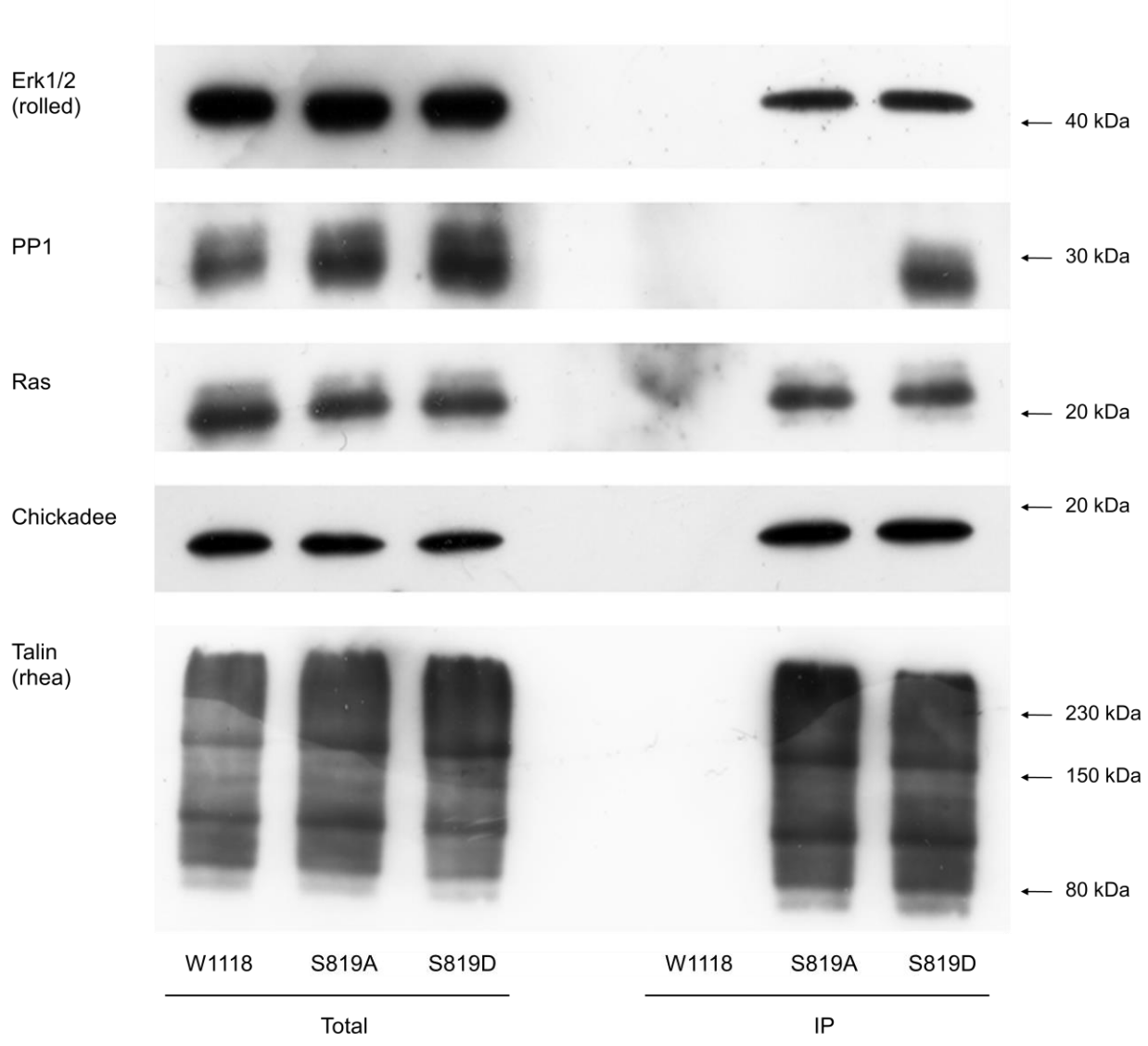

Figure 5.5.2. Immunoblots of Erk1/2, PP1, Ras, Chickadee, and Talin from Venus-Pico^{S819A} and Pico^{S819D} mutant pulldowns. Pulldowns were carried out on *hs-GAL4* flies expressing the Venus-tagged Pico^{S819A} and Pico^{S819D} mutant constructs using GFP-Trap. The samples were examined by western blot analysis to detect for the presence of Rolled, PP1, Ras, Chickadee, and Rhea. The results indicated that the non-phosphorylatable Pico^{S819A} mutant was unable to bind PP1, although it could associate with the other interaction partners. Conversely, the phosphomimetic Pico^{S819D} construct was found to bind PP1, as well as Rolled, Ras, Chickadee and Rhea, suggesting that phosphorylation of serine 819 plays a key role in PP1 binding.

Lastly, co-IPs from the Venus-tagged Pico^{S819A} and Pico^{S819D} mutant constructs were examined to determine if phosphorylation of Ser 819 had any effect on Rolled, PP1, Ras, Chickadee and Rhea interactions. The findings displayed in Figure 5.5.2. show that the dephosphorylated Pico^{S819A} mutant was unable to bind PP1, although it could associate with the other interaction partners. Conversely, the phosphomimetic Pico^{S819D} construct was found to interact with PP1, as well as Rolled, Ras, Chickadee and Rhea, indicating that phosphorylation of Ser 819 enables PP1 to bind with Pico, and that PP1 interactions do not significantly affect associations with the other binding partners.

5.6. Discussion

The work described in this chapter provides further evidence that Pico interacts with Ras, PP1, and Chickadee *in vivo* through both immunoblot analysis and mass spectrometry; supporting previous findings from yeast-two-hybrid studies of Pico, and investigations assessing the associations formed by the other MRL orthologs (Taylor, 2010, Krause et al., 2004, Lafuente et al., 2004). Indeed, taken together with the results from bioanalysis, site directed mutational examination, and yeast-two-hybrid assays, these findings strongly imply that Ras, PP1, and Chickadee bind to Pico directly. The investigations also indicated that Pico, much like Lpd and RIAM, could complex with the Talin homolog Rhea, although neither direct interaction or a protein region mediating this association was identified (Lee et al., 2009).

Unfortunately, it was not possible to verify Enabled binding to Venus-Pico by co-IP as the Enabled antibody could not be optimised for use in western blots, and mass spectrometry failed to identify any analogous peptides. It should be noted that an inability to identify proteins through mass spectrometry does not necessarily confirm an absence, as large peptides, highly folded proteins, and disulphide rich proteins are often problematic to detect (Lubec and Afjehi-Sadat, 2007). However, based on the well established interactions between MRL proteins and Ena/VASP described within the literature, in addition to findings from the yeast-two-hybrid assays, it is likely that Pico binds directly to Enabled via its C-terminal proline rich motifs (Krause et al., 2004, Lafuente et al., 2004, Taylor, 2010)

5.6.1. MRL proteins directly bind Erk1/2 via the highly conserved MAPK motif

Bioanalysis performed in Chapter 3 highlighted the presence of a highly conserved MAPK binding site adjacent to the RA domain in all MRL proteins ($MAPK^{site1}$), while a second motif positioned at the N-terminus of the RA domain was discovered in Lpd, RIAM and Mig-10 ($MAPK^{site2}$). Neither of these sites had previously been described in the literature, however, western blots of $Pico^{WT}$ and Lpd co-IPs confirmed that the Erk1/2 MAPK homolog Rolled was able to interact with both proteins *in vivo* (Colo et al., 2012b). Furthermore, Lpd and Pico constructs possessing mutations within $MAPK^{site1}$ were unable to bind Rolled, while a short RIAM peptide containing only the coiled-coil motif but not $MAPK^{site2}$ was able to interact with both Erk1/2 and Rolled. These findings revealed that the MRL proteins are able to interact directly with Erk1/2 or Rolled via the highly conserved $MAPK^{site1}$ binding site, however, the functionality of $MAPK^{site2}$ is still unclear. Recent studies have shown the coiled-coil region, within which the conserved $MAPK^{site1}$ motif is contained, is involved in homodimeric interactions in Lpd (Chang et al., 2013). As yet it is unknown how these associations affect Erk1/2 binding, or whether $MAPK^{site2}$ compensates should $MAPK^{site1}$ be blocked.

5.6.2. Rolled phosphorylates Pico at Serine 819 to enable PP1 binding

Experiments performed in this chapter indicated that Pico is capable of interacting with activated Rolled. Further studies utilising $Pico^{MAPK}$, which disrupts binding to MAPK, implicate Rolled in the phosphorylation of Serine 819, a residue situated next to the PP1 binding motif. Interestingly, PP1 was not detected in precipitates containing $Pico^{S819A}$, a non-phosphorylatable Pico mutant, by Western blotting, whilst the phosphomimetic $Pico^{S819D}$ construct was, contrastingly, shown to interact. This suggests that phosphorylation of Ser 819 allows direct associations with PP1. When combined, these findings enable a mechanism to be proposed whereby Rolled binds directly to Pico via the conserved MAPK motif and phosphorylates Ser 819 when in an activated state. This modification may cause a conformational change in Pico's structure, thereby facilitating binding to PP1.

Neither Rolled nor PP1 appeared to affect Pico's ability to complex with any of its other recognised interaction partners. Given their well established roles in regulation, this finding suggests that PP1, and possibly Rolled, may function in controlling the activity of Pico's associated proteins rather than its affinity towards them (Cohen, 2002, Nishimoto and Nishida, 2006). Consequently, until further phenotypic analysis is carried out on the respective mutants, it will not be possible to determine the overarching effects these regulatory proteins have.

5.6.3. Limitations in the procedures carried out

Idealy pulldowns would have been performed on endogenous Pico as a means of identifying complexed proteins, however, due to antibody limitations ectopic expression of a Venus-tagged peptide was required for successful and accurate precipitation. Also, while Western blot analysis of Venus-Pico co-IPs was successfully carried out to confirm interactions with Rolled, PP1, Ras, Chickadee, and Rhea, corresponding pulldowns using the associated partners as bait were not examined. This was due to the impracticalities associated with optimising co-IPs with a range of different antibodies within the time frame available. In addition, there would have been significant difficulties recognising Pico within the pulldowns as the GFP antibody could only adequately detect Venus-tagged proteins when present in high quantities, while the Pico specific antibody designed in-house did not work on immunoblots. However, it should be noted that a wealth of complementary evidence exists to support the majority of findings from the co-immunoprecipitation experiments, meaning a failure to perform corresponding pulldowns does not impede sound inferences being formed.

Next, mass spectrometry indicating potential interactions with cdc42 and Fasciclin 1 was only performed once. Usually this type of analysis would be repeated at least two more times before firm conclusions could be made, however, due to cost issues and limitations in the quality of results generated from the initial investigation, this form of assessment was not carried out again. Consequently, given the inability of cdc42 and Fasciclin 1 to be detected in pulldowns following issues surrounding antibody optimisation, it is not possible to sufficiently conclude if that these associations take place.

Lastly, due to the variable nature of *hs-GAL4* mediated expression, in addition to inconsistencies surrounding the pulldown efficiency of GFP-Trap (most notable in the disparity between Chickadee blots), it was not feasible to accurately compare subtle differences in binding affinities. As such, it was only possible to precisely corroborate either affirmative or negative associations between a construct and its interaction partner, meaning the apparent semblance in Ras binding between the $Pico^{RE}$ and $Pico^{RR}$ mutants may not be veritable.

6. Pico localisation

6.1. Introduction

A seminal paper presented by Abercrombie described three fundamental structures present within migrating cells; the lamellipodia, filopodia, and membrane ruffles (Abercrombie, 1980). The lamellipodium constitutes a thin layer of cytoplasm about 0.2 μm thick which protrudes at the front of spreading and migrating cells as shown in Figure 6.1.1. (Small et al., 2002). It is formed from the force generated by actin polymerisation pushing against the leading edge when coupled to the traction providing extracellular matrix (Ridley et al., 2003, Le Clainche and Carlier, 2008).

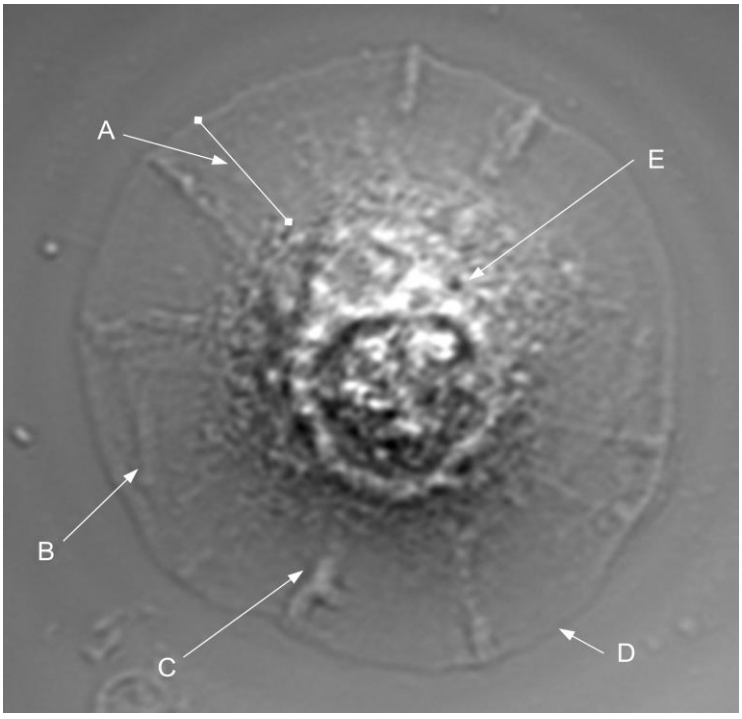

Figure 6.1.1. Illustrative cell possessing distinctive lamellipodia and membrane ruffles. Illustrative image of a cell in the process of spreading across a substrate. The annotations highlight (a) the lamellipodium, (b) lateral membrane ruffles, (c) radial membrane ruffles, (d) the leading edge, and (e) the cytoplasm.

Depending on the cell type and condition, the lamellipodium can vary from around 1 μm to 5 μm in breadth (Small et al., 2002). Contained within this structure are small bundles of actin filaments termed 'ribs', which are believed to form the precursors for finger-like filopodia protrusions that extend beyond the leading edge to sense the surrounding environment (Small, 1988, Le Clainche and Carlier, 2008). As the plasma membrane continues to expand at the cell front, material is constantly recycled from the leading edge via retrograde membrane ruffles (Wurtzel et al., 2012). These are found to occur in cellular zones undergoing rapid reorganisation of the plasma membrane and often precede the formation of a lamellipodium (Mahankali et al., 2011). When viewed down a microscope, membrane ruffles appear as regions of the lamellipodium which curl upwards, and can be found both at, or behind, the leading edge as demonstrated in Figure 6.1.1. (Abercrombie, 1980, Small et al., 2002).

6.1.1. MRL localisation

The presence of a characteristic PH domain strongly implies that MRL proteins possess the ability to localise at the cell membrane via interactions with phosphoinositides. Indeed, studies found that RIAM is present within both the cytoplasm and lamellipodia, whereas Lpd predominantly localises at the plasma membrane (Lafuente et al., 2004, Jenzora et al., 2005, Krause et al., 2004). It is thought this variation in cellular localisation is due to the differential PI binding preferences displayed by their PH domains, with RIAM primarily binding PI(3)P and PI(5)P, while Lpd interacts with $PI(3,4)P_2$ (Jenzora et al., 2005, Krause et al., 2004, Lemmon, 2008). Interestingly, MIG-10 has been found to localise asymmetrically within peripheral regions of the lamellipodia in response to external directional signals such as UNC-6 or SLT-1, enabling control over the directionality of cellular migration (Quinn et al., 2006).

In line with these findings, functional studies within single cells have revealed RIAM to be involved in promoting F-actin formation, cell spreading, and lamellipodia formation, while Lpd controls lamella protrusion velocity through regulation of actin branching density as well as F-actin levels (Lafuente et al., 2004, Krause et al., 2004). Overexpression of MIG-10 has also been found to encourage lamellipodial formation in a similar manner (Quinn et al., 2006).

Further investigations assessing co-localisation have lent additional support to previous findings generated from MRL binding analysis, with Lpd, RIAM, and MIG-10 shown to co-localise alongside Ena/VASP and F-actin at lamellipodia and filopodia tips, while RIAM was positioned together with vinculin and actin at early focal adhesions (Jenzora et al., 2005, Lafuente et al., 2004, Krause et al., 2004, Quinn et al., 2006). Contrastingly, very little work has so far been carried out assessing the subcellular localisation of Pico. This form of investigation is important not only for establishing Pico's cellular distribution, but also for determining where in the cell interactions with its associated partners are likely to take place.

6.1.2. Aims

The aim of the research presented in this chapter was to examine Pico's localisation at the subcellular level in adherent *Drosophila* S2 cells that had been induced to spread and project lamellipodia (Rogers et al., 2002, Rogers et al., 2003). Initially a time course assay was performed to ascertain how Pico's localisation changed as the cells spread on the substrate as well as enabling an optimal time for fixation to be established for immunofluorescent antibody staining. Experiments assessing the localisation of Pico's binding partners alone was carried out and the results compared to findings from the Vale lab to validate the procedures and fixation time used (Rogers et al., 2003). Co-localisation experiments were then performed to confirm if Pico and the binding proteins identified in Chapter 5 occupy overlapping subcellular distributions, which would provide support that these proteins interact *in vivo* and not just in cell extracts. The ability of the mutant constructs to localise to the same position as wild type Pico was also assessed prior to further co-localisation studies being carried out to determine if the mutants affected the distribution of Pico-binding proteins. Lastly, co-expression studies were implemented using wild type wing discs to assess if endogenous Pico and its binding partners are expressed in the same tissues at the same time.

6.2. Assessing cell spreading on ConA coated plates

Previous work reported by Rogers *et al.* 2002 demonstrated a means of inducing cell spreading and lamella formation in S2 cells through the use of ConA coated substrates. Further work carried out within the Valle lab confirmed the presence of numerous actin regulatory proteins within the lamellae and leading edge of S2 cells using similar techniques (Rogers et al., 2003). Consequently, experiments evaluating Pico's localisation within S2 cells spread on ConA coated plates were designed, however, repeated attempts to replicate the phenotype generated in these papers were unsuccessful using the recommended cell line (Rogers et al., 2002, Rogers et al., 2003). It was observed that S2 cells, normally grown in suspended cell cultures, would merely rest on the surface of the substrate and fail to attach regardless of the ConA concentration or cell density (Figure 6.2.1.a) (Schneider, 1972). Instead, the more adherent S2R+ (S2 receptor plus) cell line, differing mainly though the possession of the wingless receptors Dfrizzled-1 and Dfrizzled-2 (Yanagawa et al., 1998), was tested and found to successfully bind and spread across the ConA coated substrate leading to the formation of well defined lamellipodia (Figure 6.2.1.b). The size of the lamella varied between cells from around 1 μm to 7 μm in breadth and often contained distinctive membrane ruffles in both lateral and less frequent radial formations, however, no filopodia were detected in any of the studies carried out.

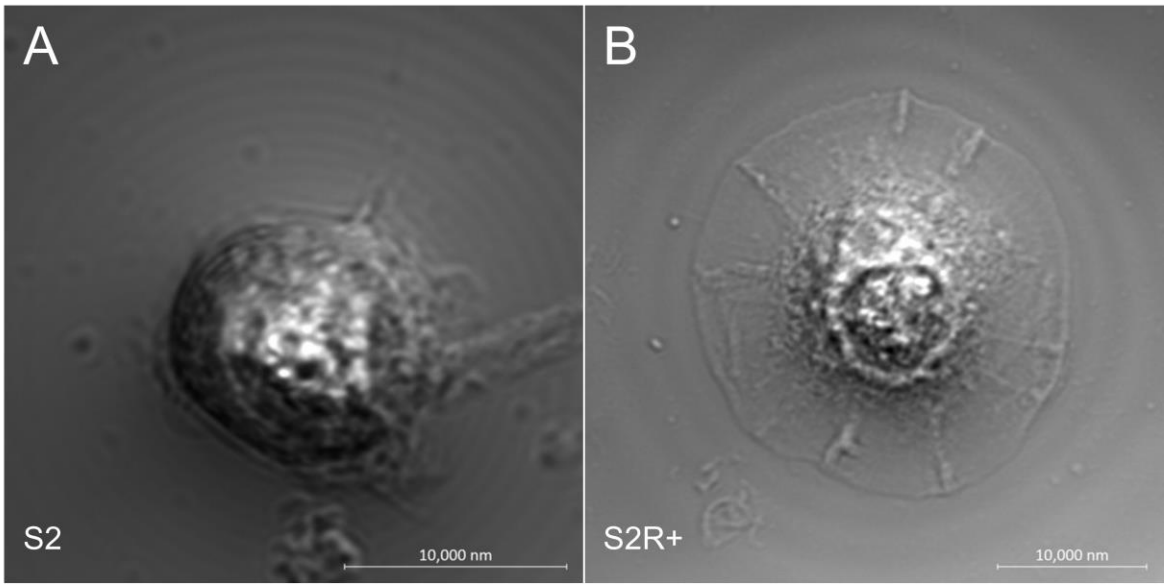

Figure 6.2.1. Capacity of S2 and S2R+ cells to spread on ConA coated substrates. Representative figures of (a) S2 and (b) S2R+ cells spread on ConA coated glass plates. S2 cells grown in suspended cultures rested on the substrate surface and failed to attach. Conversely, the more adherent S2R+ cells successfully bound and spread across the coated plates, leading to the formation of well defined lamellipodia with distinct membrane ruffles.

6.3. Pico localisation

Next, subcellular distribution of Pico during S2R+ cell spreading on ConA coated surfaces was assessed through fixed time course assays. Attempts to detect endogenous Pico using an antibody generated in-house failed to yield sufficient levels of staining for accurate imaging to be performed (data not shown). This antibody had been successfully used to stain a variety of tissues during previous research carried out within the Bennett lab (Lyulcheva, 2006, Taylor, 2010), implying that the endogenous levels of Pico may be low in S2R+ cells. Therefore, cells were transiently transfected with a plasmid capable of ectopically expressing Venus-Pico^{WT} under the control of an act5c promoter. Transfected cells were plated onto ConA coated glass plates and fixed with paraformaldehyde after different time points before confocal imaging of the Venus-tagged protein. Analysis of the resulting images showed that cells in the same field of view landed and initiated spreading across the substrate at different times, indicating a degree of

heterogeneity in the behaviour of cells within each population. Therefore to capture how the distribution of Venus-Pico might be affected during the spreading process, only cells displaying a novel morphology absent in earlier time points were analysed. Also, images were only taken of cells expressing Pico at optimal levels, as high quantities caused large aggregates to form, whereas too little prevented sufficient detection. The change in Venus-Pico distribution during the progression of cell attachment through to spreading was supported by preliminary time-lapse imaging experiments carried out when Cellfectin I was still available (data not shown).

Representative images from each time point are shown in Figure 6.3.1. Before cell spreading had commenced, ectopic Pico is distributed within the cytoplasm and generally displays a slightly heightened accumulation at the cell membrane. Within 5 minutes of adhering to the substrate, cells began to exhibit early signs of spreading, during which Pico remained localised within the cytoplasm, but could also be found in low quantities at the leading edge. As the cells continued to expand rapidly during the next 20 minutes, Pico's distribution at the leading edge began to increase, however, noticeably elevated levels of Pico were observed within highly active membrane ruffles, which form exclusively during this rapid extension phase. Pico still remained within the cytoplasm, though, after 30 minutes, cells begin to reach their maximal size and membrane ruffling was no longer observed. While cell size no longer increased, Pico was still able to accumulate at the leading edge of the lamella. However, by 45 minutes Pico had dissociated from the leading edge and was only found within the cytoplasm. When combined, these data indicated that Pico is present at the leading edge and highly active membrane ruffles only when the cells are spreading, strongly implicating Pico in processes involved in membrane remodelling and cellular migration.

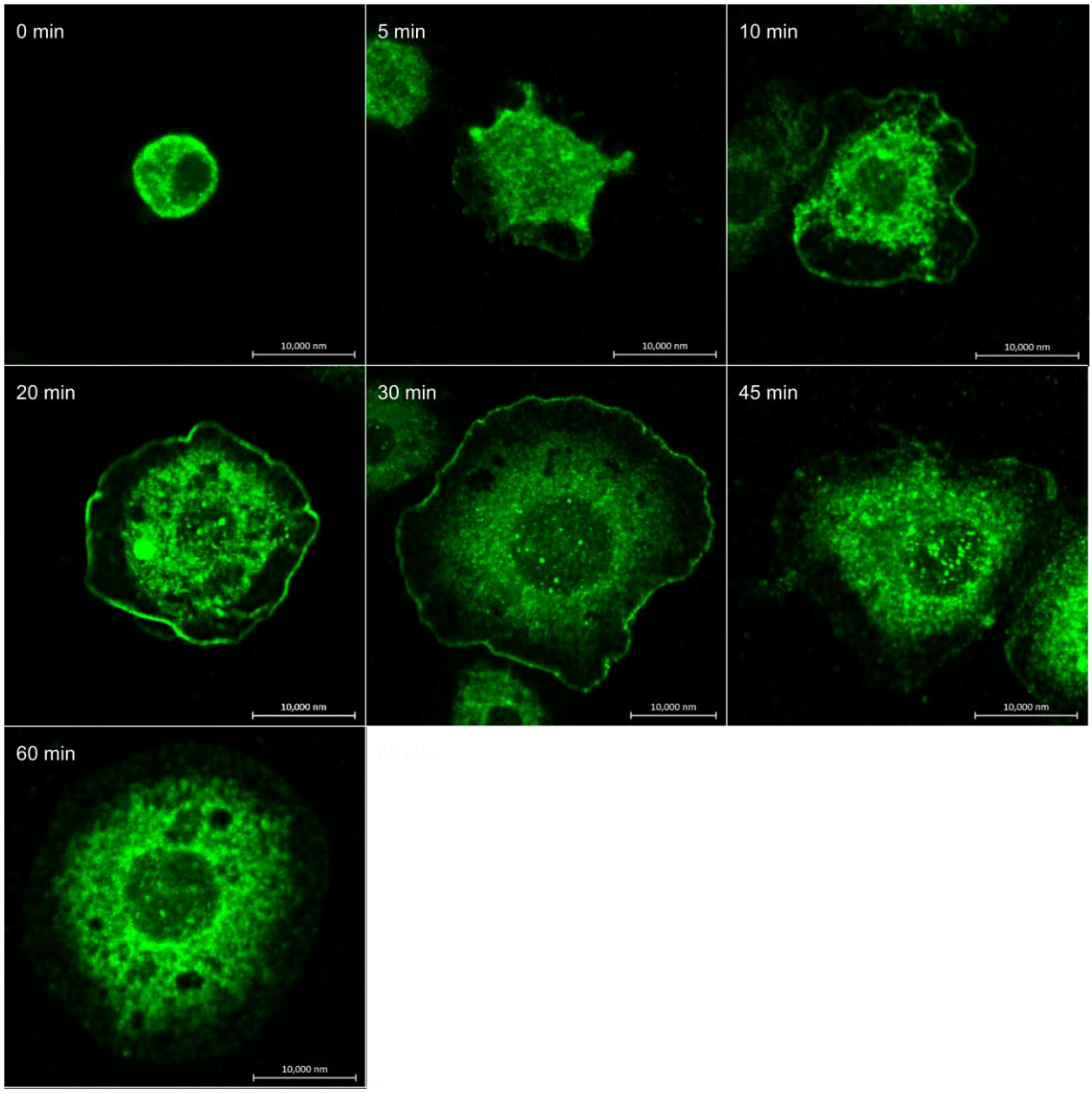

Figure 6.3.1. Time course examining the localisation of Venus-Pico during spreading of S2R+ cells. As S2R+ cells spread across the ConA coated substrate, Venus-tagged Pico localised to the leading edge and highly active membrane ruffles. Once cells reached their maximum size, membrane ruffles no longer formed and Venus-Pico gradually dissociated from the leading edge, eventually residing only within the cytoplasm.

6.4. Localisation of Pico interacting proteins

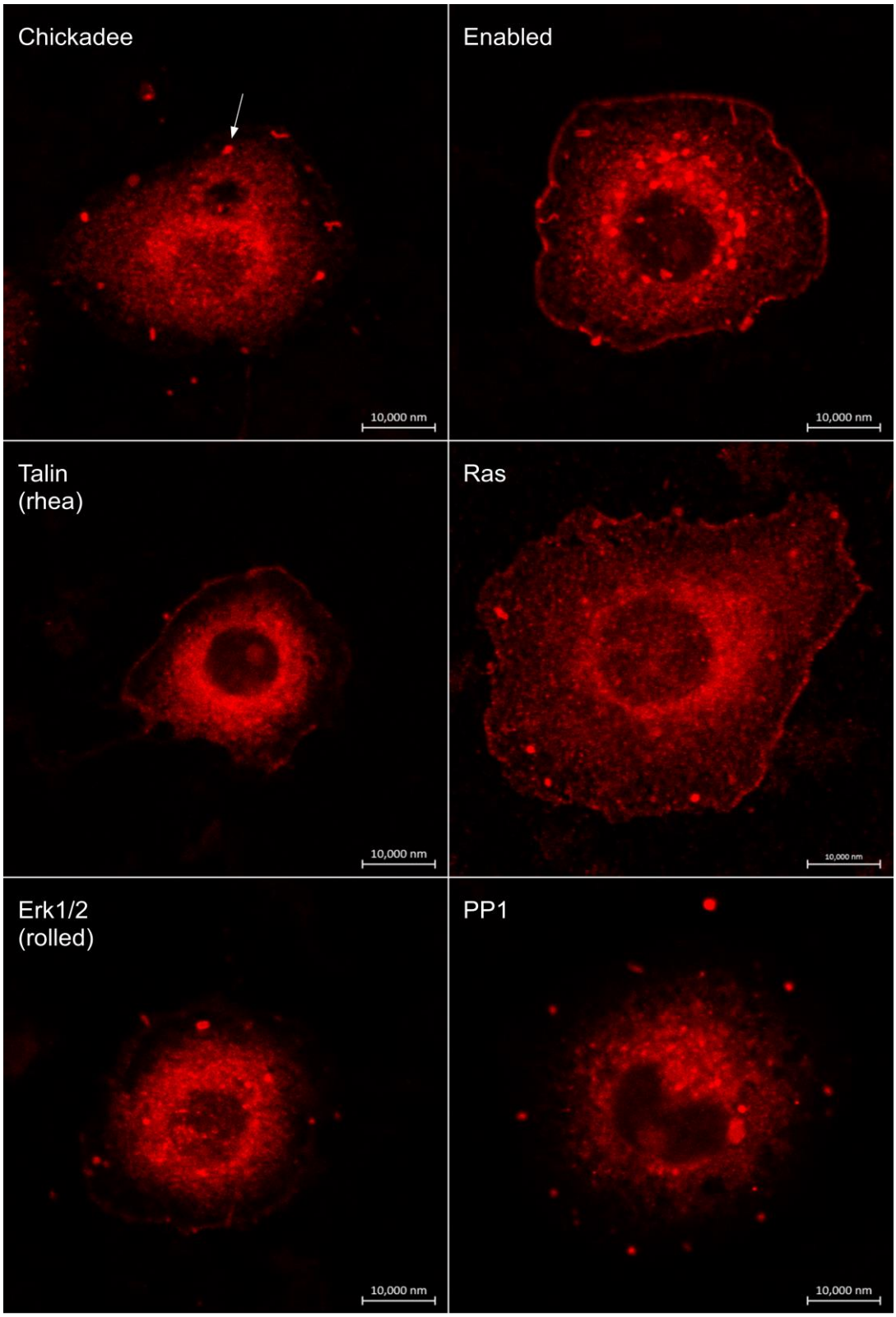

Figure 6.4.1. Localisation of Pico interacting proteins. S2R+ cells allowed to spread on ConA coated plated were fixed and stained for Chickadee, Enabled, Talin/Rhea, Ras, Erk1/2/Rolled, and PP1 to ascertain their cellular distribution. All the proteins were found to localise within the cytoplasm, however, Enabled, Rhea, Ras, and to some extent Rolled, also accumulated at the leading edge. Interestingly, both Chickadee and PP1 were observed at small 'puncta' within the lamella (indicated with arrow), while only Chickadee exhibited significant nuclear distribution.

To determine the distribution of Pico-interacting proteins, fixed S2 cells were stained by indirect immunofluorescence using primary antibodies to the proteins of interest. Based on findings from the time course assays, in addition to the methodology described by Rogers *et al.* 2003, it was decided that cells would be allowed to spread for 30 minutes on ConA treated plates before fixation and staining. This timing was proven to yield the greatest number of cells at both the rapid expansion and maximal spreading stages represented by the 20 and 30 minute images in Figure 6.3.1. respectively.

To validate the fixation and staining protocol, fixed cells were first stained for Chickadee and Enabled, whose distribution has previously been reported in S2 cells (Rogers et al., 2003). As previously reported, Chickadee was predominantly localised within the nucleus and cytoplasm, while Enabled was perceived to mainly accumulate at the leading edge and cytoplasm (Figure 6.4.1). Interestingly, small 'puncta', apparently unconnected with focal adhesions, but reported to be characteristic of Chickadee's distribution, were also observed (Rogers et al., 2003).

Next, fixed cells were stained for the Pico interacting proteins Rhea, Ras, Rolled, and PP1 (Figure 6.4.1.). Rhea was found to localise largely within the cytoplasm and modestly at the cell front, while Ras was distributed fairly evenly amongst the cytoplasm and lamella, but displayed some degree of accumulation at the leading edge. Rolled was also predominantly observed within the cytoplasm, although low levels were detected at the cell boundary. Lastly, PP1 was located almost exclusively within the cytoplasm, however, 'puncta' similar to those discovered within chickadee stained cells were also detected.

6.5. Pico co-localisation

While Enabled, Rhea, Ras, and Rolled all displayed cytoplasmic and leading edge distributions similar to that found in Pico, it did not confirm whether analogous spatial/temporal localisation to Pico occurs. Consequently, co-localisation studies were carried out to determine how the cellular distribution of Venus-Pico aligned with that of its binding partners during the rapid expansion and maximal extension stages of cell spreading.

6.5.1. Pico accumulates at membrane ruffles during the rapid expansion phase

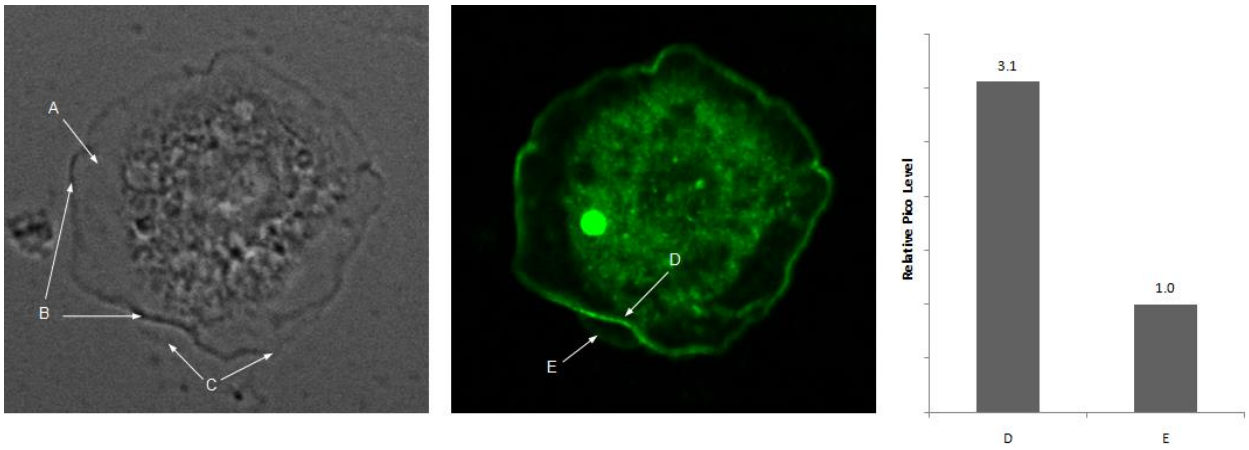

Figure 6.5.1. Pico's accumulation at membrane ruffles during the rapid spreading phase. Venus-Pico^{WT} expressing S2R+ cells were spread on ConA coated plates and fixed using paraformaldehyde. Cells exhibiting rapid expansion were examined and shown to possess characteristic (a) lamellipodia, and (b) membrane ruffles, in addition to (c) a well defined leading edge. Further analysis revealed Pico levels are significantly higher within (d) the ruffles compared to (e) the leading edge. Quantification of relative Venus-Pico levels revealed a general three-ten fold (mean 3.73, p = <0.001) difference between membrane ruffles and leading edge.

Initially, analysis of Pico's distribution during the rapid expansion phase of S2 spreading was carried out. The results shown in Figure 6.5.1 revealed Pico to predominantly accumulate within the supposedly highly active membrane ruffles which form during this period (Small et al., 2002). Indeed, further examination using the linear plot profile tool within ImageJ indicated Pico

levels are generally between 3 and 10 times higher (mean 3.73, p = <0.001, t-test) within ruffles compared to the leading edge, and that this Pico accretion is characteristic of all ruffle formation.

6.5.2. Pico co-localises with the majority of its binding partners within membrane ruffles

Next, the ability of Pico to co-localise with its identified binding partners from Chapter 5.2. was examined in S2R+ cells displaying rapid spreading. Cells transiently expressing Venus-Pico^{WT} were allowed to spread for 20 minutes before being fixed and stained with an appropriate antibody. Detected levels of Pico and the protein of interest were independent and adjusted so apparent fluorescence was broadly equivalent. Initially, co-localisation with the actin regulatory protein Chickadee was assessed. The results presented in Figure 6.5.2. indicate that within the membrane ruffles, characterised by the sizeable accumulation of Pico, both Pico and Chickadee display a notable degree of co-localisation. Contrastingly, despite the presence of reasonable levels of Pico at the leading edge, no corresponding accrual of chickadee was observed, implying associations between the two proteins only occurred within the highly active ruffles.

Co-localisation between Pico and the anti-capping protein Enabled was also analysed. The findings displayed in Figure 6.5.3. revealed Pico and Enabled exhibit considerable levels of association inside membrane ruffles, as confirmed by overlap of immunofluorescent staining (indicated in yellow within the merged image). Indeed, during this rapid cell spreading stage, Enabled is found almost exclusively within ruffled regions while very little is present at the seemingly less active areas of the leading edge (see appendix 5 for further examples). While comparatively low levels of Pico were still observed at cell boundary areas devoid of ruffles, virtually no Enabled could be detected, suggesting that Enabled, much like Chickadee, only associates with Pico in ruffled regions during expansion of the lamella.

Rhea-Pico co-localisation was assessed in cells exhibiting high levels of spreading as well. Figure 6.5.4. shows that Pico and Rhea display similarly elevated accumulation within ruffled regions, but also demonstrate analogous localisation at the leading edge as well as the cytoplasm. Taken together, these findings indicate that Pico and Rhea exhibit close associations throughout the cell during this phase of cell spreading.

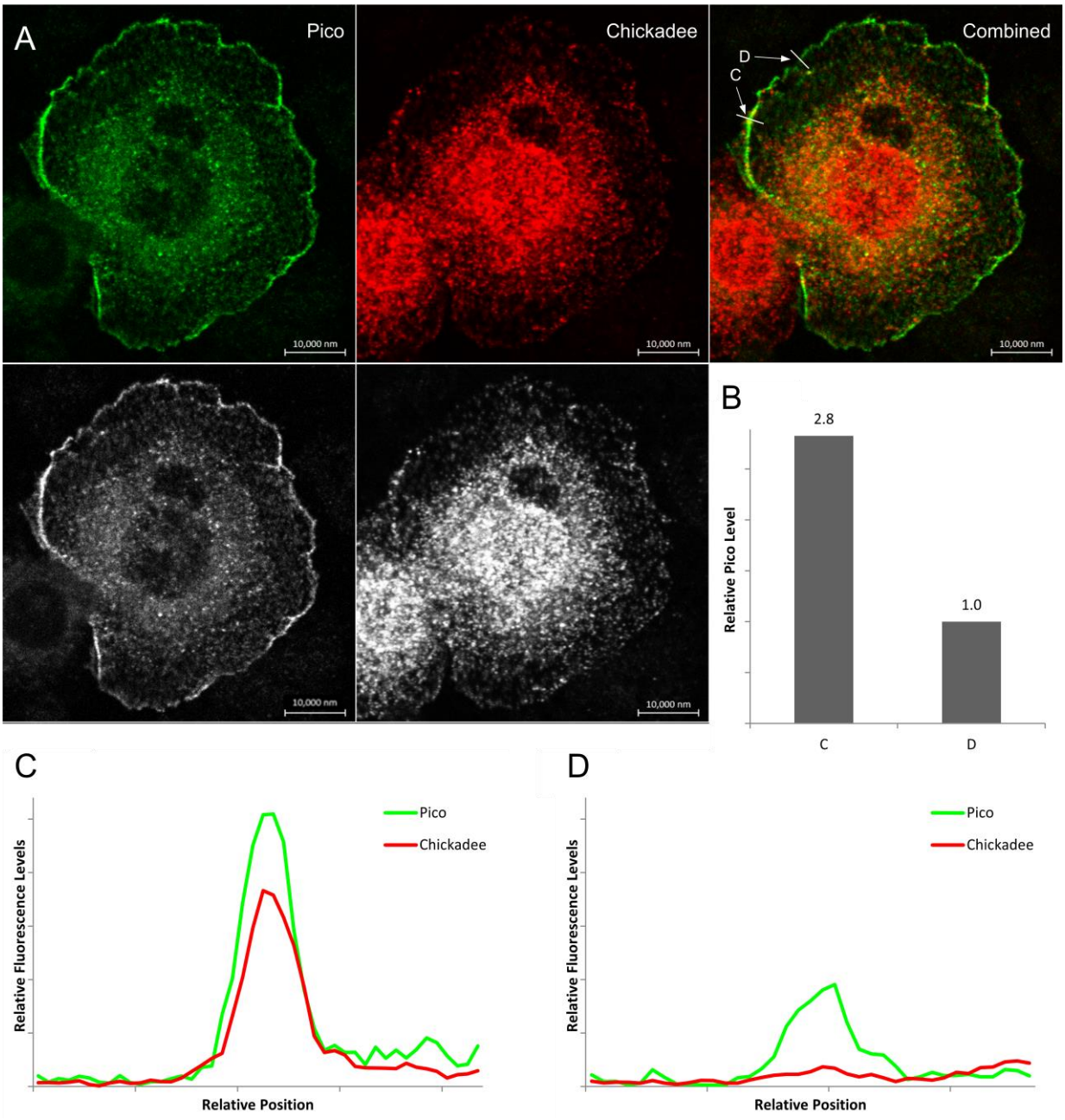

Figure 6.5.2. Co-localisation between Pico and chickadee at membrane ruffles. (a) Venus-Pico^{WT} expressing S2R+ cells spread on ConA coated plates were fixed and stained for Chickadee. Cells exhibiting rapid extension were selected and (b) relative levels of Pico examined to confirm correct identification of membrane ruffles and the leading edge. Co-localisation studies revealed that Pico associated with Chickadee in (c) membrane ruffled regions, but (d) not at the leading edge.

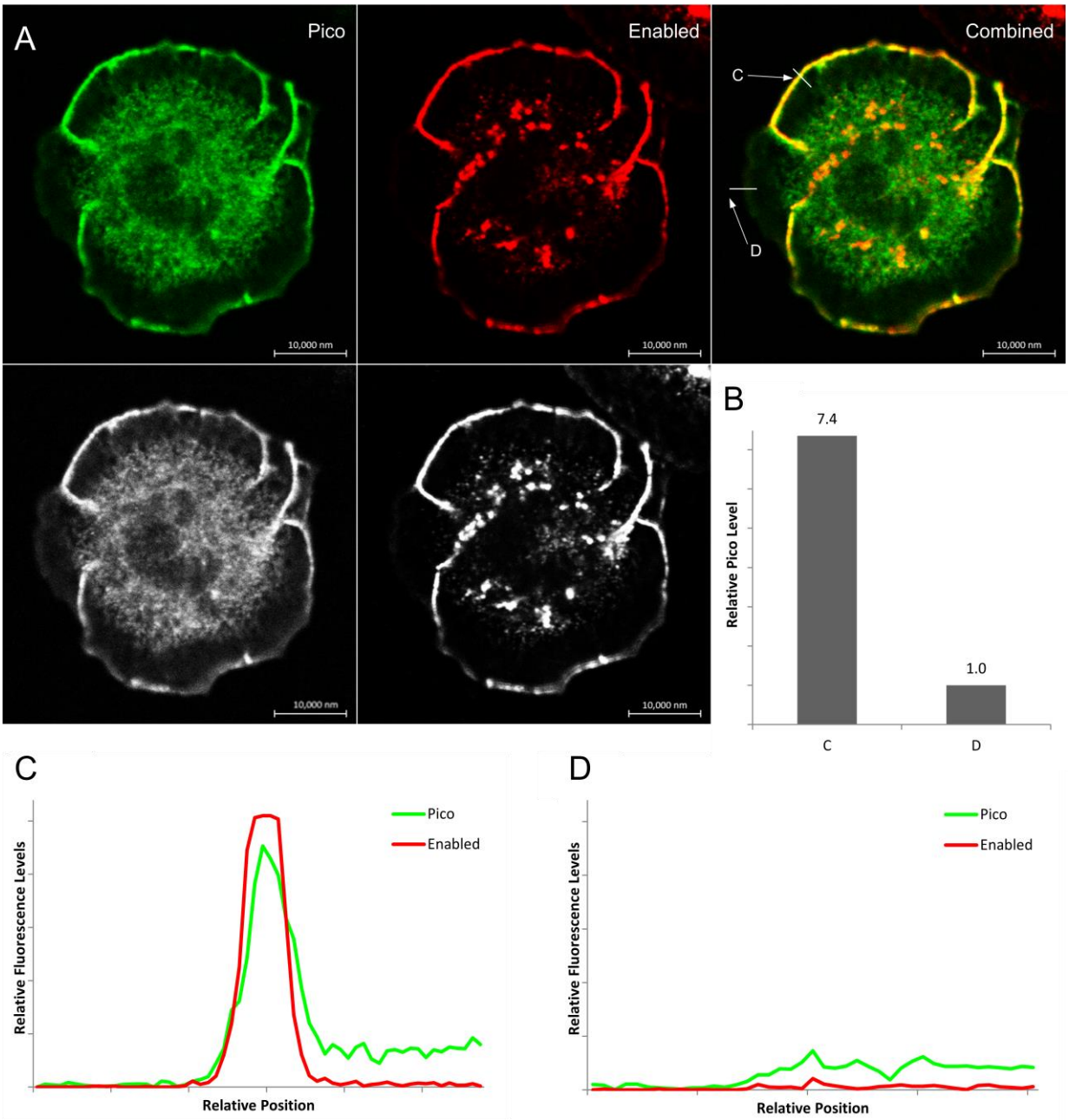

Figure 6.5.3. Assessment of Pico-enabled co-localisation at membrane ruffles. (a) S2R+ cells expressing Venus-Pico^{WT} were spread on ConA coated plates before being fixed and stained for Enabled. Cells displaying rapid expansion were selected for and (b) relative levels of Pico assessed to allow characterisation of membrane ruffles and the leading edge. Examination showed strong co-localisation between Pico and Enabled within (c) membrane ruffles, however, none was found at (d) cell boundary regions devoid of ruffles.

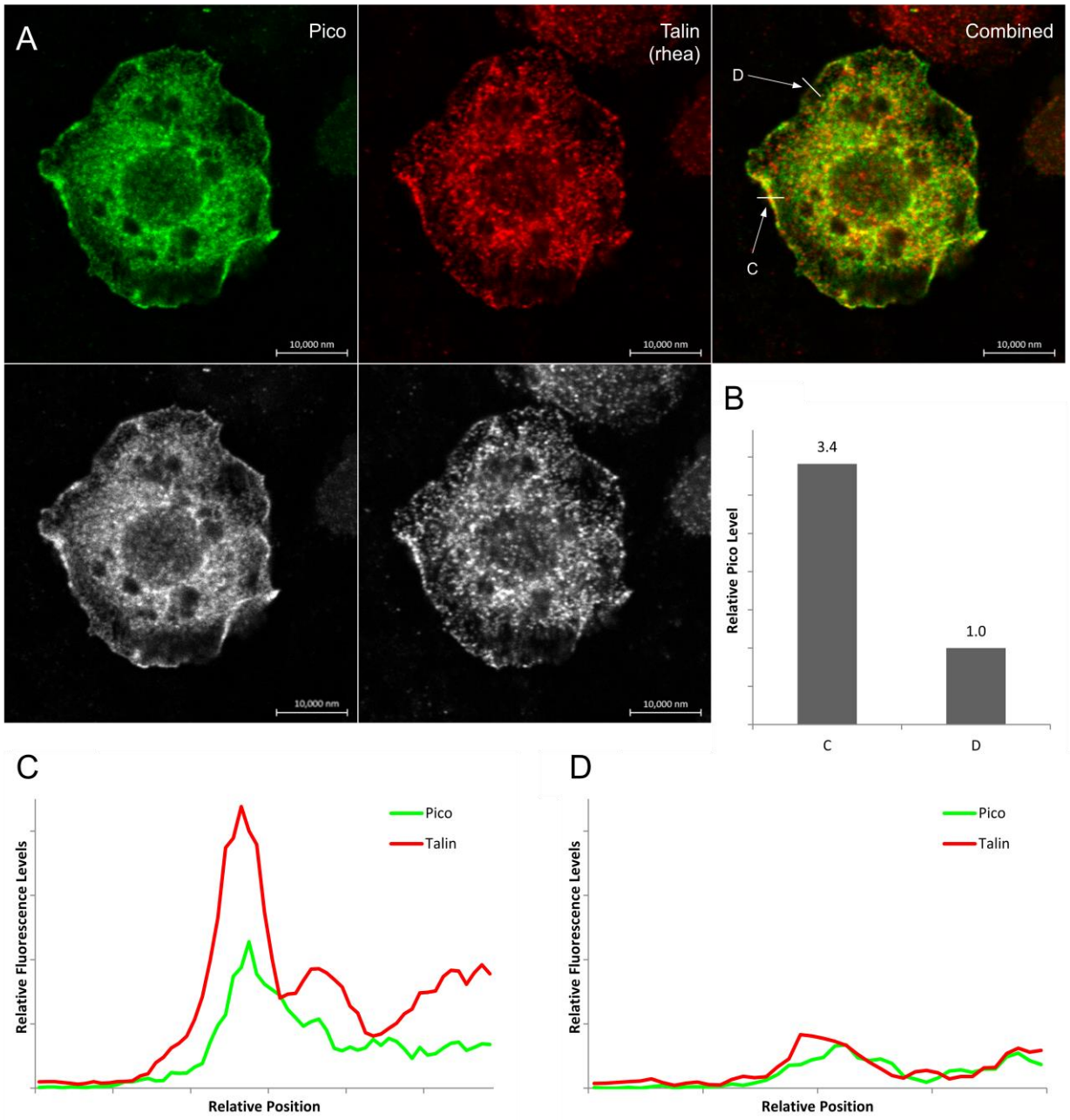

Figure 6.5.4. Associations between Pico and rhea within membrane ruffled regions. (a) Venus-Pico^{WT} expressing S2R+ cells were spread on ConA coated plates, fixed and stained for Talin (rhea). Cells exhibiting spreading were selected and (b) levels of Pico examined to enable differentiation between membrane ruffles and the leading edge. Co-localisation studies revealed that Pico associated with Rhea in both (c) membrane ruffled regions and (d) the leading edge in rapidly expanding cells.

Additional analysis was performed to assess co-localisation between Pico and Ras. The findings presented in Figure 6.5.5. reveals noticeable co-localisation between Pico and Ras within membrane ruffles, however, lower levels of both proteins were observed at the leading edge with less correlation present between their relative fluorescence levels. These results suggest Pico and Ras only co-localise within the highly active ruffled regions during this highly expansive phase.

Examination of Pico's co-localisation with the MAPK Rolled was also performed in cells exhibiting high rates of spreading. The results displayed in Figure 6.5.6. indicate that within the membrane ruffles, both Pico and Rolled display notable levels of co-localisation. Although, Pico is still present at the cell boundary, Rolled could not be detected, suggesting this association only occurs in ruffled regions during rapid expansion phase. Interestingly, the example cell presented in Figure 6.5.6. also displays radial rib-like ruffle structures sometimes found to run perpendicular to the leading edge. Much like their aforementioned counterparts, these radial structures exhibit significant Pico accumulation and display similar co-localisation results to those involved in outward cell spreading (data not shown). While an appropriate function has not yet been ascribed to these structures, it is thought they may assist in sideways expansion of the lamellipodium to prevent excessive strain being placed on the membrane as the cell develops outwards. However, given the striking similarities between both ruffle types, this report only focuses on those involved in outward extension of the cell.

Lastly, co-localisation between Pico and the phosphatase PP1 within rapidly expanding S2R+ cells was analysed. Figure 6.5.7. shows that PP1, unlike the other proteins assessed, failed to significantly associate with Pico within ruffled regions, however, it did display a similar spatial distribution at the cell boundary although levels remain low.

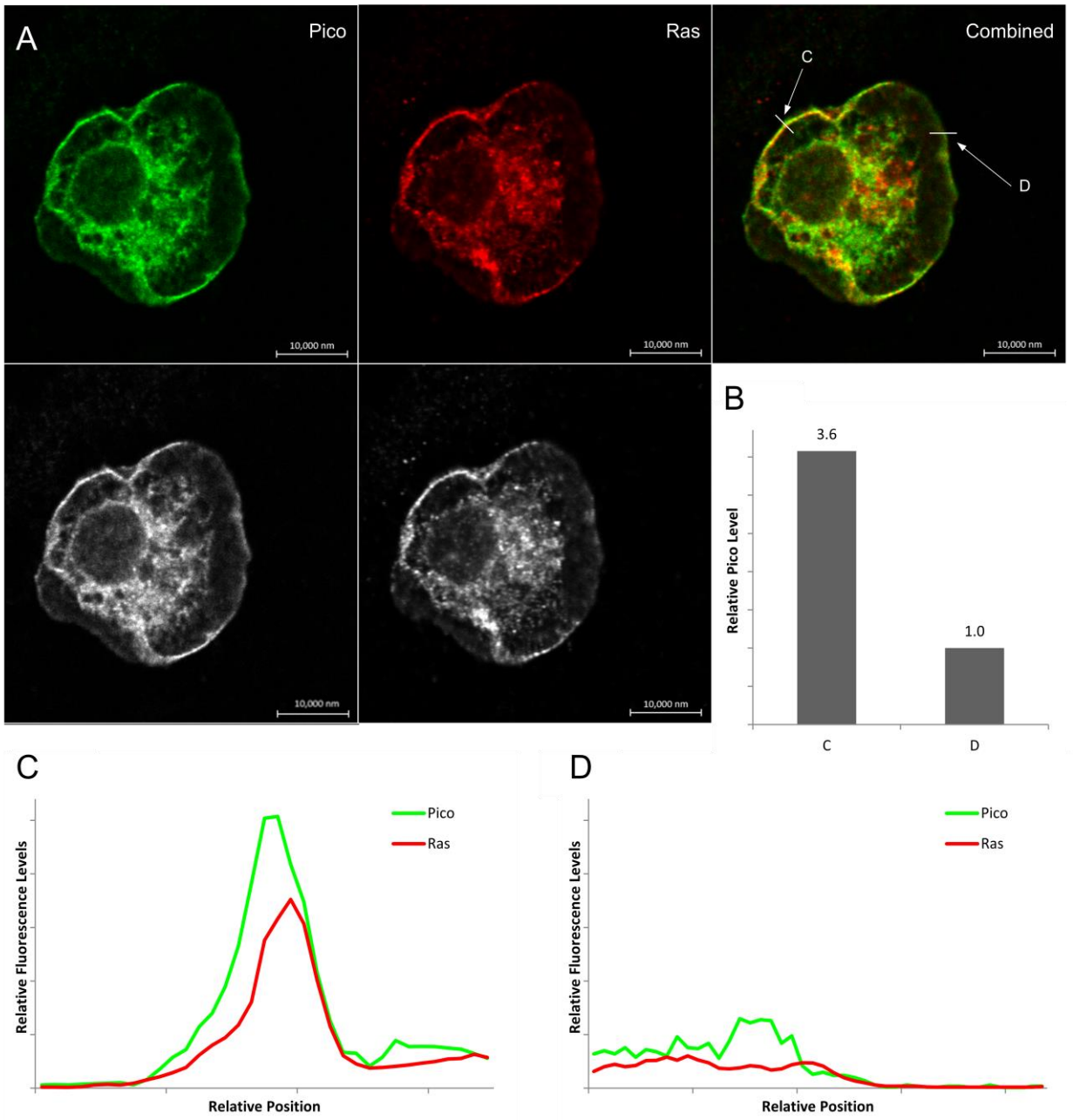

Figure 6.5.5. Co-localisation between Pico and Ras within membrane ruffles. (a) S2R+ cells expressing Venus-Pico^{WT} were spread on ConA coated plates before being fixed and stained for Ras. Cells within the rapid extension phase were selected for and (b) relative levels of Pico analysed to enable characterisation of membrane ruffles and the leading edge. Co-localisation studies revealed Pico to be closely associated with Ras within (c) membrane ruffles, however, (d) cell boundary regions exhibited significantly lower levels of both proteins with little analogy.

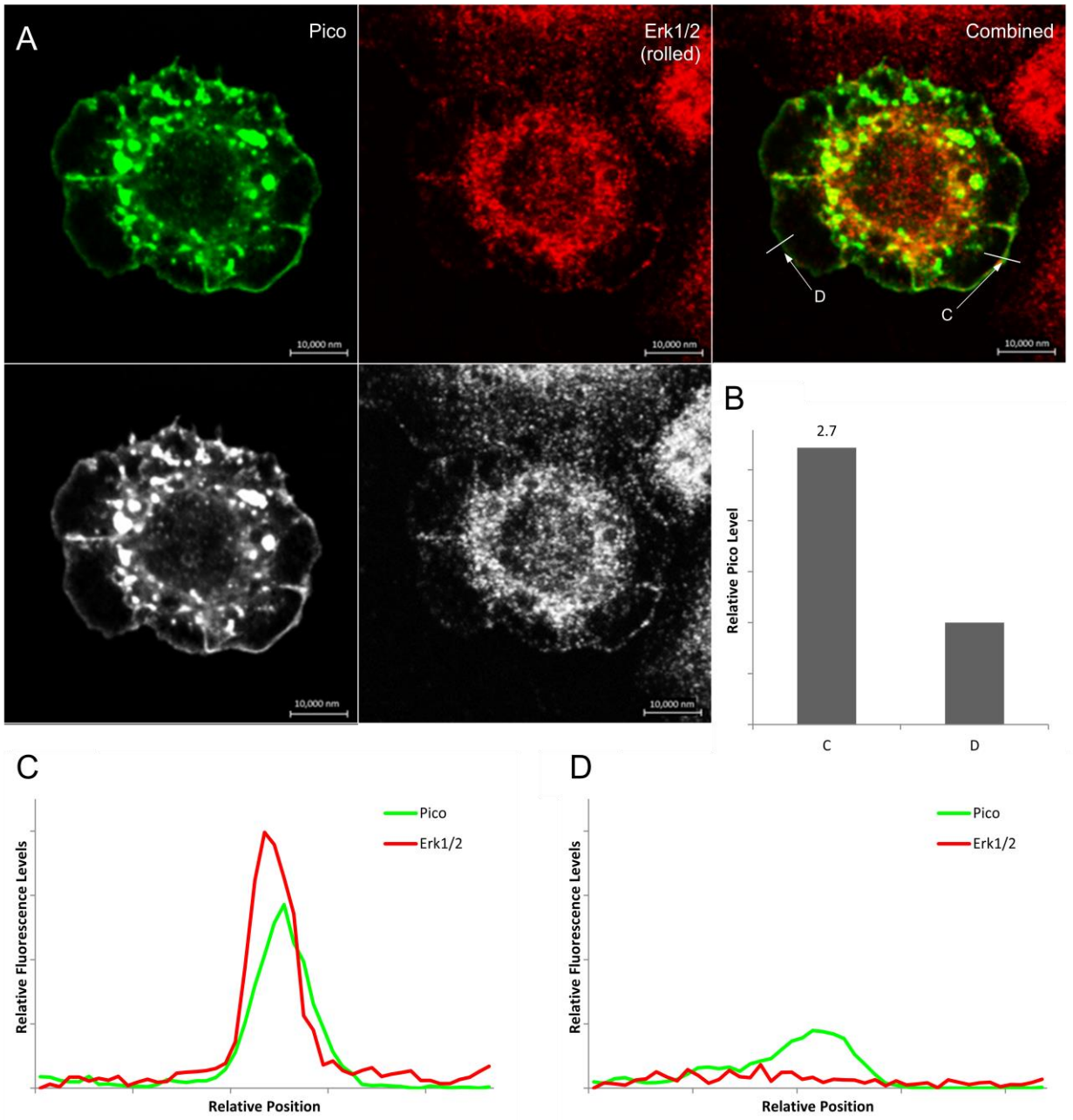

Figure 6.5.6. Associations between Pico and rolled at membrane ruffled regions. (a) Venus-Pico^{WT} expressing S2R+ cells were spread on ConA coated plates, fixed and stained for Erk1/2 (rolled). Cells exhibiting rapid spreading were selected and (b) relative levels of Pico examined to confirm correct identification of membrane ruffles and the leading edge. Examinations showed a notable degree of co-localisation between Rolled and Pico in (c) ruffled regions but (d) not at the leading edge.

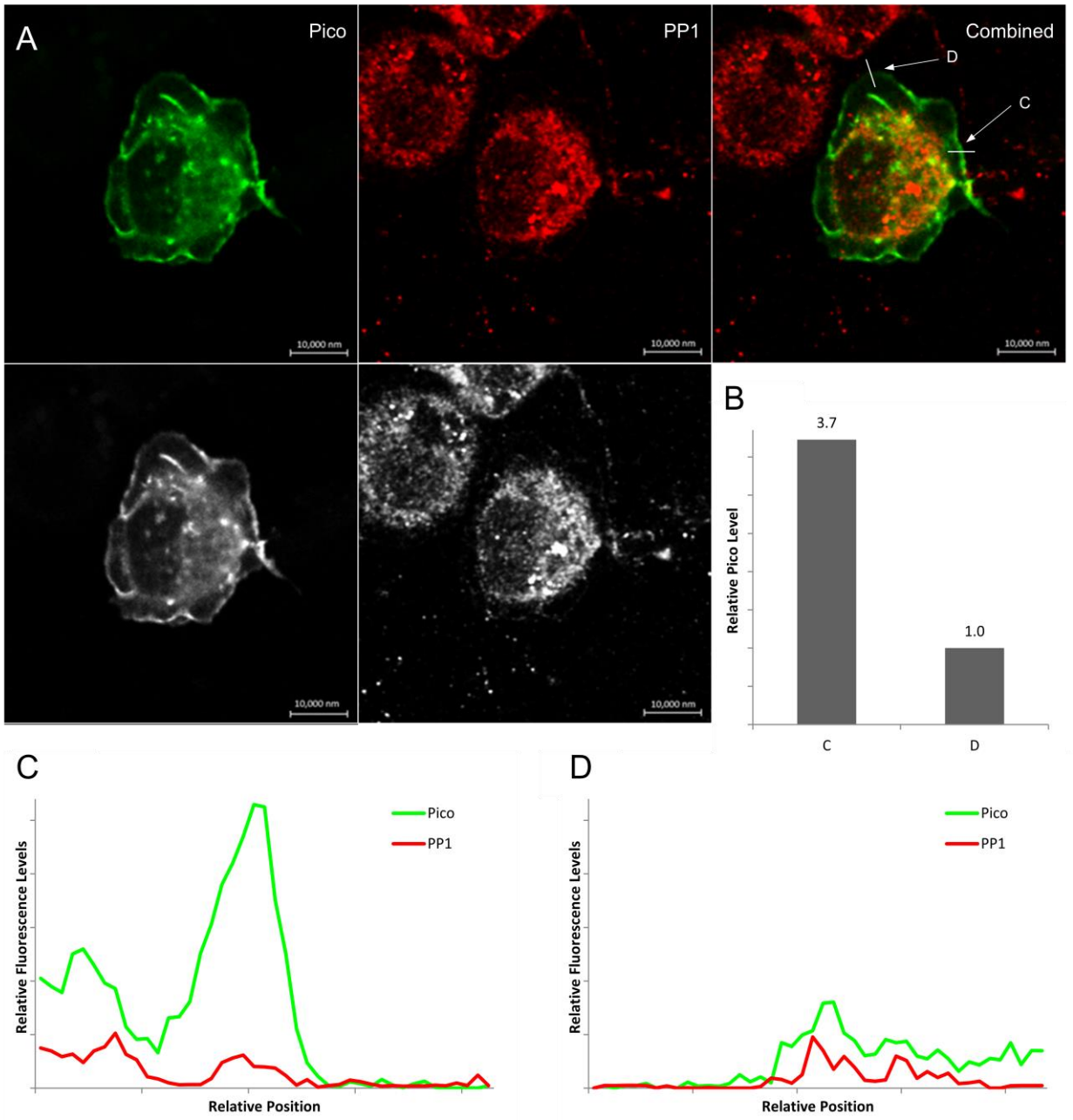

Figure 6.5.7. Examination of co-localisation between Pico and PP1 within membrane ruffles. (a) S2R+ cells expressing Venus-Pico^{WT} were spread on ConA coated plates before being fixed and stained for PP1. Cells exhibiting rapid extension were selected and (b) relative levels of Pico examined to confirm correct identification of membrane ruffles and the leading edge. Co-localisation analysis revealed that Pico does not associate with PP1 within (c) membrane ruffled regions, however, it did display some positional analogy (d) at the leading edge, although levels remain low.

6.5.3. Pico co-localises with some of its binding partners at the leading edge of maximally spread cells

Following on from analysis of cells in a rapidly expanding state, investigations were performed on those reaching the maximal extension stage of spreading where actin dynamics are thought to be lower. Cells expressing Venus-Pico were allowed to spread for 30 minutes before being fixed and stained with an appropriate antibody. Initially, co-localisation between Pico and the actin regulatory proteins Chickadee, Enabled, and Rhea was assessed at the leading edge of S2R+ cells. The results displayed in Figure 6.5.8.a indicate very little co-localisation occurs between Pico and Chickadee at the cell front as Chickadee exhibits low levels outside the nucleus and cytoplasm. Indeed, additional analysis of the relative fluorescent levels within this region, as illustrated in Figure 6.5.8.b, confirms that Pico primarily gathers at the lamella boundary whereas Chickadee levels remained low, supporting the theory that Chickadee and Pico only co-localise within active regions.

Figure 6.5.8.c implies that Pico and Enabled display significant co-localisation at the leading edge, as confirmed by the distinctive yellow areas visible in the combined image. Further verification is provided in Figure 6.5.8.d which demonstrates substantial accumulation of both proteins at the cell periphery, while considerably lower levels are present within the lamella. Interestingly, Enabled displays a reasonably even distribution throughout the lamellipodial edge at this stage, in contrast to the variegated appearance observed within the rapidly expanding cells (Figure 6.5.3.).

Rhea also displays some degree of analogous positioning with Pico at the cell front, however, Figure 6.5.8.e indicates that greater levels of co-localisation appears to occur within the cytoplasm. The relative fluorescent levels detected at the lamella boundary in Figure 6.5.8.f support these findings by revealing only a diminutive accretion of Rhea occurs at the leading edge. This finding is strikingly dissimilar to that found within the rapidly spreading cells where Pico and Rhea demonstrated strong co-localisation throughout the entire cell (Figure 6.5.4.), implying heightened association between the two proteins occurs when cells are in a highly active spreading state.

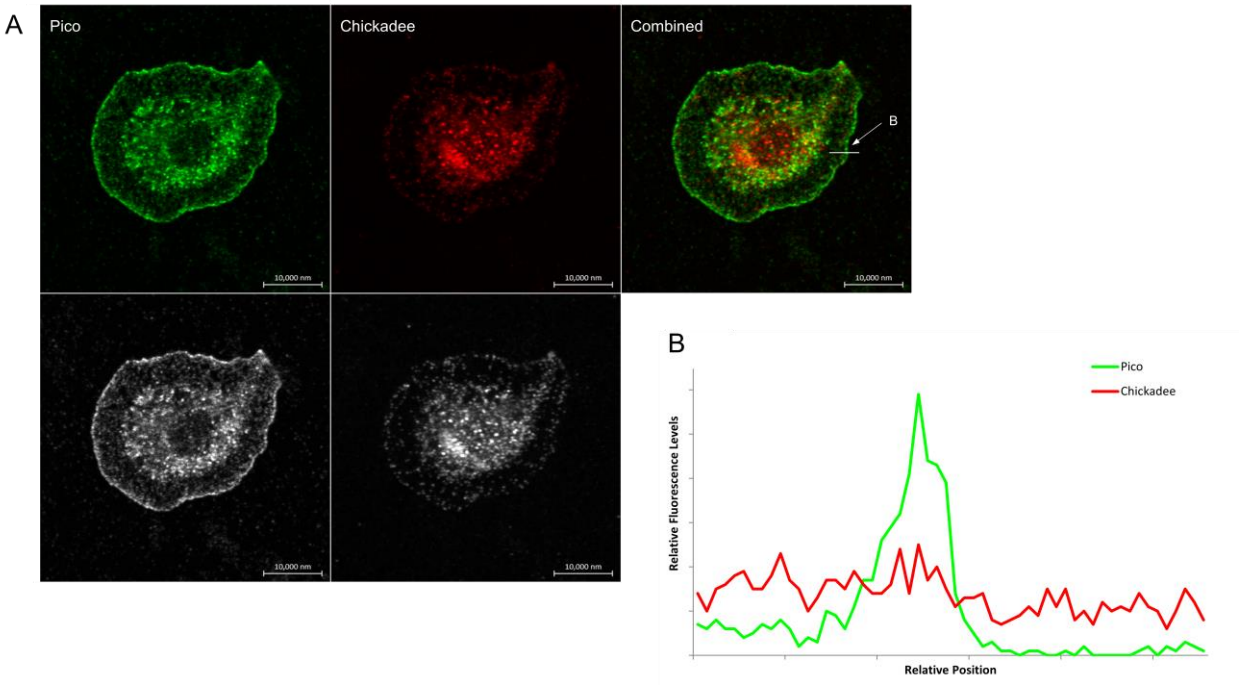
A
Pico
Chickadee
Combined
B
10,000 nm
B
Pico
Chickadee
Relative Fluorescence Levels
Relative Position

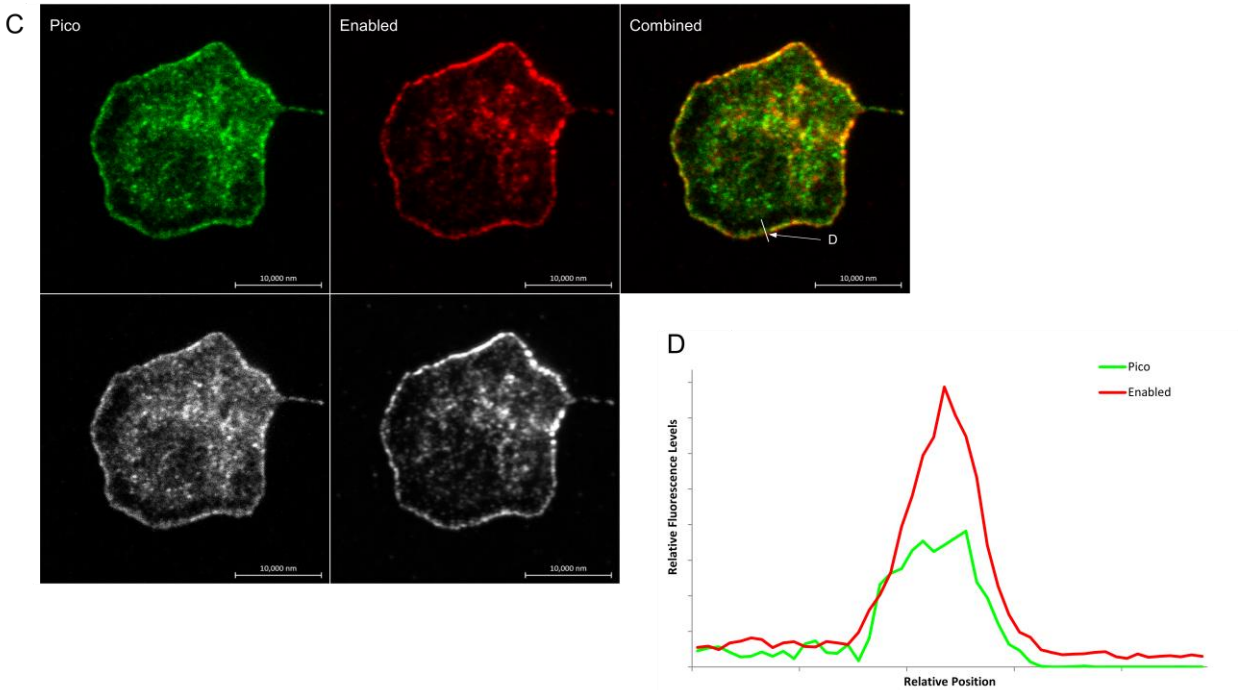
C
Pico
Enabled
Combined
D
10,000 nm
D
Pico
Enabled
Relative Fluorescence Levels
Relative Position

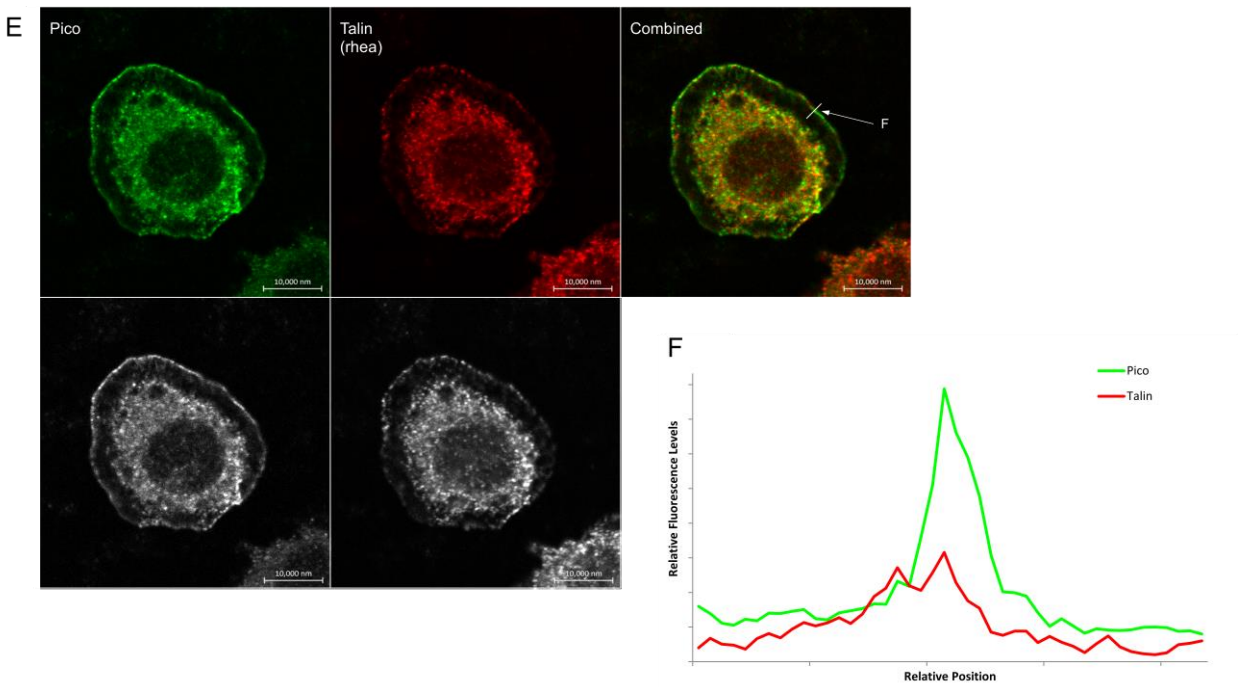

Figure 6.5.8. Co-localisation between Pico and its actin regulatory interaction partners. Venus-Pico^{WT} expressing S2R+ cells spread on ConA coated plates were fixed and stained for (a) Chickadee, (c) Enabled, and (e) Rhea, to examine co-localisation at the leading edge. The findings suggested that (b) Chickadee distribution displayed very little analogy with that observed in Pico at the cell front, while significant levels of co-localisation were detected between (d) Enabled and Pico at the leading edge. A more moderate correspondence was observed with (f) Rhea at the lamella boundary.

Pico's co-localisation with the regulatory proteins Ras, Rolled, and PP1 was also examined at the leading edge of maximally spread S2R+ cells on ConA coated plates. The findings presented in Figure 6.5.9.a revealed that the distribution of Ras was dissimilar to Pico in that it was evenly disseminated throughout the lamella and displayed no significant accumulation at the cell front. Further analysis of the relative fluorescent levels shown in Figure 6.5.9.b confirmed the dispersed nature of Ras and revealed no discernable build up in line with Pico. This finding is similar to that found in Figure 6.5.5. whereby Pico and Ras failed to strongly associate at the leading edge and only co-localised within the highly active membrane ruffles.

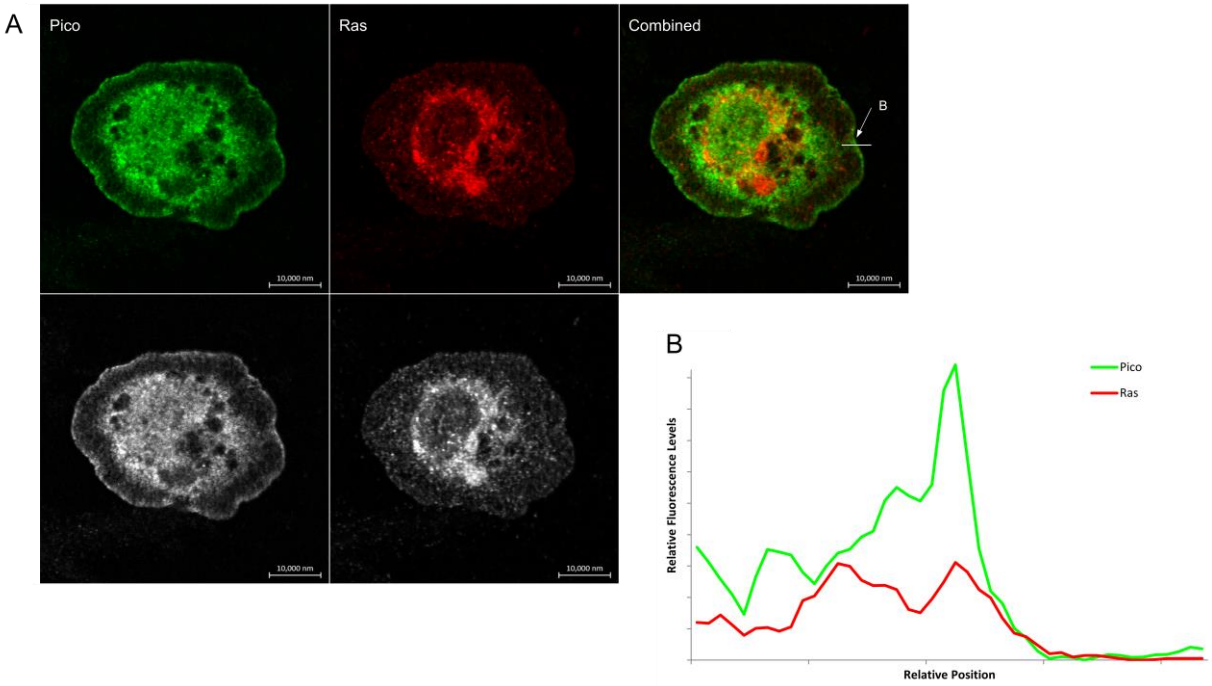
A
Pico
Ras
Combined
B
10,000 nm
B
Pico
Ras
Relative Fluorescence Levels
Relative Position

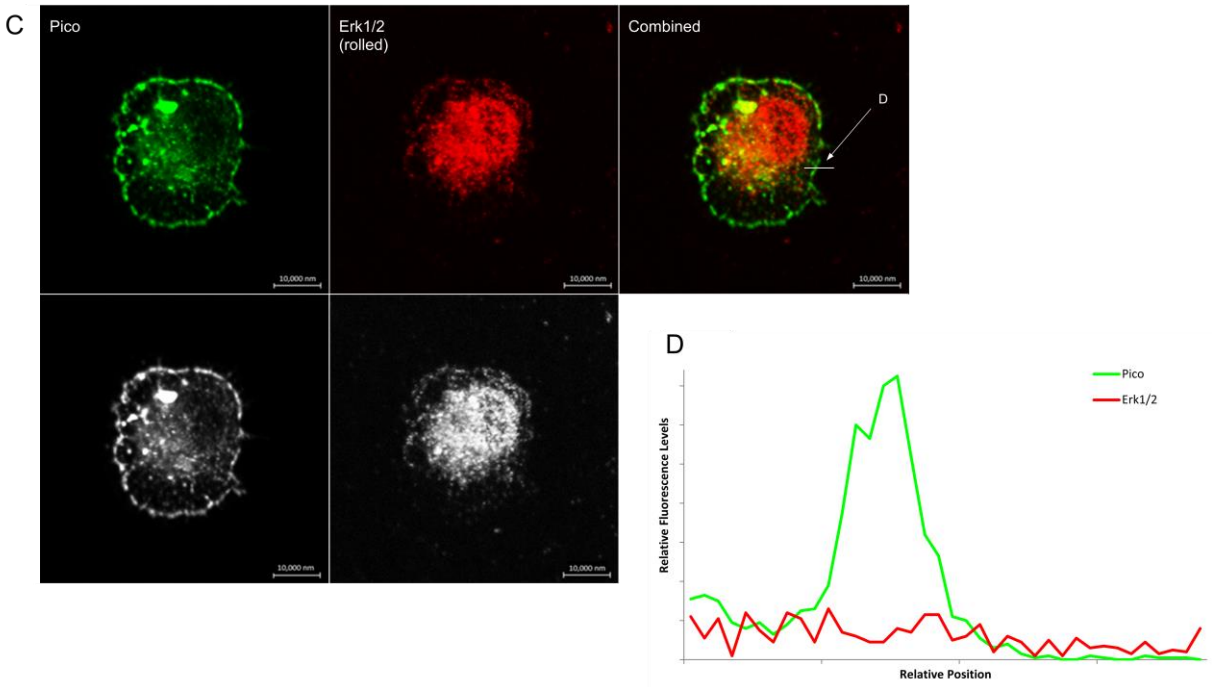
C
Pico
Erk1/2
(rolled)
Combined
D
10,000 nm
D
Pico
Erk1/2
Relative Fluorescence Levels
Relative Position

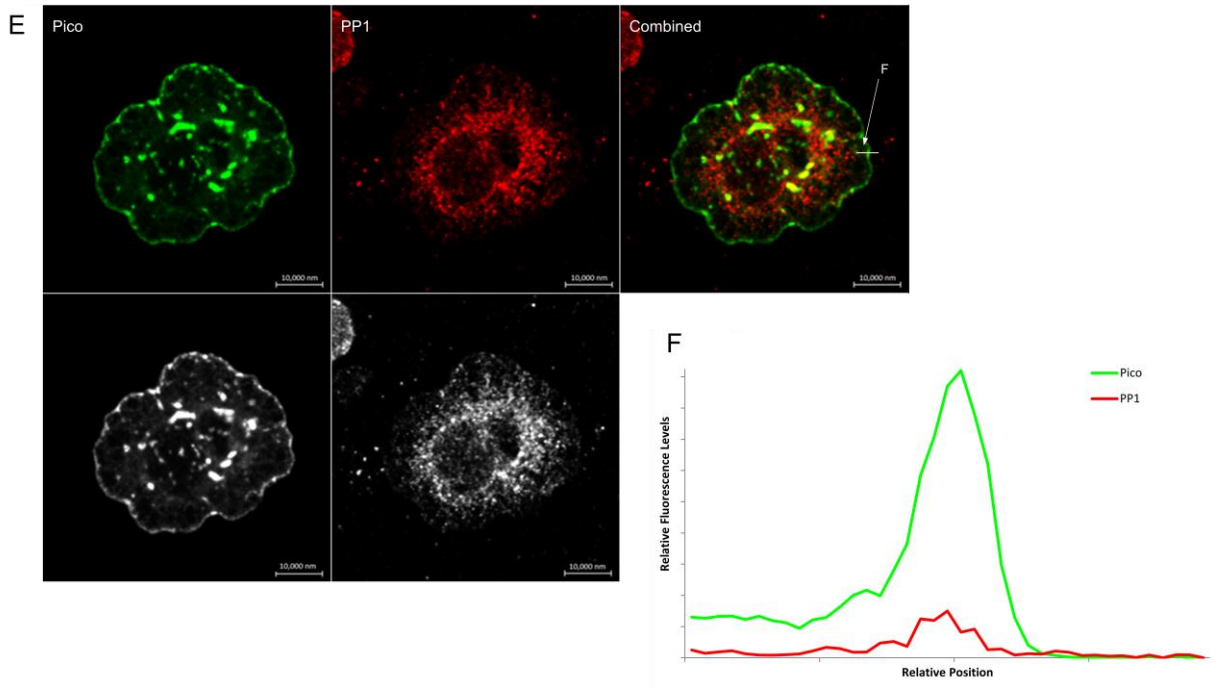

Figure 6.5.9. Co-localisation between Pico and its regulatory protein associates. S2R+ cells expressing Venus-Pico^{WT} were allowed to spread on ConA coated plates before being fixed and stained for (a) Ras, (c) Rolled, and (e) PP1 to ascertain if co-localisation occurred at the cell front. The results indicated that little positional analogy exists at the leading edge between Pico and (b) Ras, (d) Rolled, or (f) PP1.

Assessments of Rolled, illustrated in Figure 6.5.9.c, also found very little co-localisation with Pico at the leading edge, a result supported by further analysis of relative fluorescent levels within this region (Figure 6.5.9.d). Indeed, cells examined for positional analogy between Pico and PP1 also revealed very little correlation in localisation at the cell front (Figure 6.5.9.e). Figure 6.5.9.f verifies this further by demonstrating significant accumulation of Pico but not PP1 at the cell periphery.

6.6. Effects of site-directed Pico mutants on localisation of Pico and its interacting partners.

Following studies to determine distribution of wild type Pico and co-localisation with its interactors, similar experiments assessing the Pico binding and phosphorylation mutants were carried out. As with $Pico^{WT}$, S2R+ cells expressing each Venus-tagged construct under the control of an act5c promoter were allowed to spread on ConA coated plates for 20 or 30 minutes before being fixed and stained to enable analysis of rapid and maximal spread cells respectively.

6.6.1. The subcellular distribution of Pico binding and phosphorylation mutants resembled that of $Pico^{WT}$

At first, the binding and phosphorylation mutant constructs localisation within S2R+ cells exhibiting rapid spreading and maximal expansion was assessed to determine if these interactions or modifications were involved in Pico's cellular positioning. Figure 6.6.1. reveals that each mutant was capable of accumulating within the highly active membrane ruffles and localising to the lamellipodial leading edge. Consequently, these findings indicate that neither disruption of the MAPK/Rolled binding motif, the PP1 binding motif, or (de)phospho-mimetic variants of Ser 819 alter the distribution of ectopic Pico. However, due to the apparent inability of the $Pico^{LA}$, $Pico^{RE}$, and $Pico^{RR}$ mutants to interfere with Pico's confirmed interaction partners, it is not possible to establish if Chickadee, Enabled, Rhea, or Ras interactions have any discernable effects.

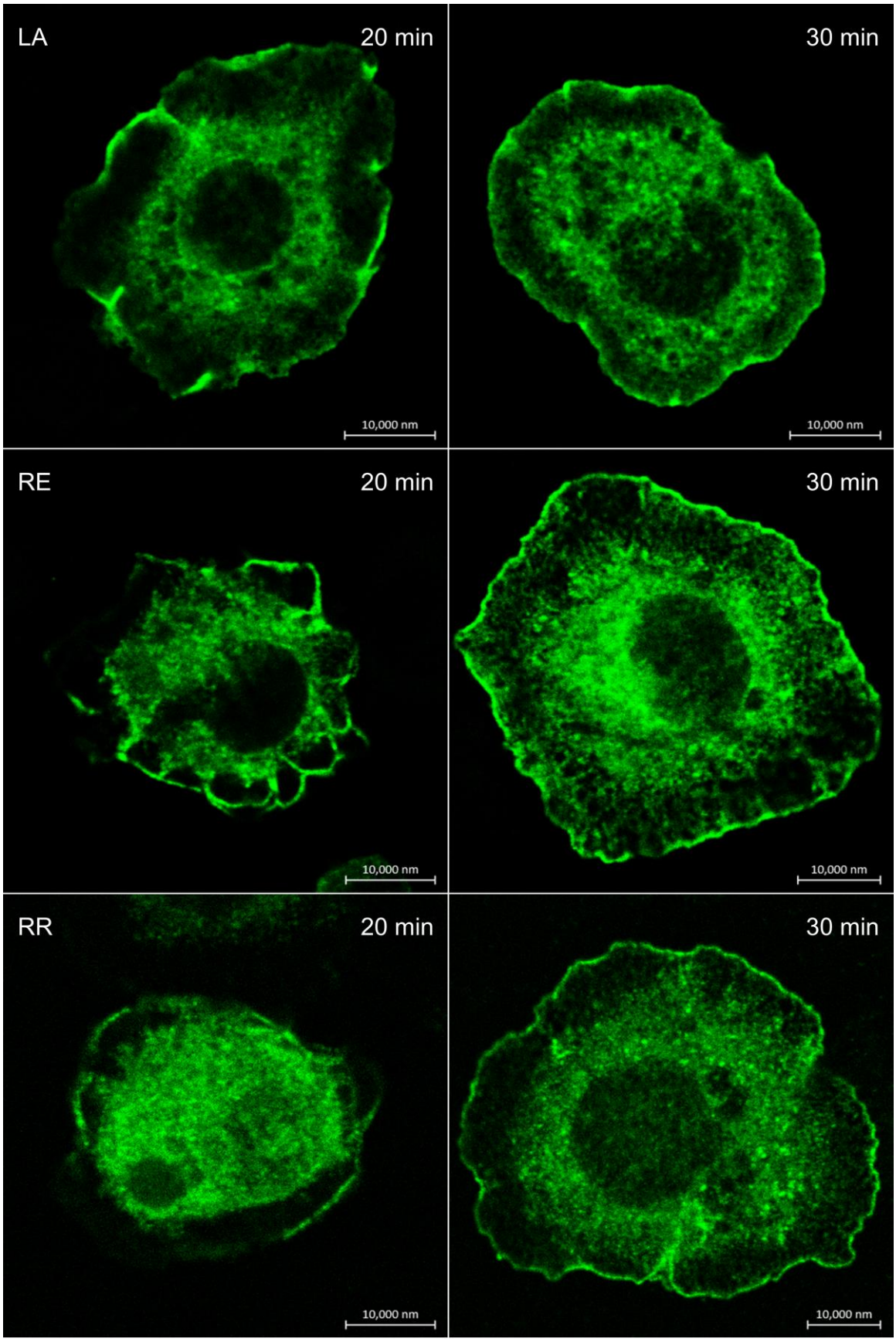
LA
20 min
10,000 nm
30 min
10,000 nm
RE
20 min
10,000 nm
30 min
10,000 nm
RR
20 min
10,000 nm
30 min
10,000 nm

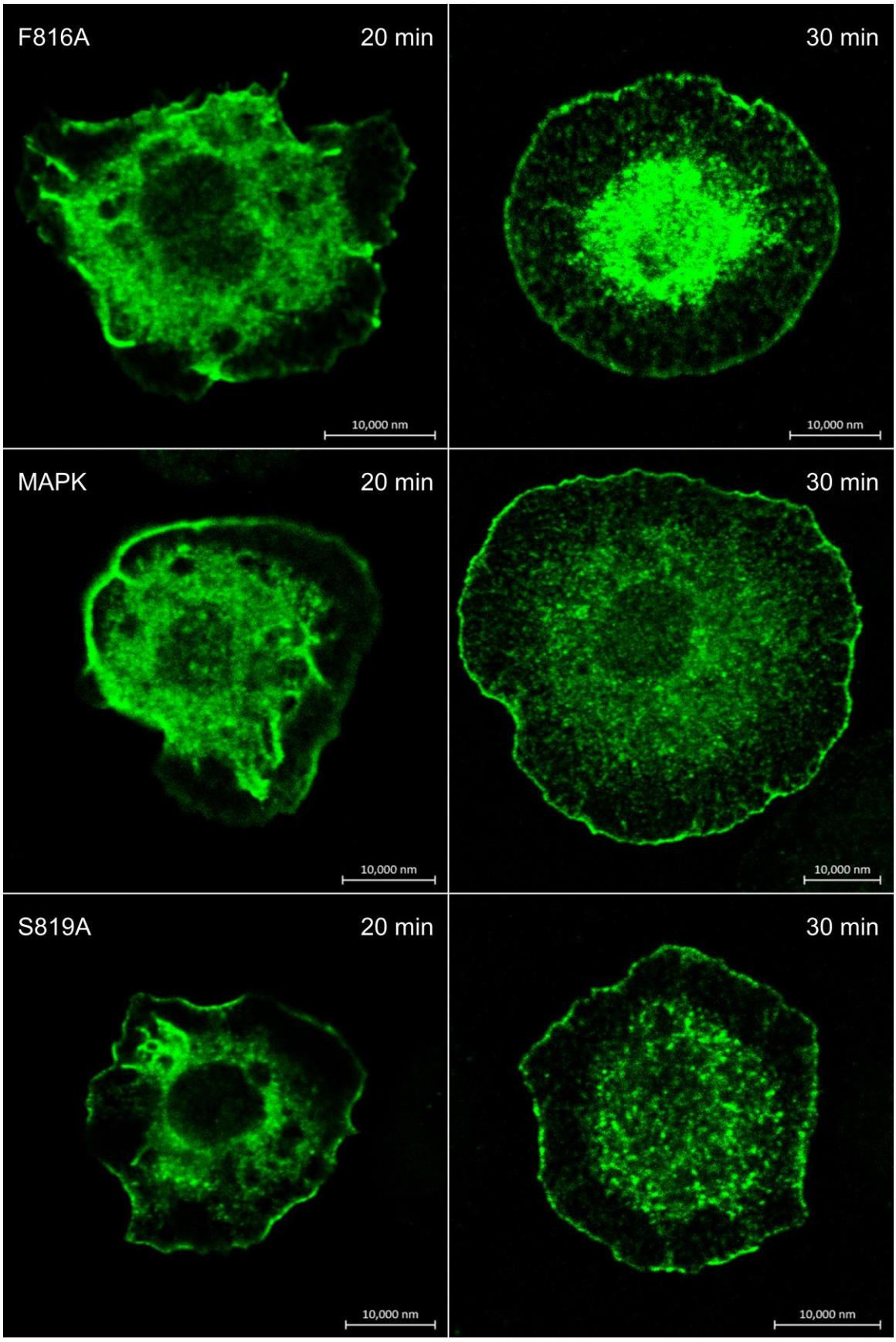
F816A
20 min
10,000 nm
30 min
10,000 nm
MAPK
20 min
10,000 nm
30 min
10,000 nm
S819A
20 min
10,000 nm
30 min
10,000 nm

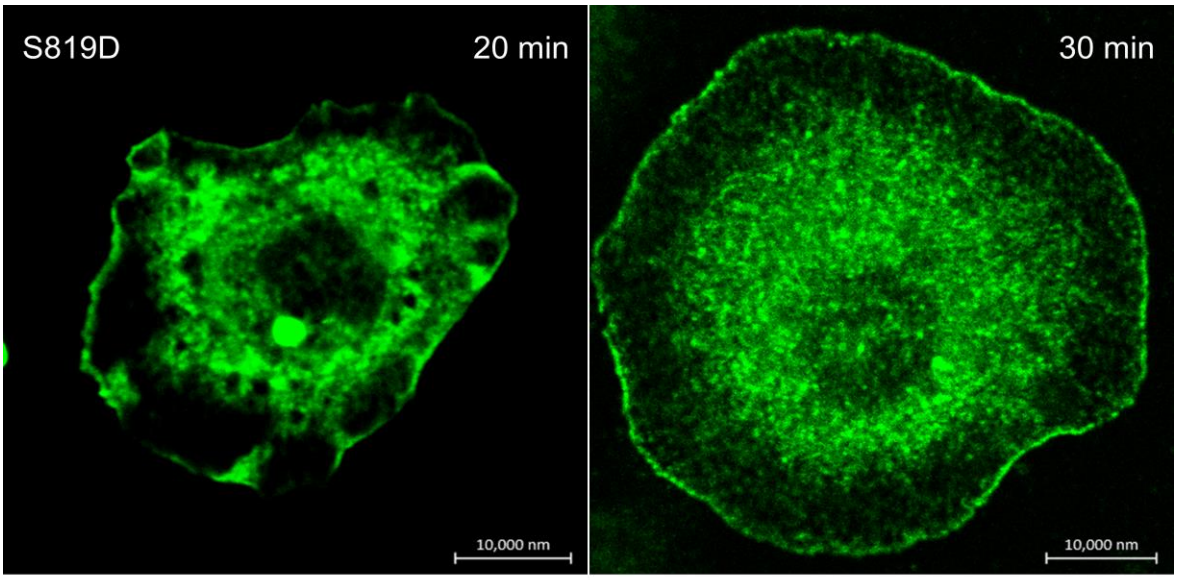

Figure 6.6.1. Subcellular localisation of ectopically expressed Pico mutants at rapid spreading and maximal expansion phases. S2R+ cells expressing the Venus-tagged Pico mutant constructs were spread on ConA coated plates and fixed with paraformaldehyde. Cells displaying rapid spreading (left) and maximal expansion (right) were imaged for each construct to determine if alterations to binding, or phosphorylation at Ser 819, prevented Pico from localising to its correct position. The results showed the changes introduced to the mutants did not alter Pico's ability to accumulate within membrane ruffles or localise at the leading edge.

6.6.2. Binding and phosphorylation mutants displayed some alterations to co-localisation

Next, the ability of the binding and phosphorylation mutant constructs to co-localise with Chickadee, Enabled, Rhea, Ras, Rolled, and PP1 was assessed and the results compared to wild type Pico. Given that $Pico^{WT}$ displayed close associations with almost all of these proteins within membrane ruffled regions, only S2R+ cells exhibiting rapid spreading were analysed. The findings revealed that the majority of mutant constructs demonstrated similar co-localisation outcomes to those displayed by the wild type protein (see appendix 5 for complete results), with only the MAPK-binding mutant and phosphomimetic $Pico^{S819D}$ construct displaying any noticeable differences.

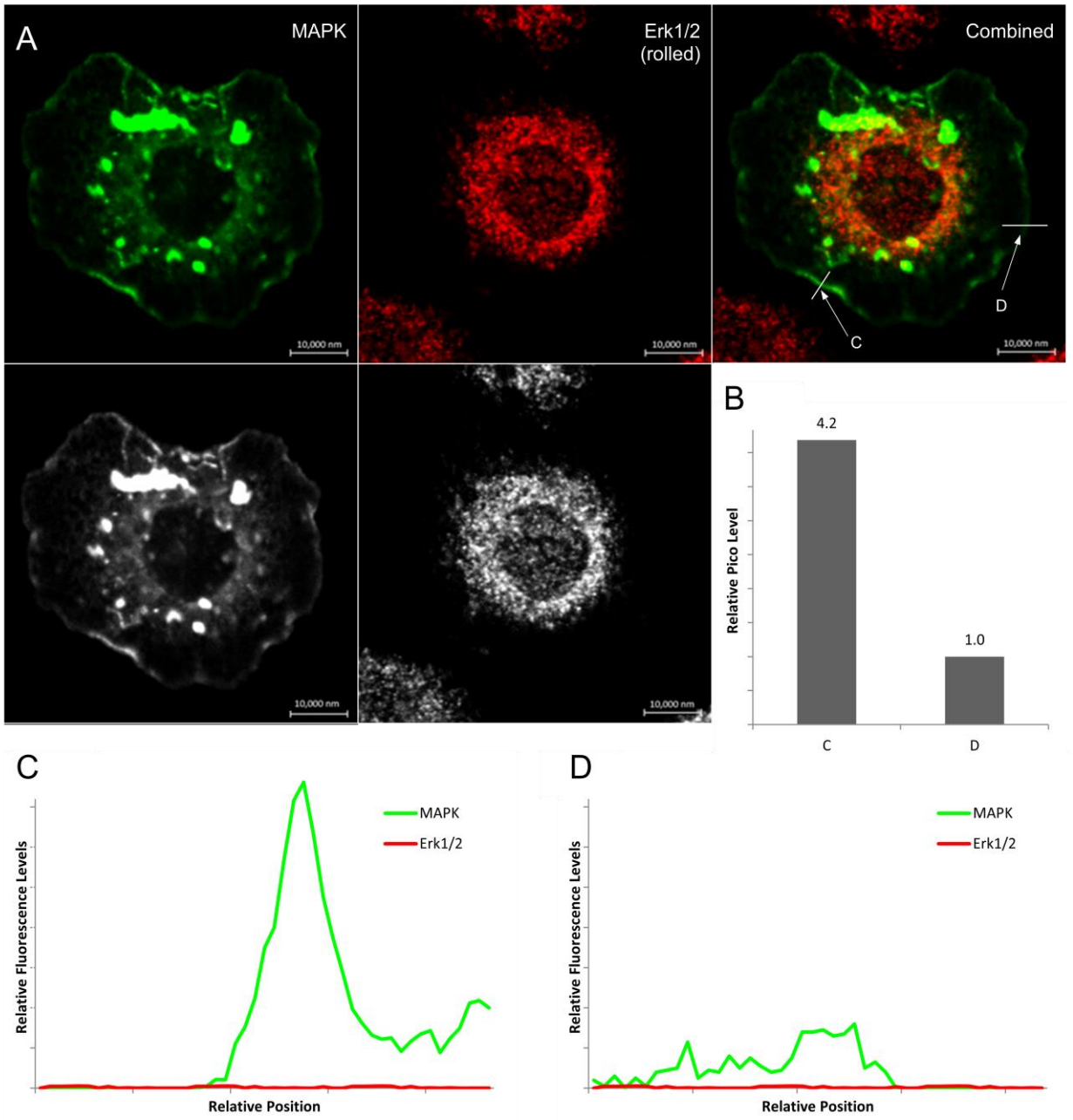

Figure 6.6.2. Examination of co-localisation between the MAPK-binding mutant and Rolled. (a) S2R+ cells expressing the Venus-Pico^{MAPK} mutant construct were spread on ConA coated plates before being fixed and stained for rolled. Cells exhibiting rapid extension were selected and (b) relative levels of Pico analysed to enable characterisation of membrane ruffles and the leading edge. Co-localisation studies revealed that the MAPK-binding mutant does not associate with Rolled in either (c) membrane ruffles or (d) at the leading edge.

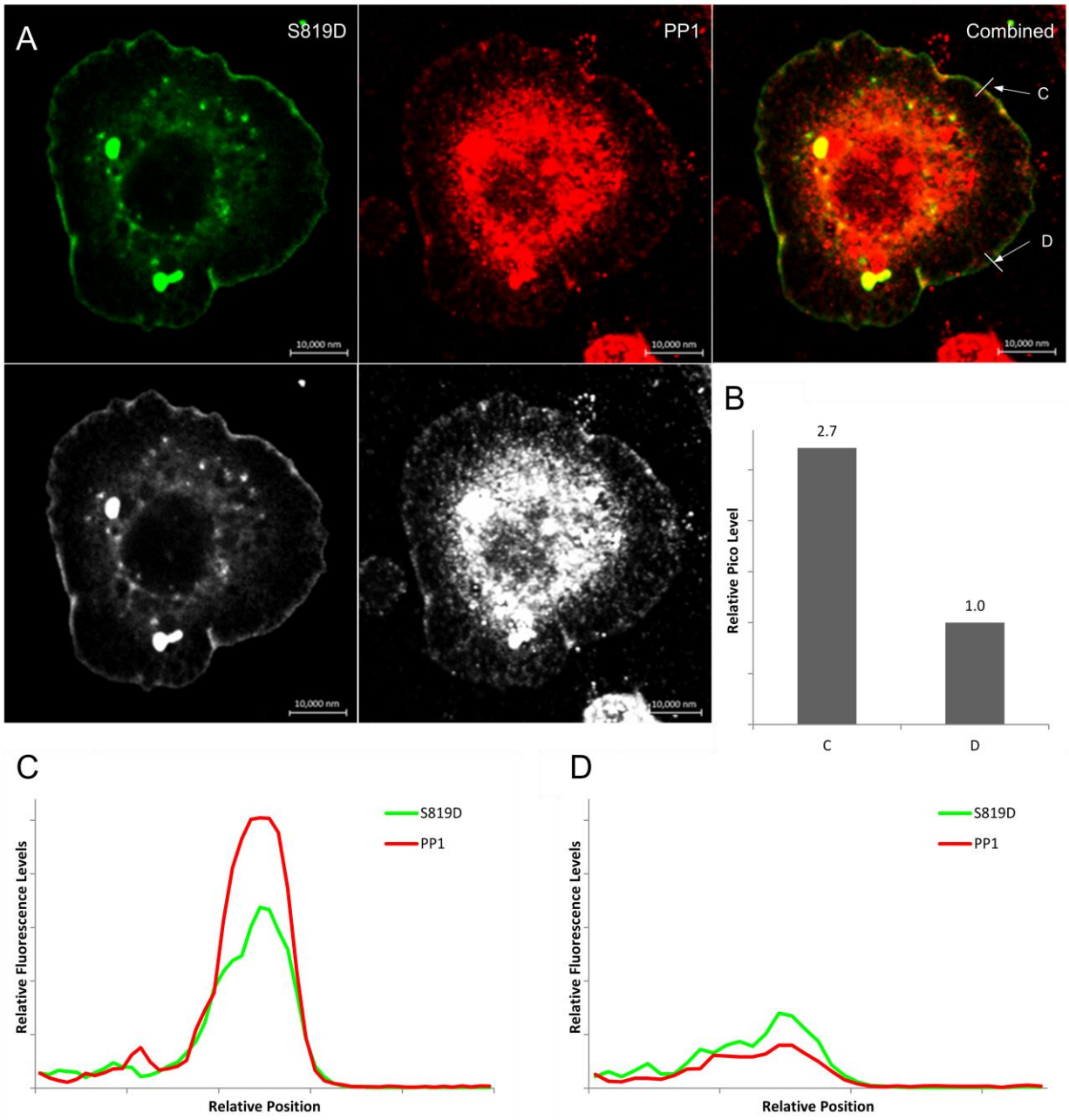

Figure 6.6.3. Co-localisation between the Pico^{S819D} mutant and PP1. (a) Venus-Pico^{S819D} expressing S2R+ cells were spread on ConA coated plates, fixed and stained for PP1. Cells exhibiting rapid spreading were selected for and (b) relative levels of Venus-Pico examined to confirm correct identification of membrane ruffles and the leading edge. Examinations showed a notable degree of co-localisation between PP1 and the Pico^{S819D} construct in both (c) membrane ruffled regions and (d) the leading edge.

The findings presented in Figure 6.6.2. revealed that the MAPK-binding mutant was unable to associate with rolled in either the membrane ruffles or at the leading edge. Indeed, one of the most striking features of these data was the complete lack of Rolled within any of the peripheral regions. This contrasted with the results generated using $Pico^{WT}$ where significant co-localisation was found to occur within ruffled regions while some accumulation of Rolled appeared to take place at the cell boundary (Figure 6.5.6.). When combined, these findings confirm the inability of the $Pico^{MAPK}$ mutant to bind with Rolled, and indicate its localisation to membrane ruffles and the leading edge is mediated by Pico.

Figure 6.6.3. demonstrates that the phosphomimetic $Pico^{S819D}$ construct strongly co-localised with PP1 at both the leading edge and membrane ruffled regions. Conversely, wild type Pico was only found to weakly accumulate alongside PP1 within boundary regions devoid of ruffles (Figure 6.5.7.). Consequently, these results support and extend the findings from chapter 5 revealing phosphorylation of Ser 819 is required for interactions with PP1, and suggest Pico may also be involved in the recruitment of PP1 to cell boundary regions.

6.7. Pico's expression and co-expression in wing discs

While analysis of S2R+ cells produced significant findings relating to the potential of ectopic Pico to associate with its binding partners during cell spreading, it was unable to confirm if Pico was actually expressed alongside these other factors in normal tissues. Due to Pico's established role in cellular growth and migration (Lyulcheva et al., 2008, Taylor, 2010), two processes found to commonly occur during early development, imaginal discs which act as progenitors for many tissue types were examined. Of these, wing discs were selected as the most appropriate organ to study owing to their ease of staining and well characterised structure and developmental fate (Klein, 2001). Wing discs, as their name suggests, form the precursor to the *Drosophila* wing and have a well defined structure by the third instar phase of larval development consisting of the wing pouch, hinge region, and adepithelium (Figure 6.7.1.a). The wing pouch gives rise to the wing blade itself, while the hinge region forms a mobile link to the body wall and flight muscles developed from myoblasts present within the adepithelium (Aldaz et al., 2010).

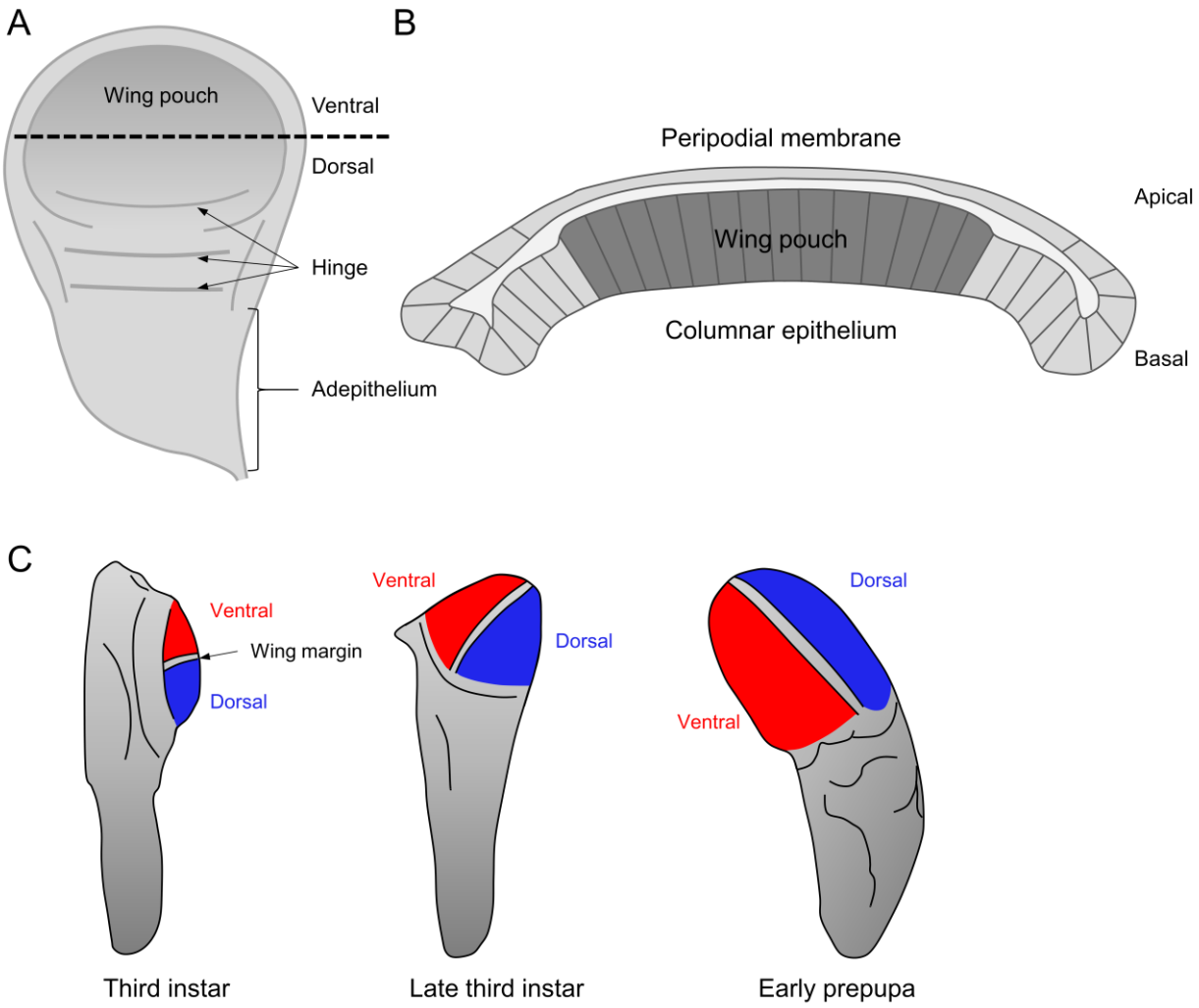

Figure 6.7.1. Wing disc structure and development. (a) Structure of complete wing disc from third instar larvae possessing a clearly defined wing pouch, hinge regions, and adepithelium containing myoblasts within the adepithial layer. The hashed line represents the dorsal-ventral wing margin. (b) X-Z cross section of the wing pouch displaying the characteristic peripodial membrane and columnar epithelium. (c) Expansion of the epithelial tissues within the wing pouch leads to repositioning of the wing margin and apposition of the dorsal and ventral compartments. During the prepupal stage the disc starts to bend and evagination of the two wing surfaces takes place (adapted from Klein, 2001 and Aldaz et al., 2010).

Two distinctive cell layers make up the wing pouch: the peripodial membrane, which eventually contributes little to the final adult structure, and the pseudo-stratified columnar epithelium that gives rise to the adult epidermis (Figure 6.7.1.b) (Aldaz et al., 2010). At the third instar stage of larval development the wing pouch is a relatively flat bilayer epithelium, with ventral and dorsal compartments positioned within the same plane (Klein, 2001). However, by late third instar, the peripodial membrane and columnar epithelium have expanded, causing the wing margin to reposition and the dorsal and ventral compartments to become apposed (Figure 6.7.1.c). At the prepupal stage, the disc starts to bend and evagination of the two wing surfaces concludes. The peripodial cells remain covering almost the entire apical surface of the columnar epithelium before retracting and eventually disintegrating at later stages of development (Klein, 2001, Aldaz et al., 2010).

Initially, studies examining regions of the wing pouch expressing Pico were carried out using W^{1118} larvae, with a representative cross section of the z-stack displayed in Figure 6.7.2. The tumour suppressor discs-large was stained for as a means of outlining the apico-lateral junctions between the columner epithelium and peripodial membrane (Janody and Treisman, 2006), while a Pico antibody developed in-house was used to detect the endogenous protein. The results revealed that Pico is predominantly expressed within basal regions of columnar epithelium in third instar larvae, while very little was detected at basal sites (Figure 6.7.2.). However, as larvae begin to enter the late third instar phase of development, Pico begins to express within basal areas of the columnar epithelium (data not shown). Eventually Pico is no longer expressed within apical columnar epithelial cells and is instead found exclusively within basal regions of the columnar epithelium (data not shown). It was not possible to display the findings from late instar larvae as the expansion and folding of the wing pouch prevented suitable z-stacks from being generated. Consequently, all future work was performed on wing discs derived from third instar larvae only.

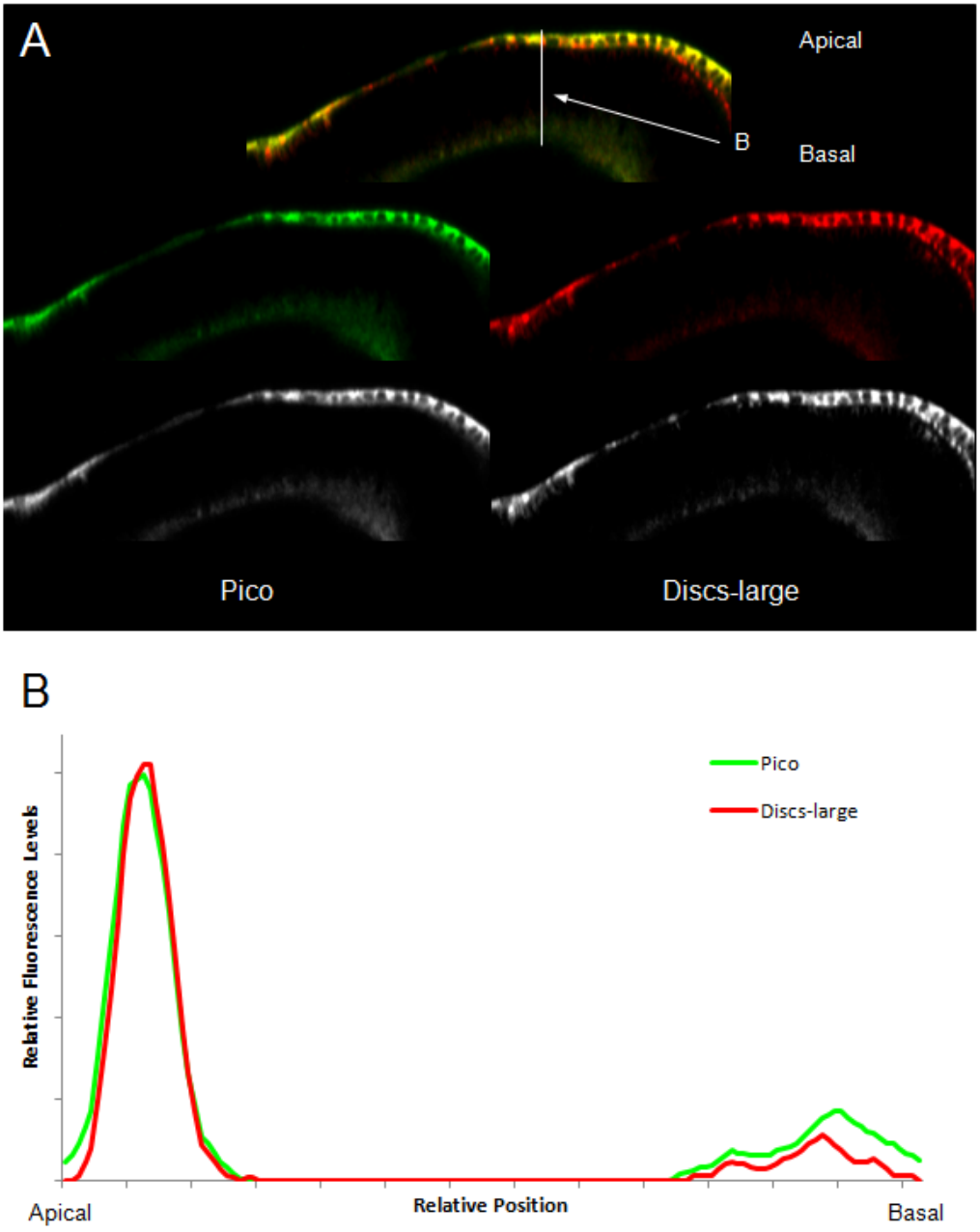

Figure 6.7.2. Expression of Pico within the wing pouch of third instar larvae. (a) Optical z-stacks were generated for wing discs from W^{1118} third instar larvae stained with discs large and Pico before appropriate X-Z cross-sections were selected. (b) Relative levels of fluorescence were analysed to determine if Pico was expressed within the peripodial membrane or columnar epithelium. The findings revealed that Pico is almost exclusively expressed within apical regions of the columnar epithelium during this stage of larval development.

6.7.1. Pico is co-expressed with all of its binding partners in wing discs

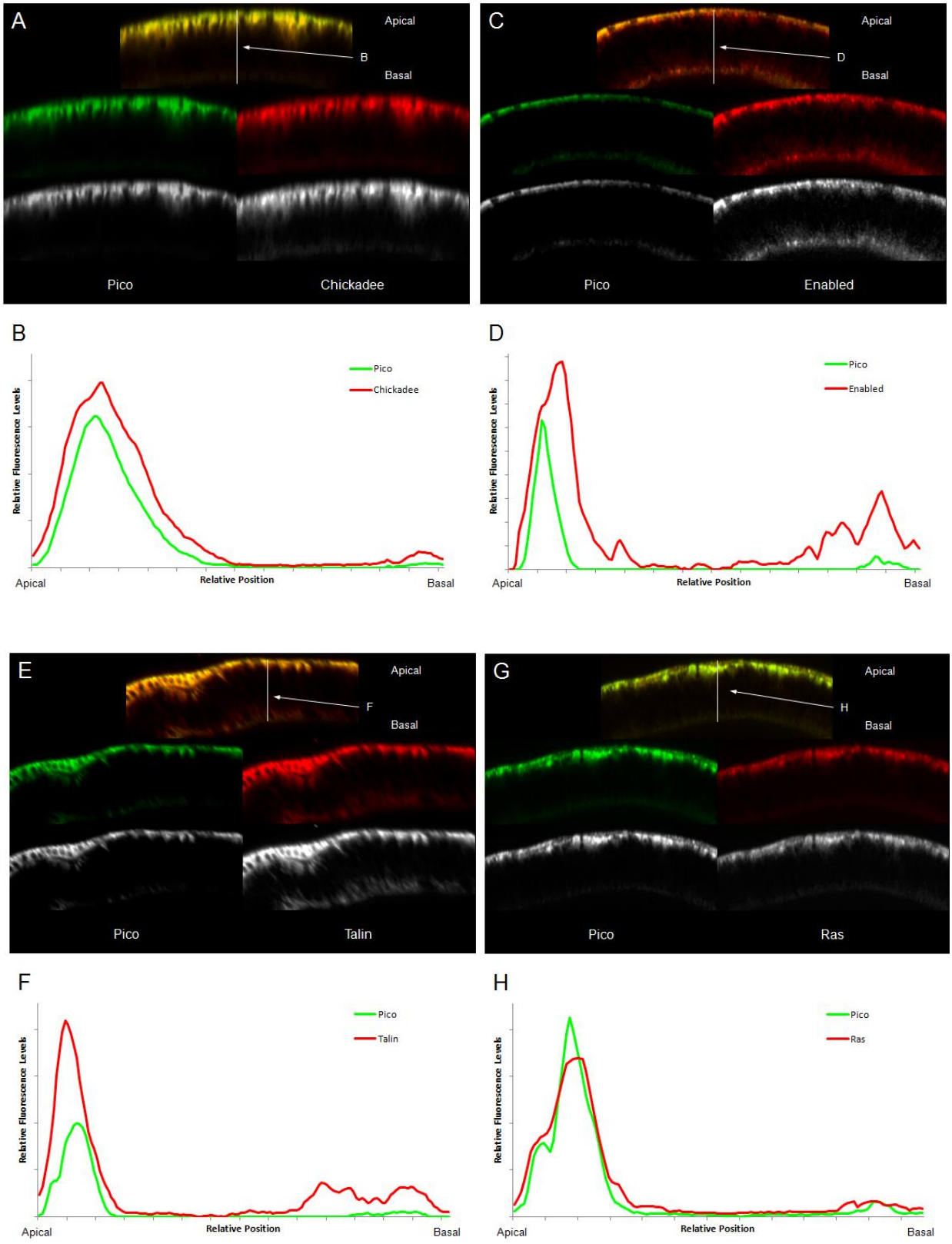

Figure 6.7.3. Co-expression of Pico and its binding partners within the wing pouch. Z-stacks were produced for W^{1118} third instar wing discs stained for Pico and (a) Chickadee, (c) Enabled, (e) Rhea, and (g) Ras. Analysis of the relative fluorescence levels shows that Pico is co-expressed with (b) Chickadee, (d) Enabled, (f) Rhea, and (h) Ras, within the apical side of the columnar epithelium, although both Enabled and Rhea are also expressed within basal regions.

Next, the degree of co-expression between Pico and its associated proteins was assessed to determine if they were naturally present in the same tissues at the same time. Co-expression analysis of Pico and Chickadee revealed both proteins are expressed almost exclusively within the apical side of columnar epithelium during the third instar stage of larval development (Figure 6.7.3.a). Enabled was also found to be expressed by apical columnar cells along with Pico, however, lower levels of Enabled were detected at basal columnar regions, implying some expression occurred here as well (Figure 6.7.3.c). Similar findings were observed following analysis Pico-Rhea co-expression. Figure 6.7.3.e. shows Rhea and Pico to be expressed at high levels within the apical columnar epithelium, while smaller quantities of Rhea are found at the basal side as well. Lastly, investigations assessing co-expression of Pico and Ras revealed strong expression of both proteins within apical columnar cells, while very little was discovered within basal regions.

As the Erk1/2, PP1, and in-house Pico antibodies were extracted from the same host species, it was not possible to co-stain wing discs with these antibodies. Consequently, wing discs were stained with Erk1/2 and PP1 alone and compared to the Pico expression studies performed earlier (Figure 6.7.2.) to determine if co-expression is likely to take place. The results presented in Figure 6.7.4.a revealed that Rolled is almost ubiquitously expressed throughout the wing pouch, with heightened levels detected in small interspersed areas of the peripodial membrane and basal regions of the columnar epithelium. PP1 was also found to be fairly evenly expressed within the wing pouch, although levels within basal regions of the columnar epithelium appeared slightly higher. While it can be concluded that Pico is co-expressed within the same tissues as Rolled and PP1, their expression pattern displays significantly less similarity than the other Pico-interacting proteins examined. This might be because MAPK and PP1 are pleiotropic enzymes with many

potential interactors, whereas Chickadee/Enabled and Rhea play more specific roles in actin regulation and adhesion signalling respectively.

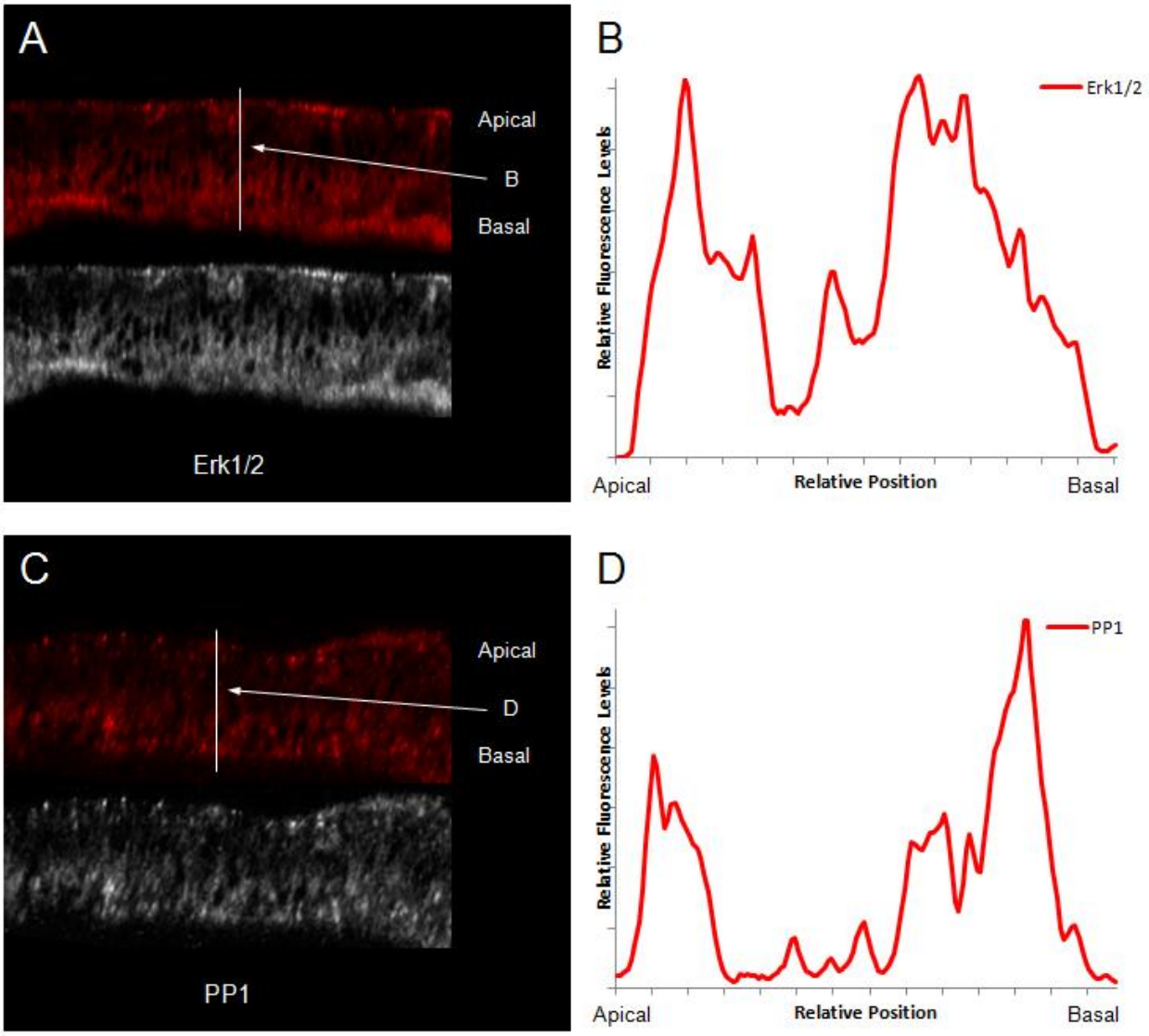

Figure 6.7.4. Expression of rolled and PP1 within the wing pouch. Optical z-stacks were generated for wing discs dissected from W^{1118} third instar larvae and stained with (a) Erk1/2 and (c) PP1. Relative levels of fluorescence were analysed and revealed that both (b) Rolled and (d) PP1 were almost ubiquitously expressed throughout the wing pouch, although Rolled was present in heightened levels in small interspersed apical and basal regions while PP1 quantities were predominantly elevated within basal regions of the columnar epithelium.

6.8. Discussion

The results presented in this chapter have shown Pico localises at the leading edge and within the cytoplasm in a similar manner to RIAM and Lpd (Lafuente et al., 2004, Krause et al., 2004). In addition, Pico possesses the ability to accumulate inside membrane ruffles, while time course assays and live imaging revealed Pico's subcellular position changes as cells spread on ConA coated substrates. Co-localisation studies confirmed associations with Chickadee, Enabled, Rhea, Ras, Rolled, and possibly PP1 occurred at some of these sites, supporting the findings from Chapter 5 and yeast-two-hybrid assays described by Taylor, 2010. Interestingly, Venus-Pico^{MAPK} displayed no positional analogy with Rolled, confirming impaired interactions and suggesting that the MAPK-binding mutant may disrupt localisation of endogenous Rolled. If Pico^{MAPK} works by competing with endogenous Pico, then this data suggests Pico is largely responsible for the normal distribution of Rolled to membrane ruffles and the leading edge during S2R+ spreading. Furthermore, the phosphomimetic Pico^{S819D} construct exhibited increased associations with PP1 compared to the wild type protein, supporting the hypothesis that phosphorylation of Ser 819 may facilitate PP1 binding. Further analysis of developing wing discs indicated that Pico is expressed alongside its binding partners, confirming that these factors do exist in the same spatial and temporal locations and therefore have the potential to come into contact naturally, validating the findings from ectopic expression studies.

6.8.1. Pico may predominantly associate with its complex partners in active regions

Time course assays and live imaging revealed Pico accumulates within highly active membrane ruffles during phases of rapid cell spreading, leading to a significant depletion at lamellipodial tips. However, as cell spreading slows down, membrane ruffles no longer form and Pico becomes uniformly positioned at the leading edge. Interestingly, co-localisation with Chickadee, Enabled, Rhea, Ras, and Rolled predominantly took place within the dynamic ruffled regions, though, as expansion of the cell decreased and Pico was repositioned to the cell boundary, only significant positional analogy was observed with Enabled. This implies that the majority of Pico's interactions with its binding partners principally occur within active regions displaying rapid membrane reorganisation following increased actin dynamics (Small et al., 2002).

Interestingly, the variable nature of Pico's co-localisation indicates that composition of the Pico mediated complexes is not the same within different subcellular locations and may depend on local concentrations of interacting factors or Pico's activation state.

6.8.2. The pattern of pico expression in developing wing discs is consistent with a role in wing growth

Immunofluorescence studies revealed Pico to be expressed almost exclusively within apico-lateral boundary regions of the wing disc columnar epithelium in early third instar larvae, however, Pico begins to express within basal columnar epithelial cells as the discs mature in middle to late third instar stages. This changing distribution may be linked to the correct development of the bag-like double epithelium which forms as the larvae prepares to enter the early prepupa phase (Figure 6.7.1.c).

In order for evagination of the wing disc to commence, enhanced growth within apical tissues occurs, causing curvature of the wing pouch as shown in Figure 6.8.1. Once apposition of the dorsal and ventral compartments has begun, further expansion of the peripodial membrane and apical/basal columnar epithelium takes place during late third instar, providing the foundations for complete evagination (Klein, 2001, Aldaz et al., 2010). Consequently, given Pico's role in growth (Lyulcheva et al., 2008), it is thought early expression in apical columnar epithelium may assist with the induction of wing pouch curvature, whilst later transcription in basal columnar epithelial cells might enable evagination to commence. As wing discs from later stage larvae were not examined, it is difficult to theorise how Pico may further function in the correct development of the wing, although, several lines of evidence suggest it promotes coordinated growth and proliferation (Lyulcheva et al., 2008, Taylor, 2010).

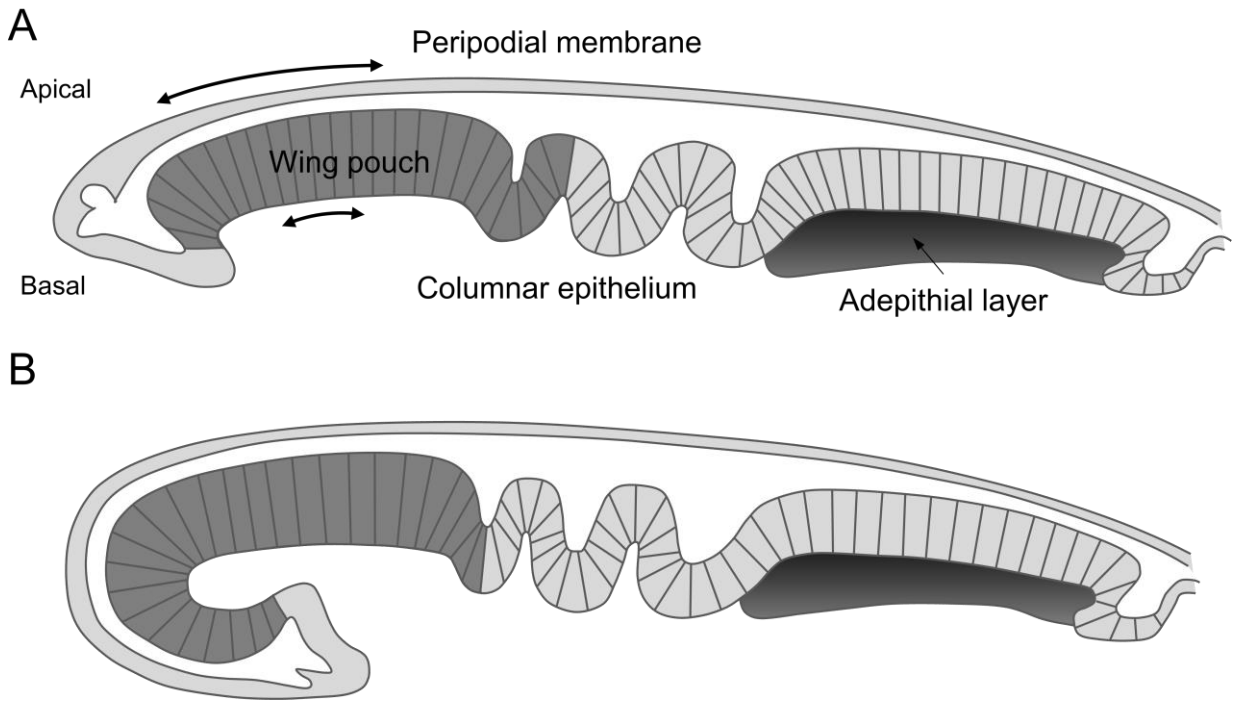

Figure 6.8.1. Schematic diagram of early wing disc evagination. (a) Schematic diagram of wing disc during the third instar stage of larval development. The arrows denote regions of growth, with length indicative of the relative proliferative levels required within the apical and basal regions of the columner epithelium to initiate the expansion and folding of the wing pouch characteristic of (b) late third instar wing discs (Klein, 2001, Aldaz et al., 2010).

Co-localisation studies revealed that Chickadee, Enabled, Rhea, and Ras were also predominantly expressed within the peripodial membrane of early third instar wing discs, whilst, Rolled and PP1 were more evenly distributed throughout the wing pouch. As Pico is believed to induce cellular proliferation through actin mediated Mal/SRF activation, highly analagous co-expression with actin regulatory proteins that bind Pico (Chapter 5.2) strongly implies shared functionality in enhanced growth of the peripodial membrane. Indeed, previous studies performed within the Bennett lab have already demonstrated the involvement of enabled in wing growth, while roles in cell proliferation have also been established for profilin, talin, and Ras (Taylor, 2010, Ding et al., 2006, Wang et al., 2011, Drosten et al., 2010). Although Rolled and PP1 are also expressed within the same tissues as Pico, a low degree of co-localisation due to their ubiquitous distribution is indicative of their pleiotropic roles.

7. Pico mediated growth

7.1. Introduction

Pico was named according to the dramatic size reduction and early growth defect observed within *pico* mutant larvae (Lyulcheva et al., 2008). Due to early lethality of homozygous *pico* mutants, RNAi-mediated silencing of *pico* was utilised to further determine role of pico during imaginal development. Knockdown of *pico* in *Drosophila* wing discs was shown to cause a significant reduction in tissue growth through reduced cellular proliferation rather than induced apoptosis (Lyulcheva et al., 2008). Further investigations demonstrated that homozygous *pico* mutant clones generated in *Drosophila* imaginal discs also exhibited severe growth and proliferation defects and were gradually extruded from the otherwise wild type tissue (Lyulcheva et al., 2008). Conversely, overexpression of Pico induced hyperplastic growth at both the tissue and whole organism level in a dose-dependent manner, owing to co-ordinated increases in both cell number and size (Lyulcheva, 2006, Lyulcheva et al., 2008).

Interestingly this growth phenotype appears to be closely linked to the actin/Mal/SRF proliferative pathway described in Chapter 1.2.2. Overexpression of *pico* was shown to increase the expression of an SRF-responsive reporter gene in mammalian cell cultures, while a hypomorphic mutation in *blistered* (*bs*), the *Drosophila* SRF homologue, impaired pico mediated wing overgrowth (Lyulcheva et al., 2008). Experiments also revealed that *pico* knockdown reduced F-actin levels, while overexpression increased the F:G actin ratio, providing a means for activating SRF through liberation of its cofactor Mal from inhibitory monomeric actin (Lyulcheva et al., 2008, Miralles et al., 2003, Settleman, 2003).

Additional findings indicated that pico's ability to regulate cell growth and proliferation is dependent on the activity of EGFR. Ectopic expression of a dominant negative form of *EGFR* ($EGFR^{DN}$), thought to interfere with signaling by forming inactive heterodimers with the wild type receptors, resulted in dramatically reduced, narrow wings (Kashles et al., 1991, Guichard et al., 1999). Wings co-expressing Pico and $EGFR^{DN}$ resembled those of $EGFR^{DN}$ alone, while

RNAi-mediated silencing of *pico* suppressed the overgrowth effects caused by ectopic EGFR (Lyulcheva et al., 2008).

Ras also functionally interacts with Pico. Eye-antennal discs overexpressing constitutively activated *Ras (Ras^{V12}*) are enlarged and exhibit a loss of morphology. Pico overexpression alone results in a slight increase in the size of the eye-antennal discs, however, the morphology of the imaginal tissues appear normal. Pico and *Ras^{V12}* co-overexpression results in dramatic overgrowth of the eye-antennal imaginal discs and an accompanying loss of morphology. Furthermore, overexpression cells (labelled with GFP) are found to invade the neighbouring tissues including the ventral nerve cord (Figure 4.8.1.) (Lyulcheva, 2006). Data from the yeast two-hybrid system indicate that Pico binds activated Ras^{V12}, and not dominant negative or wild type Ras (Taylor, 2010). In this context therefore, Pico is likely to act downstream of Ras.

As Ras acts downstream of EGFR, it is thought that EGFR activates Ras, which in turn binds to and stimulates Pico and its associated factors (Rodriguez-Viciana et al., 2004, Lyulcheva et al., 2008). This leads to an increase in F-actin formation and commensurate depletion of G-actin, alleviating inhibition on Mal's nuclear import by monomeric actin (Miralles et al., 2003, Settleman, 2003). Following translocation to the nucleus, Mal complexes with SRF to enable transcription of proliferative genes (Posern and Treisman, 2006).

7.1.1. Aims

The purpose of the research presented in this chapter was to assess the level of activity displayed by each of the mutant constructs as a means of elucidating the role interactions and phosphorylation potentially play in Pico's functionality. Initially, SRE-luciferase assays were performed to directly confirm Pico's activation of SRF within the *Drosophila* system, providing further support for the Mal/SRF mediated Pico growth pathway described by Lyulcheva *et al.*, 2008. The ability of the RNAi resistant Pico^{WT} construct to rescue *pico* knockdown phenotypes in wings was then examined to confirm specificity of *pico* RNAi lines and validate the synthetic Pico transgenes. Lastly, the ability of the Pico mutant constructs to induce overgrowth within the wings was assessed to determine their relative level of activity.

7.2. Pico overexpression enhances SRF activity

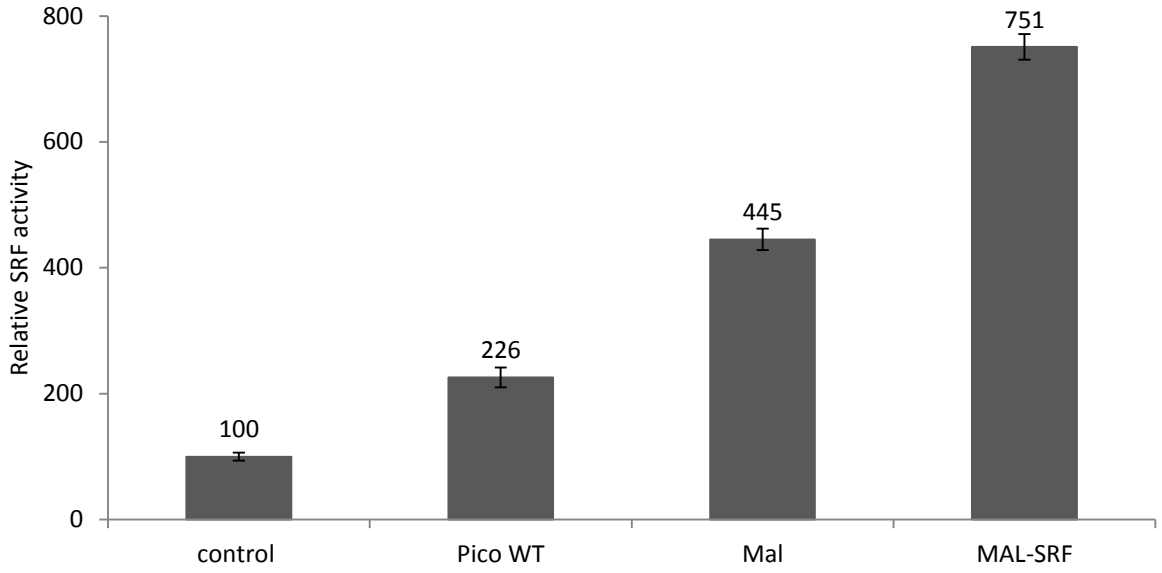

Figure 7.2.1. Assessment of Pico's ability to enhance SRF activity. Ectopic Pico was found to more than double SRF's apparent activity, while overexpresion of Mal, or Mal and SRF together causes a 4-5 and 7-8 fold increase respectively ($F(3,8) = 247$, $p = <0.001$).

While the work presented by Lyucheva *et al.*, 2008 strongly implicated the Mal/SRF pathway in Pico mediated cell growth and proliferation, this hypothesis was based on genetic analysis in flies and direct SRF activation within a heterologous mammalian system. Consequently, examinations were performed to assess Pico's ability to directly enhance SRF activity when overexpressed in a *Drosophila* system. This study utilised an SRE-responsive luciferase construct encoding the firefly luciferase reporter gene under the control of SRE tandem repeats and a minimal (m)CMV promoter. This reporter was transiently transfected into *Drosophila* S2R+ cells alongside a constitutively expressing Renilla luciferase construct, which acted as an internal control for normalising transfection efficiencies, as well as $Pico^{WT}$, Mal, or Mal and SRF. The results shown in Figure 7.2.1 indicate that ectopic Pico more than doubles the apparent activity of SRF within S2R+ cells, confirming Pico's activation of SRF within the *Drosophila* system. Mal overexpression induced SRF activity 4-5 fold, while ectopic expression of Mal and SRF together elevated SRE-firefly luciferase levels by 7-8 times, validating the approach used ($F(3,8) = 247$, $p = <0.001$, ANOVA).

7.3. RNAi resistant Pico rescues *pico* knockdown in wings

Previous research performed within the Bennett lab demonstrated that wings possessed a correct morphology but reduced size following RNAi mediated *pico* knockdown using the in-house designed picoRNAi^{IR4} inverted repeat construct, providing evidence for pico's role in growth and proliferation (Lyulcheva et al., 2008). However, this finding was challenged by Thompson, 2010 which described a blistered and crumpled wing phenotype when silencing *pico*. Instead Thompson suggested a role for Pico in maintaining actin-dependent cellular morphology and questioned Mal and SRFs role in cell proliferation and tissue growth within the *Drosophila* system (Thompson, 2010). Closer examination of available *pico* RNAi constructs revealed that the commercially available NIG-Fly RNAi lines 11940R-2 and 11940R-3 possessed numerous latent off target effects, whereas none were detected for the in-house designed picoRNAi^{IR4}, providing a potential explanation for the conflicting results.

As a means of validating the Venus-tagged Pico constructs and confirming no erroneous off-target outcomes were caused by picoRNAi^{IR4}, rescue experiments were performed by Vincent Jonchere using the RNAi resistant Venus-Pico^{WT} fly lines generated in Chapter 4. The findings presented in Figure 7.3.1. revealed that expression of picoRNAi^{IR4} by the *MS1096-GAL4* driver led to a 12% decrease (p = <0.001, t-test) in wing size and did not caused the dysmorphology phenotype described by Thompson, 2010 (Jonchere and Bennett, in press). Further analysis showed that expression of Venus-Pico^{WT} resulted in a 7% increase (p = <0.001, t-test) in adult wing size, while observations following co-expression with picoRNAi^{IR4} resembled those of ectopic Venus-Pico^{WT} alone (Figure 7.3.1.) (Jonchere and Bennett, in press). These findings proved that the Venus tag does not interfere with Pico's ability to promote growth, validating the use of Venus-tagged Pico constructs in growth studies; and indicated picoRNAi^{IR4} does not cause wing dysmorphology, supporting the findings from Lyucheva *et al.*, 2008.

To determine whether the wing dysmorphology phenotypes described by Thompson, 2010 may be the result of off-target effects by the 11940R-2 and 11940R-3 RNAi constructs, wings expressing 11940R-2 and 11940R-3 were examined by Vincent Jonchere and found to possess a blistered and crumpled morphology (data not shown). It was also established that unlike

picoRNAi^{IR4}, expression of Venus-Pico^{WT} was unable to rescue the 11940R-2/11940R-3 induced knockdown phenotype, indicating that wing dysmorphology was a result of off-target effects by the NIG-Fly constructs and refuting the conclusions from Thompson, 2010 (data not shown) (Jonchere and Bennett, in press).

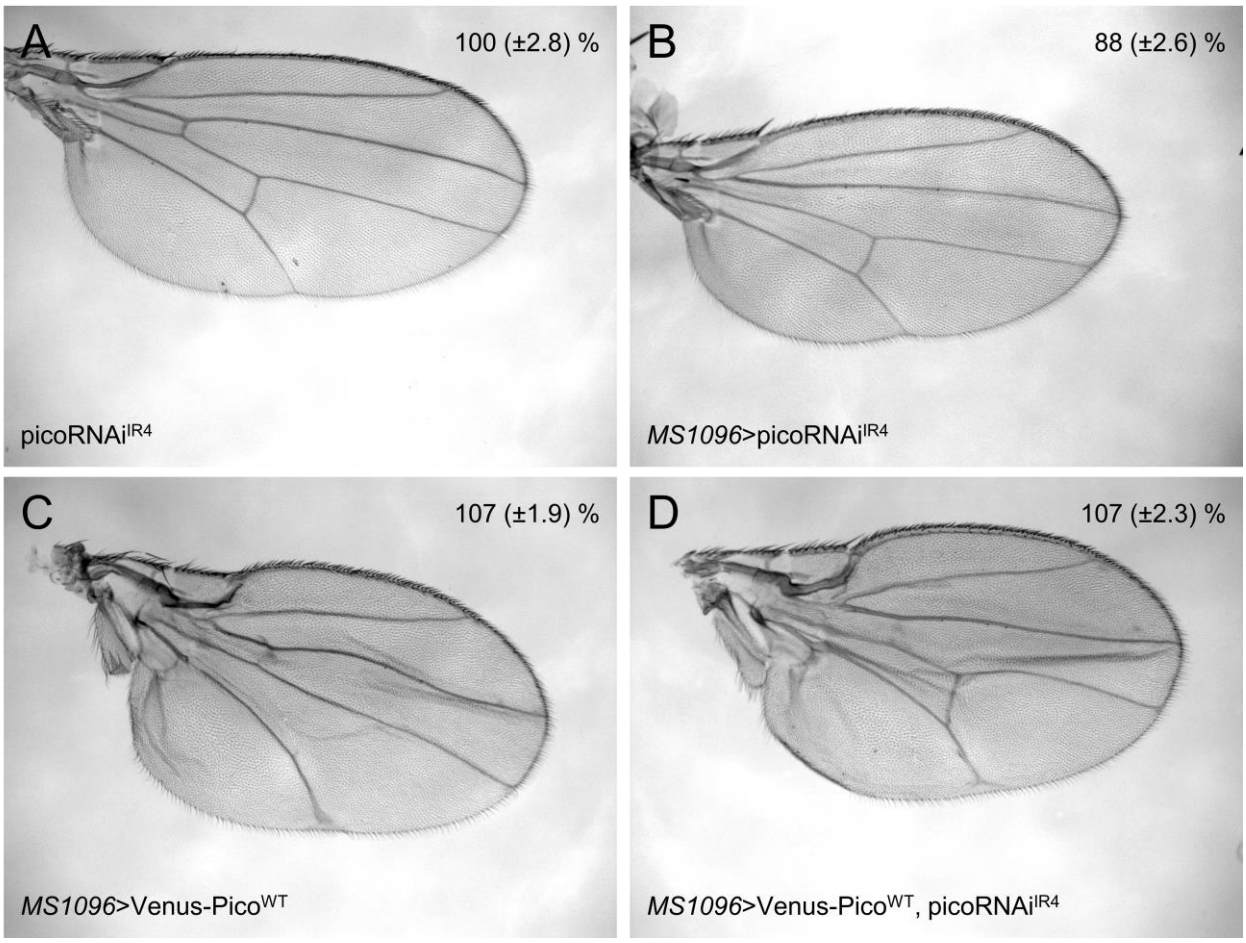

Figure 7.3.1. Venus-Pico^{WT} rescue of picoRNAi^{IR4} *pico* silencing. (a) Flies containing picoRNAi^{IR4} without a driver exhibit wing sizes comparable to W^{1118}, however, (b) expression of picoRNAi^{IR4} using the *MS1096-GAL4* driver led to a 12% decrease (p = <0.001) in wing size and caused no discernable dysmorphology. (c) *MS1096-GAL4* mediated ectopic expression of Venus-Pico^{WT} produced a 7% increase (p = <0.001) in wing size compared to *MS1096-GAL4* only flies, (d) while the phenotypic effects of Venus-Pico^{WT} expression were not modified by co-expression with picoRNAi^{IR4}, demonstrating resistance to RNAi-mediated knockdown (Jonchere and Bennett, in press).

7.4. Assessing Pico mutants ability to induce overgrowth

Following verification of the Lyucheva *et al.*, 2008 findings and confirmation that the Venus-tag does not affect Pico's functionality, analysis was carried out on the various Pico mutant constructs ability to induce overgrowth within wings to ascertain their relative level of activity.

7.4.1. Venus-Pico mediated growth does not appear to act in a dose-dependent manner

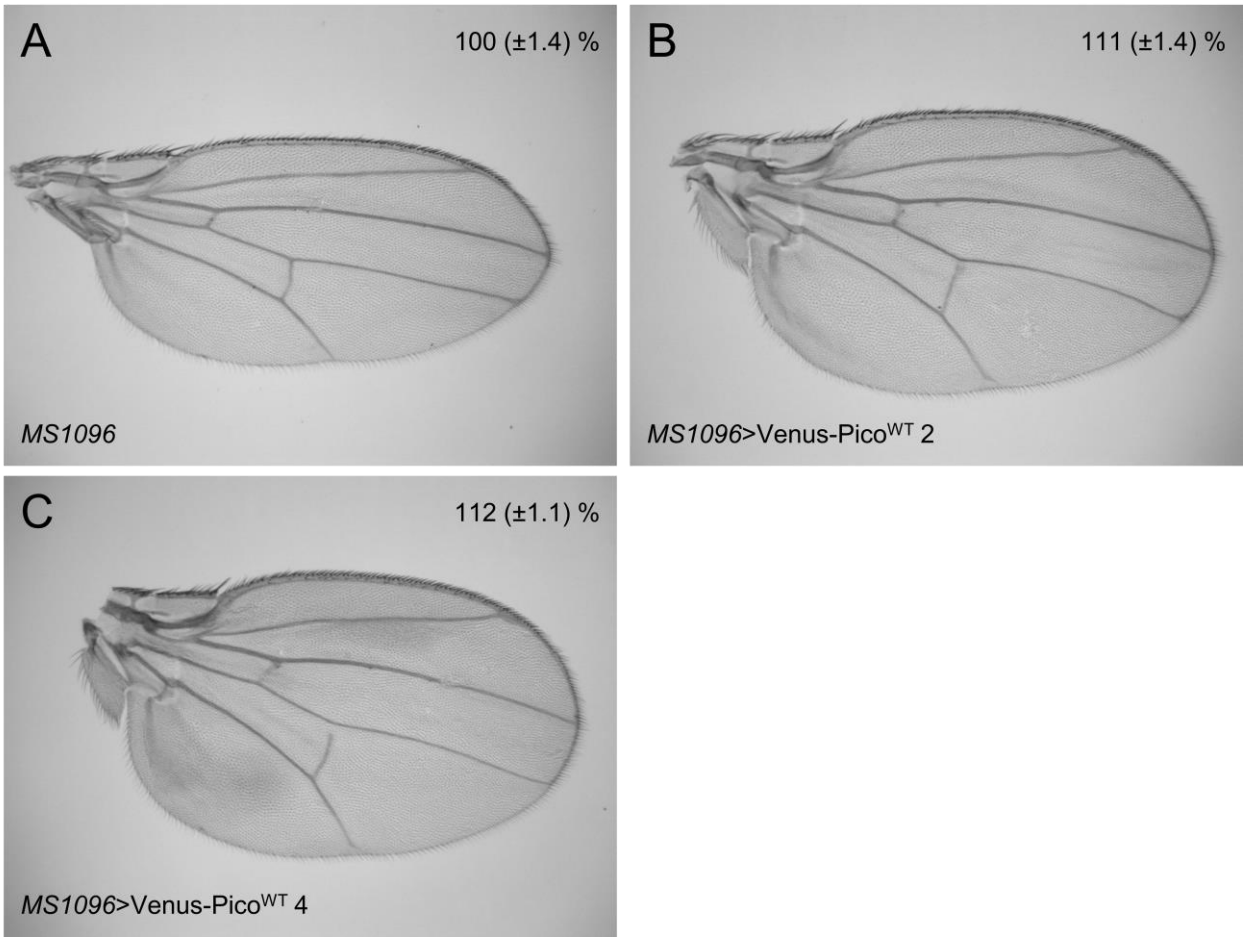

Figure 7.4.1. Venus-Pico^{WT} fails to demonstrate a dose-dependent wing growth phenotype. (a) Flies possessing the *MS1096-GAL4* driver alone display wing sizes comparable to W^{1118}. (b) Flies expressing Venus-Pico^{WT} at high levels (Line 2) under the control of *MS1096-GAL4* exhibit an 11% increase (p = <0.001) in wing size compared to their control, (c) while moderate expression (Line 4) caused a 12% increase (p = <0.001) in wing size.

Initially the ability of the high expressing Venus-Pico^{WT} 2 and moderately expressing Venus-Pico^{WT} 4 lines to promote overgrowth in wings following *MS1096-GAL4* induced expression was assessed (Chapter 4.6.3.). This enabled analysis of the dose depended effects of Pico observed in previous studies (Lyulcheva, 2006) and provided a comparable WT control for high and moderately expressed mutant constructs. 25 male flies were examined from each genotype and *MS1096-GAL4>*Venus-Pico wings compared to those from sibling *MS1096-GAL4* control flies grown in the same vials to ensure identical genetic and environmental backgrounds. The findings presented in Figure 7.4.1. revealed wings from Venus-Pico^{WT} 2 were 11% larger (p = <0.001, t-test) than the *MS1096-GAL4* control, while Venus-Pico^{WT} 4 caused a 12% increase (p = <0.001, t-test) in wing size compared to its control. The lack of any significant dose-dependent effects between the two lines indicates that either a form of control exists to regulate the activity of the Pico mediated complex, or the system may have become saturated preventing additional Pico from having an effect. Consequently, since no dose-dependent effects were observed, all future Venus-Pico mutants analysed were compared to an ectopic wild type growth figure of 11% irrespective of their relative expression level.

7.4.2. Some interactions play a key role in Pico's ability to induce growth and proliferation

Next, the Venus-tagged Pico binding mutants were examined to ascertain how Pico's associations may affect its functionality. Figure 7.4.2. reveals that ectopic expression of the Pico^{LA}, Pico^{RE}, and Pico^{RR} mutant constructs yielded an 11-12% increase (p = <0.001, t-test) in wing size over their *MS1096-GAL4* control, comparable to that observed following overexpression of Venus-Pico^{WT}. Since these mutants had displayed no alteration in their binding affinities (Chapter 5.4.) or cellular localisation (Chapter 6.6.), this finding was not unexpected. Interestingly, both the Pico^{F816A} and Pico^{MAPK} mutants displayed significantly enhanced wing overgrowth compared to their controls when ectopically expressed using *MS1096-GAL4*, with 26% and 24% increases (p = <0.001, t-test) observed respectively (Figure 7.4.2.). This effect was considerably higher than that observed in flies expressing Venus-Pico^{WT}, even though ectopic levels were similar (Chapter 4.6.3.). This indicates that disruption of the PP1- and MAPK-binding motifs potentiates the effect of ectopic Pico, identifying roles for PP1 and Rolled as potential negative regulators of Pico function.

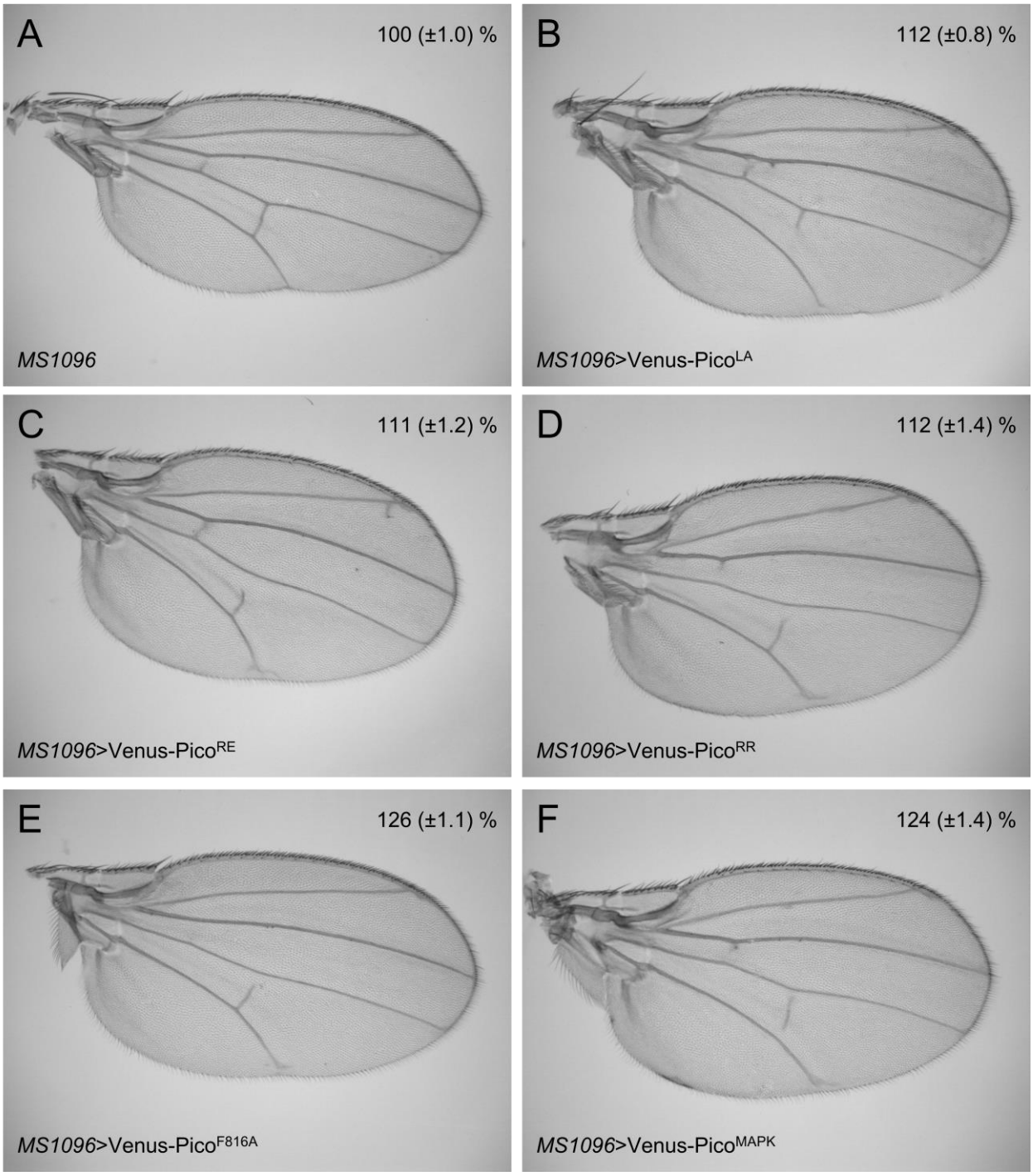

Figure 7.4.2. Ectopic expression of Pico^{MAPK} and Pico^{F816A} mutants display significant overgrowth compared to Venus-Pico^{WT}. (a) Wings from flies containing the *MS1096-GAL4* driver only were used as a comparative control. Flies expressing (b) Venus-Pico^{LA}, (c) Venus-Pico^{RE}, and (d) Venus-Pico^{RR}, under the control of the *MS1096-GAL4* driver yielded an 11-12%

increase (p = <0.001) in wing size while ectopic (e) Venus-Pico^{F816A} and (f) Venus-Pico^{MAPK} caused significant overgrowth, with 26% and 24% increases (p = <0.001) observed respectively.

7.4.3. Serine 819 is fundamental in regulating Pico's activity

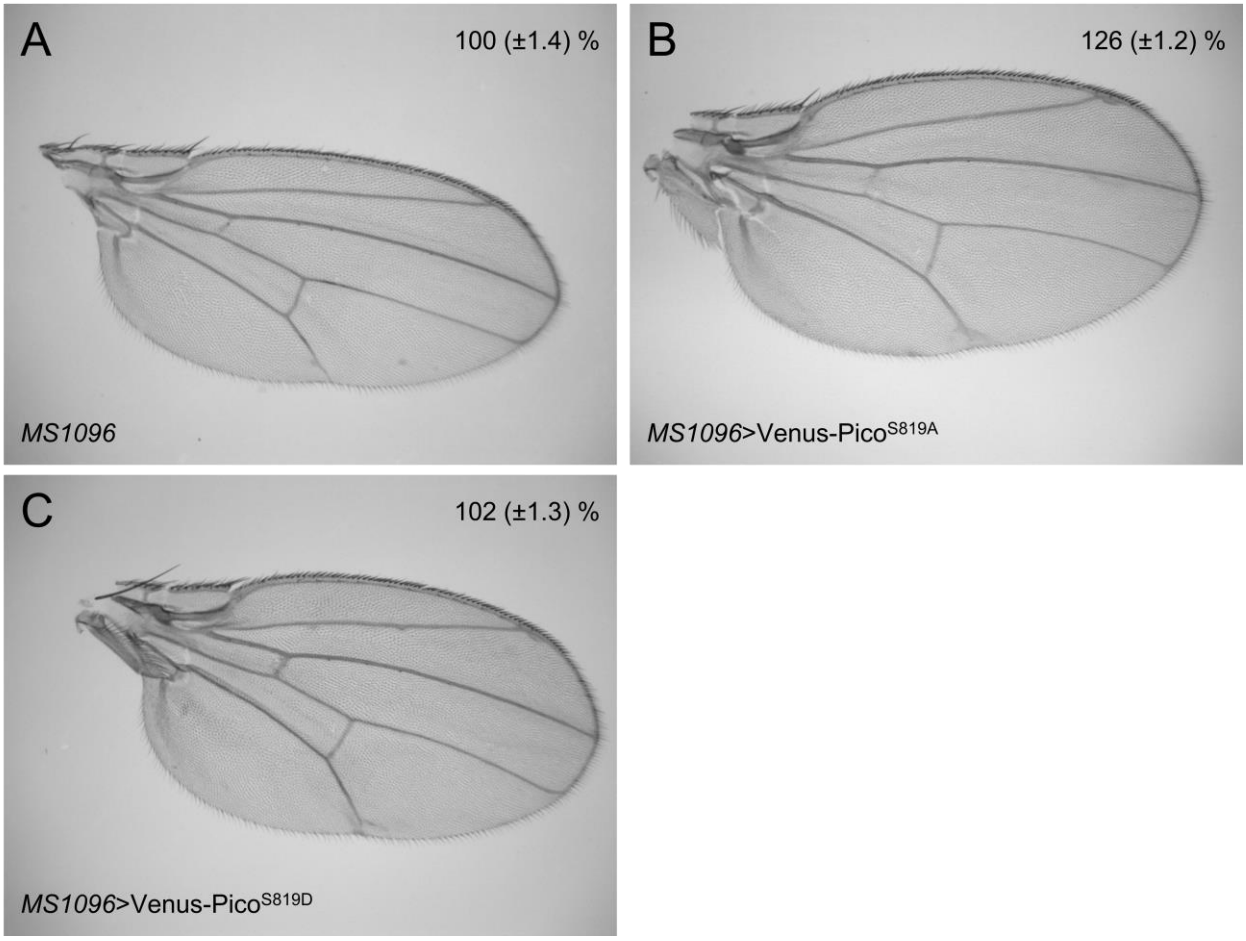

Figure 7.4.3. Serine 819 plays a key role in Pico regulation. (a) Flies containing only the *MS1096-GAL4* driver were utilised as a comparative control and exhibited wing sizes comparable to W^{1118}. (b) Flies expressing the non-phosphorylatable Venus-Pico^{S819A} construct were found to possess wings displaying a considerable 26% increase (p = <0.001) in size, whereas, (c) overexpression of phosphomimetic Venus-Pico^{S819D} only caused a negligible 2% wing overgrowth (p = <0.001).

Lastly, flies expressing the non-phosphorylatable Pico^{S819A} and phosphomimetic Pico^{S819D} constructs using the *MS1096-GAL4* driver were assessed to determine the role phosphorylation plays in regulating Pico's activity. The results presented in Figure 7.4.3. show that ectopic Pico^{S819A} causes a significant 26% increase (p = <0.001, t-test) in wing size comparable to that observed following expression of the Pico^{F816A} and Pico^{MAPK} mutant constructs. Contrastingly, overexpression of Pico^{S819D} led to a negligible 2% increase (p = <0.001, t-test) in wing size, despite expression levels being similar to Venus-Pico^{WT} 4, suggesting that phosphorylation at serine 819 may disrupt the ability of Pico to induce tissue overgrowth.

7.5. Discussion

The findings displayed in this chapter have confirmed the supposition presented by Lyucheva *et al.*, 2008 indicating Pico is involved in cellular growth and proliferation through the rescue of RNAi mediated *pico* silencing. The results also revealed that the contradictory conclusions presented by Thompson, 2010 were caused by latent off-target effects of the NIG-Fly *pico* RNAi lines used in the study. In addition, the hypothesis that Pico stimulates growth through activation of the MAL/SRF pathway was further supported by findings from SRE-luciferase assays which showed ectopic Pico increased the apparent activity of SRF.

7.5.1. PP1 and rolled appear to play a role in deactivation of the Pico mediated complex

Previous research performed within the Bennett lab had demonstrated a dose-dependent increase in wing size relative to the quantities of ectopic Pico (Lyulcheva, 2006), however, despite Pico^{WT} 2 and Pico^{WT} 4 lines displaying significantly differing expression levels, no discernable alteration in wing overgrowth was observed between the two. This implied that Venus-Pico^{WT} 2 and 4 are expressed at high enough levels for some other factor required for pico-mediated overgrowth to become limiting. Ectopic Pico^{LA}, Pico^{RE}, and Pico^{RR} also appeared to cause no difference in wing overgrowth levels when compared to flies expressing Pico^{WT}, with all constructs found to yield an 11-12% size increase (Figure 7.5.1.). This implied that each construct functioned correctly, but was limited by the same inhibitory factor that prevented a dose dependent increase being observed between Pico^{WT} 2 and Pico^{WT} 4.

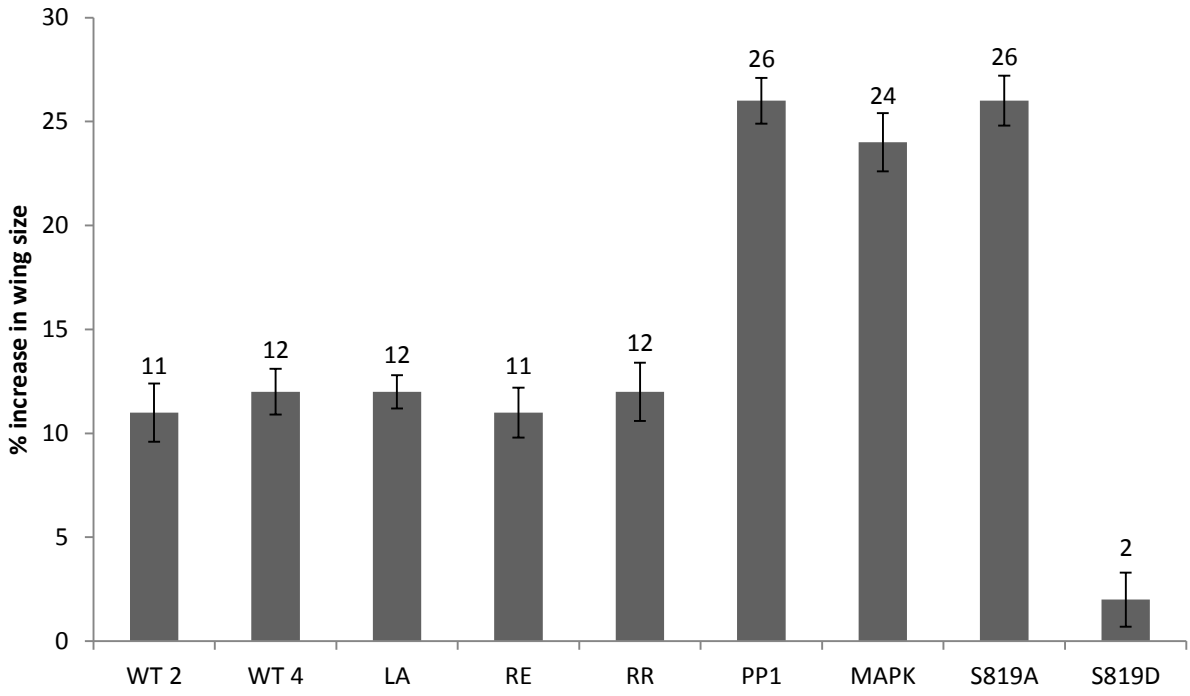

Figure 7.4.3. Overview of Pico construct induced wing overgrowth. Levels of wing overgrowth were assessed following *MS1096-GAL4* driven expression of the Venus-Pico constructs. Overexpression of Pico^{WT} 2 and Pico^{WT} 4 both caused an 11-12% increase in wing size, while expression of the Pico^{LA}, Pico^{RE}, and Pico^{RR} mutant constructs also led to an 11-12% overgrowth. Ectopic Pico^{F816A} and Pico^{MAPK} mutants brought about a significant increase in wing size of 24-26%, a level shared by non phosphorylatable Pico^{S819A}, but not the phosphomimetic Pico^{S819D} which demonstrated a negligible 2% increase.

Interestingly, the Pico^{F816A} and Pico^{MAPK} mutant constructs caused a substantial 24-26% increase in wing size when expressed using the *MS1096-GAL4* driver, strongly implying a role for both PP1 and Rolled in the negative regulation of the Pico function. Furthermore, expression of the non phosphorylatable Pico^{S819A} construct caused an equivalent overgrowth of 26% while phosphomimetic Pico^{S819D} only induced a 2% increase. These observations may not be entirely unrelated since previous data from this thesis indicate that Rolled may phosphorylate Pico at Ser 819 (Chapter 5.5.1.). Additionally, Pico^{S819D}, but not Pico^{MAPK} or Pico^{S819A}, was able to bind PP1 in cell extracts (Chapter 5.5.2.). These results suggest the existence of a potential phosphorylation cascade involving Rolled and PP1 which deactivates the Pico complex. This proposed pathway is examined in greater detail within the General Discussion (Chapter 8.2.).

8. General Discussion

8.1. A novel interaction with Erk1/2/Rolled offers a means of regulating MRL proteins

The findings presented in this report have provided evidence that Pico interacts with Chickadee, Ras, and PP1 *in vivo* (Chapter 5.2.), substantiating results from yeast-two-hybrid studies and supporting its proposed role in regulating actin dynamics (Taylor, 2010, Lyulcheva et al., 2008). Pico was also shown to interact with the Talin homologue Rhea (Chapter 5.2.1), suggesting a potential function in controlling cell adhesion as demonstrated for RIAM (Lafuente et al., 2004, Wolfenson et al., 2013, Colo et al., 2012a, Hernandez-Varas et al., 2011). However, wing dysmorphology was not observed following knockdown or overexpression of Pico, suggesting any effects during wing imaginal disc development may be minimal (Chapter 7.3.). The Pico binding partners identified were analogous to many of those discovered for other MRL orthologues, indicating a probable conserved functionality which is unsurprising given the high degree of domain homology present within the MRL family (Chapter 3.2.) (Krause et al., 2004, Lafuente et al., 2004, Lee et al., 2009)

Interestingly, this work also highlighted a novel interaction with Rolled/MAPK, the Erk1/2 homologue, not previously described within the literature (Colo et al., 2012b). MAPK binding was also found to occur with human Lpd and RIAM as well as Pico and was dependent on the presence of a highly conserved MAPK binding site adjacent to the N-terminus of the RA domain, strongly implying direct binding (Chapter 5.2.). Given the well established role Erk1/2 plays in signal transduction, this interaction could provide another means of regulating MRL proteins in addition to the contribution made by binding to Ras-like GTPases (Nishimoto and Nishida, 2006, Colo et al., 2012b). Potential functions of Pico-bound MAPK are discussed further below.

8.2. Pico interacts with most of its associated proteins within dynamic membrane regions

Previous research had shown that RIAM localises within both the cytoplasm and lamellipodia of cells in culture, whereas Lpd is predominantly found at the tips of lamellipodia and filopodia

(Lafuente et al., 2004, Krause et al., 2004). Localisation studies presented in this report revealed Pico to also accumulate within the cytoplasm and at the leading edge of *Drosophila* cells, however, time course assays and live imaging demonstrated Pico's localisation to be dynamic and change as cell spreading rates varied (Chapter 6.3.). Interestingly, Pico was shown to accumulate within active membrane ruffles, representing regions undergoing rapid reorganisation of the plasma membrane, when S2R+ cells were rapidly expanding (Chapter 6.5.1.). A similar accrual of RIAM or Lpd within these structures has not yet been reported (Colo et al., 2012b).

Furthermore, co-localisation studies established that Pico accumulated within membrane ruffles alongside the majority of its binding partners, suggesting Pico's associations may occur predominantly within areas of heightened actin remodelling (Chapter 6.5.2.). Surprisingly, Rogers *et al.*, 2003 made no mention of membrane ruffle accrual for Enabled or Chickadee when studying actin regulatory protein localisation, however, this study, much like those assessing Lpd and RIAM positioning, only examined cells which had reached their maximal size and possessed no ruffles (Lafuente et al., 2004, Krause et al., 2004).

8.3. The proposed Pico mediated growth pathway

Genetic analysis performed by Lyulcheva *et al.*, 2008 revealed that Pico acts downstream of EGFR. Pico was also shown to interact with the active form of Ras, another effector of EGFR, via the conserved RA domain (Taylor, 2010). Additional studies, such as the overgrowth analysis described in Chapter 4.8.1., have shown Pico's activity to be greatly enhanced by the presence of constitutively active Ras^{V12}, further implicating Ras-like GTPases in Pico's activation (Lyulcheva, 2006). Lyulcheva *et al.*, 2008 also suggested that Pico induces growth through alterations in the G:F actin ratio and activation of Mal/SRF, a finding further supported by the SRE luciferase assays presented in Chapter 7.2.

This led to the proposal that EGF stimulated EGFR activates Ras, which in turn binds to Pico and facilitates its function (Lyulcheva *et al.*, 2008). This causes an alteration in actin dynamics, via the actin regulators Ena and Chickadee, leading to an increase in filamentous actin levels and

a corresponding depletion of monomeric actin (Taylor, 2010). This is proposed to reduce the inhibitory binding of G-actin to MAL, enabling translocation of MAL to the nucleus where it complexes with SRF to facilitate in the transcription of SRE-containing genes involved in cellular growth and proliferation (Figure 8.3.1.) (Miralles et al., 2003, Settleman, 2003, Posern and Treisman, 2006).

Interestingly, the findings presented in this report indicate the existence of a potential deactivation pathway involving Rolled and PP1 that limits the effects of ectopic Pico on wing overgrowth (Figure 8.3.1.). Active Rolled binds Pico, most likely via the highly conserved MAPK binding motif (Chapter 5.2.4.). Once bound, Rolled phosphorylates Pico at Ser 819 allowing Pico to bind PP1 through the C-terminal PP1 binding site (Chapter 5.5.). Suppression of Pico-mediated growth by the PP1 binding phospho-mimetic $Pico^{S819D}$ variant, in addition to the enhanced proliferative effects of the non PP1 binding $Pico^{MAPK}$, $Pico^{F816A}$ and $Pico^{S819A}$ constructs compared to $Pico^{WT}$, indicate that binding to PP1 is a molecular constrain on Pico function (Chapter 7.4.). The mechanism through which PP1-mediated functional inhibition occurs remains unclear, but many of the Pico-associated proteins are phosphoproteins and might be relevant substrates for the phosphatase.

Furthermore, recent RNA-seq data has shown that overexpression of MAL leads to elevated transcription of rolled (Vincent Jonchere, personal communication). This offers a potential means of negatively regulating Pico-mediated growth through a MAL/SRF induced MAPK feedback loop. Increased levels of Rolled would enhance phosphorylation of Pico at Ser 819, causing heightened binding of and subsequent deactivation by PP1 (Figure 8.3.1.).

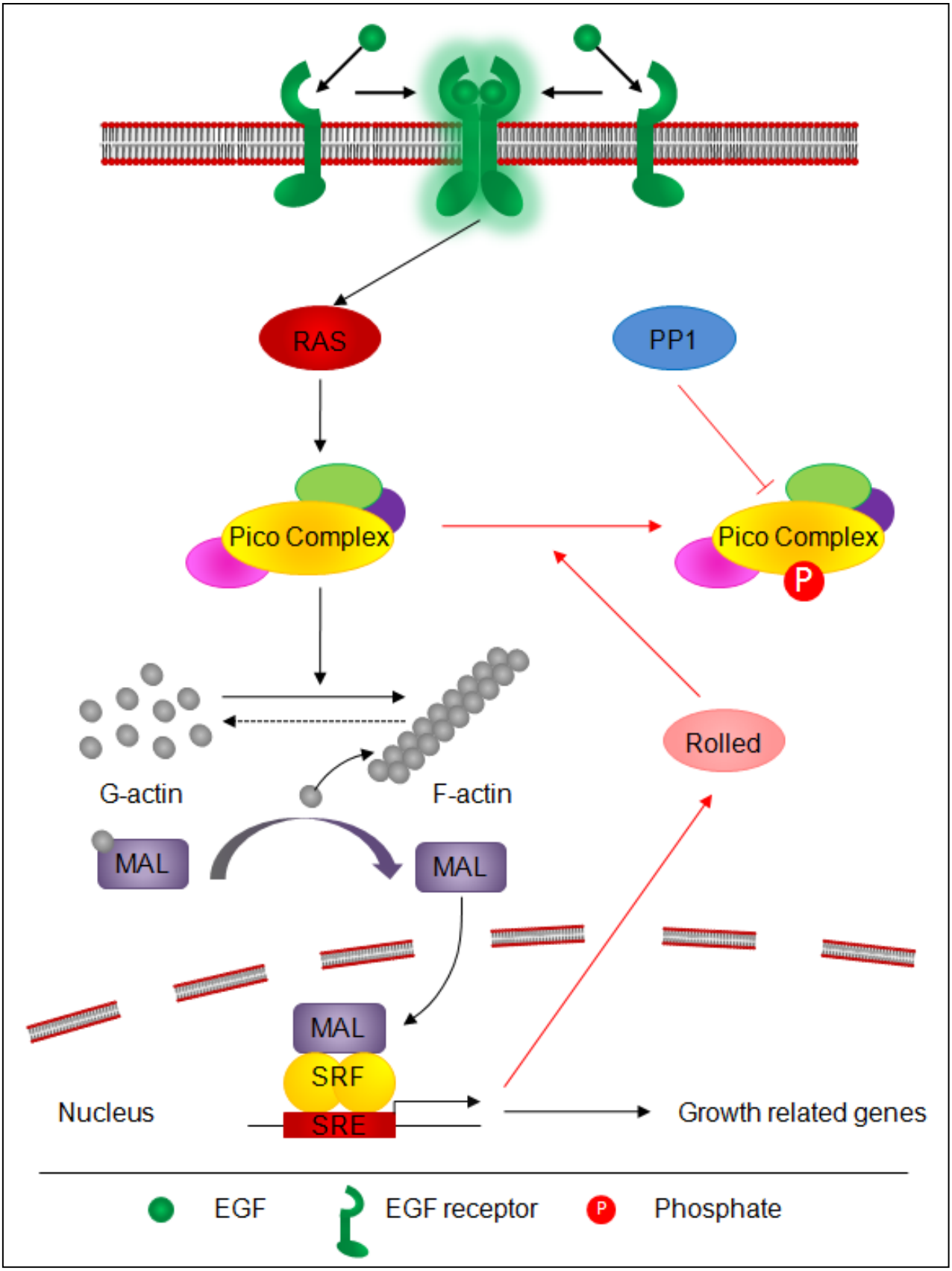
RAS
PP1
Pico Complex
Pico Complex
P
G-actin
F-actin
Rolled
MAL
MAL
MAL
SRF
SRE
Nucleus
Growth related genes
EGF
EGF receptor
P
Phosphate

Figure 8.3.1. Overview of the proposed Pico mediated growth pathway. Activated EGFR stimulates Ras which in turn binds to Pico and activates the Pico mediated complex. The activated complex enhances F-actin formation leading to depletion of G-actin and a subsequent reduction in levels of inhibitory G-actin bound to MAL. Unbound MAL translocates to the nucleus where it complexes with SRF enabling transcription of a subset of SRE-containing genes including *rolled* and those involved in cellular proliferation. Increased levels of Rolled enhances phosphorylation of Pico at Ser 819 allowing PP1 to bind and deactivate the complex. Novel conclusions are highlighted by red arrows.

It remains unclear whether Rolled/PP1 plays a role in controlling Pico's effect on cellular migration, or if a similar mechanism exists for regulating RIAM and Lpd, especially given the lack of an analogous C-terminal PP1 binding motif (Chapter 3.3.). However, a recent report by Colo *et al.*, 2012a has demonstrated that Erk1/2 activates an integrin-RIAM mediated feedback loop involved in the disassembly of FAs. In addition, RIAM silenced cells have been found to display decreased activation of Erk1/2 and PI3K, as well as impaired tumor growth and delayed metastasis, suggesting RIAM may induce activation of Erk1/2 and PI3K during a cellular proliferative process (Hernandez-Varas *et al.*, 2011). These findings, taken together with the comparable Erk1/2 binding (Chapter 5.2.4.), suggest that a similar MAPK mediated MRL deactivation loop may exist for RIAM and Lpd.

8.4. Future work

8.4.1. Validating the proposed Pico pathway

Although the work presented in this report has provided evidence of a putative Pico-mediated growth pathway, many aspects of the model require further validation. The genetic analysis performed by Lyulcheva *et al.*, 2008 intimating Pico-mediated growth downstream of EGFR is convincing, however, it could be further supported by examining synergistic enhancement of SRF activity by Pico and stimulated EGFR when co-expressed within the SRE luciferase system (Chapter 7.2). While this would provide a more direct indication of EGFR's effect on Pico,

conclusive deductions cannot be made until a suitable marker of Pico-mediated complex activation is established (e.g. Ras/Rap binding or phosphorylation at a specific site).

Discovering whether Ras-like GTPases are responsible for activation of the Pico mediated complex is also essential for accurately understanding the pathway. The current model requires assumptions to be made based upon Pico's interactions with activated Ras/Rap (Taylor, 2010, Chapter 5.2.2.), Ras/Rap functionality (Zwartkruis and Bos, 1999), and the significantly enhanced tissue overgrowth observed following co-expression of Pico with constitutively active Ras^{V12} (Lyulcheva, 2006). It is therefore crucial for a suitable Ras binding mutant of Pico to be generated either through deletion of the RA domain or introduction of more extensive alterations. This would enable interaction and functional studies to be carried out as a means of determining whether Ras/Rap binding was central to Pico's associations and activity. Further investigations assessing the effect of Ras^{V12} expression on Pico-mediated SRF activity using the SRE luciferase assay may also provide further supporting evidence (Chapter 7.3).

As the peptide array failed to identify target sequences for Erk1/2/Rolled-mediated Pico phosphorylation (Chapter 4.2.), Mass Spectrometry could instead be employed to assess potential MAPK phosphorylation sites through comparisons of $Pico^{WT}$ and $Pico^{MAPK}$ (Shou et al., 2002). This may enable further phosphomimetic and non-phosphorylatable constructs to be developed, allowing the role of Pico phosphorylation to be elucidated via additional interaction and functional studies. Mass spectrometry could also be used to assess the mechanism through which PP1 deactivates the Pico mediated complex by comparing the phosphorylation states of Pico and its associated proteins in a $Pico^{WT}$ and $Pico^{F816A}$ background.

Lastly, increased expression of rolled has only been demonstrated following overexpression of MAL (Vincent Jonchere, personal communication). As such, RT-qPCR should be carried out to confirm whether ectopic Pico can also induce elevated transcription of rolled in order to confirm whether a potential MAPK feedback loop exists. Analysis of relative Rolled protein levels could also be carried out through Western blotting of *pico* knockdown, wild type, and $Pico^{WT}$ expressing flies.

8.4.2. Further analysis of Pico

Due to time constraints it was not possible to assess Pico's effect on metastasis of Ras^{V12}-induced tumours or in the border cell migration model outlined in Chapter 4.8.1. Consequently, analysis of the Pico mutants within these systems would enable validation of the wing overgrowth results and confirm whether Rolled and PP1 play a similar role in regulating Pico's induction of cell migration. Two distinct phases of border cell invasion exist during the migration of border cells across the egg chamber; an initial rapid polarised cell behaviour followed by a slow dynamic collective migration (Bianco et al., 2007). By investigating the effect of *pico* silencing and ectopic Pico expression on border cell migration using live imaging techniques (Prasad et al., 2011) would allow further insights into Pico mediated adhesion and protrusion dynamics to be developed.

Lastly, while the co-localisation studies presented in Chapter 6.5.2 suggested that Pico predominantly associates with its binding partners within active membrane ruffles, co-localisation is not evidence of physical interaction. Consequently, Fluorescence Resonance Energy Transfer (FRET), a technique which assesses spectral absorbance between two fluorophores in close proximity (1-10nm), could also be carried out to ascertain the cellular location of Pico's interactions and validate the co-localisation findings (Chen et al., 2006). In addition, the ability of Pico's binding partners to localise within membrane ruffles or at the leading edge could be assessed in spreading S2R+ cells following *pico* knockdown. This would confirm whether Pico is crucial to the recruitment of associated factors to subcellular locations.

9. Acknowledgements

I would initially like to thank my parents, my fiancée Alison, and my future mother in-law Marilyn, for their unwavering support throughout my PhD. I am also grateful to my supervisor, Dr. Daimark Bennett, for his assistance throughout the course of the investigation and for critically reading this thesis. In addition, I wish to thank my good friend Nick Jones for sharing in the misery, and Eleanor Taylor for her consistent positive outlook in the face of ever increasing adversity; as well as other members of the Bennett lab, in particular Vincent Jonchere, Neville Cobbe, Anita Lucaci, Mirel Lucaci, and Louise Rawling.

I also wish to extend my gratitude to others within the Institute of Integrative Biology, especially James Wilson for his inescapable support, Igor Morozov for our conversations about Liverpool FC, and Jean Wood for putting up with my mess. In addition I would like to thank Lynn McLean for her invaluable assistance with mass spectrometry, Thomas Zacharchenko for supplying the shortened RIAM peptides, and Nigel Jones for use of his tissue culture facilities and noticing S2 cells failed to adhere.

10. References

ABERCROMBIE, M. 1980. The crawling movement of metazoan cells. *Proceedings of the Royal Society of London - Biological Sciences,,* 207**,** 129-147.

ADAMS, M. D. & SEKELSKY, J. J. 2002. From sequence to phenotype: reverse genetics in Drosophila melanogaster. *Nat Rev Genet,* 3**,** 189-98.

ADLER, C. E., FETTER, R. D. & BARGMANN, C. I. 2006. UNC-6/Netrin induces neuronal asymmetry and defines the site of axon formation. *Nat Neurosci,* 9**,** 511-8.

AJIRO, M., NISHIDATE, T., KATAGIRI, T. & NAKAMURA, Y. 2010. Critical involvement of RQCD1 in the EGFR-Akt pathway in mammary carcinogenesis. *Int J Oncol,* 37**,** 1085-93.

ALDAZ, S., ESCUDERO, L. M. & FREEMAN, M. 2010. Live imaging of Drosophila imaginal disc development. *Proc Natl Acad Sci U S A,* 107**,** 14217-22.

AMANN, K. J. & POLLARD, T. D. 2001. The Arp2/3 complex nucleates actin filament branches from the sides of pre-existing filaments. *Nat Cell Biol,* 3**,** 306-10.

ARMOUGOM, F., MORETTI, S., POIROT, O., AUDIC, S., DUMAS, P., SCHAELI, B., KEDUAS, V. & NOTREDAME, C. 2006. Expresso: automatic incorporation of structural information in multiple sequence alignments using 3D-Coffee. *Nucleic Acids Res,* 34**,** W604-8.

ARSENIAN, S., WEINHOLD, B., OELGESCHLAGER, M., RUTHER, U. & NORDHEIM, A. 1998. Serum response factor is essential for mesoderm formation during mouse embryogenesis. *EMBO J,* 17**,** 6289-99.

BENNETT, D., LYULCHEVA, E., ALPHEY, L. & HAWCROFT, G. 2006. Towards a comprehensive analysis of the protein phosphatase 1 interactome in Drosophila. *J Mol Biol,* 364**,** 196-212.

BEREZIAT, V., KASUS-JACOBI, A., PERDEREAU, D., CARIOU, B., GIRARD, J. & BURNOL, A. F. 2002. Inhibition of insulin receptor catalytic activity by the molecular adapter Grb14. *J Biol Chem,* 277**,** 4845-52.

BIANCO, A., POUKKULA, M., CLIFFE, A., MATHIEU, J., LUQUE, C. M., FULGA, T. A. & RORTH, P. 2007. Two distinct modes of guidance signalling during collective migration of border cells. *Nature,* 448**,** 362-5.

BISSELL, M. J. & RADISKY, D. 2001. Putting tumours in context. *Nat Rev Cancer,* 1**,** 46-54.

BODENMILLER, B., MALMSTROM, J., GERRITS, B., CAMPBELL, D., LAM, H., SCHMIDT, A., RINNER, O., MUELLER, L. N., SHANNON, P. T., PEDRIOLI, P. G., PANSE, C., LEE, H. K., SCHLAPBACH, R. & AEBERSOLD, R. 2007. PhosphoPep--a phosphoproteome resource for systems biology research in Drosophila Kc167 cells. *Mol Syst Biol,* 3**,** 139.

BOS, J. L. 2005. Linking Rap to cell adhesion. *Curr Opin Cell Biol,* 17**,** 123-8.

BOULTON, T. G. & COBB, M. H. 1991. Identification of multiple extracellular signal-regulated kinases (ERKs) with antipeptide antibodies. *Cell Regul,* 2**,** 357-71.

BOURNE, H. R., SANDERS, D. A. & MCCORMICK, F. 1990. The GTPase superfamily: a conserved switch for diverse cell functions. *Nature,* 348**,** 125-32.

BRAND, A. H. & PERRIMON, N. 1993. Targeted gene expression as a means of altering cell fates and generating dominant phenotypes. *Development,* 118**,** 401-15.

BROWN, C. M., HEBERT, B., KOLIN, D. L., ZARENO, J., WHITMORE, L., HORWITZ, A. R. & WISEMAN, P. W. 2006. Probing the integrin-actin linkage using high-resolution protein velocity mapping. *J Cell Sci,* 119**,** 5204-14.

BRUMBY, A. M. & RICHARDSON, H. E. 2005. Using Drosophila melanogaster to map human cancer pathways. *Nat Rev Cancer,* 5**,** 626-39.

BUECHNER, M. 2002. Tubes and the single C. elegans excretory cell. *Trends Cell Biol,* 12**,** 479-84.

BURRIDGE, K. & MANGEAT, P. 1984. An interaction between vinculin and talin. *Nature,* 308**,** 744-6.

CANTLEY, L. C. 2002. The phosphoinositide 3-kinase pathway. *Science,* 296**,** 1655-7.

CARGNELLO, M. & ROUX, P. P. 2011. Activation and function of the MAPKs and their substrates, the MAPK-activated protein kinases. *Microbiol Mol Biol Rev,* 75**,** 50-83.

CARLIER, M. F., LAURENT, V., SANTOLINI, J., MELKI, R., DIDRY, D., XIA, G. X., HONG, Y., CHUA, N. H. & PANTALONI, D. 1997. Actin depolymerizing factor (ADF/cofilin) enhances the rate of filament turnover: implication in actin-based motility. *J Cell Biol,* 136**,** 1307-22.

CARLIER, M. F., RESSAD, F. & PANTALONI, D. 1999. Control of actin dynamics in cell motility. Role of ADF/cofilin. *J Biol Chem,* 274**,** 33827-30.

CARY, L. A. & GUAN, J. L. 1999. Focal adhesion kinase in integrin-mediated signaling. *Front Biosci,* 4**,** D102-13.

CHANG, C., ADLER, C. E., KRAUSE, M., CLARK, S. G., GERTLER, F. B., TESSIER-LAVIGNE, M. & BARGMANN, C. I. 2006. MIG-10/lamellipodin and AGE-1/PI3K promote axon guidance and outgrowth in response to slit and netrin. *Curr Biol,* 16**,** 854-62.

CHANG, Y. C., ZHANG, H., BRENNAN, M. L. & WU, J. 2013. Crystal structure of Lamellipodin implicates diverse functions in actin polymerization and Ras signaling. *Protein Cell,* 4**,** 211-9.

CHEN, H., PUHL, H. L., 3RD, KOUSHIK, S. V., VOGEL, S. S. & IKEDA, S. R. 2006. Measurement of FRET efficiency and ratio of donor to acceptor concentration in living cells. *Biophys J,* 91**,** L39-41.

CHEN, Z., BOREK, D., PADRICK, S. B., GOMEZ, T. S., METLAGEL, Z., ISMAIL, A. M., UMETANI, J., BILLADEAU, D. D., OTWINOWSKI, Z. & ROSEN, M. K. 2010. Structure and control of the actin regulatory WAVE complex. *Nature,* 468**,** 533-8.

CHI, X., WANG, S., HUANG, Y., STAMNES, M. & CHEN, J. L. 2013. Roles of rho GTPases in intracellular transport and cellular transformation. *Int J Mol Sci,* 14**,** 7089-108.

COHEN, P. T. 2002. Protein phosphatase 1--targeted in many directions. *J Cell Sci,* 115**,** 241-56.

COLO, G. P., HERNANDEZ-VARAS, P., LOCK, J., BARTOLOME, R. A., ARELLANO-SANCHEZ, N., STROMBLAD, S. & TEIXIDO, J. 2012a. Focal adhesion disassembly is regulated by a RIAM to MEK-1 pathway. *J Cell Sci,* 125**,** 5338-52.

COLO, G. P., LAFUENTE, E. M. & TEIXIDO, J. 2012b. The MRL proteins: adapting cell adhesion, migration and growth. *Eur J Cell Biol,* 91**,** 861-8.

DATTA, S. R., DUDEK, H., TAO, X., MASTERS, S., FU, H., GOTOH, Y. & GREENBERG, M. E. 1997. Akt phosphorylation of BAD couples survival signals to the cell-intrinsic death machinery. *Cell,* 91**,** 231-41.

DAVEY, N. E., VAN ROEY, K., WEATHERITT, R. J., TOEDT, G., UYAR, B., ALTENBERG, B., BUDD, A., DIELLA, F., DINKEL, H. & GIBSON, T. J. 2012. Attributes of short linear motifs. *Mol Biosyst,* 8**,** 268-81.

DEPETRIS, R. S., WU, J. & HUBBARD, S. R. 2009. Structural and functional studies of the Ras-associating and pleckstrin-homology domains of Grb10 and Grb14. *Nat Struct Mol Biol,* 16**,** 833-9.

DESPER, R. & GASCUEL, O. 2002. Fast and accurate phylogeny reconstruction algorithms based on the minimum-evolution principle. *J Comput Biol,* 9**,** 687-705.

DI TOMMASO, P., MORETTI, S., XENARIOS, I., OROBITG, M., MONTANYOLA, A., CHANG, J. M., TALY, J. F. & NOTREDAME, C. 2011. T-Coffee: a web server for the multiple sequence alignment of protein and RNA sequences using structural information and homology extension. *Nucleic Acids Res,* 39**,** W13-7.

DIDRY, D., CARLIER, M. F. & PANTALONI, D. 1998. Synergy between actin depolymerizing factor/cofilin and profilin in increasing actin filament turnover. *J Biol Chem,* 273**,** 25602-11.

DING, Z., LAMBRECHTS, A., PAREPALLY, M. & ROY, P. 2006. Silencing profilin-1 inhibits endothelial cell proliferation, migration and cord morphogenesis. *J Cell Sci,* 119**,** 4127-37.

DINKEL, H., MICHAEL, S., WEATHERITT, R. J., DAVEY, N. E., VAN ROEY, K., ALTENBERG, B., TOEDT, G., UYAR, B., SEILER, M., BUDD, A., JODICKE, L., DAMMERT, M. A., SCHROETER, C., HAMMER, M., SCHMIDT, T., JEHL, P., MCGUIGAN, C., DYMECKA, M., CHICA, C., LUCK, K., VIA, A., CHATR-ARYAMONTRI, A., HASLAM, N., GREBNEV, G., EDWARDS, R. J., STEINMETZ, M. O., MEISELBACH, H., DIELLA, F. & GIBSON, T. J. 2012. ELM--the database of eukaryotic linear motifs. *Nucleic Acids Res,* 40**,** D242-51.

DREES, F. & GERTLER, F. B. 2008. Ena/VASP: proteins at the tip of the nervous system. *Curr Opin Neurobiol,* 18**,** 53-9.

DROSTEN, M., DHAWAHIR, A., SUM, E. Y., UROSEVIC, J., LECHUGA, C. G., ESTEBAN, L. M., CASTELLANO, E., GUERRA, C., SANTOS, E. & BARBACID, M. 2010. Genetic analysis of Ras signalling pathways in cell proliferation, migration and survival. *EMBO J,* 29**,** 1091-104.

DUFFY, J. B. 2002. GAL4 system in Drosophila: a fly geneticist's Swiss army knife. *Genesis,* 34**,** 1-15.

EDEN, S., ROHATGI, R., PODTELEJNIKOV, A. V., MANN, M. & KIRSCHNER, M. W. 2002. Mechanism of regulation of WAVE1-induced actin nucleation by Rac1 and Nck. *Nature,* 418**,** 790-3.

ELKINS, T., HORTSCH, M., BIEBER, A. J., SNOW, P. M. & GOODMAN, C. S. 1990. Drosophila fasciclin I is a novel homophilic adhesion molecule that along with fasciclin III can mediate cell sorting. *J Cell Biol,* 110**,** 1825-32.

ENDRIS, V., HAUSSMANN, L., BUSS, E., BACON, C., BARTSCH, D. & RAPPOLD, G. 2011. SrGAP3 interacts with lamellipodin at the cell membrane and regulates Rac-dependent cellular protrusions. *J Cell Sci,* 124**,** 3941-55.

ESUE, O., TSENG, Y. & WIRTZ, D. 2009. Alpha-actinin and filamin cooperatively enhance the stiffness of actin filament networks. *PLoS One,* 4**,** e4411.

ETIENNE-MANNEVILLE, S. & HALL, A. 2002. Rho GTPases in cell biology. *Nature,* 420**,** 629-35.

FORRESTER, W. C. & GARRIGA, G. 1997. Genes necessary for C. elegans cell and growth cone migrations. *Development,* 124**,** 1831-43.
FRANK, R. 2002. The SPOT-synthesis technique. Synthetic peptide arrays on membrane supports--principles and applications. *J Immunol Methods,* 267**,** 13-26.
FRANKE, T. F., YANG, S. I., CHAN, T. O., DATTA, K., KAZLAUSKAS, A., MORRISON, D. K., KAPLAN, D. R. & TSICHLIS, P. N. 1995. The protein kinase encoded by the Akt proto-oncogene is a target of the PDGF-activated phosphatidylinositol 3-kinase. *Cell,* 81**,** 727-36.
FRANTZ, J. D., GIORGETTI-PERALDI, S., OTTINGER, E. A. & SHOELSON, S. E. 1997. Human GRB-IRbeta/GRB10. Splice variants of an insulin and growth factor receptor-binding protein with PH and SH2 domains. *J Biol Chem,* 272**,** 2659-67.
FRIDMAN, M., MARUTA, H., GONEZ, J., WALKER, F., TREUTLEIN, H., ZENG, J. & BURGESS, A. 2000. Point mutants of c-raf-1 RBD with elevated binding to v-Ha-Ras. *J Biol Chem,* 275**,** 30363-71.
FRUMAN, D. A., RAMEH, L. E. & CANTLEY, L. C. 1999. Phosphoinositide binding domains: embracing 3-phosphate. *Cell,* 97**,** 817-20.
GINEITIS, D. & TREISMAN, R. 2001. Differential usage of signal transduction pathways defines two types of serum response factor target gene. *J Biol Chem,* 276**,** 24531-9.
GIOVANNONE, B., LEE, E., LAVIOLA, L., GIORGINO, F., CLEVELAND, K. A. & SMITH, R. J. 2003. Two novel proteins that are linked to insulin-like growth factor (IGF-I) receptors by the Grb10 adapter and modulate IGF-I signaling. *J Biol Chem,* 278**,** 31564-73.
GOLEY, E. D. & WELCH, M. D. 2006. The ARP2/3 complex: an actin nucleator comes of age. *Nat Rev Mol Cell Biol,* 7**,** 713-26.
GOLIC, K. G. 1991. Site-specific recombination between homologous chromosomes in Drosophila. *Science,* 252**,** 958-61.
GOULT, B. T., ZACHARCHENKO, T., BATE, N., TSANG, R., HEY, F., GINGRAS, A. R., ELLIOTT, P. R., ROBERTS, G. C., BALLESTREM, C., CRITCHLEY, D. R. & BARSUKOV, I. L. 2013. RIAM and vinculin binding to talin are mutually exclusive and regulate adhesion assembly and turnover. *J Biol Chem,* 288**,** 8238-49.
GREENSPAN, R. J. 2004. *Fly Pushing: The Theory and Practice of Drosophila Genetics,* Cold Spring Harbor Laboratory Press.
GUICHARD, A., BIEHS, B., STURTEVANT, M. A., WICKLINE, L., CHACKO, J., HOWARD, K. & BIER, E. 1999. rhomboid and Star interact synergistically to promote EGFR/MAPK signaling during Drosophila wing vein development. *Development,* 126**,** 2663-76.
GUINDON, S., DUFAYARD, J. F., LEFORT, V., ANISIMOVA, M., HORDIJK, W. & GASCUEL, O. 2010. New algorithms and methods to estimate maximum-likelihood phylogenies: assessing the performance of PhyML 3.0. *Syst Biol,* 59**,** 307-21.
HALFON, M. S., KOSE, H., CHIBA, A. & KESHISHIAN, H. 1997. Targeted gene expression without a tissue-specific promoter: creating mosaic embryos using laser-induced single-cell heat shock. *Proc Natl Acad Sci U S A,* 94**,** 6255-60.
HAN, D. C. & GUAN, J. L. 1999. Association of focal adhesion kinase with Grb7 and its role in cell migration. *J Biol Chem,* 274**,** 24425-30.
HAN, D. C., SHEN, T. L. & GUAN, J. L. 2001. The Grb7 family proteins: structure, interactions with other signaling molecules and potential cellular functions. *Oncogene,* 20**,** 6315-21.

HAN, J., LIM, C. J., WATANABE, N., SORIANI, A., RATNIKOV, B., CALDERWOOD, D. A., PUZON-MCLAUGHLIN, W., LAFUENTE, E. M., BOUSSIOTIS, V. A., SHATTIL, S. J. & GINSBERG, M. H. 2006. Reconstructing and deconstructing agonist-induced activation of integrin alphaIIbbeta3. *Curr Biol,* 16**,** 1796-806.

HANSEN, H., SVENSSON, U., ZHU, J., LAVIOLA, L., GIORGINO, F., WOLF, G., SMITH, R. J. & RIEDEL, H. 1996. Interaction between the Grb10 SH2 domain and the insulin receptor carboxyl terminus. *J Biol Chem,* 271**,** 8882-6.

HARRISON, D. A., BINARI, R., NAHREINI, T. S., GILMAN, M. & PERRIMON, N. 1995. Activation of a Drosophila Janus kinase (JAK) causes hematopoietic neoplasia and developmental defects. *EMBO J,* 14**,** 2857-65.

HASLAM, R. J., KOIDE, H. B. & HEMMINGS, B. A. 1993. Pleckstrin domain homology. *Nature,* 363**,** 309-10.

HE, W., ROSE, D. W., OLEFSKY, J. M. & GUSTAFSON, T. A. 1998. Grb10 interacts differentially with the insulin receptor, insulin-like growth factor I receptor, and epidermal growth factor receptor via the Grb10 Src homology 2 (SH2) domain and a second novel domain located between the pleckstrin homology and SH2 domains. *J Biol Chem,* 273**,** 6860-7.

HELDIN, C. H., OSTMAN, A. & RONNSTRAND, L. 1998. Signal transduction via platelet-derived growth factor receptors. *Biochim Biophys Acta,* 1378**,** F79-113.

HEMMINGS, L., REES, D. J., OHANIAN, V., BOLTON, S. J., GILMORE, A. P., PATEL, B., PRIDDLE, H., TREVITHICK, J. E., HYNES, R. O. & CRITCHLEY, D. R. 1996. Talin contains three actin-binding sites each of which is adjacent to a vinculin-binding site. *J Cell Sci,* 109 (Pt 11)**,** 2715-26.

HERBST, R. S. 2004. Review of epidermal growth factor receptor biology. *Int J Radiat Oncol Biol Phys,* 59**,** 21-6.

HERNANDEZ-VARAS, P., COLO, G. P., BARTOLOME, R. A., PATERSON, A., MEDRANO-FERNANDEZ, I., ARELLANO-SANCHEZ, N., CABANAS, C., SANCHEZ-MATEOS, P., LAFUENTE, E. M., BOUSSIOTIS, V. A., STROMBLAD, S. & TEIXIDO, J. 2011. Rap1-GTP-interacting adaptor molecule (RIAM) protein controls invasion and growth of melanoma cells. *J Biol Chem,* 286**,** 18492-504.

HILL, C. S., WYNNE, J. & TREISMAN, R. 1995. The Rho family GTPases RhoA, Rac1, and CDC42Hs regulate transcriptional activation by SRF. *Cell,* 81**,** 1159-70.

HOLT, L. J. & DALY, R. J. 2005. Adapter protein connections: the MRL and Grb7 protein families. *Growth Factors,* 23**,** 193-201.

HOLT, L. J. & SIDDLE, K. 2005. Grb10 and Grb14: enigmatic regulators of insulin action--and more? *Biochem J,* 388**,** 393-406.

HU, J., LIU, J., GHIRLANDO, R., SALTIEL, A. R. & HUBBARD, S. R. 2003. Structural basis for recruitment of the adaptor protein APS to the activated insulin receptor. *Mol Cell,* 12**,** 1379-89.

HU, K., JI, L., APPLEGATE, K. T., DANUSER, G. & WATERMAN-STORER, C. M. 2007. Differential transmission of actin motion within focal adhesions. *Science,* 315**,** 111-5.

HUANG, J. & MANNING, B. D. 2009. A complex interplay between Akt, TSC2 and the two mTOR complexes. *Biochem Soc Trans,* 37**,** 217-22.

HUMPHRIES, J. D., BYRON, A. & HUMPHRIES, M. J. 2006. Integrin ligands at a glance. *J Cell Sci,* 119**,** 3901-3.

HURWITZ, M. E., VANDERZALM, P. J., BLOOM, L., GOLDMAN, J., GARRIGA, G. & HORVITZ, H. R. 2009. Abl kinase inhibits the engulfment of apoptotic [corrected] cells in Caenorhabditis elegans. *PLoS Biol,* 7**,** e99.

HYNES, R. O. 2002. Integrins: bidirectional, allosteric signaling machines. *Cell,* 110**,** 673-87.

ISMAIL, A. M., PADRICK, S. B., CHEN, B., UMETANI, J. & ROSEN, M. K. 2009. The WAVE regulatory complex is inhibited. *Nat Struct Mol Biol,* 16**,** 561-3.

JAHN, T., SEIPEL, P., URSCHEL, S., PESCHEL, C. & DUYSTER, J. 2002. Role for the adaptor protein Grb10 in the activation of Akt. *Mol Cell Biol,* 22**,** 979-91.

JANES, P. W., LACKMANN, M., CHURCH, W. B., SANDERSON, G. M., SUTHERLAND, R. L. & DALY, R. J. 1997. Structural determinants of the interaction between the erbB2 receptor and the Src homology 2 domain of Grb7. *J Biol Chem,* 272**,** 8490-7.

JANODY, F. & TREISMAN, J. E. 2006. Actin capping protein alpha maintains vestigial-expressing cells within the Drosophila wing disc epithelium. *Development,* 133**,** 3349-57.

JENZORA, A., BEHRENDT, B., SMALL, J. V., WEHLAND, J. & STRADAL, T. E. 2005. PREL1 provides a link from Ras signalling to the actin cytoskeleton via Ena/VASP proteins. *FEBS Lett,* 579**,** 455-63.

JOHNSON, T. E. 2003. Advantages and disadvantages of Caenorhabditis elegans for aging research. *Exp Gerontol,* 38**,** 1329-32.

JONCHERE, V. & BENNETT, D. in press. Validating RNAi phenotypes in Drosophila using a synthetic RNAi-resistant transgene. *PLOS ONE*.

KAIROUZ, R., PARMAR, J., LYONS, R. J., SWARBRICK, A., MUSGROVE, E. A. & DALY, R. J. 2005. Hormonal regulation of the Grb14 signal modulator and its role in cell cycle progression of MCF-7 human breast cancer cells. *J Cell Physiol,* 203**,** 85-93.

KASHLES, O., YARDEN, Y., FISCHER, R., ULLRICH, A. & SCHLESSINGER, J. 1991. A dominant negative mutation suppresses the function of normal epidermal growth factor receptors by heterodimerization. *Mol Cell Biol,* 11**,** 1454-63.

KASUS-JACOBI, A., BEREZIAT, V., PERDEREAU, D., GIRARD, J. & BURNOL, A. F. 2000. Evidence for an interaction between the insulin receptor and Grb7. A role for two of its binding domains, PIR and SH2. *Oncogene,* 19**,** 2052-9.

KASUS-JACOBI, A., PERDEREAU, D., AUZAN, C., CLAUSER, E., VAN OBBERGHEN, E., MAUVAIS-JARVIS, F., GIRARD, J. & BURNOL, A. F. 1998. Identification of the rat adapter Grb14 as an inhibitor of insulin actions. *J Biol Chem,* 273**,** 26026-35.

KELLEHER, J. F., ATKINSON, S. J. & POLLARD, T. D. 1995. Sequences, structural models, and cellular localization of the actin-related proteins Arp2 and Arp3 from Acanthamoeba. *J Cell Biol,* 131**,** 385-97.

KELLER, R. 2005. Cell migration during gastrulation. *Curr Opin Cell Biol,* 17**,** 533-41.

KING, C. C. & NEWTON, A. C. 2004. The adaptor protein Grb14 regulates the localization of 3-phosphoinositide-dependent kinase-1. *J Biol Chem,* 279**,** 37518-27.

KLEIN, T. 2001. Wing disc development in the fly: the early stages. *Curr Opin Genet Dev,* 11**,** 470-5.

KRAUSE, M., BEAR, J. E., LOUREIRO, J. J. & GERTLER, F. B. 2002. The Ena/VASP enigma. *J Cell Sci,* 115**,** 4721-6.

KRAUSE, M., DENT, E. W., BEAR, J. E., LOUREIRO, J. J. & GERTLER, F. B. 2003. Ena/VASP proteins: regulators of the actin cytoskeleton and cell migration. *Annu Rev Cell Dev Biol,* 19**,** 541-64.

KRAUSE, M., LESLIE, J. D., STEWART, M., LAFUENTE, E. M., VALDERRAMA, F., JAGANNATHAN, R., STRASSER, G. A., RUBINSON, D. A., LIU, H., WAY, M., YAFFE, M. B., BOUSSIOTIS, V. A. & GERTLER, F. B. 2004. Lamellipodin, an Ena/VASP ligand, is implicated in the regulation of lamellipodial dynamics. *Dev Cell,* 7**,** 571-83.

KRISHNA, M. & NARANG, H. 2008. The complexity of mitogen-activated protein kinases (MAPKs) made simple. *Cell Mol Life Sci,* 65**,** 3525-44.

KUNDA, P., CRAIG, G., DOMINGUEZ, V. & BAUM, B. 2003. Abi, Sra1, and Kette control the stability and localization of SCAR/WAVE to regulate the formation of actin-based protrusions. *Curr Biol,* 13**,** 1867-75.

LAFUENTE, E. M., VAN PUIJENBROEK, A. A., KRAUSE, M., CARMAN, C. V., FREEMAN, G. J., BEREZOVSKAYA, A., CONSTANTINE, E., SPRINGER, T. A., GERTLER, F. B. & BOUSSIOTIS, V. A. 2004. RIAM, an Ena/VASP and Profilin ligand, interacts with Rap1-GTP and mediates Rap1-induced adhesion. *Dev Cell,* 7**,** 585-95.

LANGLAIS, P., DONG, L. Q., RAMOS, F. J., HU, D., LI, Y., QUON, M. J. & LIU, F. 2004. Negative regulation of insulin-stimulated mitogen-activated protein kinase signaling by Grb10. *Mol Endocrinol,* 18**,** 350-8.

LANIER, L. M. & GERTLER, F. B. 2000. From Abl to actin: Abl tyrosine kinase and associated proteins in growth cone motility. *Curr Opin Neurobiol,* 10**,** 80-7.

LAZER, G. & KATZAV, S. 2011. Guanine nucleotide exchange factors for RhoGTPases: good therapeutic targets for cancer therapy? *Cell Signal,* 23**,** 969-79.

LE CLAINCHE, C. & CARLIER, M. F. 2008. Regulation of actin assembly associated with protrusion and adhesion in cell migration. *Physiol Rev,* 88**,** 489-513.

LEE, H. S., LIM, C. J., PUZON-MCLAUGHLIN, W., SHATTIL, S. J. & GINSBERG, M. H. 2009. RIAM activates integrins by linking talin to ras GTPase membrane-targeting sequences. *J Biol Chem,* 284**,** 5119-27.

LEGG, J. A. & MACHESKY, L. M. 2004. MRL proteins: leading Ena/VASP to Ras GTPases. *Nat Cell Biol,* 6**,** 1015-7.

LEMMON, M. A. 2003. Phosphoinositide recognition domains. *Traffic,* 4**,** 201-13.

LEMMON, M. A. 2007. Pleckstrin homology (PH) domains and phosphoinositides. *Biochem Soc Symp***,** 81-93.

LEMMON, M. A. 2008. Membrane recognition by phospholipid-binding domains. *Nat Rev Mol Cell Biol,* 9**,** 99-111.

LEMMON, M. A. & FERGUSON, K. M. 2000. Signal-dependent membrane targeting by pleckstrin homology (PH) domains. *Biochem J,* 350 Pt 1**,** 1-18.

LEWIS, A. K. & BRIDGMAN, P. C. 1992. Nerve growth cone lamellipodia contain two populations of actin filaments that differ in organization and polarity. *J Cell Biol,* 119**,** 1219-43.

LI, S., BUTLER, P., WANG, Y., HU, Y., HAN, D. C., USAMI, S., GUAN, J. L. & CHIEN, S. 2002. The role of the dynamics of focal adhesion kinase in the mechanotaxis of endothelial cells. *Proc Natl Acad Sci U S A,* 99**,** 3546-51.

LO, C. M., WANG, H. B., DEMBO, M. & WANG, Y. L. 2000. Cell movement is guided by the rigidity of the substrate. *Biophys J,* 79**,** 144-52.

LUBEC, G. & AFJEHI-SADAT, L. 2007. Limitations and pitfalls in protein identification by mass spectrometry. *Chem Rev,* 107**,** 3568-84.

LUPAS, A. 1996. Coiled coils: new structures and new functions. *Trends Biochem Sci,* 21**,** 375-82.

LUSTER, A. D., ALON, R. & VON ANDRIAN, U. H. 2005. Immune cell migration in inflammation: present and future therapeutic targets. *Nat Immunol,* 6**,** 1182-90.

LYONS, R. J., DEANE, R., LYNCH, D. K., YE, Z. S., SANDERSON, G. M., EYRE, H. J., SUTHERLAND, G. R. & DALY, R. J. 2001. Identification of a novel human tankyrase through its interaction with the adaptor protein Grb14. *J Biol Chem,* 276**,** 17172-80.

LYULCHEVA, E. 2006. *Pico: a novel regulator of cell growth and proliferation.* PhD, University of Oxford.

LYULCHEVA, E., TAYLOR, E., MICHAEL, M., VEHLOW, A., TAN, S., FLETCHER, A., KRAUSE, M. & BENNETT, D. 2008. Drosophila pico and its mammalian ortholog lamellipodin activate serum response factor and promote cell proliferation. *Dev Cell,* 15**,** 680-90.

MACDONALD, A., HORWITZ, A. R. & LAUFFENBURGER, D. A. 2008. Kinetic model for lamellipodal actin-integrin 'clutch' dynamics. *Cell Adh Migr,* 2**,** 95-105.

MACHESKY, L. M., MULLINS, R. D., HIGGS, H. N., KAISER, D. A., BLANCHOIN, L., MAY, R. C., HALL, M. E. & POLLARD, T. D. 1999. Scar, a WASp-related protein, activates nucleation of actin filaments by the Arp2/3 complex. *Proc Natl Acad Sci U S A,* 96**,** 3739-44.

MAHANKALI, M., PENG, H. J., COX, D. & GOMEZ-CAMBRONERO, J. 2011. The mechanism of cell membrane ruffling relies on a phospholipase D2 (PLD2), Grb2 and Rac2 association. *Cell Signal,* 23**,** 1291-8.

MANSER, J., ROONPRAPUNT, C. & MARGOLIS, B. 1997. C. elegans cell migration gene mig-10 shares similarities with a family of SH2 domain proteins and acts cell nonautonomously in excretory canal development. *Dev Biol,* 184**,** 150-64.

MANSER, J. & WOOD, W. B. 1990. Mutations affecting embryonic cell migrations in Caenorhabditis elegans. *Dev Genet,* 11**,** 49-64.

MATTHEWS, K. A., KAUFMAN, T. C. & GELBART, W. M. 2005. Research resources for Drosophila: the expanding universe. *Nat Rev Genet,* 6**,** 179-93.

MAYER, B. J., REN, R., CLARK, K. L. & BALTIMORE, D. 1993. A putative modular domain present in diverse signaling proteins. *Cell,* 73**,** 629-30.

MCCUBREY, J. A., STEELMAN, L. S., CHAPPELL, W. H., ABRAMS, S. L., WONG, E. W., CHANG, F., LEHMANN, B., TERRIAN, D. M., MILELLA, M., TAFURI, A., STIVALA, F., LIBRA, M., BASECKE, J., EVANGELISTI, C., MARTELLI, A. M. & FRANKLIN, R. A. 2007. Roles of the Raf/MEK/ERK pathway in cell growth, malignant transformation and drug resistance. *Biochim Biophys Acta,* 1773**,** 1263-84.

MCSHEA, M. A., SCHMIDT, K. L., DUBUKE, M. L., BALDIGA, C. E., SULLENDER, M. E., REIS, A. L., ZHANG, S., O'TOOLE, S. M., JEFFERS, M. C., WARDEN, R. M., KENNEY, A. H., GOSSELIN, J., KUHLWEIN, M., HASHMI, S. K., STRINGHAM, E. G. & RYDER, E. F. 2013. Abelson interactor-1 (ABI-1) interacts with MRL adaptor protein MIG-10 and is required in guided cell migrations and process outgrowth in C. elegans. *Dev Biol,* 373**,** 1-13.

MICHAEL, M., VEHLOW, A., NAVARRO, C. & KRAUSE, M. 2010. c-Abl, Lamellipodin, and Ena/VASP proteins cooperate in dorsal ruffling of fibroblasts and axonal morphogenesis. *Curr Biol,* 20**,** 783-91.

MIKI, H., SUETSUGU, S. & TAKENAWA, T. 1998. WAVE, a novel WASP-family protein involved in actin reorganization induced by Rac. *EMBO J,* 17**,** 6932-41.
MIRALLES, F., POSERN, G., ZAROMYTIDOU, A. I. & TREISMAN, R. 2003. Actin dynamics control SRF activity by regulation of its coactivator MAL. *Cell,* 113**,** 329-42.
MONCOQ, K., BROUTIN, I., LARUE, V., PERDEREAU, D., CAILLIAU, K., BROWAEYS-POLY, E., BURNOL, A. F. & DUCRUIX, A. 2003. The PIR domain of Grb14 is an intrinsically unstructured protein: implication in insulin signaling. *FEBS Lett,* 554**,** 240-6.
MONTANER, S., PERONA, R., SANIGER, L. & LACAL, J. C. 1999. Activation of serum response factor by RhoA is mediated by the nuclear factor-kappaB and C/EBP transcription factors. *J Biol Chem,* 274**,** 8506-15.
MORRIONE, A., PLANT, P., VALENTINIS, B., STAUB, O., KUMAR, S., ROTIN, D. & BASERGA, R. 1999. mGrb10 interacts with Nedd4. *J Biol Chem,* 274**,** 24094-9.
MUDA, M., THEODOSIOU, A., RODRIGUES, N., BOSCHERT, U., CAMPS, M., GILLIERON, C., DAVIES, K., ASHWORTH, A. & ARKINSTALL, S. 1996. The dual specificity phosphatases M3/6 and MKP-3 are highly selective for inactivation of distinct mitogen-activated protein kinases. *J Biol Chem,* 271**,** 27205-8.
NAGAI, T., IBATA, K., PARK, E. S., KUBOTA, M., MIKOSHIBA, K. & MIYAWAKI, A. 2002. A variant of yellow fluorescent protein with fast and efficient maturation for cell-biological applications. *Nat Biotechnol,* 20**,** 87-90.
NANTEL, A., MOHAMMAD-ALI, K., SHERK, J., POSNER, B. I. & THOMAS, D. Y. 1998. Interaction of the Grb10 adapter protein with the Raf1 and MEK1 kinases. *J Biol Chem,* 273**,** 10475-84.
NISHIMOTO, S. & NISHIDA, E. 2006. MAPK signalling: ERK5 versus ERK1/2. *EMBO Rep,* 7**,** 782-6.
NOBES, C. D., HAWKINS, P., STEPHENS, L. & HALL, A. 1995. Activation of the small GTP-binding proteins rho and rac by growth factor receptors. *J Cell Sci,* 108 (Pt 1)**,** 225-33.
NORMAN, C., RUNSWICK, M., POLLOCK, R. & TREISMAN, R. 1988. Isolation and properties of cDNA clones encoding SRF, a transcription factor that binds to the c-fos serum response element. *Cell,* 55**,** 989-1003.
NOTREDAME, C., HIGGINS, D. G. & HERINGA, J. 2000. T-Coffee: A novel method for fast and accurate multiple sequence alignment. *J Mol Biol,* 302**,** 205-17.
OLAYIOYE, M. A. 2001. Update on HER-2 as a target for cancer therapy: intracellular signaling pathways of ErbB2/HER-2 and family members. *Breast Cancer Res,* 3**,** 385-9.
OTEY, C. A., PAVALKO, F. M. & BURRIDGE, K. 1990. An interaction between alpha-actinin and the beta 1 integrin subunit in vitro. *J Cell Biol,* 111**,** 721-9.
PAGLIARINI, R. A. & XU, T. 2003. A genetic screen in Drosophila for metastatic behavior. *Science,* 302**,** 1227-31.
PANTALONI, D., LE CLAINCHE, C. & CARLIER, M. F. 2001. Mechanism of actin-based motility. *Science,* 292**,** 1502-6.
PATSOUKIS, N., LAFUENTE, E. M., MERANER, P., KIM, J., DOMBKOWSKI, D., LI, L. & BOUSSIOTIS, V. A. 2009. RIAM regulates the cytoskeletal distribution and activation of PLC-gamma1 in T cells. *Sci Signal,* 2**,** ra79.
PINHEIRO, E. M., XIE, Z., NOROVICH, A. L., VIDAKI, M., TSAI, L. H. & GERTLER, F. B. 2011. Lpd depletion reveals that SRF specifies radial versus tangential migration of pyramidal neurons. *Nat Cell Biol,* 13**,** 989-95.

PONTING, C. P. & BENJAMIN, D. R. 1996. A novel family of Ras-binding domains. *Trends Biochem Sci,* 21**,** 422-5.
POSERN, G., MIRALLES, F., GUETTLER, S. & TREISMAN, R. 2004. Mutant actins that stabilise F-actin use distinct mechanisms to activate the SRF coactivator MAL. *EMBO J,* 23**,** 3973-83.
POSERN, G. & TREISMAN, R. 2006. Actin' together: serum response factor, its cofactors and the link to signal transduction. *Trends Cell Biol,* 16**,** 588-96.
PRASAD, M., WANG, X., HE, L. & MONTELL, D. J. 2011. Border cell migration: a model system for live imaging and genetic analysis of collective cell movement. *Methods Mol Biol,* 769**,** 277-86.
PULA, G. & KRAUSE, M. 2008. Role of Ena/VASP proteins in homeostasis and disease. *Handb Exp Pharmacol***,** 39-65.
QUINN, C. C., PFEIL, D. S., CHEN, E., STOVALL, E. L., HARDEN, M. V., GAVIN, M. K., FORRESTER, W. C., RYDER, E. F., SOTO, M. C. & WADSWORTH, W. G. 2006. UNC-6/netrin and SLT-1/slit guidance cues orient axon outgrowth mediated by MIG-10/RIAM/lamellipodin. *Curr Biol,* 16**,** 845-53.
QUINN, C. C., PFEIL, D. S. & WADSWORTH, W. G. 2008. CED-10/Rac1 mediates axon guidance by regulating the asymmetric distribution of MIG-10/lamellipodin. *Curr Biol,* 18**,** 808-13.
QUINN, C. C. & WADSWORTH, W. G. 2008. Axon guidance: asymmetric signaling orients polarized outgrowth. *Trends Cell Biol,* 18**,** 597-603.
RAJFUR, Z., ROY, P., OTEY, C., ROMER, L. & JACOBSON, K. 2002. Dissecting the link between stress fibres and focal adhesions by CALI with EGFP fusion proteins. *Nat Cell Biol,* 4**,** 286-93.
RAMEH, L. E., ARVIDSSON, A., CARRAWAY, K. L., 3RD, COUVILLON, A. D., RATHBUN, G., CROMPTON, A., VANRENTERGHEM, B., CZECH, M. P., RAVICHANDRAN, K. S., BURAKOFF, S. J., WANG, D. S., CHEN, C. S. & CANTLEY, L. C. 1997. A comparative analysis of the phosphoinositide binding specificity of pleckstrin homology domains. *J Biol Chem,* 272**,** 22059-66.
RAMEH, L. E. & CANTLEY, L. C. 1999. The role of phosphoinositide 3-kinase lipid products in cell function. *J Biol Chem,* 274**,** 8347-50.
REITER, L. T., POTOCKI, L., CHIEN, S., GRIBSKOV, M. & BIER, E. 2001. A systematic analysis of human disease-associated gene sequences in Drosophila melanogaster. *Genome Res,* 11**,** 1114-25.
REKAS, A., ALATTIA, J. R., NAGAI, T., MIYAWAKI, A. & IKURA, M. 2002. Crystal structure of venus, a yellow fluorescent protein with improved maturation and reduced environmental sensitivity. *J Biol Chem,* 277**,** 50573-8.
RIDLEY, A. J., SCHWARTZ, M. A., BURRIDGE, K., FIRTEL, R. A., GINSBERG, M. H., BORISY, G., PARSONS, J. T. & HORWITZ, A. R. 2003. Cell migration: integrating signals from front to back. *Science,* 302**,** 1704-9.
ROBERTS, D. B. 1998. *Drosophila: a practical approach,* IRL Press at Oxford University Press.
ROBINSON, P. J., SONTAG, J. M., LIU, J. P., FYKSE, E. M., SLAUGHTER, C., MCMAHON, H. & SUDHOF, T. C. 1993. Dynamin GTPase regulated by protein kinase C phosphorylation in nerve terminals. *Nature,* 365**,** 163-6.

RODRIGUEZ-VICIANA, P., SABATIER, C. & MCCORMICK, F. 2004. Signaling specificity by Ras family GTPases is determined by the full spectrum of effectors they regulate. *Mol Cell Biol,* 24**,** 4943-54.

RODRIGUEZ-VICIANA, P., WARNE, P. H., DHAND, R., VANHAESEBROECK, B., GOUT, I., FRY, M. J., WATERFIELD, M. D. & DOWNWARD, J. 1994. Phosphatidylinositol-3-OH kinase as a direct target of Ras. *Nature,* 370**,** 527-32.

ROGERS, S. L., ROGERS, G. C., SHARP, D. J. & VALE, R. D. 2002. Drosophila EB1 is important for proper assembly, dynamics, and positioning of the mitotic spindle. *J Cell Biol,* 158**,** 873-84.

ROGERS, S. L., WIEDEMANN, U., STUURMAN, N. & VALE, R. D. 2003. Molecular requirements for actin-based lamella formation in Drosophila S2 cells. *J Cell Biol,* 162**,** 1079-88.

RUBIN, G. M. & SPRADLING, A. C. 1982. Genetic transformation of Drosophila with transposable element vectors. *Science,* 218**,** 348-53.

SAMBROOK, J. 2001. Molecular cloning : a laboratory manual. *In:* RUSSELL, D. W. (ed.) 3rd ed. ed. Cold Spring Harbor, N.Y. :: Cold Spring Harbor Laboratory Press.

SANTARPIA, L., LIPPMAN, S. M. & EL-NAGGAR, A. K. 2012. Targeting the MAPK-RAS-RAF signaling pathway in cancer therapy. *Expert Opin Ther Targets,* 16**,** 103-19.

SCHAFER, D. A., JENNINGS, P. B. & COOPER, J. A. 1996. Dynamics of capping protein and actin assembly in vitro: uncapping barbed ends by polyphosphoinositides. *J Cell Biol,* 135**,** 169-79.

SCHMIDT, H. A., STRIMMER, K., VINGRON, M. & VON HAESELER, A. 2002. TREE-PUZZLE: maximum likelihood phylogenetic analysis using quartets and parallel computing. *Bioinformatics,* 18**,** 502-4.

SCHNEIDER, I. 1972. Cell lines derived from late embryonic stages of Drosophila melanogaster. *J Embryol Exp Morphol,* 27**,** 353-65.

SCHWARTZ, M. A. & GINSBERG, M. H. 2002. Networks and crosstalk: integrin signalling spreads. *Nat Cell Biol,* 4**,** E65-8.

SENTRY, J. W. & KAISER, K. 1992. P element transposition and targeted manipulation of the Drosophila genome. *Trends Genet,* 8**,** 329-31.

SETTLEMAN, J. 2003. A nuclear MAL-function links Rho to SRF. *Mol Cell,* 11**,** 1121-3.

SHAO, J. & DIAMOND, M. I. 2012. Protein phosphatase 1 dephosphorylates profilin-1 at Ser-137. *PLoS One,* 7**,** e32802.

SHATTIL, S. J., KIM, C. & GINSBERG, M. H. 2010. The final steps of integrin activation: the end game. *Nat Rev Mol Cell Biol,* 11**,** 288-300.

SHEN, T. L. & GUAN, J. L. 2004. Grb7 in intracellular signaling and its role in cell regulation. *Front Biosci,* 9**,** 192-200.

SHEN, T. L., HAN, D. C. & GUAN, J. L. 2002. Association of Grb7 with phosphoinositides and its role in the regulation of cell migration. *J Biol Chem,* 277**,** 29069-77.

SHI, Y., ALIN, K. & GOFF, S. P. 1995. Abl-interactor-1, a novel SH3 protein binding to the carboxy-terminal portion of the Abl protein, suppresses v-abl transforming activity. *Genes Dev,* 9**,** 2583-97.

SHIROUZU, M., HASHIMOTO, K., KIKUCHI, A. & YOKOYAMA, S. 1999. Double-mutant analysis of the interaction of Ras with the Ras-binding domain of RGL. *Biochemistry,* 38**,** 5103-10.

SHORE, P. & SHARROCKS, A. D. 1995. The MADS-box family of transcription factors. *Eur J Biochem,* 229**,** 1-13.
SHOU, W., VERMA, R., ANNAN, R. S., HUDDLESTON, M. J., CHEN, S. L., CARR, S. A. & DESHAIES, R. J. 2002. Mapping phosphorylation sites in proteins by mass spectrometry. *Methods Enzymol,* 351**,** 279-96.
SINGH, M. & JOHNSON, L. 2006. Using genetically engineered mouse models of cancer to aid drug development: an industry perspective. *Clin Cancer Res,* 12**,** 5312-28.
SMALL, J. V. 1988. The actin cytoskeleton. *Electron Microsc Rev,* 1**,** 155-74.
SMALL, J. V., STRADAL, T., VIGNAL, E. & ROTTNER, K. 2002. The lamellipodium: where motility begins. *Trends Cell Biol,* 12**,** 112-20.
SMITH, J. J., KURAKU, S., HOLT, C., SAUKA-SPENGLER, T., JIANG, N., CAMPBELL, M. S., YANDELL, M. D., MANOUSAKI, T., MEYER, A., BLOOM, O. E., MORGAN, J. R., BUXBAUM, J. D., SACHIDANANDAM, R., SIMS, C., GARRUSS, A. S., COOK, M., KRUMLAUF, R., WIEDEMANN, L. M., SOWER, S. A., DECATUR, W. A., HALL, J. A., AMEMIYA, C. T., SAHA, N. R., BUCKLEY, K. M., RAST, J. P., DAS, S., HIRANO, M., MCCURLEY, N., GUO, P., ROHNER, N., TABIN, C. J., PICCINELLI, P., ELGAR, G., RUFFIER, M., AKEN, B. L., SEARLE, S. M., MUFFATO, M., PIGNATELLI, M., HERRERO, J., JONES, M., BROWN, C. T., CHUNG-DAVIDSON, Y. W., NANLOHY, K. G., LIBANTS, S. V., YEH, C. Y., MCCAULEY, D. W., LANGELAND, J. A., PANCER, Z., FRITZSCH, B., DE JONG, P. J., ZHU, B., FULTON, L. L., THEISING, B., FLICEK, P., BRONNER, M. E., WARREN, W. C., CLIFTON, S. W., WILSON, R. K. & LI, W. 2013. Sequencing of the sea lamprey (Petromyzon marinus) genome provides insights into vertebrate evolution. *Nat Genet,* 45**,** 415-21, 421e1-2.
SPORN, M. B. 1996. The war on cancer. *Lancet,* 347**,** 1377-81.
SPRADLING, A. C. & RUBIN, G. M. 1982. Transposition of cloned P elements into Drosophila germ line chromosomes. *Science,* 218**,** 341-7.
ST JOHNSTON, D. 2002. The art and design of genetic screens: Drosophila melanogaster. *Nat Rev Genet,* 3**,** 176-88.
STAVOE, A. K. & COLON-RAMOS, D. A. 2012. Netrin instructs synaptic vesicle clustering through Rac GTPase, MIG-10, and the actin cytoskeleton. *J Cell Biol,* 197**,** 75-88.
STEELMAN, L. S., CHAPPELL, W. H., ABRAMS, S. L., KEMPF, R. C., LONG, J., LAIDLER, P., MIJATOVIC, S., MAKSIMOVIC-IVANIC, D., STIVALA, F., MAZZARINO, M. C., DONIA, M., FAGONE, P., MALAPONTE, G., NICOLETTI, F., LIBRA, M., MILELLA, M., TAFURI, A., BONATI, A., BASECKE, J., COCCO, L., EVANGELISTI, C., MARTELLI, A. M., MONTALTO, G., CERVELLO, M. & MCCUBREY, J. A. 2011. Roles of the Raf/MEK/ERK and PI3K/PTEN/Akt/mTOR pathways in controlling growth and sensitivity to therapy-implications for cancer and aging. *Aging (Albany NY),* 3**,** 192-222.
STEIN, E. G., GUSTAFSON, T. A. & HUBBARD, S. R. 2001. The BPS domain of Grb10 inhibits the catalytic activity of the insulin and IGF1 receptors. *FEBS Lett,* 493**,** 106-11.
STOVOLD, C. F., MILLARD, T. H. & MACHESKY, L. M. 2005. Inclusion of Scar/WAVE3 in a similar complex to Scar/WAVE1 and 2. *BMC Cell Biol,* 6**,** 11.
SVITKINA, T. M. & BORISY, G. G. 1999. Arp2/3 complex and actin depolymerizing factor/cofilin in dendritic organization and treadmilling of actin filament array in lamellipodia. *J Cell Biol,* 145**,** 1009-26.

TANI, K., SATO, S., SUKEZANE, T., KOJIMA, H., HIROSE, H., HANAFUSA, H. & SHISHIDO, T. 2003. Abl interactor 1 promotes tyrosine 296 phosphorylation of mammalian enabled (Mena) by c-Abl kinase. *J Biol Chem,* 278**,** 21685-92.

TAYLOR, E. 2010. *Using Drosophila Melanogaster to investigate the conserved roles of MRL proteins in cell growth, cell migration and metastasis.* PhD, University of Oxford.

THEODOSIOU, N. A. & XU, T. 1998. Use of FLP/FRT system to study Drosophila development. *Methods,* 14**,** 355-65.

THERIOT, J. A. & MITCHISON, T. J. 1991. Actin microfilament dynamics in locomoting cells. *Nature,* 352**,** 126-31.

THOMPSON, B. J. 2010. Mal/SRF is dispensable for cell proliferation in Drosophila. *PLoS One,* 5**,** e10077.

TREISMAN, R. 1994. Ternary complex factors: growth factor regulated transcriptional activators. *Curr Opin Genet Dev,* 4**,** 96-101.

TREISMAN, R. 1995. Journey to the surface of the cell: Fos regulation and the SRE. *EMBO J,* 14**,** 4905-13.

TSUKADA, S., SIMON, M. I., WITTE, O. N. & KATZ, A. 1994. Binding of beta gamma subunits of heterotrimeric G proteins to the PH domain of Bruton tyrosine kinase. *Proc Natl Acad Sci U S A,* 91**,** 11256-60.

VAN DER GEER, P., HENKEMEYER, M., JACKS, T. & PAWSON, T. 1997. Aberrant Ras regulation and reduced p190 tyrosine phosphorylation in cells lacking p120-Gap. *Mol Cell Biol,* 17**,** 1840-7.

VAN DYKE, T. & JACKS, T. 2002. Cancer modeling in the modern era: progress and challenges. *Cell,* 108**,** 135-44.

VANHAESEBROECK, B. & WATERFIELD, M. D. 1999. Signaling by distinct classes of phosphoinositide 3-kinases. *Exp Cell Res,* 253**,** 239-54.

VECCHIONE, A., MARCHESE, A., HENRY, P., ROTIN, D. & MORRIONE, A. 2003. The Grb10/Nedd4 complex regulates ligand-induced ubiquitination and stability of the insulin-like growth factor I receptor. *Mol Cell Biol,* 23**,** 3363-72.

VICENTE-MANZANARES, M. & HORWITZ, A. R. 2011. Adhesion dynamics at a glance. *J Cell Sci,* 124**,** 3923-7.

WACHSSTOCK, D. H., WILKINS, J. A. & LIN, S. 1987. Specific interaction of vinculin with alpha-actinin. *Biochem Biophys Res Commun,* 146**,** 554-60.

WANG, D. Z., LI, S., HOCKEMEYER, D., SUTHERLAND, L., WANG, Z., SCHRATT, G., RICHARDSON, J. A., NORDHEIM, A. & OLSON, E. N. 2002. Potentiation of serum response factor activity by a family of myocardin-related transcription factors. *Proc Natl Acad Sci U S A,* 99**,** 14855-60.

WANG, P., BALLESTREM, C. & STREULI, C. H. 2011. The C terminus of talin links integrins to cell cycle progression. *J Cell Biol,* 195**,** 499-513.

WANG, W., GOSWAMI, S., SAHAI, E., WYCKOFF, J. B., SEGALL, J. E. & CONDEELIS, J. S. 2005. Tumor cells caught in the act of invading: their strategy for enhanced cell motility. *Trends Cell Biol,* 15**,** 138-45.

WANG, W. C., ZINN, K. & BJORKMAN, P. J. 1993. Expression and structural studies of fasciclin I, an insect cell adhesion molecule. *J Biol Chem,* 268**,** 1448-55.

WANG, Y. L. 1985. Exchange of actin subunits at the leading edge of living fibroblasts: possible role of treadmilling. *J Cell Biol,* 101**,** 597-602.

WATANABE, N., BODIN, L., PANDEY, M., KRAUSE, M., COUGHLIN, S., BOUSSIOTIS, V. A., GINSBERG, M. H. & SHATTIL, S. J. 2008. Mechanisms and consequences of agonist-induced talin recruitment to platelet integrin alphaIIbbeta3. *J Cell Biol,* 181**,** 1211-22.

WEBB, D. J., PARSONS, J. T. & HORWITZ, A. F. 2002. Adhesion assembly, disassembly and turnover in migrating cells -- over and over and over again. *Nat Cell Biol,* 4**,** E97-100.

WENNERBERG, K., ROSSMAN, K. L. & DER, C. J. 2005. The Ras superfamily at a glance. *J Cell Sci,* 118**,** 843-6.

WICK, K. R., WERNER, E. D., LANGLAIS, P., RAMOS, F. J., DONG, L. Q., SHOELSON, S. E. & LIU, F. 2003. Grb10 inhibits insulin-stimulated insulin receptor substrate (IRS)-phosphatidylinositol 3-kinase/Akt signaling pathway by disrupting the association of IRS-1/IRS-2 with the insulin receptor. *J Biol Chem,* 278**,** 8460-7.

WIESNER, S., HELFER, E., DIDRY, D., DUCOURET, G., LAFUMA, F., CARLIER, M. F. & PANTALONI, D. 2003. A biomimetic motility assay provides insight into the mechanism of actin-based motility. *J Cell Biol,* 160**,** 387-98.

WITTINGHOFER, A. & NASSAR, N. 1996. How Ras-related proteins talk to their effectors. *Trends Biochem Sci,* 21**,** 488-91.

WOLFENSON, H., LAVELIN, I. & GEIGER, B. 2013. Dynamic regulation of the structure and functions of integrin adhesions. *Dev Cell,* 24**,** 447-58.

WURTZEL, J. G., KUMAR, P. & GOLDFINGER, L. E. 2012. Palmitoylation regulates vesicular trafficking of R-Ras to membrane ruffles and effects on ruffling and cell spreading. *Small GTPases,* 3**,** 139-53.

YANAGAWA, S., LEE, J. S. & ISHIMOTO, A. 1998. Identification and characterization of a novel line of Drosophila Schneider S2 cells that respond to wingless signaling. *J Biol Chem,* 273**,** 32353-9.

YARMOLA, E. G. & BUBB, M. R. 2006. Profilin: emerging concepts and lingering misconceptions. *Trends Biochem Sci,* 31**,** 197-205.

YUAN, T. L. & CANTLEY, L. C. 2008. PI3K pathway alterations in cancer: variations on a theme. *Oncogene,* 27**,** 5497-510.

ZWARTKRUIS, F. J. & BOS, J. L. 1999. Ras and Rap1: two highly related small GTPases with distinct function. *Exp Cell Res,* 253**,** 157-65.

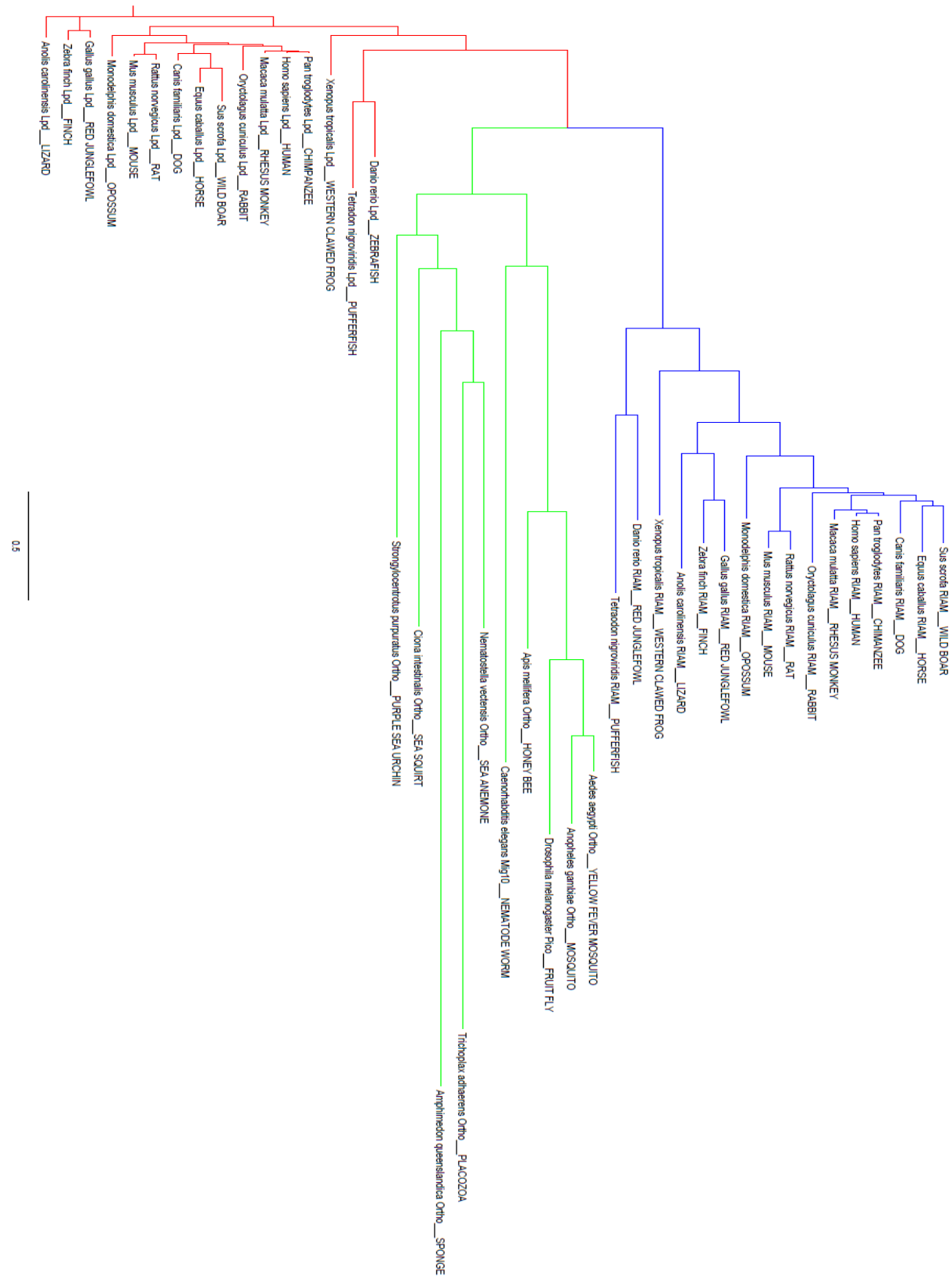
Sus scrofa RIAM__WILD BOAR
Equus caballus RIAM__HORSE
Canis familiaris RIAM__DOG
Pan troglodytes RIAM__CHIMANZEE
Homo sapiens RIAM__HUMAN
Macaca mulatta RIAM__RHESUS MONKEY
Oryctolagus cuniculus RIAM__RABBIT
Rattus norvegicus RIAM__RAT
Mus musculus RIAM__MOUSE
Monodelphis domestica RIAM__OPOSSUM
Gallus gallus RIAM__RED JUNGLEFOWL
Zebra finch RIAM__FINCH
Anolis carolinensis RIAM__LIZARD
Xenopus tropicalis RIAM__WESTERN CLAWED FROG
Danio rerio RIAM__RED JUNGLEFOWL
Tetraodon nigroviridis RIAM__PUFFERFISH
Aedes aegypti Ortho__YELLOW FEVER MOSQUITO
Anopheles gambiae Ortho__MOSQUITO
Drosophila melanogaster Flo__FRUIT FLY
Apis mellifera Ortho__HONEY BEE
Caenorhabditis elegans Mig10__NEMATODE WORM
Nematostella vectensis Ortho__SEA ANEMONE
Trichoplax adhaerens Ortho__PLACOZOA
Amphimedon queenslandica Ortho__SPONGE
Ciona intestinalis Ortho__SEA SQUIRT
Strongylocentrotus purpuratus Ortho__PURPLE SEA URCHIN
Danio rerio Lpd__ZEBRAFISH
Tetraodon nigroviridis Lpd__PUFFERFISH
Xenopus tropicalis Lpd__WESTERN CLAWED FROG
Pan troglodytes Lpd__CHIMPANZEE
Homo sapiens Lpd__HUMAN
Macaca mulatta Lpd__RHESUS MONKEY
Oryctolagus cuniculus Lpd__RABBIT
Sus scrofa Lpd__WILD BOAR
Equus caballus Lpd__HORSE
Canis familiaris Lpd__DOG
Rattus norvegicus Lpd__RAT
Mus musculus Lpd__MOUSE
Monodelphis domestica Lpd__OPOSSUM
Gallus gallus Lpd__RED JUNGLEFOWL
Zebra finch Lpd__FINCH
Anolis carolinensis Lpd__LIZARD
0.5

1. WTETKKQSFKQTG
2. LEKIGEGTYGTVF
3. PTAENPEYLGLDV
4. GRKGSGDYMPMSP
5. LLPTPPLSPSRRS
6. KEFGVERSVRPTD
7. KSNVKIQSTPVKQ
8. LVEPLTPSGEAPN
9. IHFWSTLSPIAPR
10. GSRSRTPSLPTPP
11. ASATVSKTETSQV
12. MANLEDSQESELDQILGE
13. MANLEDAQESELDQILGE
14. ANLEDSQESELDQILGEL
15. ANLEDSQEAELDQILGEL
16. LDQILGELSLLEAQISYT
17. LDQILGELALLEAQISYT
18. LDQILGELSLLEAQIAFA
19. SLLEAQISYTEASMLPAM
20. SLLEAQIAYTEASMLPAM
21. ALLEAQISFAEAAMLPAM
22. SLLEAQISETEASMLPAM
23. ALLEAQIAYAEAAMLPAM
24. SLLEAQISYAEASMLPAM
25. ALLEAQIAFTEAAMLPAM
26. AQISYTEASMLPAMCAPS
27. AQISYTEAAMLPAMCAPS
28. AQIAFAEASMLPAMCAPA
29. MLPAMCAPSAGAQIAPPP
30. MLPAMCAPAAGAQIAPPP
31. QIAPPPGVTQLPGSAPTM
32. QIAPPPGVAQLPGSAPTM
33. QIAPPPGVTQLPGAAPAM
34. PGVTQLPGSAPTMVSMSA
35. PGVTQLPGAAPTMVSMSA
36. PGVAQLPGSAPAMVAMAA
37. TQLPGSAPTMVSMSASSS
38. TQLPGSAPAMVSMSASSS
39. AQLPGAAPTMVAMAAAAA
40. PGSAPTMVSMSASSSRSH
41. PGSAPTMVAMSASSSRSH
42. PGAAPAMVSMAAAAARAH
43. SAPTMVSMSASSSRSHRT
44. SAPTMVSMAASSSRSHRT
45. AAPAMVAMSAAAARAHRA
46. TMVSMSASSSRSHSRTNS
47. TMVSMSAASSRSHSRTNS
48. AMVAMAASAARAHARANA
49. TMVSMSASASRSHSRTNS
50. AMVAMAAASARAHARANA
51. TMVSMSASSARSHSRTNS
52. AMVAMAAAASRAHARANA
53. SMSASSSRSHSRTNSTIS
54. SMSASSSRAHSRTNSTIS
55. AMAAAAARSHARANAAIA
56. SASSSRSHSRTNSTISAD
57. SASSSRSHARTNSTISAD
58. AAAAARAHSRANAAIAAD
59. SSSRSHSRTNSTISADVS
60. SSSRSHSRANSTISADVS
61. AAARAHARTNAAIAADVA
62. SRSHSRTNSTISADVSSC
63. SRSHSRTNATISADVSSC
64. ARAHARANSAIAADVAAC
65. SRSHSRTNSAISADVSSC
66. ARAHARANATIAADVAAC
67. HSRTNSTISADVSSCSSS
68. HSRTNSTIAADVSSCSSS
69. HARANAAISADVAACAAA
70. NSTISADVSSCSSSGISE
71. NSTISADVASCSSSGISE
72. NAAIAADVSACAAAGIAE
73. NSTISADVSACSSSGISE
74. NAAIAADVASCAAAGIAE
75. SADVSSCSSSGISENGHG
76. SADVSSCASSGISENGHG
77. AADVAACSAAGIAENGHG
78. SADVSSCSASGISENGHG
79. AADVAACASAGIAENGHG
80. SADVSSCSSAGISENGHG
81. AADVAACAASGIAENGHG
82. SSCSSSGISENGHGLGLV
83. SSCSSSGIAENGHGLGLV
84. AACAAAGISENGHGLGLV
85. GLVLGGPGSAGMMVQPPP
86. GLVLGGPGAAGMMVQPPP
87. QPPPPGGMTMGITLGVVT
88. QPPPPGGMAMGITLGVVT
89. QPPPPGGMTMGIALGVVA
90. PGGMTMGITLGVVTPREP
91. PGGMTMGIALGVVTPREP
92. PGGMAMGITLGVVAPREP
93. MGITLGVVTPREPRTESP
94. MGITLGVVAPREPRTESP
95. MGIALGVVTPREPRAEAP
96. VVTPREPRTESPDNDSAF
97. VVTPREPRAESPDNDSAF
98. VVAPREPRTEAPDNDAAF
99. TPREPRTESPDNDSAFSD
100. TPREPRTEAPDNDSAFSD
101. APREPRAESPDNDAAFAD
102. RTESPDNDSAFSDTVSLL
103. RTESPDNDAAFSDTVSLL
104. RAEAPDNDSAFADAVALL
105. SPDNDSAFSDTVSLLSSE
106. SPDNDSAFADTVSLLSSE
107. APDNDAAFSDAVALLAAE
108. DNDSAFSDTVSLLSSESS
109. DNDSAFSDAVSLLSSESS
110. DNDAAFADTVALLAAEAA
111. DSAFSDTVSLLSSESSAS
112. DSAFSDTVALLSSESSAS
113. DAAFADAVSLLAAEAAAA
114. FSDTVSLLSSESSASSNT
115. FSDTVSLLASESSASSNT
116. FADAVALLSAEAAAAANA
117. FSDTVSLLSAESSASSNT
118. FADAVALLASEAAAAANA
119. TVSLLSSESSASSNTSLQ
120. TVSLLSSEASASSNTSLQ
121. AVALLAAESAAAANAALQ
122. TVSLLSSESAASSNTSLQ
123. AVALLAAEASAAANAALQ
124. LLSSESSASSNTSLQQQQ
125. LLSSESSAASNTSLQQQQ
126. LLAAEAAASANAALQQQQ
127. LLSSESSASANTSLQQQQ
128. LLAAEAAAASNAALQQQQ
129. SESSASSNTSLQQQQQQQ
130. SESSASSNASLQQQQQQQ
131. AEAAAAAANTALQQQQQQQ
132. SESSASSNTALQQQQQQQ
133. AEAAAAAANASLQQQQQQQ
134. HGQHGGQQSGANSITKAD
135. HGQHGGQQAGANSITKAD
136. HGQHGGQQSGANAIAKAD
137. GGQQSGANSITKADKIQL
138. GGQQSGANAITKADKIQL
139. GGQQAGANSIAKADKIQL
140. QQSGANSITKADKIQLAL
141. QQSGANSIAKADKIQLAL
142. QQAGANAITKADKIQLAL
143. QLALHKLESAPIRRLFVK
144. QLALHKLEAAPIRRLFVK
145. RRLFVKAFTSDGASKSLL
146. RRLFVKAFASDGASKSLL
147. RRLFVKAFTADGAAKALL
148. RRLFVKAFTADGASKSLL
149. RRLFVKAFASDGAAKALL
150. KAFTSDGASKSLLVDERM
151. KAFTSDGAAKSLLVDERM
152. KAFAADGASKALLVDERM
153. FTSDGASKSLLVDERMGC
154. FTSDGASKALLVDERMGC
155. FAADGAAKSLLVDERMGC
156. ERMGCGHVTRLLADKNHV
157. ERMGCGHVARLLADKNHV
158. DKNHVQMQSNWALVEHLG
159. DKNHVQMQANWALVEHLG
160. ELLVDNLMTWHSDAGNRV
161. ELLVDNLMAWHSDAGNRV
162. VDNLMTWHSDAGNRVLFQ
163. VDNLMTWHADAGNRVLFQ
164. FQQRPDKVTLFLRPELYL
165. FQQRPDKVALFLRPELYL
166. FQQRPDKVTLFLRPELEL
167. TLFLRPELYLPGPQMAPG
168. TLFLRPELELPGPQMAPG
169. ALFLRPELYLPGPQMAPG
170. PGCQHDEQTRQMLLDEFF
171. PGCQHDEQARQMLLDEFF
172. MLLDEFFDSHNQLQMDGP
173. MLLDEFFDAHNQLQMDGP
174. QLQMDGPLYMKADPKKGW
175. QLQMDGPLEMKADPKKGW
176. DPKKGWKRYHFVLRSSGL
177. DPKKGWKRFHFVLRSSGL
178. DPKKGWKRYHFVLRAAGL
179. KRYHFVLRSSGLYYFPKE
180. KRYHFVLRASGLYYFPKE
181. KRFHFVLRSAGLFFFPKE
182. KRYHFVLRSAGLYYFPKE
183. KRFHFVLRASGLFFFPKE
184. FVLRSSGLYYFPKEKTKN
185. FVLRSSGLFYFPKEKTKN
186. FVLRAAGLYFFPKEKAKN

187. FVLRSSGLYFFPKEKTKN
188. FVLRAAGLFYFPKEKAKN
189. LYYFPKEKTKNTRDLACL
190. LYYFPKEKAKNTRDLACL
191. LFFFPKEKTKNARDLACL
192. FPKEKTKNTRDLACLNLF
193. FPKEKTKNARDLACLNLF
194. FPKEKAKNTRDLACLNLF
195. NLFHGHNVYTGLGWRKKW
196. NLFHGHNVFTGLGWRKKW
197. NLFHGHNVYAGLGWRKKW
198. LGWRKKWKSPTDYTFGFK
199. LGWRKKWKAPTDYTFGFK
200. LGWRKKWKSPADFAFGFK
201. WRKKWKSPTDYTFGFKAV
202. WRKKWKSPADYTFGFKAV
203. WRKKWKAPTDFAFGFKAV
204. KKWKSPTDYTFGFKAVGD
205. KKWKSPTDFTFGFKAVGD
206. KKWKAPADYAFGFKAVGD
207. KKWKSPTDYAFGFKAVGD
208. KKWKAPADFTFGFKAVGD
209. FGFKAVGDSSLGKSCRSL
210. FGFKAVGDASLGKSCRSL
211. FGFKAVGDSALGKACRAL
212. FGFKAVGDSALGKSCRSL
213. FGFKAVGDASLGKACRAL
214. VGDSSLGKSCRSLKMLCA
215. VGDSSLGKACRSLKMLCA
216. VGDAALGKSCRALKMLCA
217. SSLGKSCRSLKMLCAEDL
218. SSLGKSCRALKMLCAEDL
219. AALGKACRSLKMLCAEDL
220. MLCAEDLPTLDRWLTAIR
221. MLCAEDLPALDRWLTAIR
222. MLCAEDLPTLDRWLAAIR
223. LPTLDRWLTAIRVCKYGK
224. LPTLDRWLAAIRVCKYGK
225. LPALDRWLTAIRVCKFGK
226. LTAIRVCKYGKQLWDSHK
227. LTAIRVCKFGKQLWDSHK
228. LAAIRVCKYGKQLWDAHK
229. KYGKQLWDSHKSLLEDLC
230. KYGKQLWDAHKSLLEDLC
231. KFGKQLWDSHKALLEDLC
232. KQLWDSHKSLLEDLCLSR
233. KQLWDSHKALLEDLCLSR
234. KQLWDAHKSLLEDLCLAR
235. SLLEDLCLSRDDAVSQSS
236. SLLEDLCLARDDAVSQSS
237. ALLEDLCLSRDDAVAQAA
238. CLSRDDAVSQSSFAASMR
239. CLSRDDAVAQSSFAASMR
240. CLSRDDAVSQAAFAAAMR
241. SRDDAVSQSSFAASMRSE
242. SRDDAVSQASFAASMRSE
243. ARDDAVAQSAFAAAMRAE
244. SRDDAVSQSAFAASMRSE
245. ARDDAVAQASFAAAMRAE
246. VSQSSFAASMRSESISSI
247. VSQSSFAAAMRSESISSI
248. VAQAAFAASMRAEAIAAI
249. SSFAASMRSESISSISSA
250. SSFAASMRAESISSISSA
251. AAFAAAMRSEAIAAIAAA
252. FAASMRSESISSISSAVP
253. FAASMRSEAISSISSAVP
254. FAAAMRAESIAAIAAAVP
255. ASMRSESISSISSAVPSQ
256. ASMRSESIASISSAVPSQ
257. AAMRAEAISAIAAAVPAQ
258. ASMRSESISAISSAVPSQ
259. AAMRAEAIASIAAAVPAQ
260. RSESISSISSAVPSQCGS
261. RSESISSIASAVPSQCGS
262. RAEAIAAISAAVPAQCGA
263. RSESISSISAAVPSQCGS
264. RAEAAAIASAVPAQCGA
265. SSISSAVPSQCGSVSSAI
266. SSISSAVPAQCGSVSSAI
267. AAIAAAVPSQCGAVAAAI
268. SAVPSQCGSVSSAISSMS
269. SAVPSQCGAVSSAISSMS
270. AAVPAQCGSVAAAIAAMA
271. VPSQCGSVSSAISSMSNS
272. VPSQCGSVASAISSMSNS
273. VPAQCGAVSAAIAAMANA
274. VPSQCGSVSAAISSMSNS
275. VPAQCGAVASAIAAMANA
276. CGSVSSAISSMSNSTSGR
277. CGSVSSAIASMSNSTSGR
278. CGAVAAAISAMANAAAGR
279. CGSVSSAISAMSNSTSGR
280. CGAVAAAIASMANAAAGR
281. VSSAISSMSNSTSGRTSR
282. VSSAISSMANSTSGRTSR
283. VAAAIAAMSNAAAGRAAR
284. AISSMSNSTSGRTSRASS
285. AISSMSNATSGRTSRASS
286. AIAAMANSAAGRAARAAA
287. AISSMSNSASGRTSRASS
288. AIAAMANATAGRAARAAA
289. AISSMSNSTAGRTSRASS
290. AIAAMANAASGRAARAAA
291. MSNSTSGRTSRASSSSSS
292. MSNSTSGRASRASSSSSS
293. MANAAAGRTARAAAAAAA
294. MSNSTSGRTARASSSSSS
295. MANAAAGRASRAAAAAAA
296. SGRTSRASSSSSSGCLSD
297. SGRTSRAASSSSSGCLSD
298. AGRASRASAAAAAGCLAD
299. SGRTSRASASSSSGCLSD
300. AGRASRAASAAAAGCLAD
301. SGRTSRASSASSSGCLSD
302. AGRASRAAASAAAGCLAD
303. TSRASSSSSSGCLSDDNN
304. TSRASSSASSGCLSDDNN
305. AARAAAASAAGCLADDNN
306. TSRASSSSASGCLSDDNN
307. AARAAAAASAGCLADDNN
308. TSRASSSSSAGCLSDDNN
309. AARAAAAAASGCLADDNN
310. SSSSSGCLSDDNNAFDSE
311. SSSSSGCLADDNNAFDSE
312. AAAAAGCLSDDNNAFDAE
313. SDDNNAFDSEFTTGTIKR
314. SDDNNAFDAEFTTGTIKR
315. ADDNNAFDSEFAAGAIKR
316. NNAFDSEFTTGTIKRKPS
317. NNAFDSEFATGTIKRKPS
318. NNAFDAEFTAGAIKRKPA
319. NNAFDSEFTAGTIKRKPS
320. NNAFDAEFATGAIKRKPA
321. FDSEFTTGTIKRKPSMKP
322. FDSEFTTGAIKRKPSMKP
323. FDAEFAAGTIKRKPAMKP
324. TGTIKRKPSMKPNLPLTT
325. TGTIKRKPAMKPNLPLTT
326. AGAIKRKPSMKPNLPLAA
327. SMKPNLPLTTMTRQLKEV
328. SMKPNLPLATMTRQLKEV
329. AMKPNLPLTAMARQLKEV
330. SMKPNLPLTAMTRQLKEV
331. AMKPNLPLATMARQLKEV
332. PNLPLTTMTRQLKEVGEI
333. PNLPLTTMARQLKEVGEI
334. PNLPLAAMTRQLKEVGEI
335. QLKEVGEITICESAGGDA
336. QLKEVGEIAICESAGGDA
337. QLKEVGEITICEAAGGDA
338. VGEITICESAGGDASSPE
339. VGEITICEAAGGDASSPE
340. VGEIAICESAGGDAAAPE
341. CESAGGDASSPERSGTLT
342. CESAGGDAASPERSGTLT
343. CEAAGGDASAPERAGALA
344. CESAGGDASAPERSGTLT
345. CEAAGGDAASPERAGALA
346. GDASSPERSGTLTRRHSR
347. GDASSPERAGTLTRRHSR
348. GDAAAPERSGALARRHAR
349. ASSPERSGTLTRRHSRRK
350. ASSPERSGALTRRHSRRK
351. AAAPERAGTLARRHARRK
352. SPERSGTLTRRHSRRKSQ
353. SPERSGTLARRHSRRKSQ
354. APERAGALTRRHARRKAQ
355. SGTLTRRHSRRKSQESNG
356. SGTLTRRHARRKSQESNG
357. AGALARRHSRRKAQEANG
358. TRRHSRRKSQESNGSGTL
359. TRRHSRRKAQESNGSGTL
360. ARRHARRKSQEANGAGAL
361. HSRRKSQESNGSGTLKRR
362. HSRRKSQEANGSGTLKRR
363. HARRKAQESNGAGALKRR
364. RKSQESNGSGTLKRRPIA
365. RKSQESNGAGTLKRRPIA
366. RKAQEANGSGALKRRPIA
367. SQESNGSGTLKRRPIAVP
368. SQESNGSGALKRRPIAVP
369. AQEANGAGTLKRRPIAVP
370. RPIAVPVATVVKQTEPMG
371. RPIAVPVAAVVKQTEPMG
372. RPIAVPVATVVKQAEPMG

373. PVATVVKQTEPMGSASST
374. PVATVVKQAEPMGSASST
375. PVAAVVKQTEPMGAAAAA
376. VKQTEPMGSASSTSSSSN
377. VKQTEPMGAASSTSSSSN
378. VKQAEPMGSAAAAAAAAN
379. TEPMGSASSTSSSSNSTP
380. TEPMGSAASTSSSSNSTP
381. AEPMGAASAAAAAANSAP
382. TEPMGSASATSSSSNSTP
383. AEPMGAAASAAAAANAAP
384. TEPMGSASSASSSSNSTP
385. AEPMGAAAATAAAANAAP
386. PMGSASSTSSSSNSTPTP
387. PMGSASSTASSSNSTPTP
388. PMGAAAAASAAANAAPAP
389. PMGSASSTSASSNSTPTP
390. PMGAAAAAASAANAAPAP
391. PMGSASSTSSASNSTPTP
392. PMGAAAAAAASANAAPAP
393. SASSTSSSSNSTPTPTPS
394. SASSTSSSANSTPTPTPS
395. AAAAAAAASNAAPAPAPA
396. SSTSSSSNSTPTPTPSIC
397. SSTSSSSNATPTPTPSIC
398. AAAAAAANSAPAPAPAIC
399. SSTSSSSNSAPTPTPSIC
400. AAAAAAANATPAPAPAIC
401. SSSSNSTPTPTPSICAKP
402. SSSSNSTPAPTPSICAKP
403. AAAANAAPTPAPAICAKP
404. SSNSTPTPTPSICAKPPP
405. SSNSTPTPAPSICAKPPP
406. AANAAPAPTPAICAKPPP
407. NSTPTPTPSICAKPPPGD
408. NSTPTPTPAICAKPPPGD
409. NAAPAPAPSICAKPPPGD
410. CAKPPPGDSASLMCSSTL
411. CAKPPPGDAASLMCSSTL
412. CAKPPPGDSAALMCAAAL
413. KPPPGDSASLMCSSTLDS
414. KPPPGDSAALMCSSTLDS
415. KPPPGDAASLMCAAALDA
416. DSASLMCSSTLSLDSLPP
417. DSASLMCASTLSLDSLPP
418. DAAALMCSAALALDALPP
419. DSASLMCSATLSLDSLPP
420. DAAALMCASALALDALPP
421. DSASLMCSSALSLDSLPP
422. DAAALMCAATLALDALPP
423. SLMCSSTLSLDSLPPPPP
424. SLMCSSTLALDSLPPPPP
425. ALMCAAALSLDALPPPPP
426. CSSTLSLDSLPPPPPPPA
427. CSSTLSLDALPPPPPPPA
428. CAAALALDSLPPPPPPPA
429. PPPPALDGSEDQDVYGSQ
430. PPPPALDGAEDQDVYGSQ
431. PPPPALDGSEDQDVFGAQ
432. DGSEDQDVYGSQLSLASL
433. DGSEDQDVFGSQLSLASL
434. DGAEDQDVYGAQLALAAL
435. SEDQDVYGSQLSLASLPP
436. SEDQDVYGAQLSLASLPP
437. AEDQDVFGSQLALAALPP
438. QDVYGSQLSLASLPPPPP
439. QDVYGSQLALASLPPPPP
440. QDVFGAQLSLAALPPPPP
441. YGSQLSLASLPPPPPPED
442. YGSQLSLAALPPPPPPED
443. FGAQLALASLPPPPPPED
444. PEDVLAMNYAEPSSPSTP
445. PEDVLAMNFAEPSSPSTP
446. PEDVLAMNYAEPAAPAAP
447. LAMNYAEPSSPSTPTPMS
448. LAMNYAEPASPSTPTPMS
449. LAMNFAEPSAPAAPAPMA
450. LAMNYAEPSAPSTPTPMS
451. LAMNFAEPASPAAPAPMA
452. NYAEPSSPSTPTPMSTPM
453. NYAEPSSPATPTPMSTPM
454. NFAEPAAPSAPAPMAAPM
455. NYAEPSSPSAPTPMSTPM
456. NFAEPAAPATPAPMAAPM
457. EPSSPSTPTPMSTPMIMP
458. EPSSPSTPAPMSTPMIMP
459. EPAAPAAPTPMAAPMIMP
460. SPSTPTPMSTPMIMPNSN
461. SPSTPTPMATPMIMPNSN
462. APAAPAPMSAPMIMPNAN
463. SPSTPTPMSAPMIMPNSN
464. APAAPAPMATPMIMPNAN
465. STPMIMPNSNGSLPPAVP
466. STPMIMPNANGSLPPAVP
467. AAPMIMPNSNGALPPAVP
468. MIMPNSNGSLPPAVPAKP
469. MIMPNSNGALPPAVPAKP
470. MIMPNANGSLPPAVPAKP
471. GGLKAAPPYKAPPDYVGP
472. GGLKAAPPFKAPPDYVGP
473. GGLKAAPPYKAPPDFVGP
474. PPYKAPPDYVGPALLPGP
475. PPYKAPPDFVGPALLPGP
476. PPFKAPPDYVGPALLPGP
477. PPPAQKKVSFADSPVLLR
478. PPPAQKKVAFADSPVLLR
479. PPPAQKKVSFADAPVLLR
480. QKKVSFADSPVLLRRKMC
481. QKKVSFADAPVLLRRKMC
482. QKKVAFADSPVLLRRKMC
483. VLLRRKMCSPEPVLPQRS
484. VLLRRKMCAPEPVLPQRS
485. VLLRRKMCSPEPVLPQRA
486. PEPVLPQRSPSTTLSCHS
487. PEPVLPQRAPSTTLSCHS
488. PEPVLPQRSPAAALACHA
489. VLPQRSPSTTLSCHSSSS
490. VLPQRSPATTLSCHSSSS
491. VLPQRAPSAALACHAAAA
492. VLPQRSPSATLSCHSSSS
493. VLPQRAPATALACHAAAA
494. VLPQRSPSTALSCHSSSS
495. VLPQRAPAATLACHAAAA
496. QRSPSTTLSCHSSSSAGS
497. QRSPSTTLACHSSSSAGS
498. QRAPAAALSCHAAAAAGA
499. STTLSCHSSSSAGSAYQT
500. STTLSCHASSSAGSAYQT
501. AAALACHSAAAAGAAFQA
502. STTLSCHSASSAGSAYQT
503. AAALACHASAAAGAAFQA
504. STTLSCHSSASAGSAYQT
505. AAALACHAASAAGAAFQA
506. TLSCHSSSSAGSAYQTYA
507. TLSCHSSSAAGSAYQTYA
508. ALACHAAASAGAAFQAFA
509. CHSSSSAGSAYQTYAPGP
510. CHSSSSAGAAYQTYAPGP
511. CHAAAAAGSAFQAFAPGP
512. SSSSAGSAYQTYAPGPML
513. SSSSAGSAFQTYAPGPML
514. AAAAAGAAYQAFAPGPML
515. SSAGSAYQTYAPGPMLPP
516. SSAGSAYQAYAPGPMLPP
517. AAAGAAFQTFAPGPMLPP
518. SSAGSAYQTFAPGPMLPP
519. AAAGAAFQAYAPGPMLPP
520. PRADVARLSSLSNGSSSE
521. PRADVARLASLSNGSSSE
522. PRADVARLSALANGAAAE
523. PRADVARLSALSNGSSSE
524. PRADVARLASLANGAAAE
525. DVARLSSLSNGSSSEVTS
526. DVARLSSLANGSSSEVTS
527. DVARLAALSNGAAAEVAA
528. LSSLSNGSSSEVTSPKRL
529. LSSLSNGASSEVTSPKRL
530. LAALANGSAAEVAAPKRL
531. LSSLSNGSASEVTSPKRL
532. LAALANGASAEVAAPKRL
533. LSSLSNGSSAEVTSPKRL
534. LAALANGAASEVAAPKRL
535. SNGSSSEVTSPKRLQESA
536. SNGSSSEVASPKRLQESA
537. ANGAAAEVTAPKRLQEAA
538. SNGSSSEVTAPKRLQESA
539. ANGAAAEVASPKRLQEAA
540. TSPKRLQESASNPPRDFL
541. TSPKRLQEAASNPPRDFL
542. AAPKRLQESAANPPRDFL
543. PKRLQESASNPPRDFLKD
544. PKRLQESAANPPRDFLKD
545. PKRLQEAASNPPRDFLKD
546. QKCKAEPAITPHEVLGFR
547. QKCKAEPAATPHEVLGFR
548. QKCKAEPATAPHEVLGFR
549. EVLGFRDFSNEDLLAAHN
550. EVLGFRDFANEDLLAAHN
551. LLAAHNLNSGANSSHYYR
552. LLAAHNLNAGANSSHYYR
553. LLAAHNLNSGANAAHFFR
554. HNLNSGANSSHYYRETAN
555. HNLNSGANASHYYRETAN
556. HNLNAGANSAHFFREAAN
557. HNLNSGANSAHYYRETAN
558. HNLNAGANASHFFREAAN

559. NSGANSSHYYRETANVSH
560. NSGANSSHFYRETANVSH
561. NAGANAAHYFREAANVAH
562. NSGANSSHYFRETANVSH
563. NAGANAAHFYREAANVAH
564. NSSHYYRETANVSHWVRK
565. NSSHYYREAANVSHWVRK
566. NAAHFFRETANVAHWVRK
567. YYRETANVSHWVRKHYEY
568. YYRETANVAHWVRKHYEY
569. FFREAANVSHWVRKHFEF
570. VSHWVRKHYEYAHNALYE
571. VSHWVRKHFEYAHNALYE
572. VAHWVRKHYEFAHNALFE
573. HWVRKHYEYAHNALYENV
574. HWVRKHYEFAHNALYENV
575. HWVRKHFEYAHNALFENV
576. YEYAHNALYENVHAQSAA
577. YEYAHNALFENVHAQSAA
578. FEFAHNALYENVHAQAAA
579. LYENVHAQSAAAAGVPGS
580. LYENVHAQAAAAAGVPGS
581. LFENVHAQSAAAAGVPGA
582. AAAAGVPGSGEATTPPLP
583. AAAAGVPGAGEATTPPLP
584. AAAAGVPGSGEAAPPLP
585. GVPGSGEATTPPLPPPPG
586. GVPGSGEAATPPLPPPPG
587. GVPGAGEATAPPLPPPPG
588. GVPGSGEATAPPLPPPPG
589. GVPGAGEAATPPLPPPPG
590. PLPPPPGNSVAAKKRPPP
591. PLPPPPGNAVAAKKRPPP
592. PPPPPPKRSDKTHLTNRV
593. PPPPPPKRADKTHLTNRV
594. PPPPPPKRSDKAHLANRV
595. PPPPPPKRSDKAHLTNRV
596. PPPPPPKRADKTHLANRV
597. PPPPPPKRSDKTHLANRV
598. PPPPPPKRADKAHLTNRV

>Pico^{WT} (size=3108bp)

ATGGCGAATCTCGAAGACAGCCAAGAGAGCGAACTCGATCAAATTTTGGGAGAACTGTCCCTCCTCGAAGCCCAGAT
CTCCTATACCGAAGCGAGCATGTTACCGGCGATGTGCGCCCCCAGTGCCGGAGCGCAGATCGCCCCACCCCCAGGCG
TCACCCAGCTCCCCGGATCGGCCCCCACCATGGTGAGCATGAGCGCGAGCAGCAGCCGCAGCCACAGCCGCACGAAC
TCGACGATAAGCGCCGATGTGTCCAGCTGTAGCTCCAGCGGCATCAGCGAAAACGGCCATGGCCTCGGCTTGGTGCT
GGGAGGACCGGGGCTCCGCCGGCATGATGGTCCAACCGCCCCCACCAGGTGGAATGACGATGGGCATCACCCTCGGAG
TGGTGACCCCACGCGAGCCCCCGGACGGAGAGCCCCGATAACGATAGCGCCTTCTCGGATACCGTGAGCCTGCTGAGC
TCCGAGAGCAGCGCCAGCTCCAACACCAGCCTGCAACAGCAACAACAGCAACAGCAGCAGCAACACCATCAGCATCA
GCAGCATCACCAGCACCAGCAACAGCAACAGAAGCCGCAGCTGGCCGGAGCCGAGAAGCTGCACCACCACGGCGTGC
ACGGACAGCACGGCGGCCAGCAGAGCGGCGCCAACTCGATCACCAAGGCCGATAAGATCCAGCTGGCCCTGCACAAG
CTGGAGAGCGCCCCCATCCGCCGCCTGTTTGTGAAGGCCTTTACCTCCGATGGTGCGAGCAAGTCCCTGCTGGTCGA
TGAGCGCATGGGCTGCGGACACGTGACCCGCCTGCTGGCCGACAAGAACCACGTGCAGATGCAGAGCAACTGGGCCC
TGGTGGAGCACCTGGGCGATCTGCAGATGGAGCGCCTGTTCGAGGATCACGAGCTGCTGGTCGACAACCTGATGACC
TGGCACTCCGATGCCGGCAACCGCGTGCTGTTCCAGCAGCGCCCCGATAAGGTGACCCTGTTCCTGCGCCCCGAGCT
GTACCTGCCAGGCCCACAGATGGCCCCAGGATGCCAGCACGATGAGCAGACCCGCCAGATGCTGCTGGATGAGTTCT
TCGATAGCCACAACCAGCTGCAGATGGATGGCCCCCTGTACATGAAGGCCGATCCCAAGAAGGGCTGGAAGCGCTAC
CACTTCGTGCTGCGCTCCTCCGGCCTGTACTACTTCCCCAAAGAAAAGACCAAGAACACCCGCGATCTGGCCTGCCT
GAACCTGTTCCACGGCCACAACGTGTACACCGGCCTGGGCTGGCGCAAGAAGTGGAAGAGCCCCACCGATTACACCT
TCGGCTTCAAGGCCGTCGGTGATAGCAGCCTGGGAAAGAGCTGCCGCAGCCTGAAGATGCTGTGCGCCGAGGATCTG
CCAACCCTGGATCGCTGGCTGACCGCCATCCGCGTGTGCAAGTACGGCAAGCAGCTGTGGGATTCCCACAAGTCGCT
GCTGGAGGATCTGTGCCTGAGCCGCGACGATGCCGTGAGCCAGAGCAGCTTCGCCGCCAGCATGCGCAGCGAGTCCA
TCAGCTCCATCTCCAGCGCCGTGCCAAGCCAGTGCGGCAGCGTGTCCAGCGCCATCTCCTCCATGAGCAACAGCACC
TCCGGCCGCACCAGCCGCGCCTCCAGCAGCTCCTCCAGCGGCTGCCTGAGCGACGATAACAACGCCTTCGATAGCGA
GTTCACCACCGGCACCATCAAGCGCAAGCCCAGCATGAAGCCCAACCTGCCCCTGACCACCATGACCCGCCAACTCA
AAGAAGTCGGAGAGATAACGATTTGCGAATCGGCCGGAGGTGACGCGAGCAGCCCCGAGAGAAGCGGCACCCTGACC
CGCCGGCACTCCCGCAGAAAGAGCCAAGAATCCAATGGATCCGGAACCCTGAAACGTCGTCCAATCGCGGTCCCGT
CGCGACCGTGGTGAAACAACCGAACCCATGGGATCCGCGTCCTCCACCTCCAGCTCCTCGAATTCCACCCCGACCC
CGACCCCATCCATCTGTGCCAAGCCCCCACCCGGCGATAGCGCCAGCCTGATGTGCAGCTCCACCCTGAGCCTGGAT
AGCCTGCCACCACCCCCCCCACCACCCGCCCTGGATGGCAGCGAGGATCAGGATGTGTACGGCAGCCAGCTGTCGCT
GGCCTCCCTGCCGCCACCGCCACCCCCCGAGGACGTGCTGGCCATGAACTACGCCGAGCCCAGCTCCCCCAGCACCC
CAACCCCCATGAGCACCCCCATGATCATGCCCAACAGCAACGGATCCCTGCCCCCAGCCGTGCCAGCCAAGCCCATG
AAGCCCGCCGTGAAGCAGGCCGCGGGCGGACTGAAGGCCGCCCCACCCTACAAGGCCCCACCCGACTACGTGGGCCC
AGCGCTGCTGCCCGGACCCCCCCTGCCGCCACCACCGCCAGCCCAGAAGAAGGTCTCCTTCGCCGATAGCCCCGTGC
TGCTGCGCCGCAAGATGTGCAGCCCAGAGCCAGTGCTGCCCCAGCGCTCCCCCAGCACCACCCTGTCCTGCCATAGC
AGCAGCTCCGCCGGAAGCGCCTATCAGACCTACGCCCCAGGCCCTATGTTGCCACCACGCGCCGACGTCGCCCGCCT
GAGCAGCCTGTCCAACGGCAGCTCCAGCGAGGTGACCAGCCCAAAGCGCCTGCAGGAAAGCGCCTCCAACCCCCCCC
GCGATTTCCTGAAGGATCTGCAGCGCGTGATGCGCAAGAAGTGGCAGGTCGCCCAGAAGTGCAAGGCCGAGCCAGCC
ACCACGCCGCATGAGGTGCTGGGCTTCCGCGATTTCAGCAACGAGGACCTGCTGGCCGCCCACAATCTGAACTCCGG
CGCCAACAGCTCCCACTACTACCGCGAGACCGCCAACGTGTCCCACTGGGTGCGCAAGCACTACGAGTACGCCCACA
ACGCCCTGTACGAGAACGTGCATGCCCAGTCGGCCGCCGCTGCCGGAGTGCCCGGCTCCGGCGAGGCTACGACGCCA
CCGCTGCCGCCACCGCCAGGCAACAGCGTGGCCGCCAAGAAGCGCCCACCGCCCCCACCCCCCAAGCGCAGCGATAA
GACCCACCTGACCAACCGCGTGTAATAG

MANLEDSQESELDQILGELSLLEAQISYTEASMLPAMCAPSAGAQIAPPPG
VTQLPGSAPTMVSMSASSSRSHSRTNSTISADVSSCSSSGISENGHGLGLVL
GGPGSAGMMVQPPPPGGMTMGITLGVVTPREPRTESPDNDSAFSDTVSLLS
SESSASSNTSLQQQQQQQQQQHHQHQQHHQHQQQQQKPQLAGAEKLHH
HGVHGQHGGQQSGANSITKADKIQLALHKLESAPIRRLFVKAFTSDGASKS
LLVDERMGCGHVTRLLADKNHVQMQSNWALVEHLGDLQMERLFEDHEL
LVDNLMTWHSDAGNRVLFQQRPDKVTLFLRPELYLPGPQMAPGCQHDEQ
TRQMLLDEFFDSHNQLQMDGPLYMKADPKKGWKRYHFVLRSSGLYYFPK
EKTKNTRDLACLNLFHGHNVYTGLGWRKKWKSPTDYTFGFKAVGDSSLG
KSCRSLKMLCAEDLPTLDRWLTAIRVCKYGKQLWDSHKSLLEDLCLSRDD
AVSQSSFAASMRSESISSISSAVPSQCGSVSSAISSMSNSTSGRTSRASSSSSS
GCLSDDNNAFDSEFTTGTIKRKPSMKPNLPLTTMTRQLKEVGEITICESAGG
DASSPERSGTLTRRHSRRKSQESNGSGTLKRRPIAVPVATVVKQTEPMGSA
SSTSSSSNSTPTPTPSICAKPPPGDSASLMCSSTLSLDSLPPPPPPPALDGSED
QDVYGSQLSLASLPPPPPPEDVLAMNYAEPSSPSTPTPMSTPMIMPNSNGSL
PPAVPAKPMKPAVKQAAGGLKAAPPYKAPPDYVGPALLPGPPLPPPPPAQ
KKVSFADSPVLLRRKMCSPEPVLPQRSPSTTLSCHSSSSAGSAYQTYAPGP
MLPPRADVARLSSLSNGSSSEVTSPKRLQESASNPPRDFLKDLQRVMRKK
WQVAQKCKAEPATTPHEVLGFRDFSNEDLLAAHNLNSGANSSHYYRETA
NVSHWVRKHYEYAHNALYENVHAQSAAAAGVPGSGEATTPPLPPPPGNS
VAAKKRPPPPPPKRSDKTHLTNRV

Accessory gland-specific peptide 26Aa OS=Drosophila melanogaster GN=Acp26Aa PE=1 SV=2 - [MS2A_DROME]
Accessory gland-specific peptide 70A OS=Drosophila sechellia GN=Acp70A PE=2 SV=1 - [A70A_DROSE]
Ataxin-2 homolog OS=Drosophila melanogaster GN=Atx2 PE=1 SV=1 - [ATX2_DROME]
Box A-binding factor OS=Drosophila melanogaster GN=srp PE=1 SV=2 - [SRP_DROME]
Calmodulin OS=Drosophila melanogaster GN=Cam PE=1 SV=2 - [CALM_DROME]
Cdc42 homolog OS=Drosophila melanogaster GN=Cdc42 PE=1 SV=1 - [CDC42_DROME]
Centaurin-gamma-1A OS=Drosophila melanogaster GN=cenG1A PE=1 SV=2 - [CEG1A_DROME]
Centrosome-associated zinc finger protein CP190 OS=Drosophila melanogaster GN=Cp190 PE=1 SV=2 - [CP190_DROME]
Chromatin-remodeling complex ATPase chain Iswi OS=Drosophila melanogaster GN=Iswi PE=1 SV=1 - [ISWI_DROME]
Copia protein OS=Drosophila melanogaster GN=GIP PE=1 SV=3 - [COPIA_DROME]
Defective chorion-1 protein (Fragments) OS=Drosophila erecta GN=dec-1 PE=3 SV=2 - [DEC1_DROER]
Ejaculatory bulb-specific protein 1 OS=Drosophila melanogaster GN=Peb PE=1 SV=1 - [PEB1_DROME]
Enhancer of mRNA-decapping protein 3 OS=Drosophila melanogaster GN=Edc3 PE=1 SV=1 - [EDC3_DROME]
Heat shock protein 22 OS=Drosophila melanogaster GN=Hsp22 PE=1 SV=4 - [HSP22_DROME]
Heat shock protein 68 OS=Drosophila melanogaster GN=Hsp68 PE=1 SV=1 - [HSP68_DROME]
Kinesin-like protein Klp59C OS=Drosophila melanogaster GN=Klp59C PE=1 SV=1 - [KI59C_DROME]
Major heat shock 70 kDa protein Ba OS=Drosophila melanogaster GN=Hsp70Ba PE=2 SV=2 - [HSP72_DROME]
Maternal protein exuperantia OS=Drosophila melanogaster GN=exu PE=1 SV=2 - [EXU_DROME]
Muscle segmentation homeobox OS=Drosophila melanogaster GN=Dr PE=2 SV=2 - [HMSH_DROME]
PERQ amino acid-rich with GYF domain-containing protein CG11148 OS=Drosophila melanogaster GN=CG11148 PE=1 SV=1 - [PERQ1_DROME]
Phosrestin-1 OS=Drosophila melanogaster GN=Arr2 PE=1 SV=2 - [ARRB_DROME]
Phosrestin-2 OS=Drosophila melanogaster GN=Arr1 PE=1 SV=1 - [ARRA_DROME]
Probable RNA-binding protein orb2 OS=Drosophila melanogaster GN=orb2 PE=1 SV=1 - [ORB2_DROME]
Profilin OS=Drosophila melanogaster GN=chic PE=1 SV=1 - [PROF_DROME]

Protein encore OS=Drosophila melanogaster GN=enc PE=1 SV=2 - [ENC_DROME]
Putative mitochondrial inner membrane protein OS=Drosophila melanogaster GN=CG6455 PE=2 SV=4 - [IMMT_DROME]
Ras-like protein 1 OS=Drosophila mojavensis GN=Ras85D PE=3 SV=1 - [RAS1_DROMO]
Ras-related protein Rab-3 OS=Drosophila melanogaster GN=Rab3 PE=1 SV=1 - [RAB3_DROME]
Serine/threonine-protein phosphatase alpha-1 isoform OS=Drosophila melanogaster GN=Pp1alpha-96A PE=1 SV=1 - [PP11_DROME]
Serine/threonine-protein phosphatase beta isoform OS=Drosophila melanogaster GN=flw PE=1 SV=1 - [PP1B_DROME]
Transient-receptor-potential-like protein OS=Drosophila melanogaster GN=trpl PE=1 SV=2 - [TRPL_DROME]
Transport and Golgi organization protein 1 OS=Drosophila melanogaster GN=Tango1 PE=1 SV=2 - [TGO1_DROME]
UPF0363 protein CG9853 OS=Drosophila melanogaster GN=CG9853 PE=1 SV=1 - [U363_DROME]
UPF0505 protein CG8202 OS=Drosophila melanogaster GN=CG8202 PE=2 SV=3 - [U505_DROME]

Acetylcholinesterase OS=Drosophila melanogaster GN=Ace PE=1 SV=1 - [ACES_DROME]
Atlastin OS=Drosophila melanogaster GN=atl PE=1 SV=1 - [ATLAS_DROME]
Cathepsin L OS=Drosophila melanogaster GN=Cp1 PE=1 SV=2 - [CATL_DROME]
Interference hedgehog OS=Drosophila willistoni GN=iHog PE=3 SV=1 - [IHOG_DROWI]
Longitudinals lacking protein, isoforms J/P/Q/S/Z OS=Drosophila melanogaster GN=lola PE=1 SV=4 - [LOLA5_DROME]
Polycomb group protein Pc OS=Drosophila melanogaster GN=Pc PE=1 SV=1 - [PC_DROME]
Protein lap4 OS=Drosophila melanogaster GN=scrib PE=1 SV=1 - [LAP4_DROME]
Salivary glue protein Sgs-8 OS=Drosophila melanogaster GN=Sgs8 PE=2 SV=1 - [SGS8_DROME]
WD repeat-containing protein on Y chromosome OS=Drosophila grimshawi GN=WDY PE=4 SV=1 - [WDY_DROGR]

Appendix 5

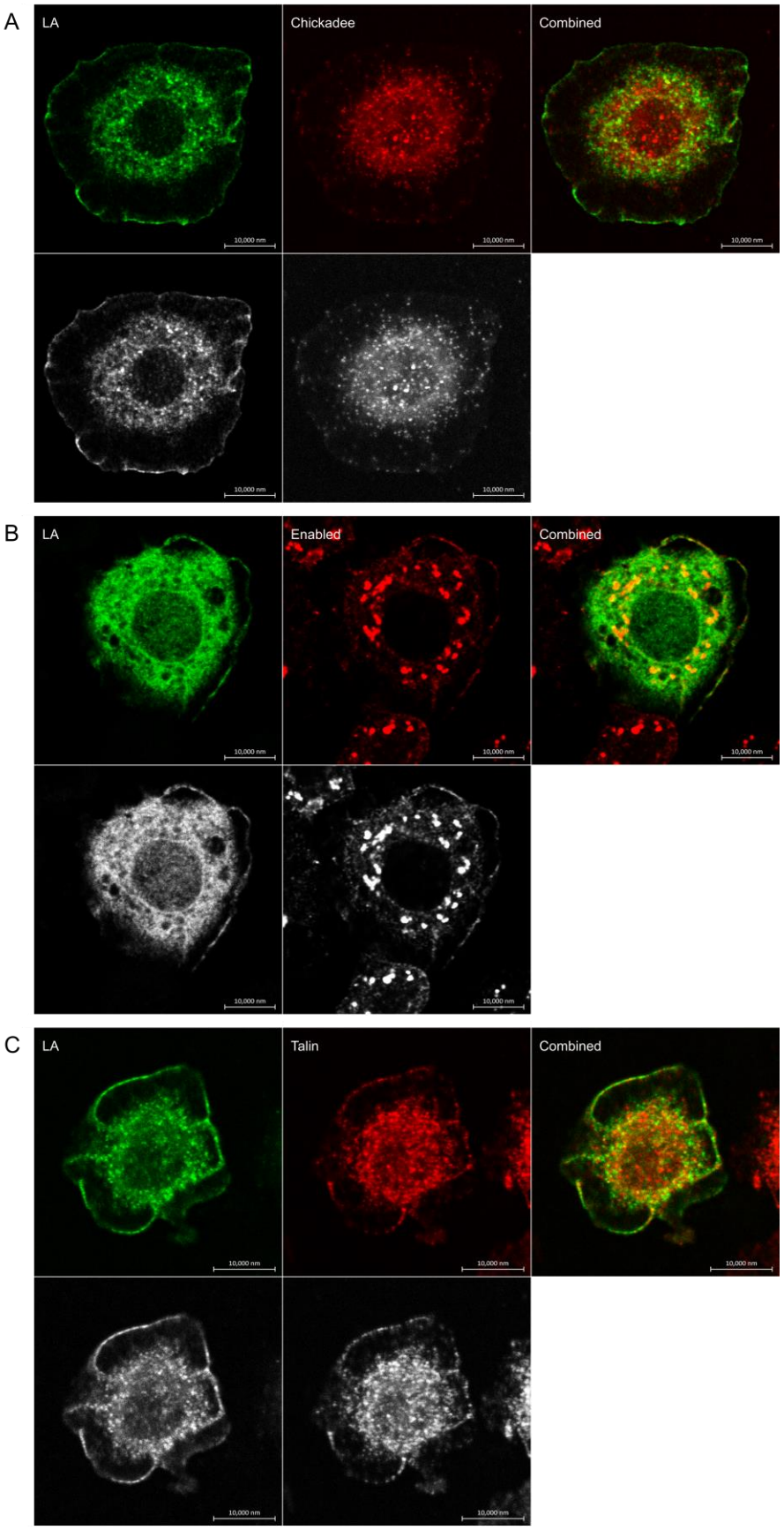
A
LA
Chickadee
Combined
B
LA
Enabled
Combined
C
LA
Talin
Combined

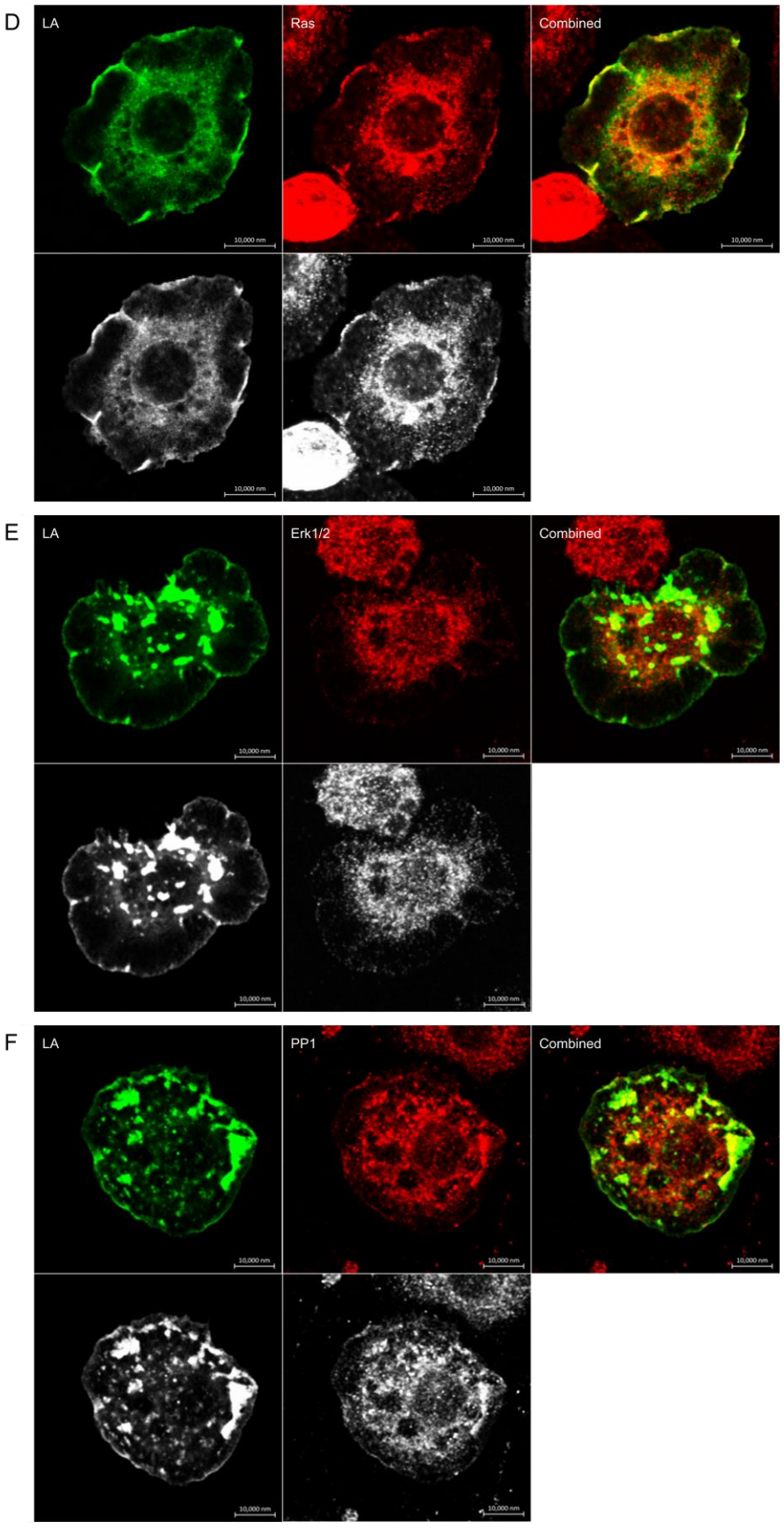
D
LA
Ras
Combined
E
LA
Erk1/2
Combined
F
LA
PP1
Combined

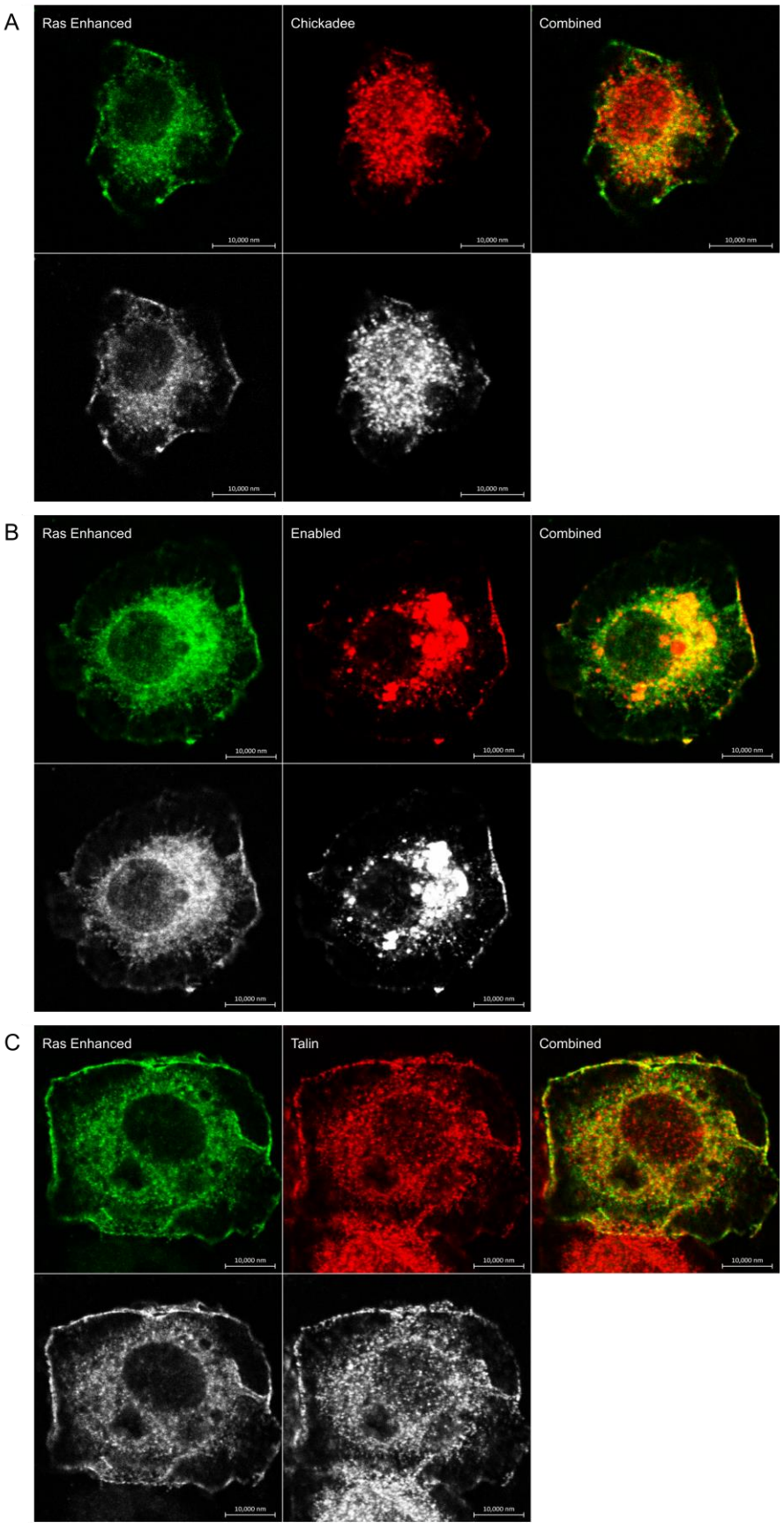
A
Ras Enhanced
Chickadee
Combined
B
Ras Enhanced
Enabled
Combined
C
Ras Enhanced
Talin
Combined

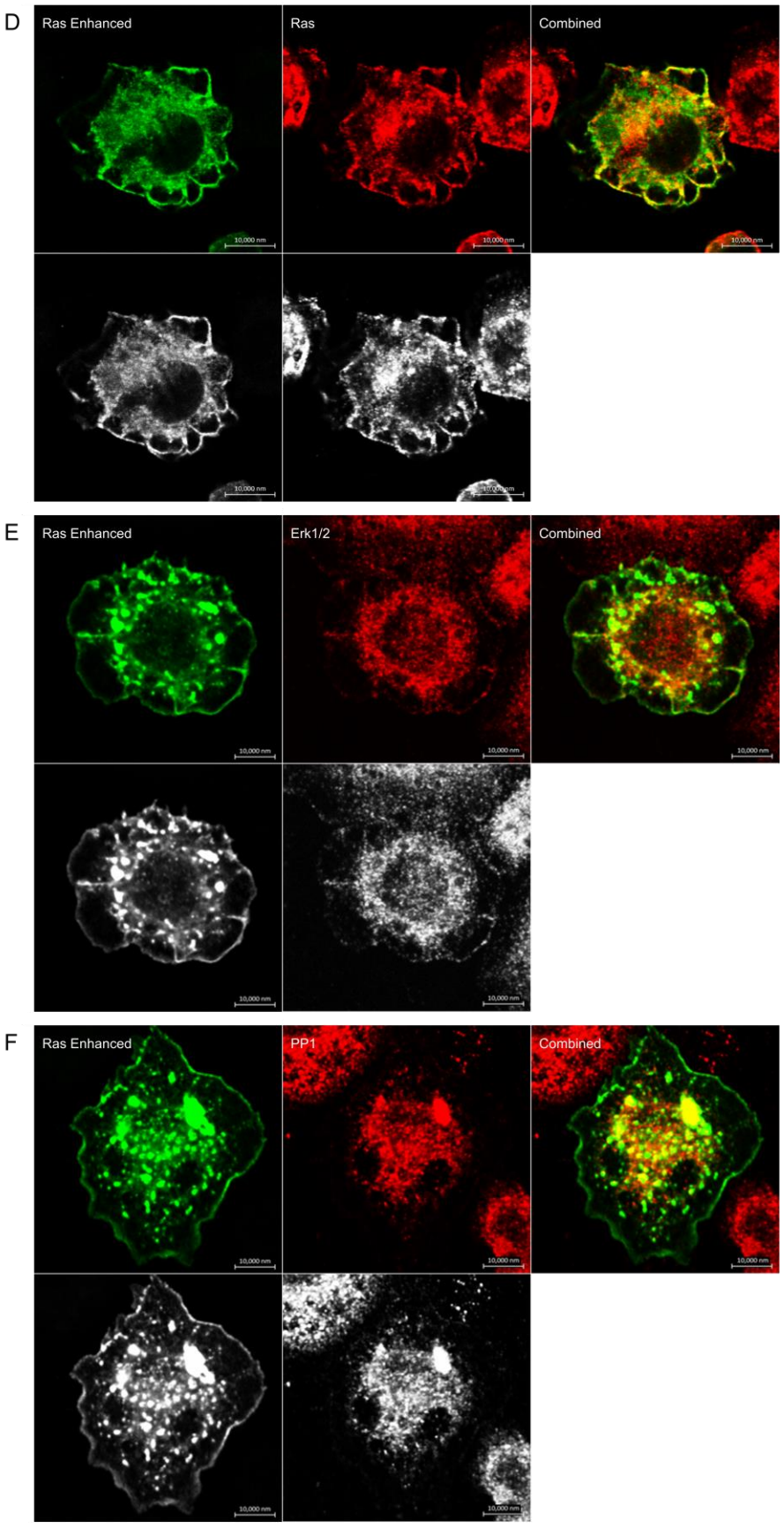
D
Ras Enhanced
Ras
Combined
E
Ras Enhanced
Erk1/2
Combined
F
Ras Enhanced
PP1
Combined

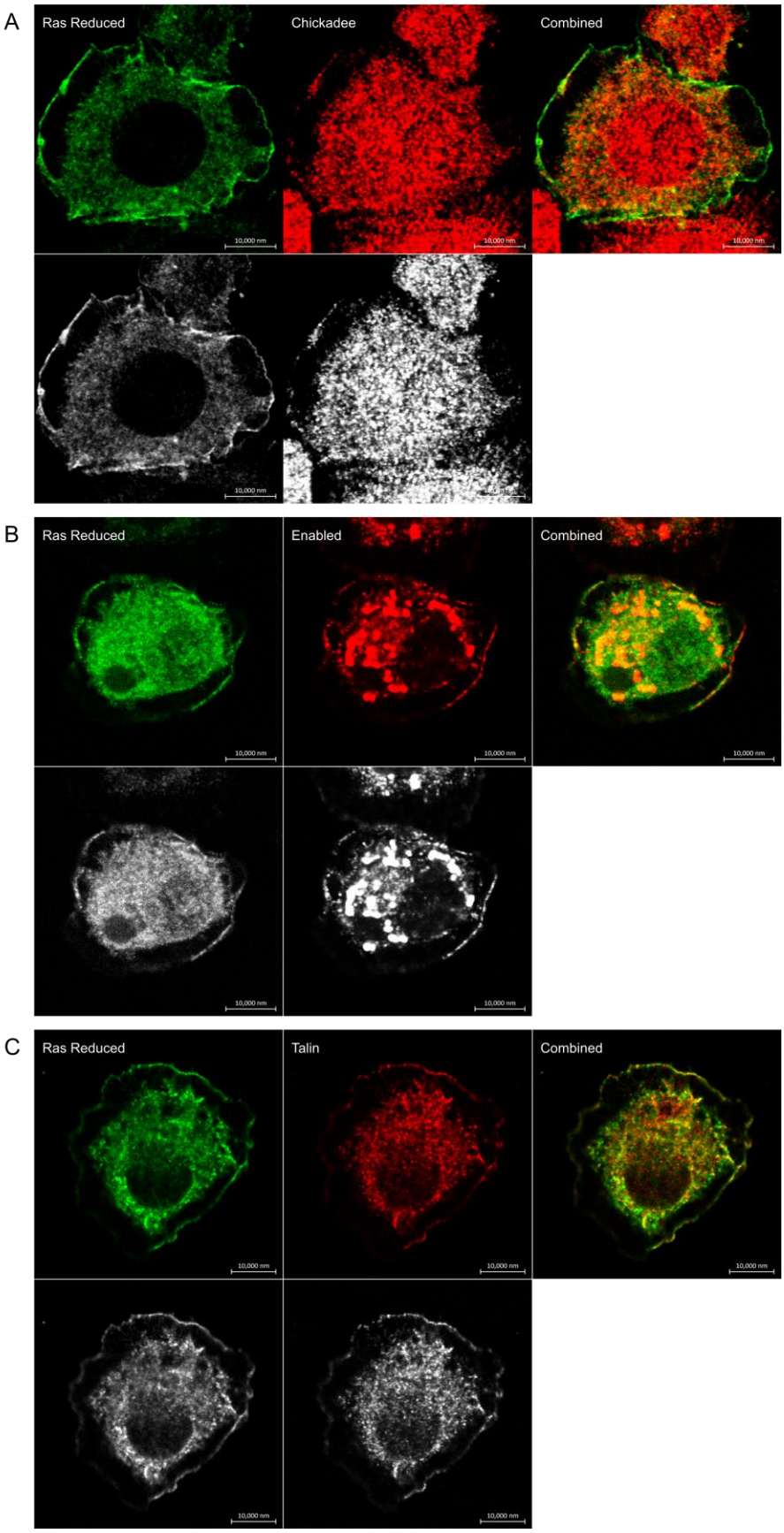
A
Ras Reduced
Chickadee
Combined
B
Ras Reduced
Enabled
Combined
C
Ras Reduced
Talin
Combined

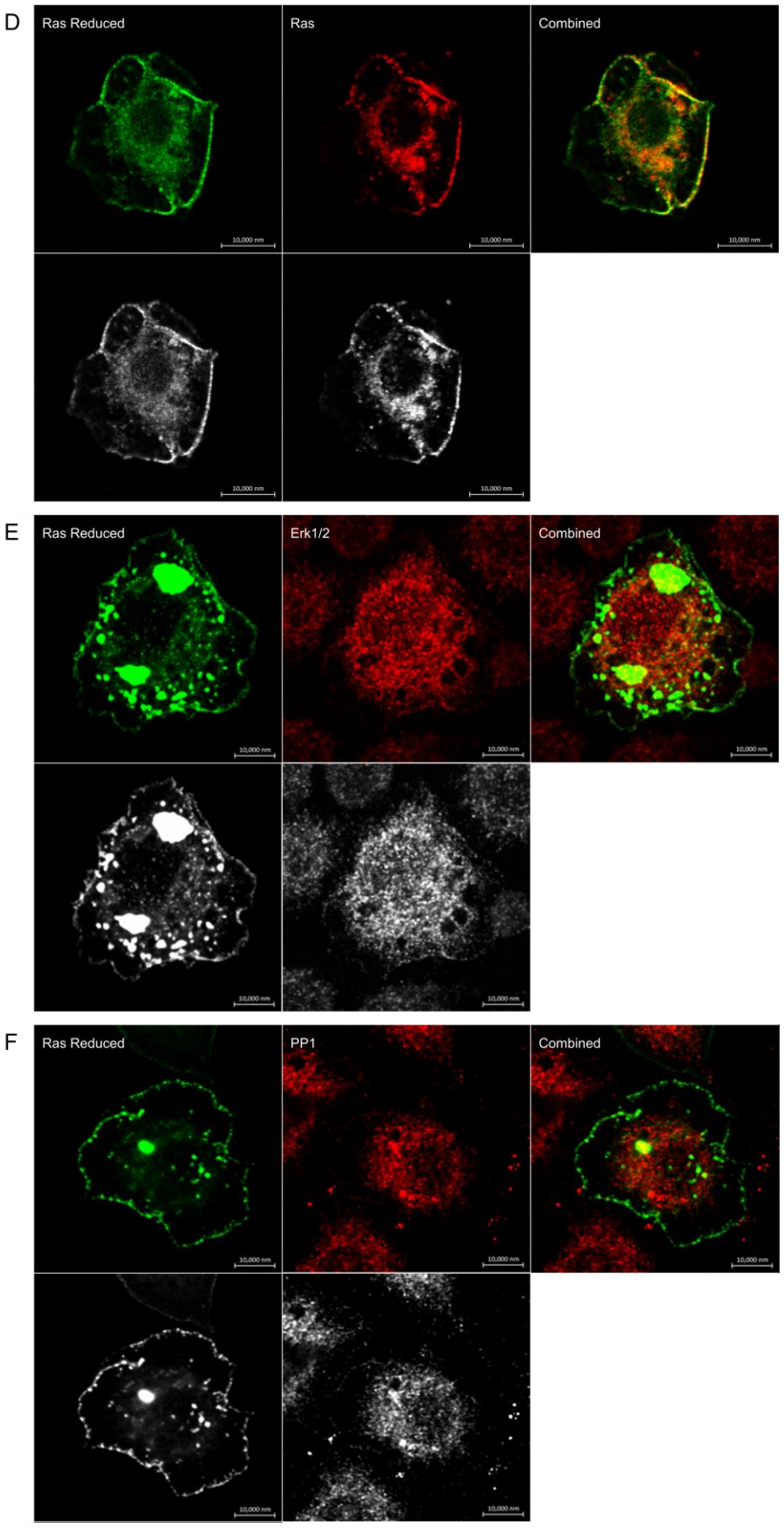
D
Ras Reduced
Ras
Combined
E
Ras Reduced
Erk1/2
Combined
F
Ras Reduced
PP1
Combined

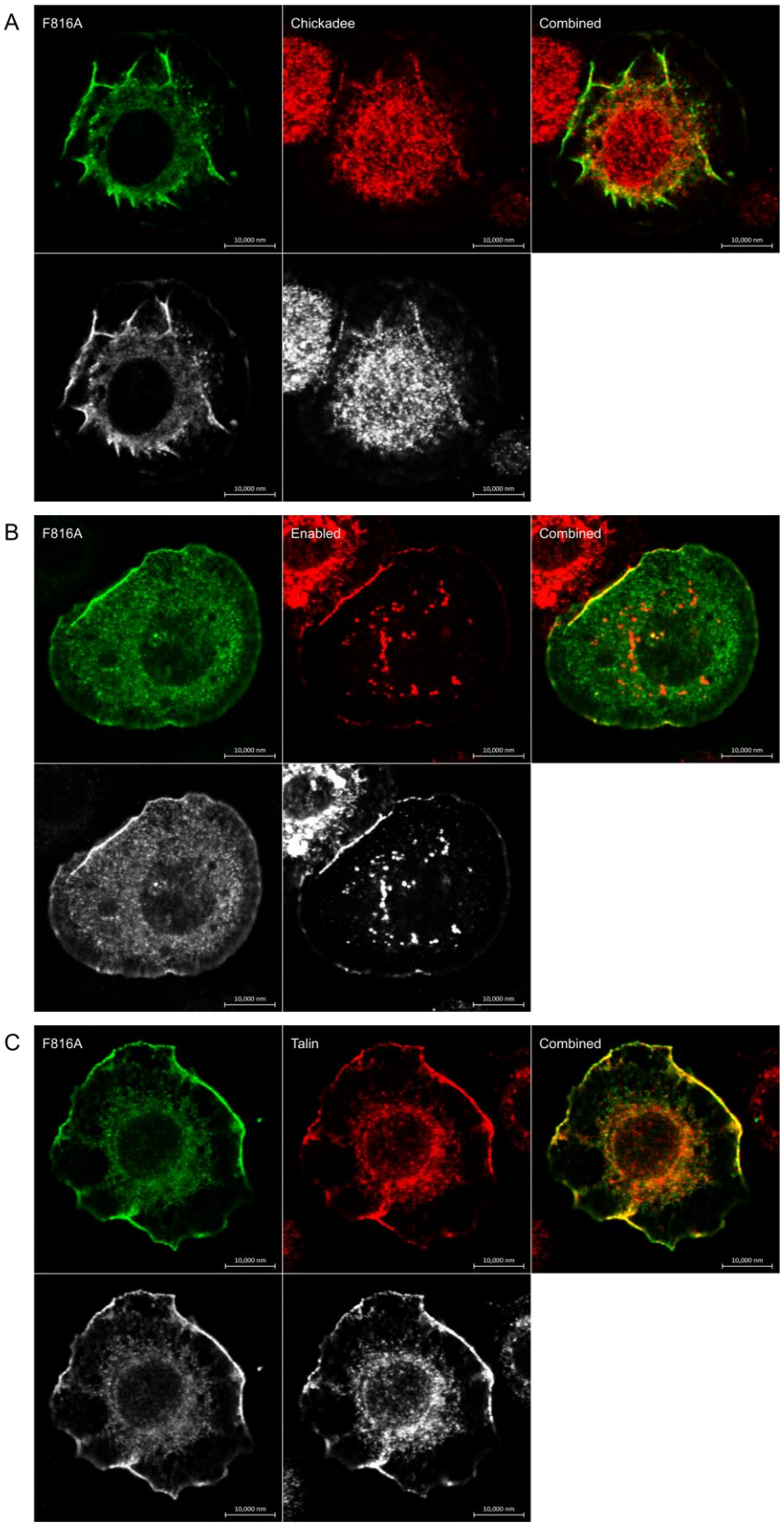
A
F816A
Chickadee
Combined
B
F816A
Enabled
Combined
C
F816A
Talin
Combined

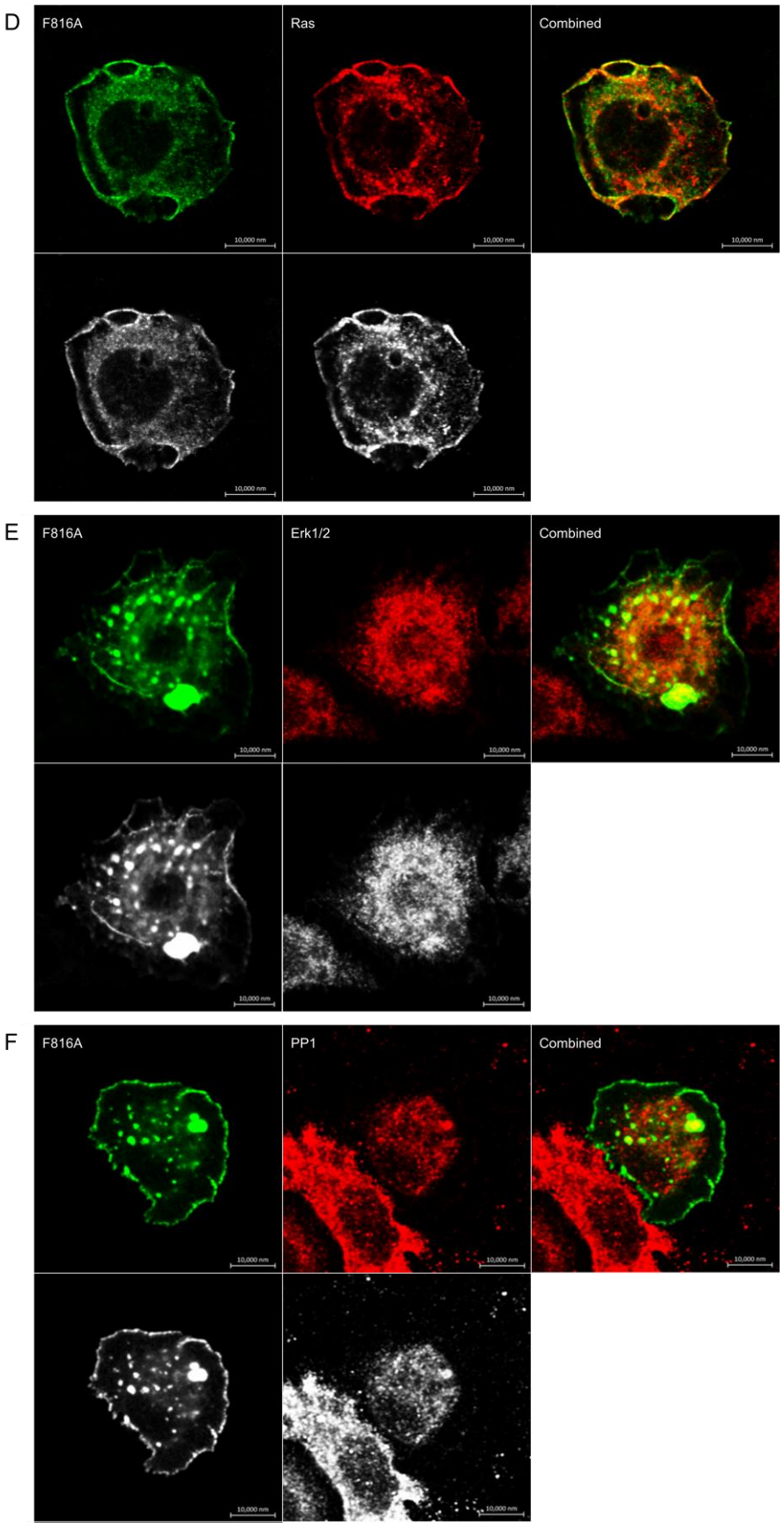
D
F816A
Ras
Combined
E
F816A
Erk1/2
Combined
F
F816A
PP1
Combined

Appendix 5

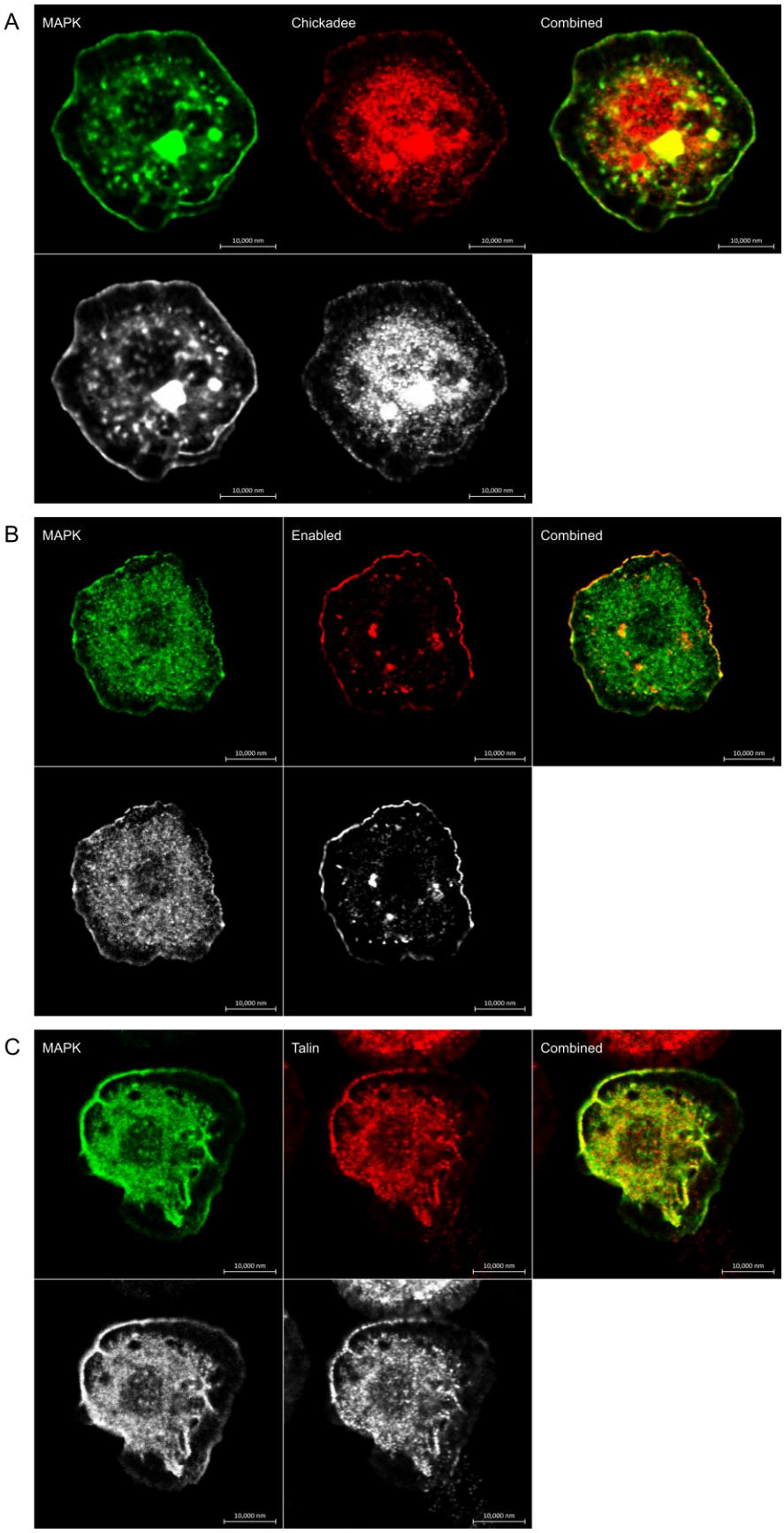
A
MAPK
Chickadee
Combined
B
MAPK
Enabled
Combined
C
MAPK
Talin
Combined

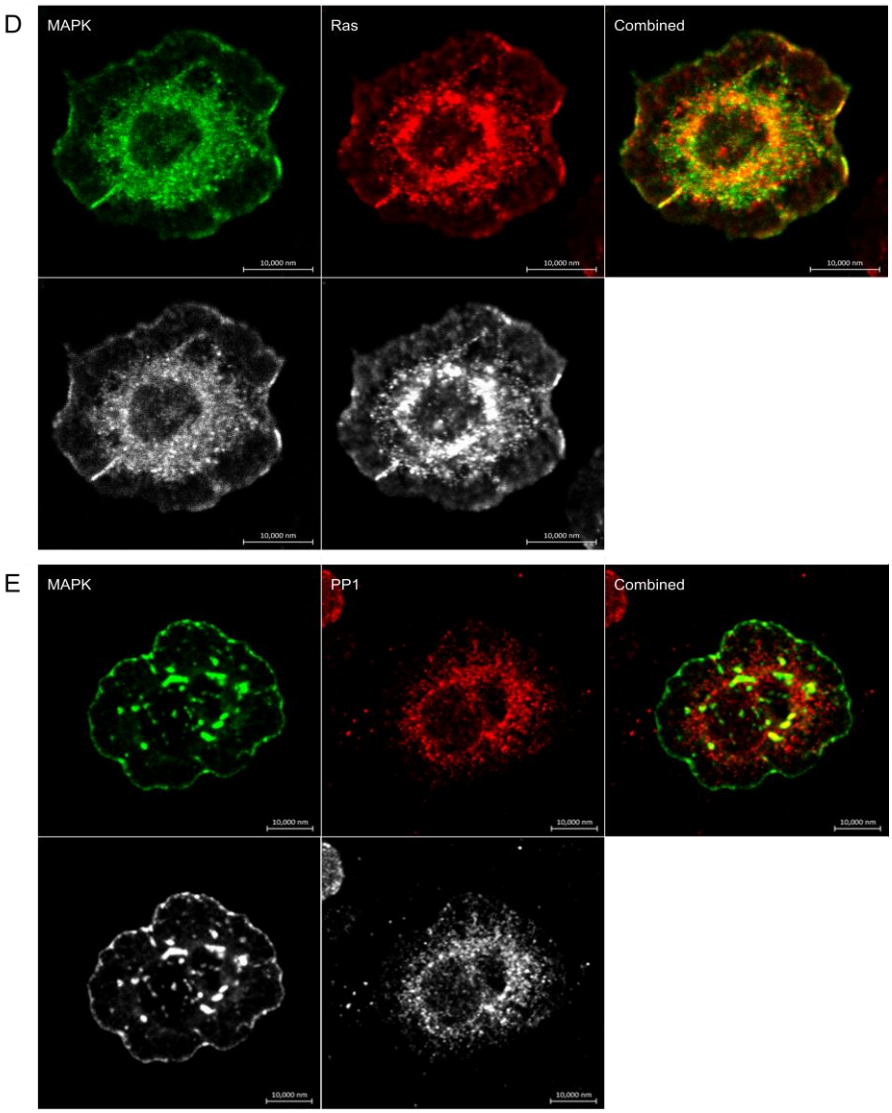
D
MAPK
Ras
Combined
E
MAPK
PP1
Combined

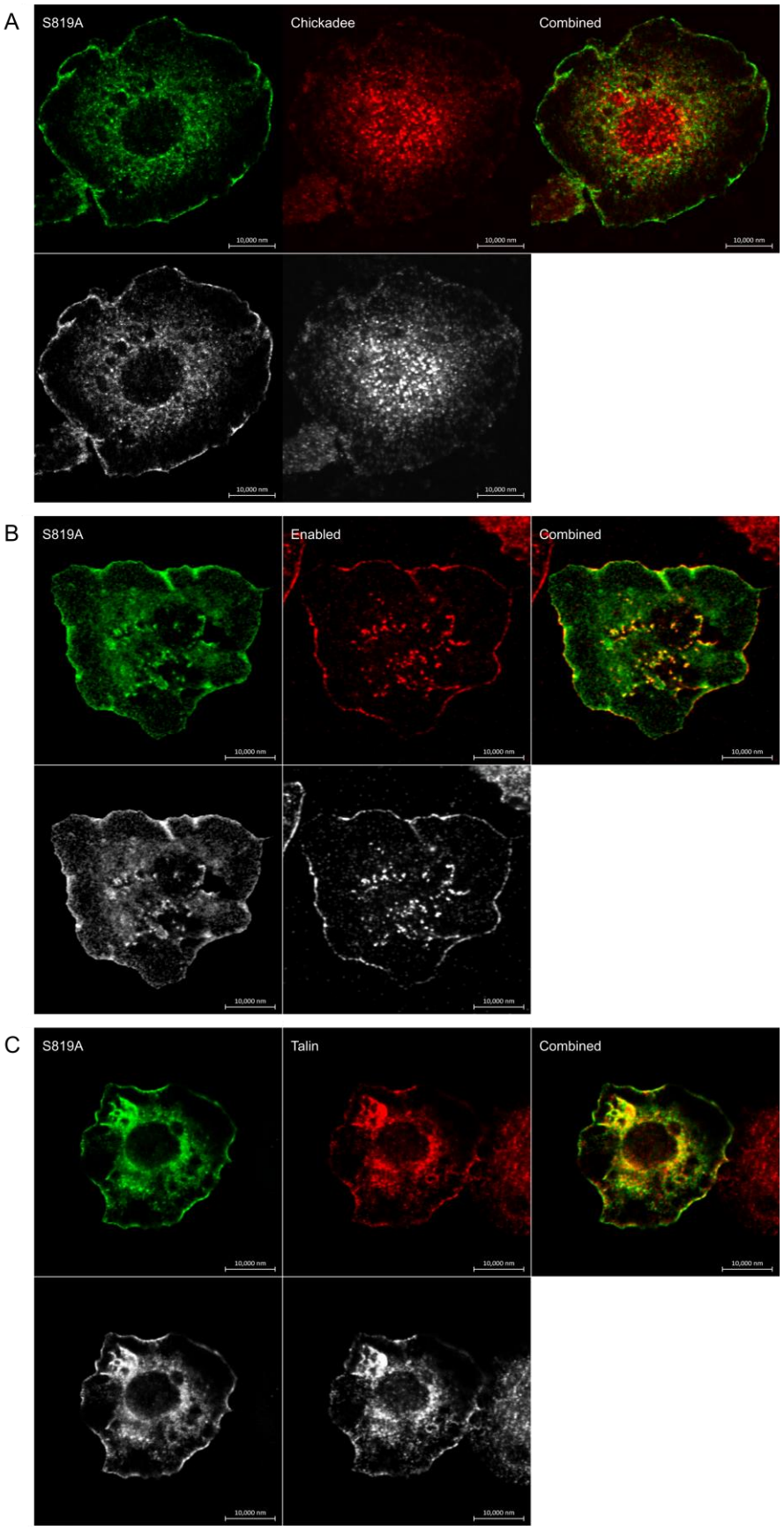
A
S819A
Chickadee
Combined
B
S819A
Enabled
Combined
C
S819A
Talin
Combined

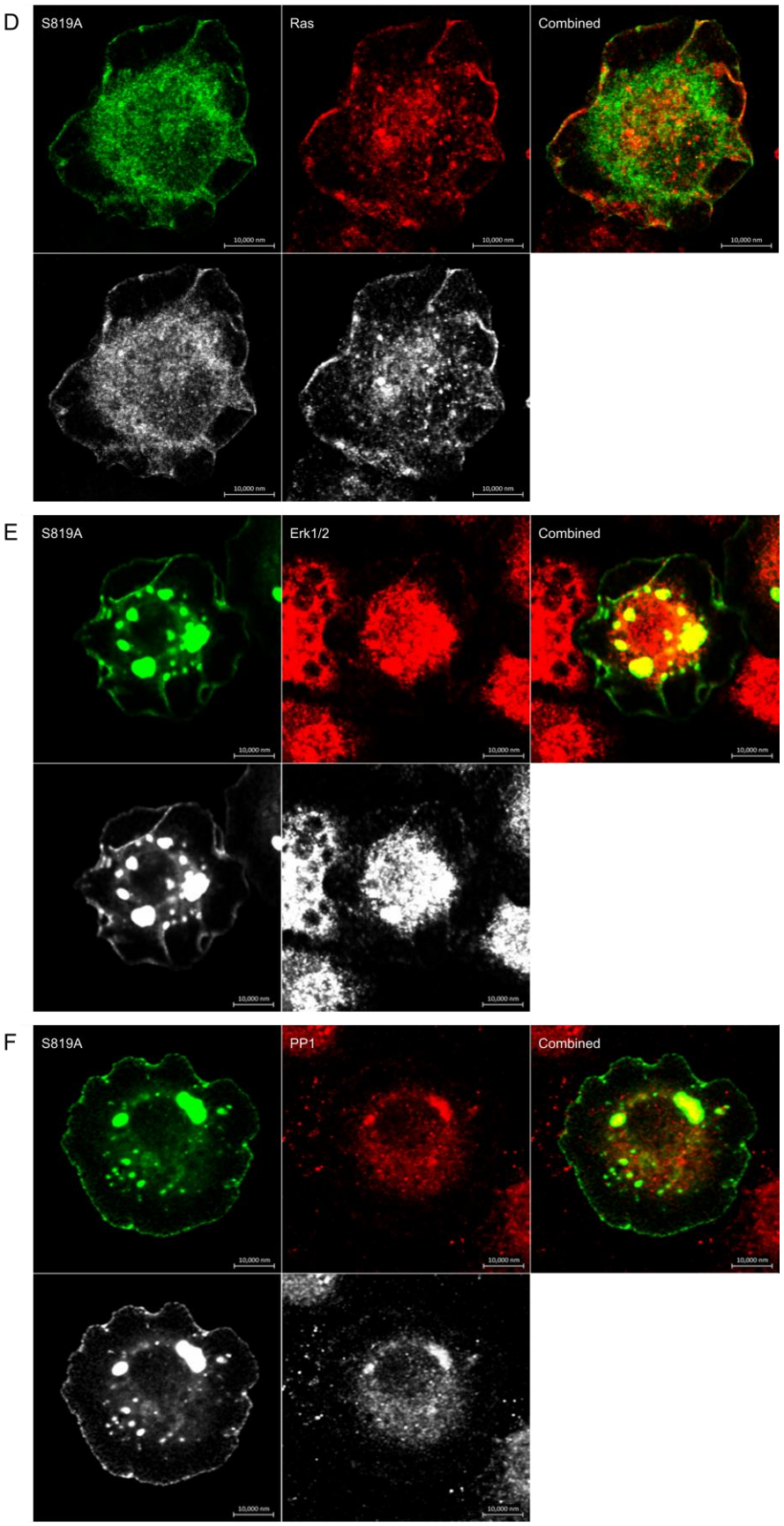
D
S819A
Ras
Combined
E
S819A
Erk1/2
Combined
F
S819A
PP1
Combined

Appendix 5

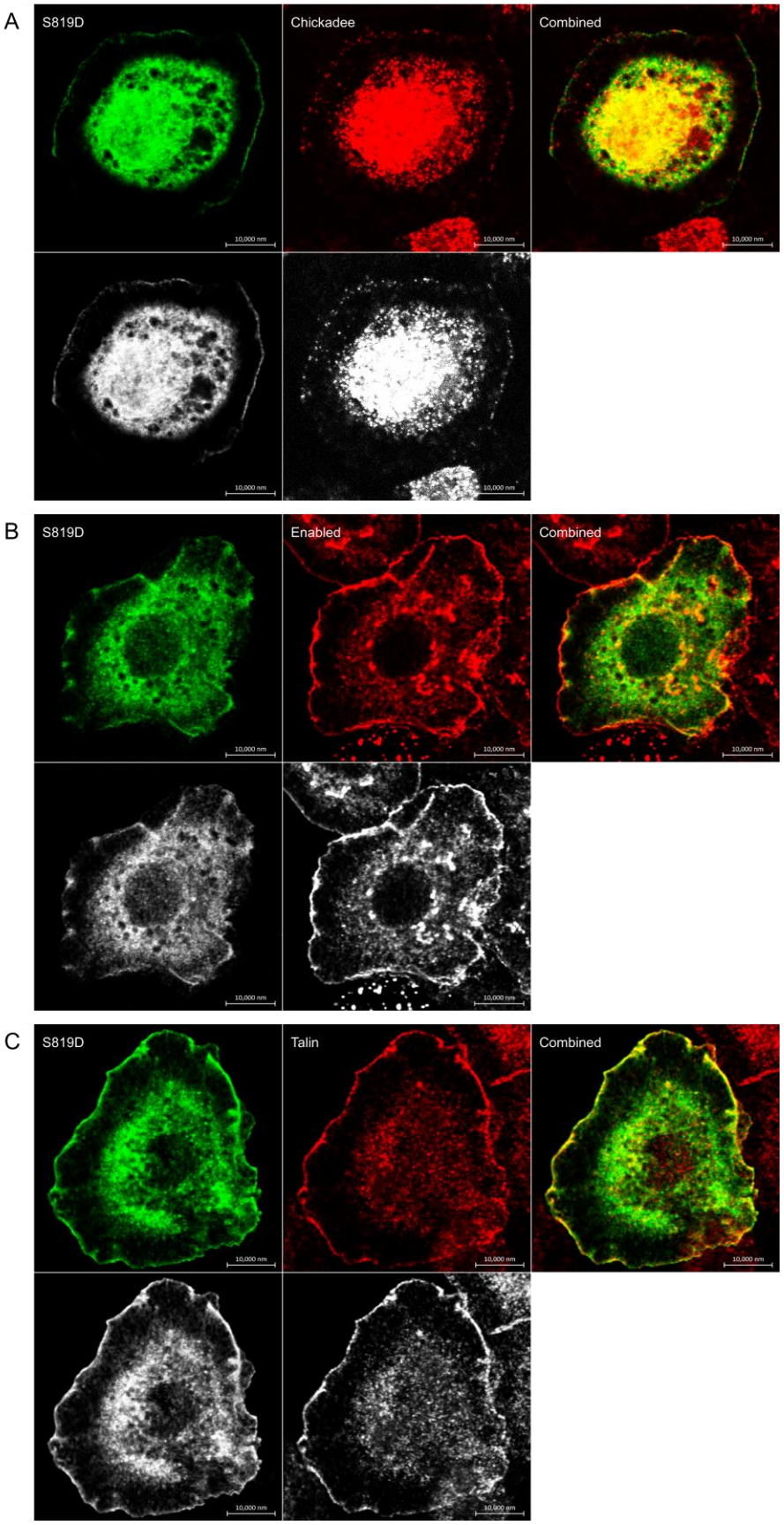
A
S819D
Chickadee
Combined
B
S819D
Enabled
Combined
C
S819D
Talin
Combined

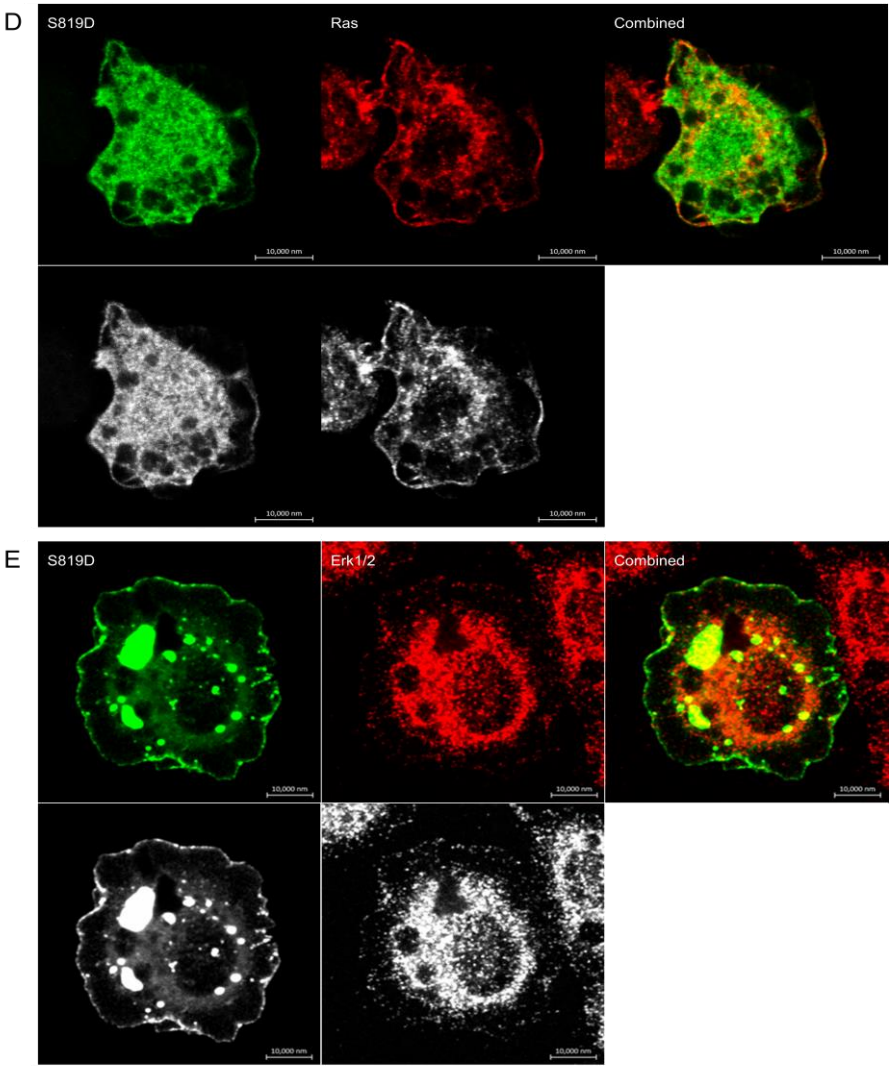
D
S819D
Ras
Combined
E
S819D
Erk1/2
Combined

Appendix 5

(Bennett et al., 2006)